



Deliverable 1.33

Innovative Turbine Concepts - Multi-Rotor System

August 2015

Agreement n.:	308974
Duration	November 2012 – October 2017
	DTU Wind



The research leading to these results has received funding from the European Community's Seventh Framework Programme under grant agreement

PROPRIETARY RIGHTS STATEMENT

This document contains information, which is proprietary to the "INN WIND.EU" Consortium. Neither this document nor the information contained herein shall be used, duplicated or communicated by any means to any third party, in whole or in parts, except with prior written consent of the "INN WIND.EU" consortium.

Document information

Document Name:	Innovative Turbine Concepts – Multi-Rotor System
Document Number:	Deliverable 1.33
Author:	P Jamieson, M Branney and K Hart (University of Strathclyde) P K Chaviaropoulos and G Sieros (CRES), S Voutsinas, P Chasapogiannis, J M Prospathopoulos (National Technical University of Athens)
Document Type	Report
Dissemination level	PU
Review:	W. E. Leithead (University of Strathclyde)
Date:	September 2015
WP:	WP1: Conceptual Design
Task:	Task 1.3: Innovation and assessment at the WT Level
Approval:	Approved by WP Leader

TABLE OF CONTENTS

LIST OF FIGURES & TABLES	7
CHAPTER 1 INTRODUCTION	13
1.1 Scope and Objectives	13
1.2 Overview of report contents	13
CHAPTER 2 BACKGROUND	15
2.1 History of technology – the motivation	15
2.2 Status and development needs of MRS prior to Innwind	16
CHAPTER 3 SYSTEM CONCEPT DESIGN.....	17
3.1 Structure concept.....	17
3.2 Layout shape.....	18
3.3 Scale issues.....	18
3.4 Wind Turbine Operational Characteristics.....	19
3.5 Rotor and drive train module	20
3.6 System Yawing	21
3.7 Assembly and Installation Concept.....	22
3.8 O&M Concept	23
CHAPTER 4 AERODYNAMIC EVALUATION OF THE MULTI ROTOR CONCEPT	25
4.1 Introduction	25
4.2 Numerical Models	25
4.2.1 CRES-flowNS RANS solver.....	25
4.2.2 The GENUVP vortex method.....	31
4.3 Results.....	37
4.4 Discussion of the results	47
CHAPTER 5 MULTI ROTOR SYSTEM LOADS	49
5.1 General	49
5.2 Loads Simulation Tool an7d Capability	49
5.3 Design Load Cases.....	50
5.4 Wind turbine parameters.....	53
5.5 LOAD CASE ANALYSIS	57
5.5.1 DLC-1.2 (NTM) - Fatigue loads.....	57
5.5.2 DLC-1.3 (ETM) - Ultimate Loads in Power Production	57
5.5.3 DLC-1.4 (ECD) - Ultimate loads during power production	67
5.5.4 DLC-2.3 (EOG) - Ultimate Loads During Production with Electrical Fault	70

5.5.5	DLC-4.1 (NWP) - Fatigue Loads During Shutdown	75
5.5.6	DLC-4.2 (EOG) - Ultimate Loads During Shutdown	75
5.5.7	DLC-6.1 (EWM) - Idling Ultimate Loads due to 50 Year Gust	80
5.5.8	DLC-6.2 (EWM) - Idling Ultimate Loads due to 50 Year Gust and Grid Loss (Effectively Yaw System Non-Operational).....	83
5.5.9	DLC-6.3 (EWM) - Idling Ultimate Loads with 1 Year Gust & Extreme Yaw Misalignment .	84
5.6	LOAD CASE OVERVIEW.....	86
5.7	DISCUSSION	88
5.7.1	Load Averaging	88
5.7.2	Turbulence Loading.....	92
5.7.3	Phased Shutdowns.....	93
5.7.4	Addition of Turbulence to Coherent Load Cases	97
5.8	LOAD CASE COMPARISON	99
5.9	DISCUSSION	100
CHAPTER 6 MULTI ROTOR SYSTEM SUPPORT STRUCTURE DESIGN		101
6.1	Brief description of the structural analysis tool.....	101
6.2	Initial shape	102
6.3	Selection of candidate cross sections	103
6.4	Load cases	105
6.5	Preliminary Designs	106
6.6	Final Design.....	107
6.7	Structural Analysis - Eigenvalue analysis.....	109
6.8	Structural Analysis - Ultimate Loading.....	111
6.9	Structural Analysis - Fatigue Loading.....	114
6.10	Structural Analysis – Robustness	118
CHAPTER 7 FLOATING PLATFORM – PRELIMINARY DESIGN		122
7.1	Scope	122
7.2	Design method and assumptions made.....	123
7.3	Results.....	125
7.4	Discussion on the results	129
CHAPTER 8 ELECTRICAL SYSTEMS DESIGN		130
8.1	General	130
8.2	Electrical Infrastructure	130
8.2.1	Inverters	130
8.2.2	Electrical Clusters	130
8.2.3	Provisional wiring arrangement for MRS.....	134

8.2.4	Control strategy.....	134
8.2.5	Resistors for load dump	135
CHAPTER 9 YAWING OF THE MRS		138
9.1	Yaw system design.....	138
9.1.1	Yaw moments due to structure drag	138
9.1.2	Effect of yaw system centre location on yaw stability	140
9.1.3	Active control of yaw using rotor thrust	142
9.2	Engineering of yaw systems	144
9.2.1	Concepts for yawing	144
9.2.2	Development of tower-frame concepts	145
9.2.3	Yaw bearing solutions	149
9.3	Overview of yaw system issues	153
9.3.1	Yaw torques and operational aspects.....	153
9.3.2	Bearing design and interaction with structural solutions.....	154
CHAPTER 10 OPERATION AND MAINTENANCE		155
10.1	O&M Modelling of the MRS	155
10.2	Validation of baseline O&M impact of LCOE	156
10.3	Results for the MRS	156
CHAPTER 11 COST OF ENERGY EVALUATION		160
11.1	General	160
11.2	Energy Capture – Impact of Wind Turbulence.....	160
11.3	Energy Capture – Effect of Rotor Interaction	163
11.4	LCOE Cost Model.....	164
11.5	CAPEX Comparisons.....	167
11.6	Baseline LCOE Comparison	171
11.7	LCOE Sensitivity Study	173
11.8	40 MW MRS	178
CHAPTER 12 CONCLUSIONS AND OVERALL EVALUATION		180
CHAPTER 13 MRS CONCEPT OVERVIEW		183
13.1	Evaluation of MRS as an innovation	183
13.2	The level of benefit.....	183
13.3	Feasibility, economics and possible show stoppers	184
13.4	Perception of the MRS concept.....	186
13.5	Status of MRS at conclusion of Task 1.33	187



REFERENCES	188
APPENDIX A FATIGUE ANALYSIS OF THE SUPPORT STRUCTURE MEMBERS, S-N CURVES	191

LIST OF FIGURES & TABLES

Figure 2-1 Honnef's vision of large scale wind energy systems.	15
Figure 3-1 Outline of MRS support structure.....	17
Figure 3-2: MRS design based on cantilevered support structure.....	18
Figure 3-3: Drive train efficiency comparison.....	21
Figure 3-4: Initial floater concept as a barge.....	21
Figure 3-5: Previous design of a 5 MW MRS.	22
Figure 4-1: Polar grid definition on the rotor disk plane. Δr and $\Delta\psi$ define the spacing in the radial and azimuth direction respectively.....	28
Figure 4-2: Numerical grid at the rotors plane $x=0$ for the 7 MRS.....	30
Figure 4-3: Numerical grid at the rotors plane $x=0$ for the 45 MRS.....	31
Figure 4-4: The notations of the grid on the bodies and the wake.....	33
Figure 4-5: (a) The three sub steps per time step in GENUVP, (b) The integration scheme	35
Figure 4-6: The surface grid.....	36
Figure 4-7: GENUVP: Perspective and back view of a 7 MRS. Red dots correspond to vortex blobs. In the Right figure the wake expansion, the tendency of the wake to mix and the overall swirling can be seen.....	36
Figure 4-8: The $C_p - \lambda$ curve of the rotor	37
Figure 4-9: Per cent increase in thrust and power estimation of a 7 MRS in comparison to the single rotor performance. Simulations were performed using the CRES-flowNS actuator disk and the GENUVP vortex methods.....	38
Figure 4-10: Per cent increase in thrust and power estimation of a 7 and a 45 MRS in comparison to the single rotor performance. Simulations were performed using the CRES-flowNS actuator disk method.....	39
Figure 4-11. Axial velocity contours normalized by U_{ref} at $z=227m$ (TSR=9). Predictions obtained using CRES-flowNS. <i>Left: Single rotor, Right: 7 multi rotor system.</i>	40
Figure 4-12: Axial velocity contours normalized by U_{ref} at $z=245.5m$ (TSR=9) for the 45 MRS. Predictions obtained using CRES-flowNS. <i>Left: Distance between centers of rotors is $1.05 D$, Right: Distance between centers of rotors is $1.025 D$.</i>	40
Figure 4-13: Axial velocity contours normalized by U_{ref} on the vertical plane $y=0$ (TSR=9) Predictions obtained using CRES-flowNS <i>Left: Single rotor, Right: 7 MRS.</i>	41
Figure 4-14: Axial velocity contours normalized by U_{ref} on the vertical plane $y=0$ (TSR=9) for the 45 MRS. Predictions obtained using CRES-flowNS. <i>Left: Distance between the centers of the rotors is $1.05 D$. Right: Distance between the centers of the rotors is $1.025 D$.</i>	42
Figure 4-15: Axial velocity contours normalized by U_{ref} on the vertical plane $y=0$ (TSR=9) for the 7 MRS. <i>Left: CRES-flowNS, Right: GENUVP</i>	43

Figure 4-16: Axial velocity contours normalized by U_{ref} at $z=227m$ (TSR=9) for the 7 MRS. *Left: CRES-flowNS, Right: GENUVP* 43

Figure 4-17: Axial velocity contours normalized by U_{ref} on the rotor-plane $x=0$ (TSR=9) for the 7 MRS. *Left: CRES-flowNS, Right: GENUVP*..... 44

Figure 4-18: Axial velocity contours normalized by U_{ref} at the $x=0.1D$ downstream position (TSR=9) for the 7 MRS. *Left: CRES-flowNS, Right: GENUVP* 44

Figure 4-19: Axial velocity contours normalized by U_{ref} (TSR=9) for the 45 MRS. Predictions obtained using CRES-flowNS. *Left: Rotor plane $x=0$, Right: Downstream position $x=0.1 D$* 45

Figure 4-20: Axial velocity contours normalized by U_{ref} (TSR=9) for the 45 MRS. Focus is made on the 7 central rotors of the system. Predictions obtained using CRES-flowNS. *Left: Rotor plane $x=0$, Right: Downstream position $x=0.1 D$* 45

Figure 4-21: Snapshots of the normalized axial velocity: (a) on the rotor plane and (b) at $x=0.1D$ downstream at azimuth angle $\psi=0^\circ$ (results obtained with the vortex model) 46

Figure 4-22: Blade loading history for the central and the off-set rotors, TSR=9, sheared inflow. 47

Figure 4-23: Blade loading means and amplitudes for the central and the off-set rotors. The rotor at the center is labeled as CR_1, while the off-set rotors as OR_2, OR_3,, etc..... 47

Figure 5-1 - Graphical Representation of the 45-rotor 20MW MRS Modelled in Bladed..... 52

Figure 5-2 - Rotor Numbering System 53

Figure 5-3 - Hub Fx by Row (DLC1.3a1) 59

Figure 5-4: Comparison of aerodynamic thrust loading..... 60

Figure 5-5 - Hub Fx by Rotor (DLC1.3a3) 60

Figure 5-6 - Hub Fx by Rotor (DLC1.3a3) 62

Figure 5-7 - DLC1.3a1; Comparison of MRS Average Hub Fx with Rotor 24 Hub Fx..... 63

Figure 5-8 - DLC1.3a3; Comparison of MRS Average Hub My with Rotor 2 Hub My..... 64

Figure 5-9 - Comparison of MRS Average Hub Mz with Rotor 30 Hub Mz (DLC 1.3a3) 65

Figure 5-10 - DLC1.3a3; Hub Fx Comparison (Fx), 20MW SR + MRS 66

Figure 5-11 - DLC1.3a3; Overturning Moment Comparison (My), 20MW SR + MRS 66

Figure 5-12 - DLC1.3a3; Yaw Moment Comparison (Mz), 20MW SR + MRS..... 67

Figure 5-13 - DLC1.4: Combined Hub Fx and Fy Loading (+ve)..... 69

Figure 5-14 - DLC2.3: Effect of Gust Phasing on Total Hub Fx 71

Figure 5-15 - DLC2.3; Comparison of Combined Fx during E-Stop around Rated 72

Figure 5-16 - Pitch Rate Comparison During E-stop 73

Figure 5-17 - Effect of Random Starting Azimuth Angles 74

Figure 5-18 - DLC4.2: Effect of Gust Phasing on Total Hub Fx 77

Figure 5-19 - Comparison of Shutdown Cases DLC2.3a3 and DLC4.2a3 (Safety Factors Applied).. 77

Figure 5-20 - Comparison of Hub Fx Loading at Rated and Cutout Wind Speeds.....	78
Figure 5-21 - Comparison of Total Hub Fx in all Examined Cases (Safety Factors Applied)	79
Figure 5-22 - DLC6.1a1; Comparison of Turbulent and Coherent Wind in the 50-Year Gust (Safety Factors Applied).....	81
Figure 5-23 - DLC6.1b1; Individual Hub Fx Statistics.....	82
Figure 5-24 - DLC6.2; 50 Year Gust and Extreme Yaw Misalignment (Safety Factors Applied)	84
Figure 5-25 - DLC6.3; 1 Year Gust and Yaw Misalignment of +-30 (Safety Factors Applied)	85
Figure 5-26 - Comparison of Total Hub Fx Loading (All Cases).....	87
Figure 5-27 - Hub Fx Characteristic Curve	88
Figure 5-28 - Hub Fx vs. Wind Speed for Whole Multi-Rotor Array	91
Figure 5-29 - Combined Fx Loading on MRS in Various Wind Classes.....	93
Figure 5-30 - DLC4.2; Pair and Quad Phased Normal Shutdown (Safety Factors Applied)	95
Figure 5-31 - DLC2.3; Comparison of Two Group and Four Group Shutdown (Safety Factors Applied)	96
Figure 5-32 - Comparison of Shutdown Loads with Power Production Loads in Extreme Turbulence (Safety Factors Applied)	97
Figure 5-33 - Normal Stop Loading Comparisons (No Safety Factors).....	98
Figure 6-1: Layout (left) of the multi-rotor system and first design of its support structure (right) .	103
Figure 6-2: Left: Optimal sectional properties as a function of the axial compression load (F_{ax}). The y-axes present the outer diameter of the cylinder D_o and the mean radius over thickness RoT . Right: RoT vs D_o	104
Figure 6-3: Front and side view of the 'Final Design' members following for cross-sections identification (I_{mat} increases from smaller to larger diameters)	109
Figure 6-4: First nine eigenmodes of the "Final Design"	110
Figure 6-5: Maximum loading under DLC 6.2. From top to bottom, front and side views of: equivalent stress (in MPa), lateral buckling (BI1) and local buckling (BI2).	112
Figure 6-6: Maximum loading under DLC 3.1 Dynamic". From top to bottom, front and side views of: equivalent stress (in MPa), lateral buckling (BI1) and local buckling (BI2).	113
Figure 6-7: Spectral analysis of the displacements for nodes 11-15	115
Figure 6-8: Cross sections properties of the 'Fatigue-driven Design'	116
Figure 6-9: Equivalent load at 10^7 cycles for all members of the support structure.....	117
Figure 6-10: Life "consumption" for all members of the support structure.....	118
Figure 6-11: S_{max} of the remaining members when one is missing.....	121
Figure 7-1: Floater configurations considered: a) rectangular barge, b) cylindrical barge, c) annular floater with a solid bottom ring and d) four cylindrical floaters on a solid plate.....	122
Figure 7-2: MRS forces for floater design	124

Figure 7-3: Cost-frequency dependence of a cylindrical barge for the 20MW MRS.....	127
Figure 8-1 - Small Clusters of 2, 3, or 4 Machines.....	131
Figure 8-2 - Wind Longitudinal Component Point History of Turbines 31, 32 and 39	132
Figure 8-3 - Medium Clusters.....	133
Figure 8-4 - Large Clusters.....	134
Figure 8-5: Optimised Electrical Interconnections with Redundancy.....	134
Figure 8-6 - Turbine Side Load Dump Resistor	136
Figure 9-1 Axes definition in relation to structure	138
Figure 9-2 Yaw moments due to drag on the structure	139
Figure 9-3 Yaw moment from drag on the structure in 90° yaw error.....	140
Figure 9-4 Yaw moment from drag on the structure with h=4m	141
Figure 9-5 Yaw moment from drag on the structure with h=4m	142
Figure 9-6 Available thrust per rotor depending on operational state	142
Figure 9-7 Yawing bearing arrangements for a 20 MW MRS	144
Figure 9-8 Reference design for development of yaw bearing solutions.....	146
Figure 9-9 Full tower (left) and semi-tower solutions.....	147
Figure 9-10 Hydrostatic bearing designs for a yaw system of 500 kW wind turbine	150
Figure 9-11 Bearing concepts for MRS	151
Figure 9-12 Friction torque related to bearing concepts	152
Figure 10-1 O&M Methodology.....	155
Figure 10-2 Distribution of O&M Cost	156
Figure 10-3 Distribution of O&M costs.....	157
Figure 10-4 Average Monthly Wind Farm Costs (RWT).....	159
Figure 10-5 Average Monthly Wind Farm Costs (MRS)	159
Figure 11-1: Energy gain comparison.....	161
Figure 11-2: Turbulence intensity.....	161
Figure 11-3: Power curve.	162
Figure 11-4: Gain in AEP.	163
Figure 11-5 Comparison of mass – MRS v 2 x RWT.....	169
Figure 11-6 Comparisons of cost – MRS v 2 x RWT	169
Figure 11-7: CAPEX breakdown of the MRS.....	172
Figure 11-8: CAPEX breakdown of 10MW RWT	172
Figure 11-9 Sensitivity to cost factors of MRS Design A (tower-frame concept)	174

Figure 11-10 Sensitivity to cost factors of MRS Design B (base yaw bearing)..... 174

Figure 11-11 Comparison of cost sensitivities of MRS and RWT..... 175

Figure 11-12: MRS LCOE sensitivity to Wake losses..... 175

Figure 11-13: MRS LCOE sensitivity to MRS aerodynamic losses..... 176

Figure 11-14 Individual Wind Turbine Rated Power (kW) 177

Figure 11-15 Individual Wind Turbine Rated Power (kW) 178

Table 4-1 Rotor general characteristics 37

Table 5-1 - Abbreviated Load Cases taken from IEC61400-3 51

Table 5-2 - Statistics of Hub Fx DLC1.3a3 61

Table 5-3 - Statistics of Hub Fx DLC1.3b4 62

Table 5-4 - Statistics of Hub Fx DLC1.4a1 (+ve)..... 69

Table 5-5 - Statistics of Hub Fx DLC1.4b1 (-ve)..... 70

Table 5-6 - Statistics of Hub Fx DLC2.3a3 75

Table 5-7 - Statistics of Hub Fx DLC4.2..... 80

Table 5-8 - Statistics of Hub Fx DLC6.1..... 82

Table 5-9 - DLC Comparison Summary; 1st column - load case name, 2nd column - results..... 86

Table 5-10 - Maximum Steady-State Thrust in Coherent Load Case DLC4.2a3..... 89

Table 5-11 - Full Load Case Comparison 99

Table 6-1: The selected family of welded pipes cross-sections 104

Table 6-2: Static variant of DLC 1.3a1. CRES' coordinate system is now used. Row numbering: bottom to top 105

Table 6-3: Mass of the support structure as a function of the bottom depth and the safety factor applied on the transient loads 107

Table 6-4: Load cases and load and material safety factors for the 'Final Design' 108

IMAT	MASS (kg)	IMAT	MASS (kg)	IMAT	MASS (kg)
1	25,256	6	297,212	11	300,860
2	75,303	7	150,655	12	187,409
3	66,837	8	64,850	13	707,235
4	148,183	9	286,532	14	215,116
5	187,797	10	225,258	15	0

Table 6-5: 'Final Design', mass per cross-sections family member 108

Table 6-6: Gross properties of the 'Final Design' 108

Table 6-7: Eigenvalues of 'Final Design'	110
Table 6-8: Gross properties of the 'Fatigue-driven Design'	116
Table 6-9: Critical members for robustness check.....	119
Table 6-10: Consequences of missing members on S-max of the remaining ones	119
Table 7-1: Assumptions made for concrete floaters	124
Table 7-2: Alternative designs for the rectangular barge (a)	126
Table 7-3: Alternative designs for the cylindrical barge (b).....	126
Table 7-4: Alternative designs for the annular barge with a solid concrete bottom ring (c)	128
Table 7-5: Alternative designs for the four cylindrical floaters on a solid plate (d)	129
Table 9-1 Yaw moment components	140
Table 9-2 Tubular cross sections	147
Table 9-3 Design Comparisons based on DLC1.3a1 excluding load safety factors.	148
Table 9-4 Final Design Comparisons of System Mass.....	149
Table 9-5 Design characteristics of a hydrostatic bearing for the 20 MW MRS	151
Table 11-1 Mass and CAPEX of MRS Options	168
Table 11-2: Cost comparison between MRS and RWT.....	171
Table 11-3 CAPEX Comparison of 20 and 40 MW MRS	179
Table 11-4 LCOE Comparisons.....	179

CHAPTER 1 INTRODUCTION

1.1 Scope and Objectives

This work forms part of Task 1.3 of the Innwind.EU project. Within this task several innovative concepts are developed and evaluated using design tools and information often from other supporting tasks. The specific concept of Task 1.33 is of a multi rotor system (MRS) in which many rotors are placed on a single structure. Resources are not available for a detailed engineering design. The scope is also restricted to have a primary focus on turbine capital cost (CAPEX) and so balance of plant and O&M concepts and costs are broad-brushed.

The principle aim of the task work is to develop a design to a sufficient level that there is reasonable credibility about loads and performance leading to mass and cost estimates that will enable a top level evaluation of the potential for reduction in levelised cost of energy (LCOE).

1.2 Overview of report contents

The historical background and development of the case for multi rotor systems is first discussed. Before any more detailed evaluation could proceed, an outline conceptual design of the system and its operation was required. This is presented and the rationale of concept design choices is explained. Following that some more detailed design and analysis work is reviewed. This comprises:

- System aerodynamic performance evaluation by NTUA
- System loads determination by UoS supported by DNV
- Rotor support structure design by CRES
- Floating platform design by CRES
- Electrical systems design by UoS

There is then an LCOE evaluation phase conducted by UoS comprising a discussion of energy capture issues followed by extensive use of the design tool [1] for LCOE developed in Task 1.2 in which the LCOE is predicted and multiple sensitivities examined.

Finally conclusions are summarised and attention is drawn to important aspects of the MRS concept beyond LCOE concerning implementation (potential for rapid TRL progression), capability of the technology to meet EU renewables targets, technology



development facilitation and de-risking financing and investment. This is all in comparison with the conventional offshore wind farm based on large single rotors.

CHAPTER 2 BACKGROUND

2.1 History of technology – the motivation

Multi rotor technology has a long history and the multi-rotor concept persists in a variety of modern innovative systems but the concept had generally fallen out of consideration in mainstream design from a perception that it is complex and unnecessary as very large single wind turbine units are now technically feasible. Multi rotor systems (MRS) such as in Figure 2-1 (Honnef¹ 1930) arose out of a vision of how wind power may be deployed as large scale units at a time when steel was the only practical material for rotor blades and when, especially due to the enormous weight of large scale steel blades, very large capacity single turbines were not feasible. Neither the basic concept of the MRS nor its deployment offshore is a recent thought.

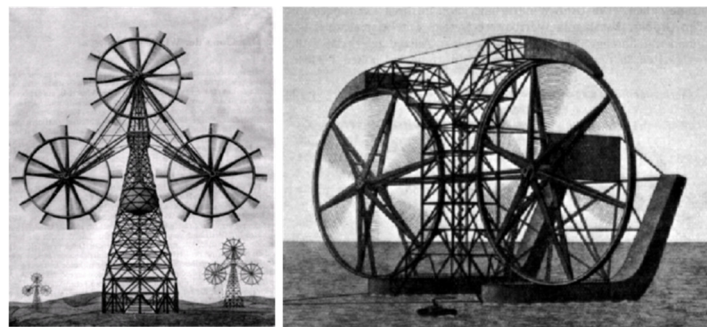


Figure 2-1 Honnef's vision of large scale wind energy systems.

In the 1970's Heronemus advocated multi rotor systems noting advantages of standardisation of rotor and drive train components and "scale-ability"; the fact that very large system capacities could be realised without overstressing the capability to up-scale individual rotors. In 1995 in work on innovative wind turbine concepts for UK DTI, Jamieson [2] noted the up-scaling advantage as related to area to volume ratio potentially allowing very large savings in materials and CAPEX of rotor and nacelle systems. Thus not only was the MRS in view of the scale-ability noted by Heronemus a feasible route to very large unit capacity but it was potentially a very advantageous solution. In summary:

- 1930 Honnef introduced the concept but for a defensive motive – very big blades could not be made in steel
- 1970 Heronemus designed systems (land based and offshore) noting scalability and advantages of component standardisation

¹ Honnef's vision encompassed direct drive rim generators, urban and offshore applications.

- 1995 Jamieson drew attention to fundamentally obvious scaling rules that suggested the MRS concept not only rendered very large unit capacities feasible but potentially a cost effective solution

This short account reviews only the history of the motivation for the MRS. Many varied concept designs exist in patent documents and other publications. A few systems were manufactured such as the 6 rotor design of Lagerwey but the rotors were not closely spaced and the support structure was of the cantilevered “tree” type. Both these factors are considered undesirable for a highly economic design. Laboratory testing of Smulders [3] of 2 closely spaced (5% of diameter, D , minimum spacing) rotors in the 1980s suggested that there was no adverse effect on power performance with this close spacing. Later tests on an array of 7 small commercial rotors each of 1 m diameter in the NASA Langley wind tunnel in Virginia [4] confirmed this. The most recent work within this project indicates that a 45 rotor array spaced with 5% D spacing or even as little as 2.5% D will not only avoid power loss but may have significant power gains. In this discussion “gain” or “loss” means that n rotors in an MRS array will produce more or less power than nP where P is the power of a single rotor operating in isolation.

2.2 Status and development needs of MRS prior to Innwind

1. Prior to this project there has been testing (but not on a large array) suggesting that the aerodynamic performance of closely spaced rotors would be satisfactory
2. A few design studies of the MRS have been conducted as for example related to reference [4] but many details are commercially confidential.
3. There was no available modelling capability to predict loads in turbulent wind conditions on a large array of independently controlled wind turbine rotors. In prior work, simplifying assumptions were made for load prediction which as it turns out were very conservative and failed to capture some major load mitigation effects specific to MRS.

CHAPTER 3 SYSTEM CONCEPT DESIGN

3.1 Structure concept

The MRS support structure is shown in Figure 3-1.

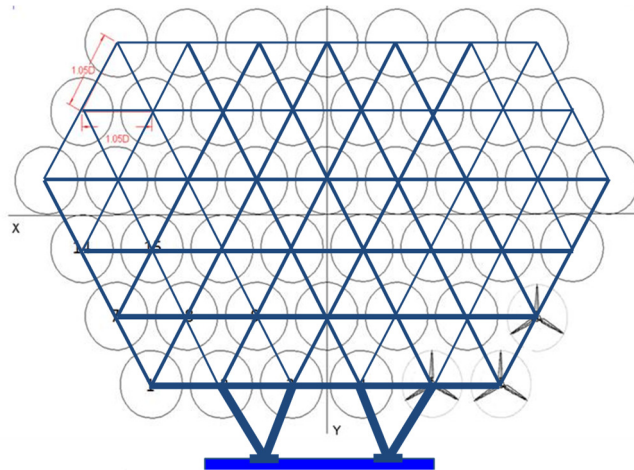


Figure 3-1 Outline of MRS support structure

Only a lattice structure with tubular members has been considered for the MRS. There is no other good option for two main reasons:

- The lattice structure is the most efficient type of support structure in minimising mass of materials for any large loaded structure (jackets in deep water, electricity pylons etc.)
- Tubes are optimum for omni-directional aerodynamic loading when self-induced wind loading on the structural members is significant for design or design driving.

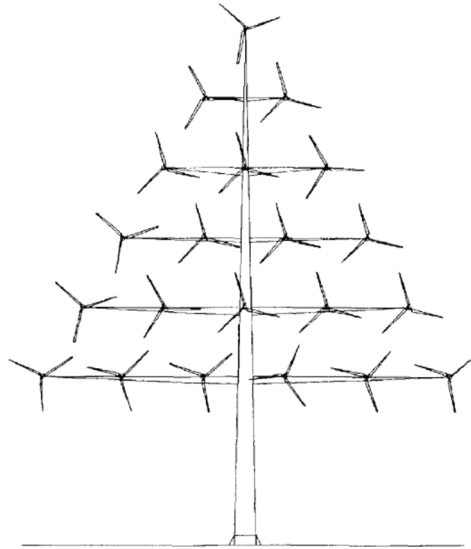


Figure 3-2: MRS design based on cantilevered support structure.

A tree structure as a complete system of cantilevers (Figure 3-2 from [5]) is almost certainly much heavier in total, more subject to vibrational loading issues and, if made most economically with significant flexibility, may even be problematic in terms of displacements and rotor blade interference.

3.2 Layout shape

The layout shape of Figure 3-1 has not been optimised. It is arbitrarily developed having consideration to being in the form of an equiangular triangular lattice. To minimise support structure spatial extent (frontal projected area) and thereby possibly key loads, weight and cost, the most compact arrangement that approximated circular would be optimum. However base overturning moment is assumed to be significant for design. Thus reducing layout height, accepting some added lateral spread whilst avoiding too big a footprint, led to the layout design of Figure 3-1. The tools but not the resource have existed within this project to vary layouts and optimise for minimum mass/cost.

3.3 Scale issues

An MRS system of 20 MW rating was chosen for two main reasons. A major advantage of the MRS is in the capability to provide much larger capacity at a single maintenance site than with the single rotor concept. So it was important that a rating above the reference wind turbine (RWT) rating of 10 MW should be chosen. Although no 20 MW single rotor exists, a design was developed in UPWIND [6] and this provides a useful base of information for comparison of multi and single rotor concepts at 20 MW scale. In an MRS system the keys to economic advantage relating to scaling are;

- The MRS can be up-scaled to any desired rated power level without decreasing the ratio of active swept area to rotor and nacelle mass. Alternatively put, the MRS avoids the penalty associated with the square cube law in up-scaling the single turbine concept.
- As unit rating increases the number of MRSs per installed MW of wind farm capacity decreases. This benefits balance of plant and O&M costs per installed MW especially offshore and is the core reason for the present technology development battle to upscale the standard wind turbine concept.
- The huge savings in rotor and nacelle mass and CAPEX more than offset increased support structure costs of the MRS. Above water, the MRS support structure will most probably scale cubically and this will set an economic limit to system scale but probably at a level (50- 100 MW?) far beyond what is realistic with single rotor systems.
- Detailed evaluation will always be necessary but from the logic that floater stability relies on a moment due to displaced water weight and that mass related moments scale as 4th power of linear dimensions, the floater mass and cost may upscale more favourably than the above water support structure.

3.4 Wind Turbine Operational Characteristics

Preliminary thinking about the MRS was to have rotor systems that were as simple as possible and so stall regulated rotors were considered. Work at UoS within the PhD study of M Branney in the year preceding this Innwind project [7] considered the MRS system in outline comparing extreme loading of a system with stall regulated rotors with that of pitch regulated rotors. A clear conclusion was that employing stall regulation would put a large premium on support structure mass and cost. There is a huge difference in rotor thrust loading and in blade out of plane bending moments between a rotor with blades pitched at full feather and a stall regulated rotor where the blade surface is almost flat on to wind incurring large drag loads. This is true providing that the wind flow is uniform and perfectly aligned with the wind. In reality in turbulent wind a single rotor with blades feathered in extreme storm conditions encounters inflow angles that generate maximum lift on a blade and there may be little difference between pitch and stall regulated rotors in ultimate wind loading on blades. Within the MRS, a rotor with blades feathered may also experience maximum lift in turbulent wind but the probability of all or many rotors experiencing this simultaneously and coherently so that their impact on structure loading is additive is negligible. Thus for an MRS design, in extreme storm conditions, much more so than for the single rotor design, blade pitching avoids large loads from the rotors that may drive or add substantially to structure design demand.

The concept design decision was thus that the rotors of the MRS were chosen to be of industry standard variable speed, pitch regulated design. Each rotor was then conceived as a fully independent wind turbine (except obviously in respect of yawing control) and has its own permanent magnet generator and power converter. Power converters are a significant reliability concern for the wind industry but having fewer converters of higher rating would not improve overall availability. There are many options for electrical system integration including clustering of rotors that may save component costs. Electrical clustering was considered and is discussed in Chapter 8. However as the benefits of independent rotor operation became apparent in early loading work, it was decided to focus effort on the simplest arrangement where each rotor is operating essentially as individual rotors in a conventional wind farm. The optimisation of collective and individual aspects of the MRS rotors as impacts on electrical hardware and system control is subtle may in future lead to further cost benefit for the MRS.

3.5 Rotor and drive train module

Although not detailed within this project, it is intended that the MRS system shall have built-in maintenance capability such as a high level crane rail that will enable rotor handling possibly under automated control from base level. For this to be effective it is essential that the rotor and drive train assembly be designed as a “plug-in” module. Among precedents for this would be the fixing of an aero engine which is necessarily very securely held but can be removed by releasing only a few connections.

At the present high level conceptual design stage, the nacelle assembly is conceived as a compact cylinder, containing generator and converter with rotor assembly on front and electrical power terminations at rear. To realise a particularly high efficiency, lightweight drive train, the pseudo direct drive (PDD) generator of, Innwind partner, Magnomatics Ltd (Sheffield, UK) is employed. The technology of Magnomatics has been laboratory tested and their design methods validated. Their system incorporates a stage of magnetic gearing integrated with a PMG all in a compact coaxial arrangement. As in conventional drive trains, gearing increases the air gap velocity and reduces generator size and mass but the Magnomatics design achieves this in an integrated system without physically contacting gears avoiding associated concerns of wear and lubrication. The overall drive train efficiency of the proposed design of PDD is compared in Figure 3-3 with data typical of a DFIG (doubly fed, induction generator) which has been the prevalent drive train choice in the wind industry.

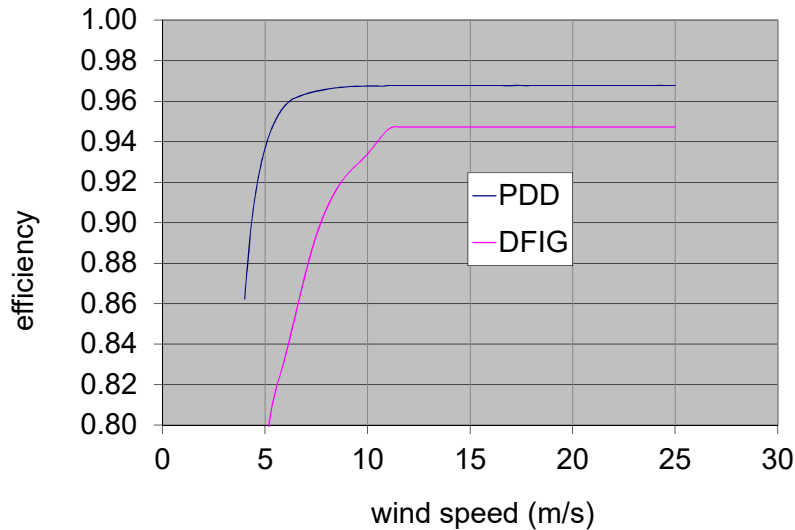


Figure 3-3: Drive train efficiency comparison.

3.6 System Yawing

At present several designs have been considered based on how the complete system may be yawed to preserve alignment with wind direction. A floater that yaws in the sea is shown in Figure 3-4 and floater design is developed in Chapter 7.

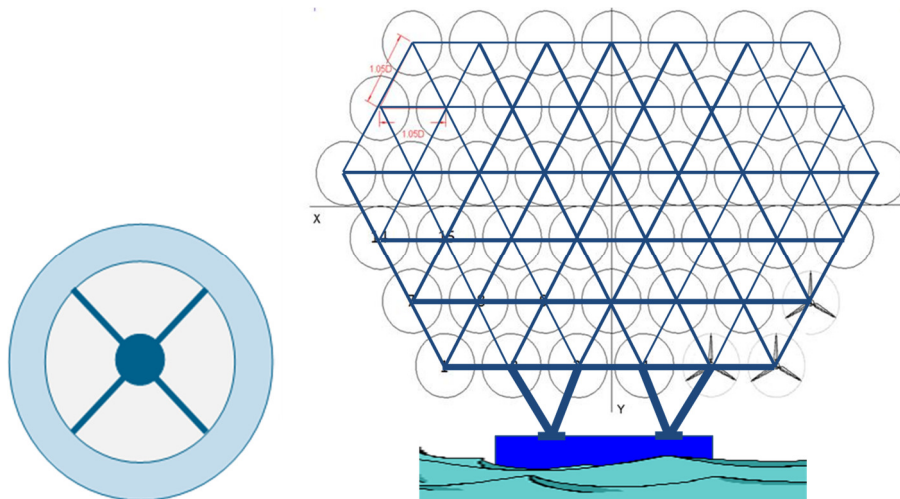


Figure 3-4: Initial floater concept as a barge.

This removes yaw system costs entirely from the rotors and support structure above waterline. The technology for large marine swivel joints is established in offshore loading buoys and other offshore equipment although it will be a very special design for the MRS and will add significant additional cost to the mooring system. In water depths up to about

50 m jackets are generally more cost effective than floaters but obviously floating systems can access deep water resource that cannot otherwise be exploited.

In a study by GL Garrad Hassan for OWES LLC (details commercial in confidence but the illustration here, Figure 3-5, was previously published with permission of OWES [8] an alternative bearing system was developed for an MRS of 5 MW rating.



Figure 3-5: Previous design of a 5 MW MRS.

The scaling rules determined that the whole rotor support structure including rotors and nacelles was lighter than the rotor and hub of a typical 5 MW wind turbine and yaw system and tower loads were generally less. Thus there was no reason for the yaw bearing and actuation system to be much more expensive than for the equivalent single turbine. This design concept put some further premium on structure cost in having both tower and space frame but still promised very favourable overall economics for the MRS. The space frame, yawing on tower concept is explored in Section 9.2.2 and it also looks to be the most cost effective solution at 20 MW as it was at 5MW scale.

3.7 Assembly and Installation Concept

The complete MRS structure will be built in dry dock, turbines assembled and plugged into the structure and the system commissioned and tested prior to being installed at site.

In the case of jacket foundations, the system will be floated out and jacked or craned on to the jacket connection members. Largest offshore cranes have 8000 t lift capability and this system will be about half that weight. Prior to de-commissioning this should be the only time that any giant offshore crane is brought to site as maintenance operations will be done by automatic control of a travelling crane attached to the top of the MRS structure.

In the case of a floating system, the complete MRS system will be floated out and installed by connection to a pre-established mooring turret which will also provide for electrical connection. In comparison with any concept involving turbine erection offshore (nacelle and rotor lifts) which is generally the case with present offshore wind farms, the MRS should have much simpler and less expensive installation.

3.8 O&M Concept

A major consideration in O&M is that a local turbine fault in an MRS will not disable a large proportion of output capacity.

At equal reliability per turbine with a single large turbine, faults in an n rotor multi rotor system would be n times more frequent than for a single turbine but mostly have n times less impact in lost production. With easy access for repair and no restrictions on wind or wave climate affecting maintenance, comparing MRS and single turbine, overall availability would be similar and O&M would perhaps be favourable for the large single turbine in costs as fewer site visits may be incurred. However, this is very far from the real situation. The need to access site, possibly with very large scale equipment (jack up barges or floating cranes) and only in favourable weather conditions can lead to substantial loss of availability and expensive O&M for single large turbines. Individual turbine faults in an MRS can be ignored for longer periods, some spares may be held on site and there would be no requirement to bring large scale equipment to site. So unscheduled maintenance may largely be avoided and costs associated with developing equipment for O&M in more demanding environmental conditions (as is presently being considered) will be avoided.

Although as discussed, O&M should be more favourable for the MRS without the small turbines having any reliability advantage over larger units, there is a clear case that the smaller turbines, with a faster manufacture and development cycle in greater quantity production and somewhat simpler in concept without individual yaw systems can be more reliable per unit than a large turbine.

A further factor reducing the O&M cost in comparison to single turbine wind farm solutions is that no single turbine will have as great capacity as a MRS. Thus in the present case of comparing O&M of a 500 MW wind farm of 20 MW MRS with one of 10 MW RWTs the number (25) of maintenance site associated with the MRS is half of the number (50) associated with the DTU 10 MW. Maintenance cost per installed MW is thus reduced with MRS technology.

Another key factor in O&M is in the design of the MRS structure to facilitate maintenance. The access concept is not yet developed but for a relatively stable barge floater requiring to be accessed only in benign weather conditions, there may not be any special demands and less than for single large turbines. The concept for turbine maintenance is to have a top level or near top level crane rail with a travelling crane that can handle complete rotor modules. This is still conceptual and is not developed in the present project with neither

the capital cost impact nor the O&M benefits being evaluated. However it seems to be feasible to avoid any major vessels (floating cranes or jack up barges) being required for maintenance operations on turbine units.

Finally it will be evident (Figure 11-6) that the total cost of rotor-nacelle assemblies of the MRS is much less than for the RWT.

CHAPTER 4 AERODYNAMIC EVALUATION OF THE MULTI ROTOR CONCEPT

4.1 Introduction

A main feature of the present MRS is that 45 rotors are closely clustered in a single actuator plane. The aerodynamic performance of closely spaced rotors has been studied experimentally in the past but, as discussed previously, only for small arrays of 2 and 7 rotors. A detailed analysis of flow characteristics of 7 and 45 rotor MRSs is now discussed.

4.2 Numerical Models

Two different aerodynamic tools have been applied: a RANS flow solver in which a rotor is simulated as an actuator disk (flowNS) and a Vortex solver in which the blades are rotating and represented in their true geometry (GENUVP). The two methods are complementary with respect to the kind of information they can deliver. The RANS solver considers turbulent flow but runs in steady-state mode and therefore can deliver average flow information. Unsteady flow computations in this context would require modelling of all rotating blades at least as actuator lines, a very dense space grid and a small time step, which all together lead to prohibitively high cost. On the contrary the Vortex solver is by definition running in unsteady mode and therefore could deliver the underlying dynamics of the system behaviour, but suppresses viscous effects and therefore the flow information obtained is idealized. By introducing a posteriori viscous corrections, it is possible to obtain realistic loading predictions on the blades, but these corrections would have no effect on the flow field development. By suppressing viscous effects the cost of Vortex solvers becomes manageable but not low. Vortex methods track the wake of its blade separately by means of vortex blobs, with their number to increase in time. Usually 10 full revolutions are needed until steady state convergence is reached while in aeroelastic simulations the number of revolutions should correspond to ~ 10 min. The resulting CPU is high and requires substantial computer power.

4.2.1 CRES-flowNS RANS solver

Description of the solver

The CRES-flowNS RANS solver [9] is applied for the simulation of the flow field around the multi-rotor system. The governing equations for incompressible fluid flow are numerically integrated by means of an implicit pressure correction scheme, where Wind Turbines (WT) are modelled as momentum absorbers by means of their thrust coefficient. A matrix-free algorithm for pressure updating is introduced, which maintains the compatibility of the velocity and pressure field corrections, allowing the use of high time step values within the time integration process. Spatial discretization is performed on a computational domain,

resulting from a body-fitted coordinate transformation, using finite difference/finite volume techniques. The convection terms in the momentum equations are handled by a second order upwind scheme bounded through a limiter. Centred second order schemes are employed for the discretization of the diffusion terms. The Cartesian velocity components are stored at grid-nodes while pressure is computed at mid-cells. This staggering technique allows for pressure field computation without any explicit need of pressure boundary conditions. A linear fourth order dissipation term is added into the continuity equation to prevent the velocity-pressure decoupling. The governing equations are discretized and solved in their non-dimensional form:

$$\nabla \cdot \vec{u} = 0$$

$$\frac{\partial \vec{u}}{\partial t} + (\vec{u} \cdot \nabla) \vec{u} - \frac{1}{\text{Re}} \nabla \cdot \left\{ (1 + \nu_T) \left[\nabla \vec{u} + (\nabla \vec{u})^T \right] \right\} + \nabla p_{\text{eff}} = 0 \quad (1)$$

In the above equations, the velocity vector \vec{u} is normalized by the free stream wind speed U_{ref} , the effective pressure $p_{\text{eff}} = p + 2k/3$ by ρU_{ref}^2 , ν_T is the turbulent viscosity normalized by the laminar viscosity ν , and $\text{Re} = U_{\text{ref}} \cdot D / \nu$ is the Reynolds number with respect to the rotor diameter D .

Turbulence closure is achieved using Wilcox's k - ω model [10]

$$\frac{\partial k}{\partial t} + \vec{u} \cdot \nabla k - \frac{1}{\text{Re}} \nabla \cdot \left[(1 + \sigma^* \nu_T) \nabla k \right] = \frac{1}{\text{Re}} P_k - \beta^* k \omega$$

$$\frac{\partial \omega}{\partial t} + \vec{u} \cdot \nabla \omega - \frac{1}{\text{Re}} \nabla \cdot \left[(1 + \sigma \nu_T) \nabla \omega \right] = \frac{1}{\text{Re}} \alpha P_k \frac{\omega}{k} - \beta \omega^2 \quad (2)$$

$$P_k = \frac{1}{2} \nu_T \left[\nabla \vec{u} + (\nabla \vec{u})^T \right]^2$$

where k is the turbulent kinetic energy (TKE), ω is the specific rate of dissipation of TKE, ν_T is estimated as $\text{Re} k / \omega$, and P_k is the production of TKE. In order to account for atmospheric flows, modified coefficients for the k - ω model are established using the boundary condition for the TKE at the wall, $TKE = u_*^2 / \sqrt{\beta^*}$ and the fact that u_*^2 / TKE has been measured close to 0.182 for neutral conditions in flat terrain [11]. This corresponds to a value of $\beta_* = 0.033$. Using the procedure described in [12], the following constants of the k - ω model are derived:

$$\begin{aligned} \alpha &= 0.3706, \quad \beta = 0.0275, \quad \beta_* = 0.033, \\ \sigma &= 0.5, \quad \sigma_* = 0.5 \end{aligned} \quad (3)$$

The overestimation of TKE in the near wake is corrected using Durbin's constraint for the turbulent time scale:

$$T = \min\left(\frac{1}{\omega}, \frac{2}{3} \sqrt{\frac{3}{8S^2}}\right) \quad (4)$$

where $S^2 = S_{ij} \cdot S_{ji}$ and $S_{ij}, i = j = 1, 2, 3$ is the strain tensor given by the relationship:

$$S_{ij} = \frac{1}{2} \left(\frac{\partial U_i}{\partial x_j} + \frac{\partial U_j}{\partial x_i} \right) \quad (5)$$

Wind turbine modelling

The rotor disks are simulated as momentum absorbers according to the actuator disk theory. This type of modelling adds axial body forces in the corresponding momentum equation for the cells in which the rotor disks are contained. Let, ΔS denote the surface area of the numerical cell with width Δr (Figure 4-1), ρ the air density, U_{ax} the local axial velocity and C_T the local thrust coefficient. Then, the axial force is defined as

$$F_{ax} = \frac{1}{2} \rho U_{ax}^2 C_T \Delta S \quad (6)$$

The local C_T in (6) is calculated using the blade element theory

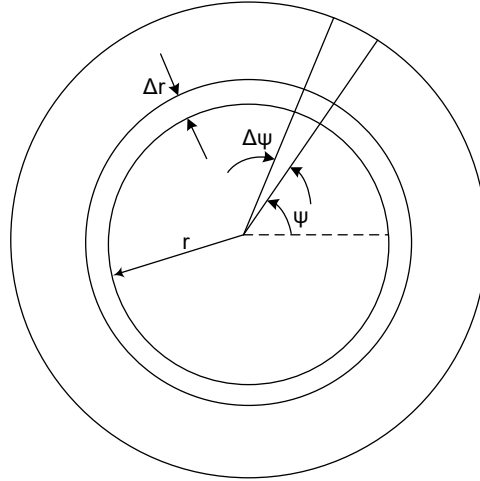


Figure 4-1: Polar grid definition on the rotor disk plane. Δr and $\Delta\psi$ define the spacing in the radial and azimuth direction respectively

Let U_{ax} , U_{cir} denote the axial and circumferential flow velocities at a cell containing part of the rotor disk. Since these components also contain the effect of induction, they also define the angle of attack α and through look-up tables the corresponding lift and drag forces L , D :

$$L = 0.5\rho C_L U_t^2 c \Delta r, \quad D = 0.5\rho C_D U_t^2 c \Delta r \quad (7)$$

where $U_t = \sqrt{U_{ax}^2 + (\omega r)^2}$ is the total relative velocity and ω is the angular velocity of the rotor. Taking into account the angle of incidence $\varphi = \tan^{-1}(U_{ax} / U_{cir})$, the axial force exerted from the first blade on the fluid, at a point (r, ψ) of the rotor disk surface is

$$F_{x,1} = F_x(r, \psi) = L \cos \varphi + D \sin \varphi \quad (8)$$

where the azimuth is given by $\psi = \omega \cdot t$. The other two blades present a phase difference of 120° and 240° respectively, so the axial forces are

$$F_{x,2} = F_x(r, \psi + 2\pi/3) \quad \text{and} \quad F_{x,3} = F_x(r, \psi + 4\pi/3) \quad (9)$$

Rotor loading in the non-rotating frame can be obtained by applying a Fourier coordinate transformation that is also referred to as the Coleman's transformation, so that:

$$F_{bl}(r, \psi) = F_o + F_C \cos \psi + F_S \sin \psi \quad (10)$$

with

$$F_o = \frac{1}{3} \sum_{n=1}^3 F_{x,n}, \quad F_C = \frac{2}{3} \sum_{n=1}^3 \left(F_{x,n} \cos \left(\psi + (n-1) \frac{2\pi}{3} \right) \right),$$

$$F_S = \frac{2}{3} \sum_{n=1}^3 \left(F_{x,n} \sin \left(\psi + (n-1) \frac{2\pi}{3} \right) \right) \quad (11)$$

The local C_T in Eq.(1) can now be calculated as

$$C_T = \frac{3 F'_{bl}}{\pi \rho r \Delta r U^2} \quad (12)$$

where F'_{bl} is the $F_{bl}(r, \psi)$ interpolated in the yz Cartesian mesh at the rotor disk surface.

Boundary conditions and computational grid

At the inlet of the computational domain the velocity and k - ω profiles are given by the Monin-Obukhov theory for neutral conditions [13]:

$$U_x = U_{ref} \frac{\ln(z / z_o)}{\ln(z_{hub} / z_o)}, \quad k = \frac{u_*^2}{\sqrt{\beta_*}}, \quad \omega = \frac{u}{\sqrt{\beta_*} \cdot K \cdot z} \quad (13)$$

where K is the von-Karman constant, z_o is the roughness length and U_{ref} is the reference velocity at the hub height z_{hub} . Here, z_{hub} is the hub height of the central W/T rotor. Neumann conditions are applied at the outlet boundary as well as at the side boundaries of the domain. The boundary layer height is set equal to 800m (20 D) and the velocity is considered constant above this height, $U=U_\infty$. As a result, the velocity is set equal to U_∞ at the top boundary and the TKE is set equal to zero (laminar flow approach). On the ground boundary all velocities are zero. Logarithmic wall functions are used to compute the velocity at the first grid point above ground.

The computational domain is extended to $20 D$ downstream of the rotors level in the axial direction and $11 D$ off the central rotor in the lateral direction. The height of the domain is $25 D$. In this way, the flow is not restricted by the numerical boundaries, where free-stream Dirichlet conditions are imposed. The inlet boundary is positioned $9 D$ upstream of the rotors level, so that a sufficient distance is provided for the flow to develop. The x - and y -axes are selected so that their origin coincides with the hub height of the central rotor. The grid spacing in the x -direction reduces to its minimum value of $0.05 D$ at the rotors level and increases outwards following a geometrical progression with a ratio of 1.15 until the maximum dimension of the domain is reached. In the vertical direction, the first grid-line is positioned at a height of $0.035 D$ a.g.l., and then the grid spacing follows a successive coarsening and refinement up to the lower tips of the two lower rotors at a height of $4.267 D$ or $2.826 D$ (for the 7 or the 45 MRS respectively). The grid spacing is kept uniform and equal to $0.04 D$ from the lower tips of the lower rotors up to the higher tips of the two upper rotors and then follows a geometrical progression with a ratio of 1.15 up to the height of the domain (see Figures Figure 4-2, Figure 4-3). In the lateral direction the grid spacing is kept uniform and equal to $0.03 D$ all over the area of the 7 or 45 W/T rotor disks, and it follows a geometrical progression with a ratio of 1.2 outwards up to the side boundaries of the domain (see Figures Figure 4-2, Figure 4-3). The mesh generated in this way comprises $75 \times 137 \times 175$ and $75 \times 281 \times 213$ grid points for the 7 and the 45 MRS respectively. The same mesh is used for the single W/T case in order to ensure a fair comparison of the predictions.

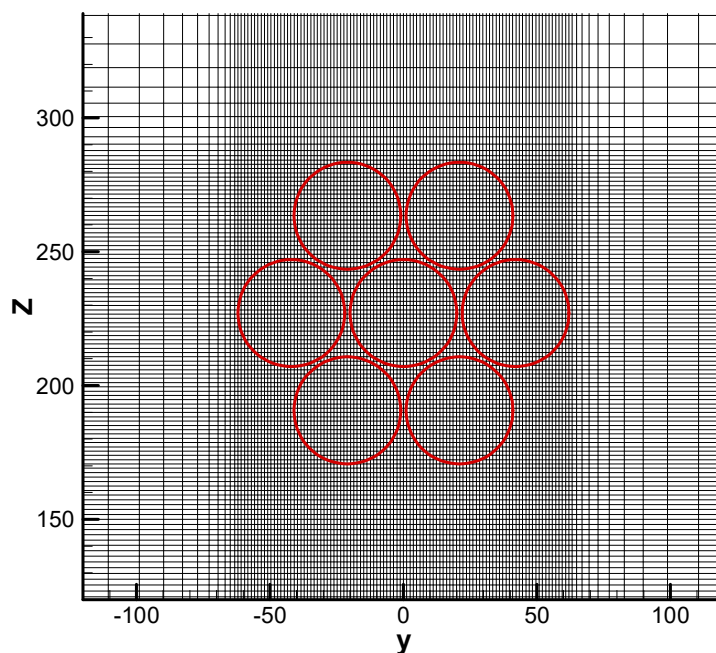


Figure 4-2: Numerical grid at the rotors plane $x=0$ for the 7 MRS.

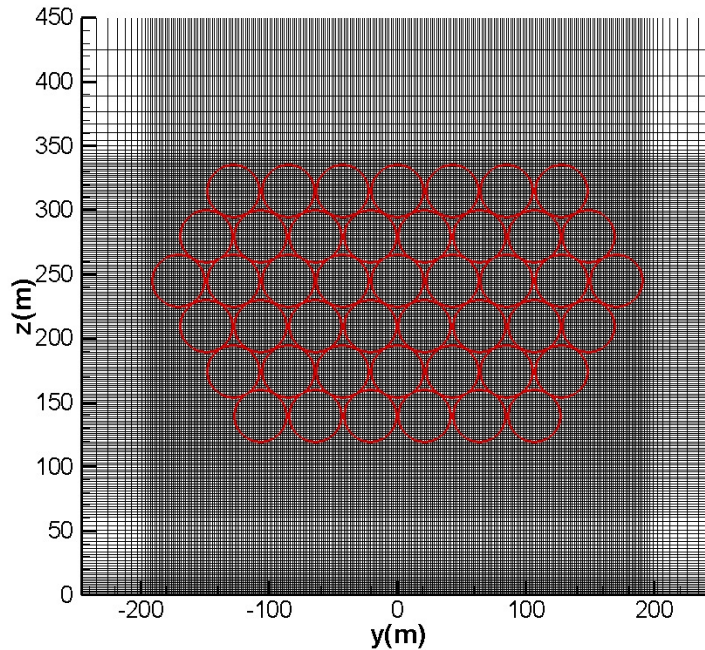


Figure 4-3: Numerical grid at the rotors plane $x=0$ for the 45 MRS.

4.2.2 The GENUVP vortex method

Description of the method

GENUVP is an unsteady potential flow solver in which the effect of solid boundaries is represented by means of surface source and/or dipole distributions while the wakes are modelled by means of freely moving vortex blobs [14].

Based on Helmholtz's decomposition, flow velocity is decomposed into a potential part and a vertical one:

$$\vec{u}(\vec{x}; t) = \vec{U}_\infty(\vec{x}; t) + \nabla\varphi(\vec{x}; t) + \vec{u}_\omega(\vec{x}; t), \vec{x} \in \mathcal{D} \quad (14)$$

where $\vec{U}_\infty(\cdot; t)$ is the infinite velocity field, $\varphi(\cdot; t)$ the disturbance velocity potential and $\vec{u}_\omega(\cdot; t)$ is the free vorticity induced field.

In the present work, the blades are approximated as thin lifting surfaces. In this case dipole distributions μ are defined over their surface and their wakes. Let N_B denote the number of blades defined by their mean surfaces \mathcal{S}_k and their wakes \mathcal{S}_{Wk} with their orientation given by the normal vector \vec{v} . Then,

$$\varphi(\vec{x}_0; \mathbf{t}) = - \sum_{k=1}^{N_B} \left\{ \int_{S_k} \frac{\boldsymbol{\mu}_k(\vec{x}; \mathbf{t}) \vec{\mathbf{v}}(\vec{x}; \mathbf{t}) \cdot (\vec{x}_0 - \vec{x})}{4\pi |\vec{x}_0 - \vec{x}|^3} dS(\vec{x}) + \int_{S_{Wk}} \frac{\boldsymbol{\mu}_{Wk}(\vec{x}; \mathbf{t}) \vec{\mathbf{v}}_W(\vec{x}; \mathbf{t}) \cdot (\vec{x}_0 - \vec{x})}{4\pi |\vec{x}_0 - \vec{x}|^3} dS_W(\vec{x}) \right\} \quad (15)$$

where, $\boldsymbol{\mu}_k(\cdot; \mathbf{t})$ is the dipole distribution of the k-th thin lifting surface (1st term) and $\boldsymbol{\mu}_{Wk}(\cdot; \mathbf{t})$ is the dipole distribution of the vortex sheet originating for the k-th lifting body (2nd term). In order to determine the unknown fields the following conditions are applied:

(a) The solid boundary condition:

$$\vec{\mathbf{v}}(\vec{x}_0; \mathbf{t}) \cdot \nabla \varphi(\vec{x}_0; \mathbf{t}) = \frac{\partial \varphi}{\partial \mathbf{v}}(\vec{x}_0; \mathbf{t}) = \vec{\mathbf{v}}(\vec{x}_0; \mathbf{t}) \cdot (\vec{U}_{Bk} - \vec{U}_\infty - \vec{U}_\omega), \quad (16)$$

$$\vec{x}_0 \in S_k, k = 1, N_B$$

where $\vec{U}_B(\cdot; \mathbf{t})$ denotes the body velocity distribution on the blades and includes both the rigid body velocity component as well as the elastic movement component.

(b) The evolution of the wake in Lagrangian form:

$$\frac{d\vec{x}_W}{dx} = \vec{U}_\infty(\vec{x}_W, \mathbf{t}) + \nabla \varphi(\vec{x}_W, \mathbf{t}) + \vec{U}_\omega(\vec{x}_W, \mathbf{t}) \quad (17)$$

(c) The wake dynamic condition, requiring zero pressure jump across S_{Wk} . Using Kelvin's theorem, it follows that the wake dynamic condition is equivalent to material conservation of $\boldsymbol{\mu}_W$:

$$\frac{d\boldsymbol{\mu}_W}{dt} = \mathbf{0} \quad (18)$$

Therefore the intensity of the surface distributions $\boldsymbol{\mu}_k(\cdot; \mathbf{t})$ is determined by (16), the wake intensities $\boldsymbol{\mu}_{Wk}(\cdot; \mathbf{t})$ by (18) and the wake geometry by (17).

Theoretical results as well as experimental and numerical evidence suggest that in time, free vortex sheets due to intense roll-up lose their smoothness and flow calculations become singular. In order to overcome this difficulty, the wake is considered to carry

vorticity which in the case of a vortex sheet approximated by piecewise constant dipole distribution is defined per panel $S_W^e(t)$ as,

$$\vec{\omega}_{S_W}(\vec{x}, t) = \nabla \times \vec{u}_\mu(\vec{x}, t) = \underbrace{\delta_{\partial S_W}(\vec{x} - \vec{x}_{\partial S_W}) \vec{t}(\vec{x}_{\partial S_W}, t) \mu_W(\vec{x}_{\partial S_W}, t)}_{\text{line term}} \quad (19)$$

where $\delta_{\partial S_W}(\cdot)$ denotes the line Dirac functions defined on the boundary of $S_W^e(t)$ and $\vec{t}(\cdot, t)$ the unit tangential to $\partial S_W(t)$ vector (see Figure 4-4). In the numerical implementation applied in GENUVP, the wake of every blade is decomposed into its near S_{Wk}^A and far part S_{Wk}^* . It is the far part that is transformed into vorticity while the near part which is produced during the current time step retains its surface character.

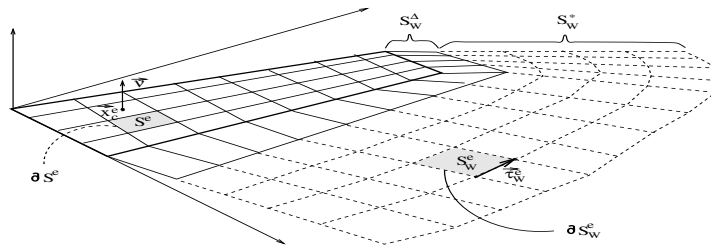


Figure 4-4: The notations of the grid on the bodies and the wake.

Far wake vorticity in GENUVP is approximated by freely moving vortex blobs defined by their intensity $\vec{\Omega}_j(t)$ and position $\vec{Z}_j(t)$,

$$\vec{\omega}_W(\vec{x}, t) = \sum_{j \in J(t)} \vec{\Omega}_j(t) \zeta_\varepsilon(\vec{x} - \vec{Z}_j(t)) \quad (20)$$

where $J(t)$ the index set for the vortex particles and $\zeta_\varepsilon(\mathbf{r})$ the cut-off function:

$$\zeta_\varepsilon(\mathbf{r}_j) = \frac{1}{\varepsilon^3} \exp\left(-\left(\frac{r_j}{\varepsilon}\right)^3\right), \quad r_j = |\vec{x} - \vec{Z}_j(t)| \quad (21)$$

Using (20), $\vec{u}_\omega(\cdot, t)$ takes the form:

$$\vec{u}_\omega(\vec{x}_0, t) = \sum_{j \in J(t)} \frac{\vec{\Omega}_j(t) \times (\vec{x} - \vec{Z}_j(t))}{4\pi|\vec{x} - \vec{Z}_j(t)|^3} \left(1 - \exp\left(-\left(\frac{|\vec{x} - \vec{Z}_j(t)|}{\varepsilon}\right)^3\right) \right) \quad (22)$$

while the evolution of wake vorticity is defined by

$$\frac{d\vec{Z}_j(t)}{dt} = \vec{u}(\vec{Z}_j; t), \quad j \in J(t), \quad \frac{d\vec{\Omega}_j(t)}{dt} = (\vec{\Omega}_j(t) \cdot \nabla) \vec{u}(\vec{Z}_j; t) \quad (23)$$

In the above formulation the potential will now only include the contributions by the solid surfaces and the near wakes.

Vorticity is shed continuously along the trailing edge. The amount of vorticity released in the near wake is determined by the Kutta condition which requires finite velocity at the trailing edge which is satisfied by setting the near wake dipole intensity equal to that on the blade along the trailing edge. Once the solid boundary condition and the Kutta condition are fulfilled, the wake is convected to its new position. At their new positions the near wake panels are transformed into vortex blobs by integrating (19) (Figure 4-5).

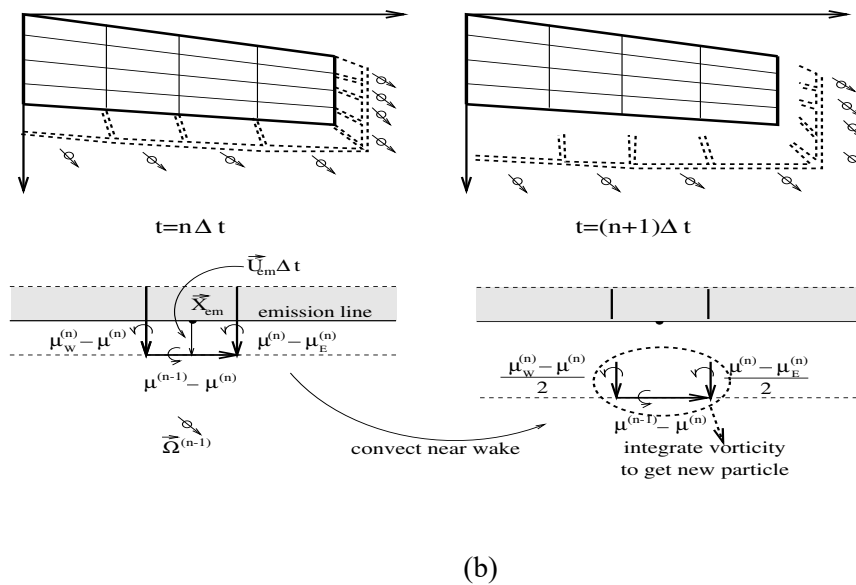
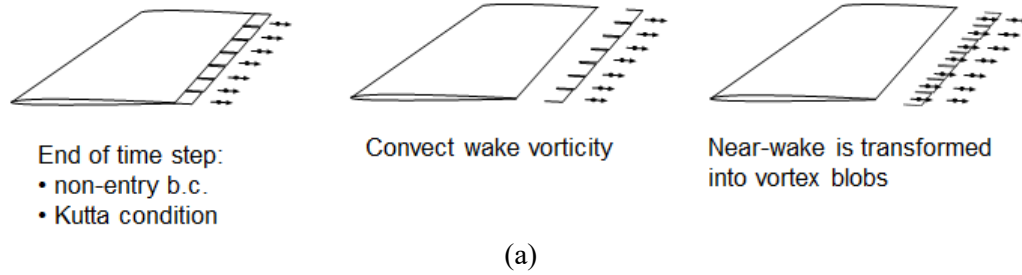


Figure 4-5: (a) The three sub steps per time step in GENUVP, (b) The integration scheme

Loads are obtained by integrating the surface pressure distribution given by the solver. By definition, they do not include any viscous effect and therefore viscous corrections are needed in order to obtain realistic load estimations. In GENUVP, viscous corrections are introduced through the ONERA model [15] which uses the effective angle of attack and relative velocity as calculated by the flow solver and sectional steady C_L - C_D data.

Numerical details

A surface grid of 26 (chordwise) x 13 (radial) nodes per blade is used (Figure 4-6), while the time step corresponds to an azimuthal step of 7.5°.

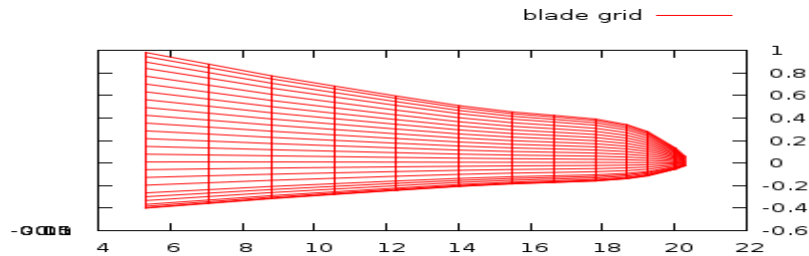


Figure 4-6: The surface grid

It is noted that the aerodynamic modelling of the blade starts at $r=5.30m$. The reason is that the inner part is close to a cylinder and therefore undergoes massive separation which is beyond the capabilities of the current Vortex solver. The expected effect of cutting the inner part of the blade is that the root section wherefrom the root vortex originates is set further outboard than in reality and therefore reduces the performance of the root blade sections. This effect is local and does not affect the overall performance of the rotor as already confirmed within the INN WIND WP2 activities (Benchmark of aerodynamic modelling). However excluding the hub region will channel the inflow through and generate an acceleration of the flow.

In Figure 4-7 the blades of the 7 rotors and their wakes are shown. The distribution of vortex blobs (red dots) indicates the expansion of the wakes and their tendency to mix. Also an overall swirling of the wake under the influence of the mutual interaction of the wakes is noted.

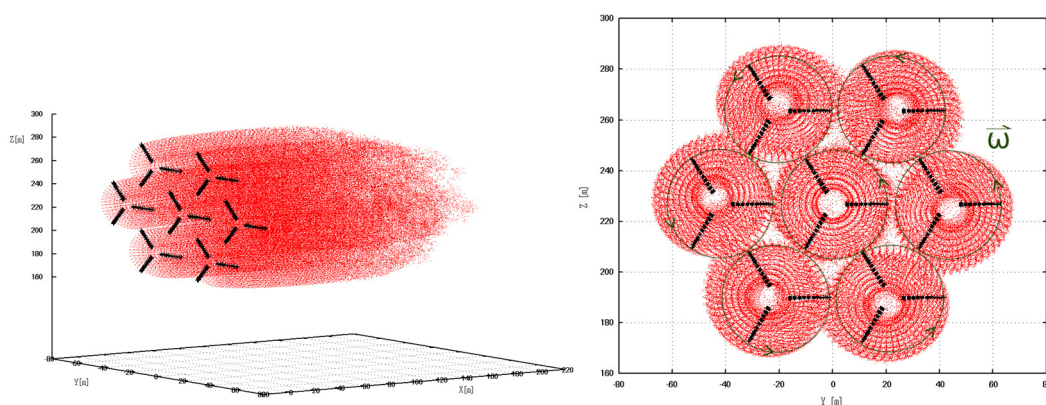


Figure 4-7: GENUVP: Perspective and back view of a 7 MRS. Red dots correspond to vortex blobs. In the Right figure the wake expansion, the tendency of the wake to mix and the overall swirling can be seen.

With respect to the viscous correction of the loads, the 2D polars for the various sections of the blade are needed. To this end 2D flow predictions were carried out using FOIL2W [16]. The data thus obtained were next used in power curve calculations for different pitch

angles (Figure 4-8) in order to check the correspondence to the anticipated power curve of the rotor.

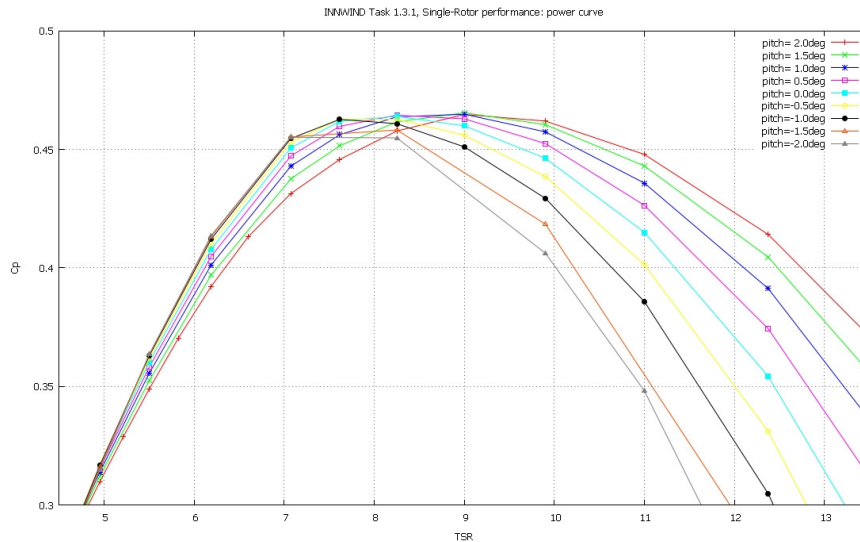


Figure 4-8: The $C_p - \lambda$ curve of the rotor

4.3 Results

The test cases

Two case studies have been considered. The first one refers to the simulation of a 7 rotor MRS (7_MRS) for which flow predictions have been obtained with both aerodynamic solvers. The second case refers to the full configuration with 45 rotors (45_MRS) which has been simulated with the RANS flow solver. The increase of the number of surrounding rotors is expected to produce more blocking of the flow at the internal rotors. By comparing the results for the 7_ and 45_MRS information on how the concept scales up is obtained.

Table 4-1 Rotor general characteristics

3-bladed, UPWIND, pitch-variable speed regulated rotor	
Rotor diameter:	40.55m
Rated power:	444KW
Hub height:	227.06m
Airfoil sections:	NACA634xx

The performance of a 7 and a 45 MRS is examined, assuming the sheared inflow defined in (13), at nominal operating conditions (TSR=9) corresponding to a $Re=3\cdot 10^7$ for the CFD simulations. The single rotor case is considered in similar operational conditions at the

same hub height ($H=227\text{m}$, which is the hub height proposed for the 45 MRS) and the corresponding results are used as reference values. The rotors are synchronized in speed and azimuth angle which would perhaps not be the case in real operation. It is also noted that neither pitch nor rotational speed control are active. With respect to rotor spacing, the default value was set to $1.05D$. For the 45 MRS case a spacing of $1.025 D$ is also considered.

Performance results

In Figure 4-9 the predicted thrust and power for the 7_MRS is compared to the performance of the single rotor case. Both models predict an increase of similar level which suggests that the blockage of the flow is not expected to negatively affect the performance. In fact there is an increase of $\sim 2.5\%$ in power generation alongside with an increase of $\sim 2\%$ in thrust. It is noted that the single rotor and the central rotor of the 7_MRS were placed at the same hub height and the calculated loading of the single rotor was multiplied by 7 in order to compare it with the MRS system loading. The single rotor has the same rotor diameter as each of the rotors of the 7_MRS. Choosing the same hub height for both systems means that the single rotor is placed higher as compared to the standard $1D$ above ground level. Therefore in sheared inflow the single rotor will benefit from higher wind speeds and its performance will be somehow promoted.

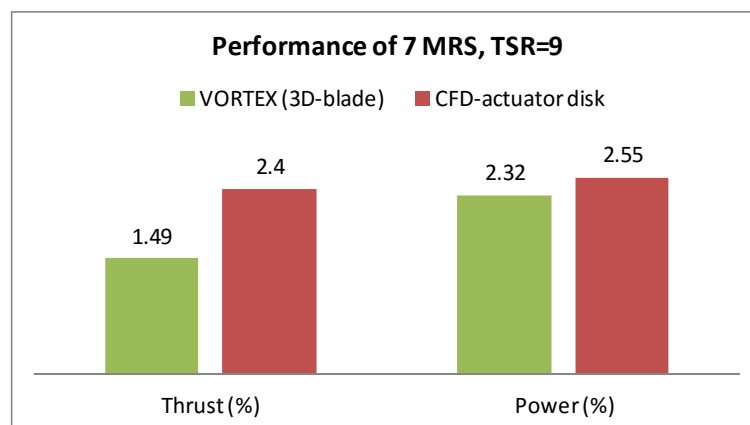


Figure 4-9: Per cent increase in thrust and power estimation of a 7 MRS in comparison to the single rotor performance. Simulations were performed using the CRES-flowNS actuator disk and the GENUVP vortex methods.

For the 45_MRS simulations are performed using the CRES-flowNS actuator disk method for a distance of $1.05 D$ and $1.025 D$ between the centres of neighbouring rotors. The excessive blockage of the flow at the internal rotors produces an acceleration of the flow higher than that of the 7 MRS, which results in a higher performance of the system, but also higher thrust. Therefore, the increase in both thrust and power generation compared to the single rotor is $\sim 8\%$, significantly higher than that of the 7_MRS as shown in Figure 7.

Changing the distance between the centres of neighbouring rotors from 1.05 to 1.025 D does not seem to affect the mean thrust and power production (Figure 4-10).

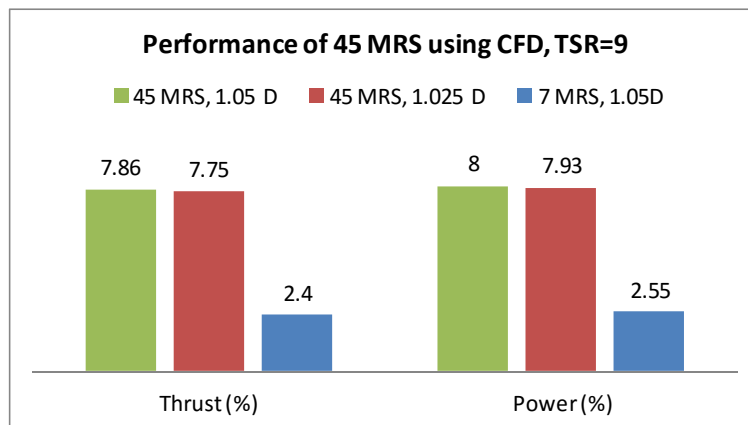


Figure 4-10: Per cent increase in thrust and power estimation of a 7 and a 45 MRS in comparison to the single rotor performance. Simulations were performed using the CRES-flowNS actuator disk method.

Flow results

Figure 4-11 shows the axial velocity contours at the hub height (227m a.g.l.) normalized by U_{ref} , in the case of the single rotor and the 7_MRS. Noticeable flow acceleration is found in the regions amongst the rotors. By comparing the extent of the wake cores, the effect of the extra mixing in the 7 MRS case can be noted. The individual wake cores of the 7 MRS merge into one wake at a distance which is comparable to the core length of the single rotor. In the single rotor case, flow recovery starts at $\sim 100\text{m}$, while in the 7 MRS case at $\sim 300\text{m}$ giving a 1:3 ratio which coincides with the diameter ratio of the two systems. In non-dimensional terms the same decrease in the velocity deficit is observed at the same distance. In the 45 MRS case the mean hub height of 227m a.g.l lies between the 3rd and 4th rows of rotors (208.42 and 245.5 m a.g.l respectively).

In Figure 4-12, the axial velocity contours at the plane of the 4th row (245.5 m a.g.l.) are plotted for the 45 MRS case. At a distance of more than 800m the velocity deficit is still significant exhibiting a slower flow recovery in non-dimensional terms than the single rotor and the 7MRS case. When the distance between the centers of the rotors is decreased to 1.025 D , the flow recovery becomes even slower. This comparison indicates that the results from the simulation of the 7 MRS cannot be generalized to the 45 MRS. The same conclusion was derived for the performance of the system in the previous section.

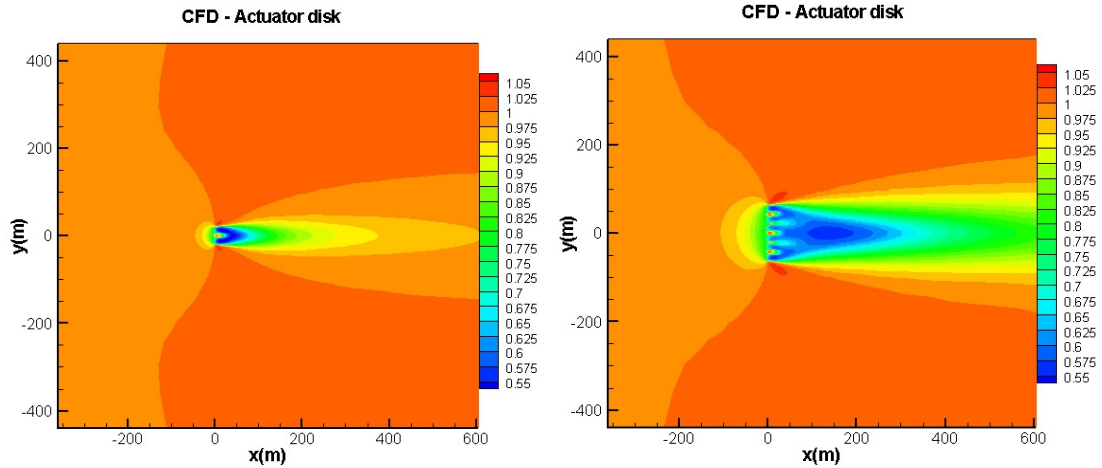


Figure 4-11. Axial velocity contours normalized by U_{ref} at $z=227m$ (TSR=9). Predictions obtained using CRES-flowNS. Left: Single rotor, Right: 7 multi rotor system.

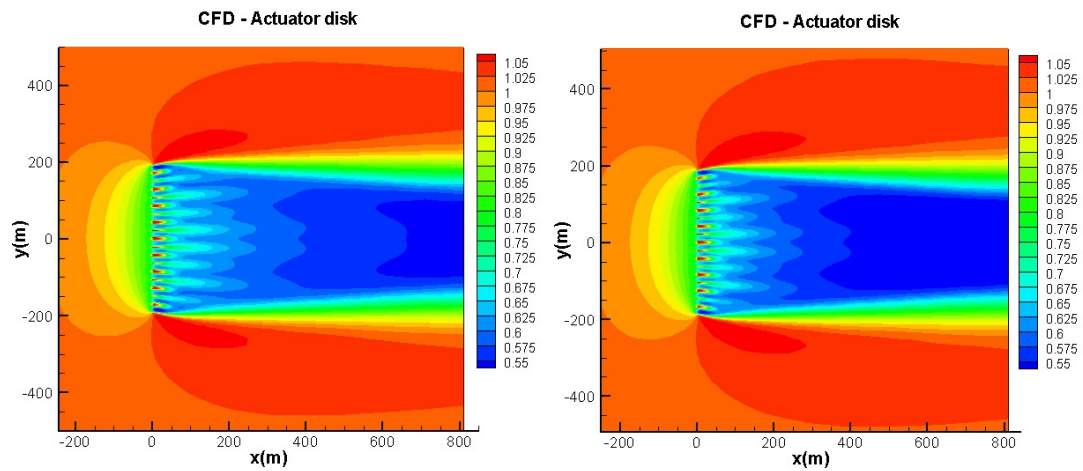


Figure 4-12: Axial velocity contours normalized by U_{ref} at $z=245.5m$ (TSR=9) for the 45 MRS. Predictions obtained using CRES-flowNS. Left: Distance between centers of rotors is $1.05 D$, Right: Distance between centers of rotors is $1.025 D$.

The extent of a MRS wake will be longer and therefore, in a wind farm design context, the next MRS system will be placed at a longer distance as compared to a design using single rotors. Assuming that the rows in a single rotor wind farm design contain the same number of rotors with the MRS, over the same wind farm area more rows could be fitted and more energy could be produced. However if the coverage of the wind farm area in the cross wind direction is also considered, more MRS systems would be placed. A clear comparison between MRS and single rotor wind farms would also require an account on the relevant

costs and therefore a detailed investigation is needed before conclusions can be drawn in this respect.

The effect of the multiple rotors on the wake deficit is also shown in Figure 4-13, Figure 4-14, where the axial velocity contours on the vertical plane $y=0$ are presented. Similar remarks can be made regarding the wake evolution. In these plots the effect of shear is also shown. Note that as the number of rotors increases from 1 to 7 and then to 45, the lower part of the rotor system comes closer to the ground level which explains the local higher flow acceleration as well as a slightly slower flow recovery.

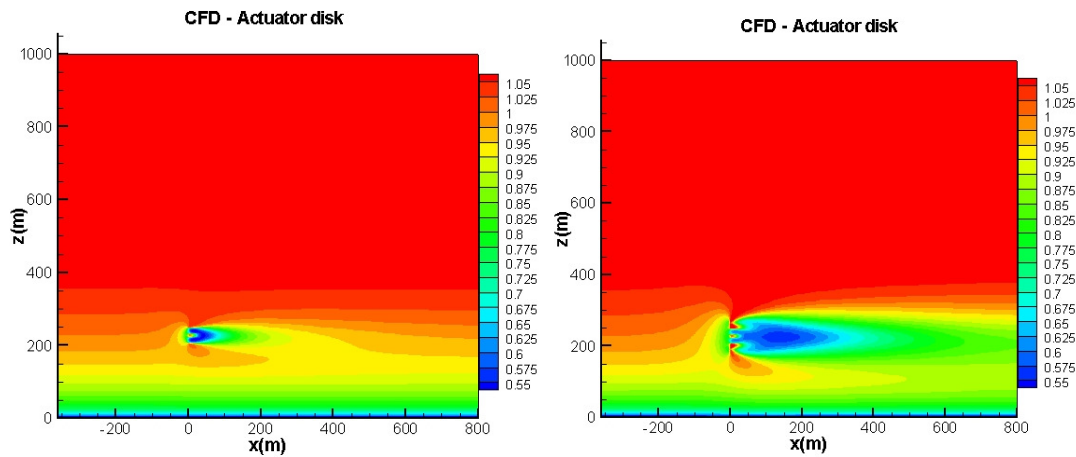


Figure 4-13: Axial velocity contours normalized by U_{ref} on the vertical plane $y=0$ (TSR=9) Predictions obtained using CRES-flowNS Left: Single rotor, Right: 7 MRS.

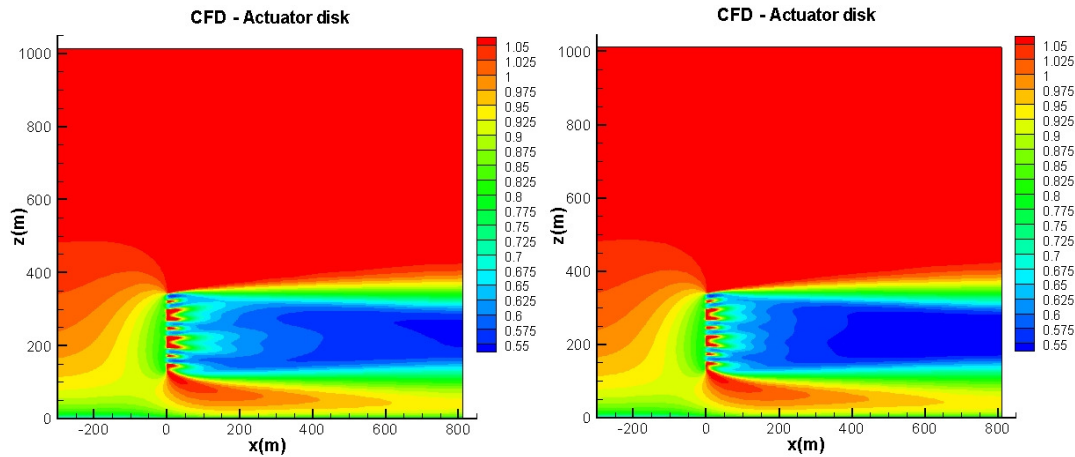


Figure 4-14: Axial velocity contours normalized by U_{ref} on the vertical plane $y=0$ (TSR=9) for the 45 MRS. Predictions obtained using CRES-flowNS. Left: Distance between the centers of the rotors is $1.05 D$. Right: Distance between the centers of the rotors is $1.025 D$.

In Figures Figure 4-15, Figure 4-16 the flow field predictions are compared as obtained by the two models. Since the vortex model is an unsteady solver by definition, mean flow field predictions (averaged over a full rotation) are used. Figure 4-15 presents a focused view of the axial velocity contours normalized by U_{ref} at $y=0$ plane. The lack of viscosity in GENUVP is responsible for the long range conservation of the deficit indicated by the long blue strips in the plots. In the near wake the deficit gradually develops over a long range towards the theoretical $U(1-2a)$ value given by the actuator disk theory. The acceleration seen over the gaps in between the rotors is also conserved as indicated by the red strips in the plots. Instead, in the CFD results, viscous mixing results in a different development of the velocity deficit and a quick damping of the acceleration obtained over the gaps. Similar remarks can be made on the results obtained on the $z=227\text{m}$ hub height horizontal plane (Figure 4-16).

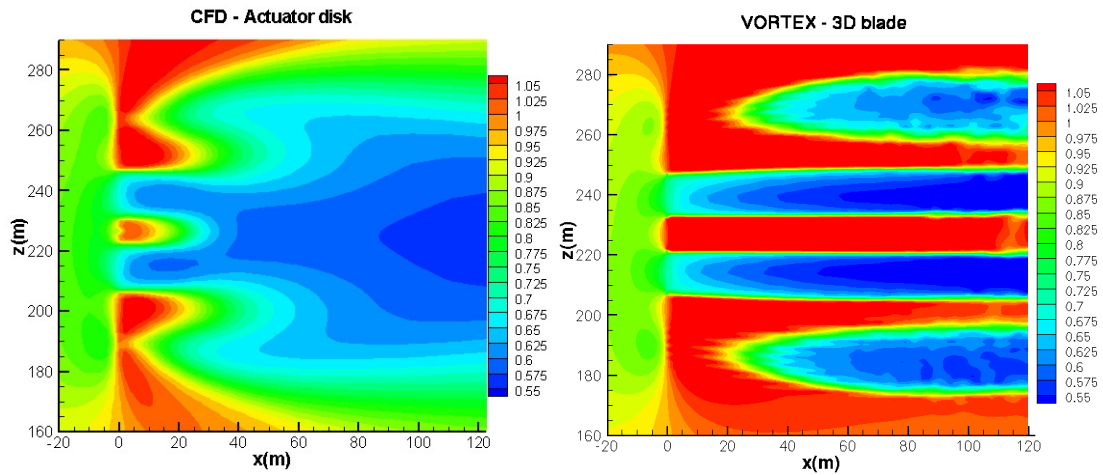


Figure 4-15: Axial velocity contours normalized by U_{ref} on the vertical plane $y=0$ (TSR=9) for the 7 MRS. Left: CRES-flowNS, Right: GENUVP

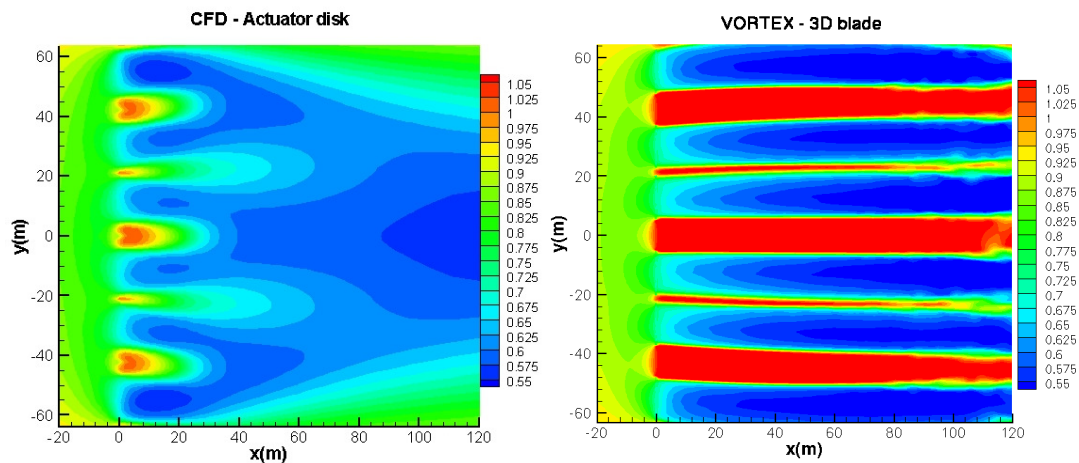


Figure 4-16: Axial velocity contours normalized by U_{ref} at $z=227m$ (TSR=9) for the 7 MRS. Left: CRES-flowNS, Right: GENUVP

The acceleration of the flow due to blockage is also depicted in Figures Figure 4-17-Figure 4-20. Figure 4-17 and Figure 4-18 show the normalized axial velocity contours as obtained from CRES-flowNS and GENUVP for the 7 MRS on the rotor plane ($x=0$) and on a downstream plane at $x=0.1D$. On the rotor plane both methods predict a flow acceleration of approximately 1.025 (relative to U_{ref}) through the "triangular" free spaces, which increases to almost 1.1 downstream at $x=0.1D$ ($x=4m$). This explains the 2.5% increase in performance presented in Figure 4-9. Higher axial flow velocities are also seen through the hub regions of the rotors. In the CFD simulations, over this part of the disk, a constant drag coefficient is assumed, while in the vortex simulations only this part is completed open to

the flow. This explains why the acceleration in the GENUVP results is more pronounced in this region.

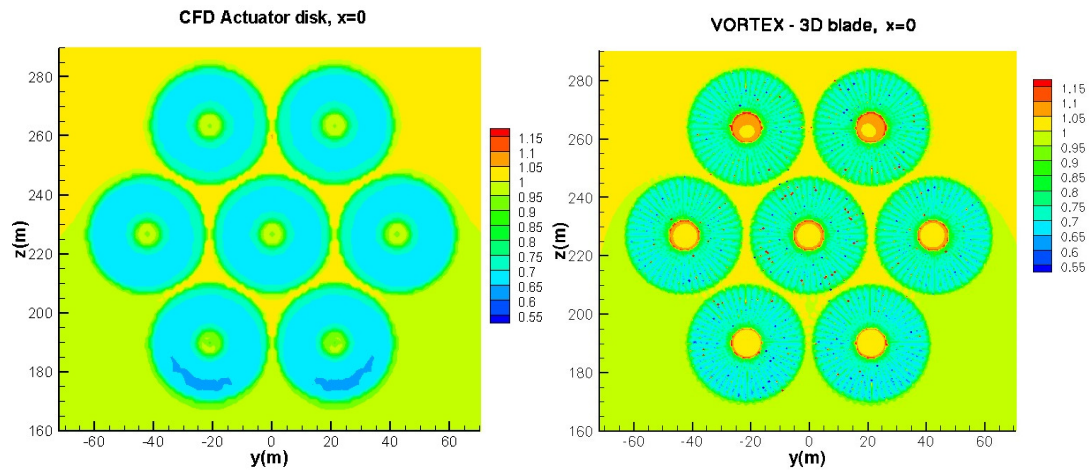


Figure 4-17: Axial velocity contours normalized by U_{ref} on the rotor-plane $x=0$ (TSR=9) for the 7 MRS. Left: CRES-flowNS, Right: GENUVP

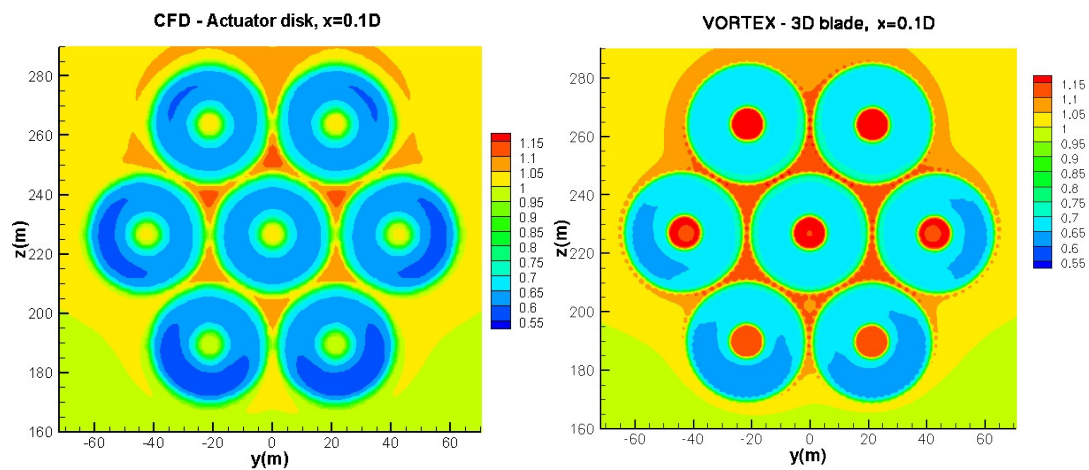


Figure 4-18: Axial velocity contours normalized by U_{ref} at the $x=0.1D$ downstream position (TSR=9) for the 7 MRS. Left: CRES-flowNS, Right: GENUVP

Figure 4-19 presents the axial velocity contours on the same planes for the 45 MRS when the distance between the centers of the rotors is $1.05D$. At a first glance the contour plot on the downstream plane $x=0.1D$ shows that a significant flow acceleration occurs at the internal “triangular” free spaces. This acceleration is the cause for the significant increase of almost 8% in performance shown in Figure 4-10. When the distance between the centres of the rotors reduces to $1.025D$ no significant difference is observed in the

velocity contour plots justifying the fact that the power production remains essentially the same. Figure 4-20 presents a focused view on the group of the internal 7 rotors which are located at the same position with the 7 MRS. Note that the vertical position is not exactly the same since the $z=227\text{m}$ hub height does not pass through the centers of the rotors. In this plot it is observed that the flow acceleration through the triangular spaces on the rotor plane increases to approximately 1.05 whereas the flow acceleration through the triangular spaces on the plane $x=0.1D$ increases to more than 1.15. The increase of flow acceleration in comparison to the 7_MRS is responsible for the increase in power production from 2.5% to 8% as depicted in Figure 4-9 and Figure 4-10.

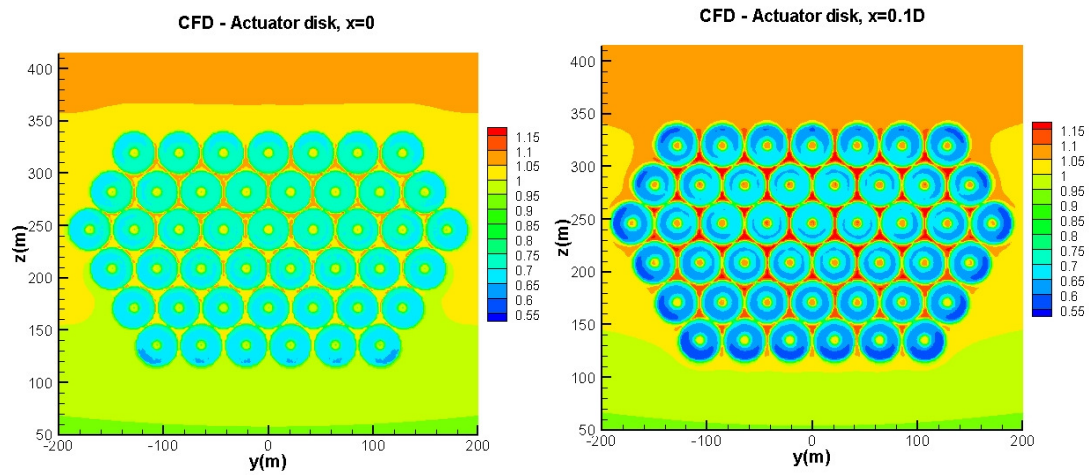


Figure 4-19: Axial velocity contours normalized by U_{ref} (TSR=9) for the 45 MRS. Predictions obtained using CRES-flowNS. Left: Rotor plane $x=0$, Right: Downstream position $x=0.1D$.

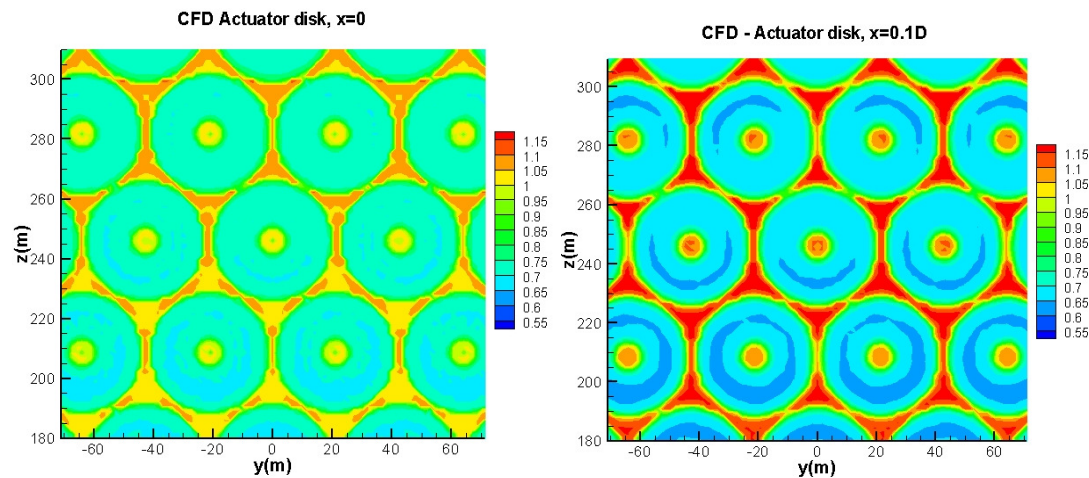


Figure 4-20: Axial velocity contours normalized by U_{ref} (TSR=9) for the 45 MRS. Focus is made on the 7 central rotors of the system. Predictions obtained using CRES-flowNS. Left: Rotor plane $x=0$, Right: Downstream position $x=0.1D$.

Loading characteristics

The loading characteristics of the multi-rotor system can be obtained from the output time signals of the vortex model. Snapshots of the normalized axial velocity at azimuth angle $\psi=0^\circ$ are shown in Figure 4-21 on planes $x=0$ and $x=0.1D$. As expected, the axial velocity distribution over each of the system disks follows the rotating motion of the blades. The flow field outside the area occupied by the rotors, as a whole, is only slightly affected. On the contrary the acceleration within the triangular shaped gaps that are formed in between the individual rotors seems to follow the rotation of the blades. In fact this acceleration is triggered by the close passing of the blades. A similar pattern is seen at $x=0.1D$ as regards the distribution of the velocity deficit which also follows the blade passage.

These flow variations induce similar variations in the blade loading as shown in Figure 4-22, where the MRS blade axial loading T is normalized by the single rotor blade axial loading T_{ref} . A clear 6P frequency is found in the loading of the central rotor blade (CR_1). The behaviour and performance of the off-set rotors (OR_2~7), depend on the vertical location of the rotor within the MRS. The main excitation is at 1P and secondarily at 6P.

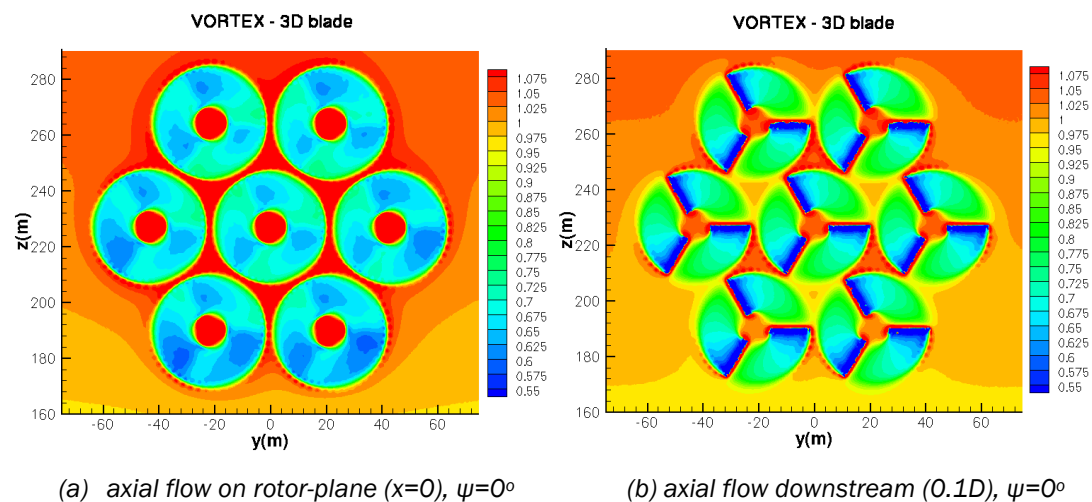


Figure 4-21: Snapshots of the normalized axial velocity: (a) on the rotor plane and (b) at $x=0.1D$ downstream at azimuth angle $\psi=0^\circ$ (results obtained with the vortex model)

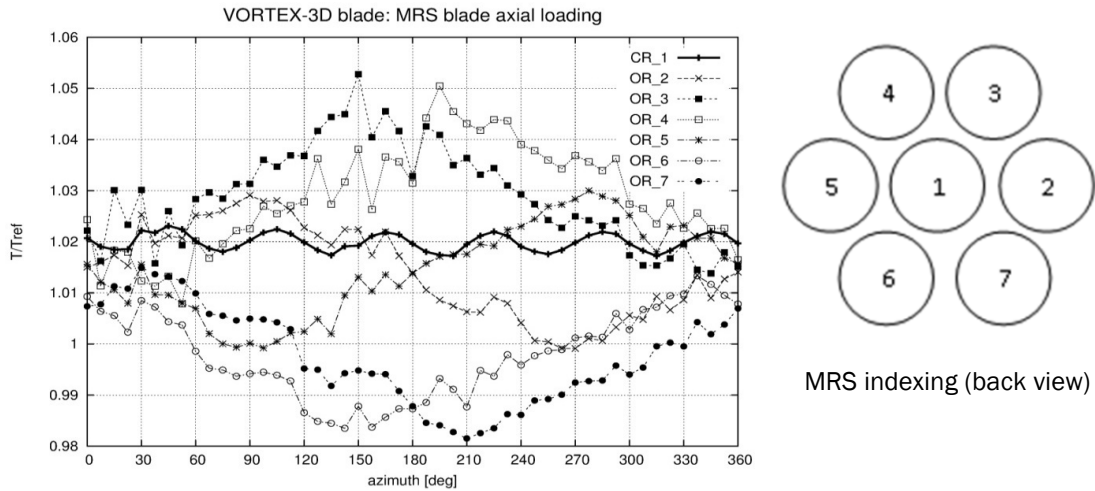


Figure 4-22: Blade loading history for the central and the off-set rotors, TSR=9, sheared inflow.

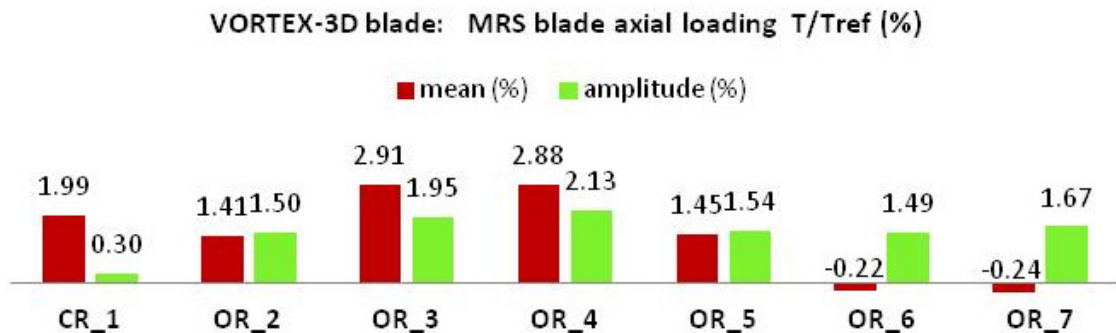


Figure 4-23: Blade loading means and amplitudes for the central and the off-set rotors. The rotor at the center is labeled as CR_1, while the off-set rotors as OR_2, OR_3, ..., etc.

In terms of axial loading, the central rotor (CR_1) receives 2% more average loading and slightly higher amplitude of 0.3%, in comparison to the single rotor case. For the off-set rotors the increase in average loading varies from -0.22 to 2.91% depending on the vertical position of the rotor in the sheared inflow (Figure 4-23), while the amplitude in the loading signals increases from 1.49 to 2.13%. These variations could have implications on the blade fatigue loads and should be further examined through aeroelastic simulations

4.4 Discussion of the results

The aerodynamic implication of close spacing in multi-rotor systems was investigated using two different simulation procedures: a CFD actuator disk and a vortex method. The CFD model was used in order to give a realistic prediction of the mean flow field, whereas the vortex model which can realistically take into account the blade geometry, was used in order to assess the dynamic implications of such a system. Both models predicted no penalty in performance for a 7 MRS at rated tip speed ratio. For the 7_MRS an increase of

~2.5% in power production was obtained alongside with an increase in thrust of ~2%. This suggests that at least from an aerodynamic point of view, the 7_MRS will perform equally well with 7 stand-alone rotors. Regarding the dynamic implications it was found that at blade level, there is an increase in the loading amplitude ranging from 0.3 to 2.13%.

Simulation of a 45 MRS using the CFD actuator disk method showed that by increasing the number of rotors power production also increases. A ~8% gain in power production was obtained alongside with a ~8% increase in thrust as compared to the stand-alone rotor case. Therefore, CFD predictions suggest that moving from the stand-alone machines to the multi-rotor systems results in an increase in power and thrust at almost the same percentage. However the thrust can be regulated by pitch control as it peaks near rated wind speed so that most of the power gain can be exploited to produce extra energy without affecting design driving loads.

In terms of loading, the unsteady vortex method indicated a penalty in the loading amplitude. Further detailed aerodynamic and aeroelastic analysis are needed in order to quantify the gains and penalties of using a multi-rotor system.

CHAPTER 5 MULTI ROTOR SYSTEM LOADS

5.1 General

Within the present project loads were generated by UoS primarily for the purpose of enabling CRES to develop a structure design for the MRS. In subsequent discussion loads, represented as the sum of individual loading on each of the 45 rotors, are often presented to assist understanding and make comparisons with single rotor system loads. However the only output to CRES used directly for their structure design was in the form of complete time histories of the 6 load components at the hub centre of each rotor.

5.2 Loads Simulation Tool an7d Capability

GL Garrad Hassan (now DNV GL Renewables Advisory) had developed software (extension of GLGH Bladed) to model loads and performance of a small array of tidal turbines, thus essentially a multi- rotor system. They further developed this within the present project to enable loads and performance evaluation of the 45 rotor MRS subject to 3 dimensional turbulent wind input. As a basis for checking and grounding comparisons, some parallel loading evaluation was done on the UPWIND 20 MW rotor [6].

The capability of the Bladed software, although very substantial, was necessarily restricted with so many independent rotors and some simplifications were introduced. In summary:

1. Only limited aeroelastic interaction with the structure was able to be modelled.
2. Closed loop control of each turbine was independent but supervisory control was collective
3. The spatial resolution in the turbulence modelling was fully adequate for the 20 MW single rotor system but gave rather poor resolution over single rotors of the multi-rotor system
4. Structure aerodynamic interference was modelled using standard “tower shadow” models, for the effect of each structure tube that was located immediately downwind of a rotor

Regarding supervisory control being collective, this had the unfortunate effect that, should one rotor shut down due to local wind conditions or a fault, then the whole array would shut down. Moreover although straightforward in principle to change the modelling to enable independent supervisory control of rotors, this would have consumed too much project resource. Work-around solutions were found so that this did not impede getting suitable system loads. Regarding the spatial resolution of turbulence, again there was no fundamental difficulty increasing resolution, but run times were already long even with the

comparatively low resolution files. The solution adopted was to inject additional 1P and 3P harmonics into the load spectra of the rotors, compare with signals from a single rotor where the wind field had high resolution and then verify that augmenting the harmonic content in this way as compared with using the low resolution data directly had negligible effect on design load levels.

5.3 Design Load Cases

The Innwind project concept was to develop top level evaluations of several innovative wind turbine systems. Due to this and to the computationally arduous nature of modelling 45 rotors, a much reduced set of load cases (as compared with loads evaluation as required by accepted design standards) was chosen.

Two equivalently rated 20MW systems (a single rotor and a 45-rotor MRS) are compared based on the IEC 61400-1 standards [17], [18]; DLC 1.3-1.4, DLC 2.3, DLC4.x and DLC6.x specifications. Although the system rating is the same, UPWIND 20 MW rotor design (250 m diameter) would require to be 275 m diameter to have the same total swept area as the MRS. The main concern is to identify which loads drive the design of the support structure. It is assumed that the individual rotors have already been designed to withstand the environment they are subjected to and therefore there is no consideration of blade bending moments or blade forces. The loading information provided for support structure design comprised the 6 forces and moments acting at hub centre of each rotor. Whilst simplification of the scope of load calculations is very desirable, it is also to a large extent quite justifiable. Fault cases that may be important or critical for single rotor design, for example a blade stuck in pitch, are of little consequence for overall loading of the MRS structure.

Table 5-1 shows an abbreviated list of the design cases taken from the standard. The table highlights the conditions and types of analysis presented in this paper. The abbreviations in the table are; F - fatigue load, U - ultimate load, A - abnormal safety factor (1.1), N - normal safety factor (1.35), NTM - normal turbulence model, ETM - extreme turbulence model, ECD - Extreme Gust with Change of Direction, EOG - Extreme Operating Gust, EWM - Extreme Wind Model, NWP - Normal Wind Profile.

Design situation	DL C	Wind condition	Other conditions	Type of analysis	Partial safety factors
1) Power production	1.2	NTM $V_{in} < V_{hub} < V_{out}$		F	*
	1.3	ETM $V_{in} < V_{hub} < V_{out}$		U	N
	1.4	ECD $V_{hub} = V_r - 2 \text{ m/s}, V_r, V_r + 2 \text{ m/s}$		U	N
2) Power production plus occurrence of fault	2.3	EOG $V_{hub} = V_r \pm 2 \text{ m/s}$ and V_{out}	External or internal electrical fault including loss of electrical network	U	A
4) Normal shut down	4.1	NWP $V_{in} < V_{hub} < V_{out}$		F	*
	4.2	EOG $V_{hub} = V_r \pm 2 \text{ m/s}$ and V_{out}		U	N
6) Parked (standing still or idling)	6.1	EWM 50-year recurrence period		U	N
	6.2	EWM 50-year recurrence period	Loss of electrical network connection	U	A
	6.3	EWM 1-year recurrence period	Extreme yaw misalignment	U	N
	6.4	NTM $V_{hub} < 0,7 V_{ref}$		F	*

Table 5-1 - Abbreviated Load Cases taken from IEC61400-3

For the purposes of loads prediction, the structure was modelled using the inbuilt multi-member tower function of GH Bladed (v 4.1). The initial objective was to generate design loads for a first iteration of structural design and for this purpose the structure was assumed to be rigidly connected to base level by 4 tubes. The numbering system for the 45 rotors is as depicted in Figure 5-2, with numbers running from left to right beginning with the bottom row.

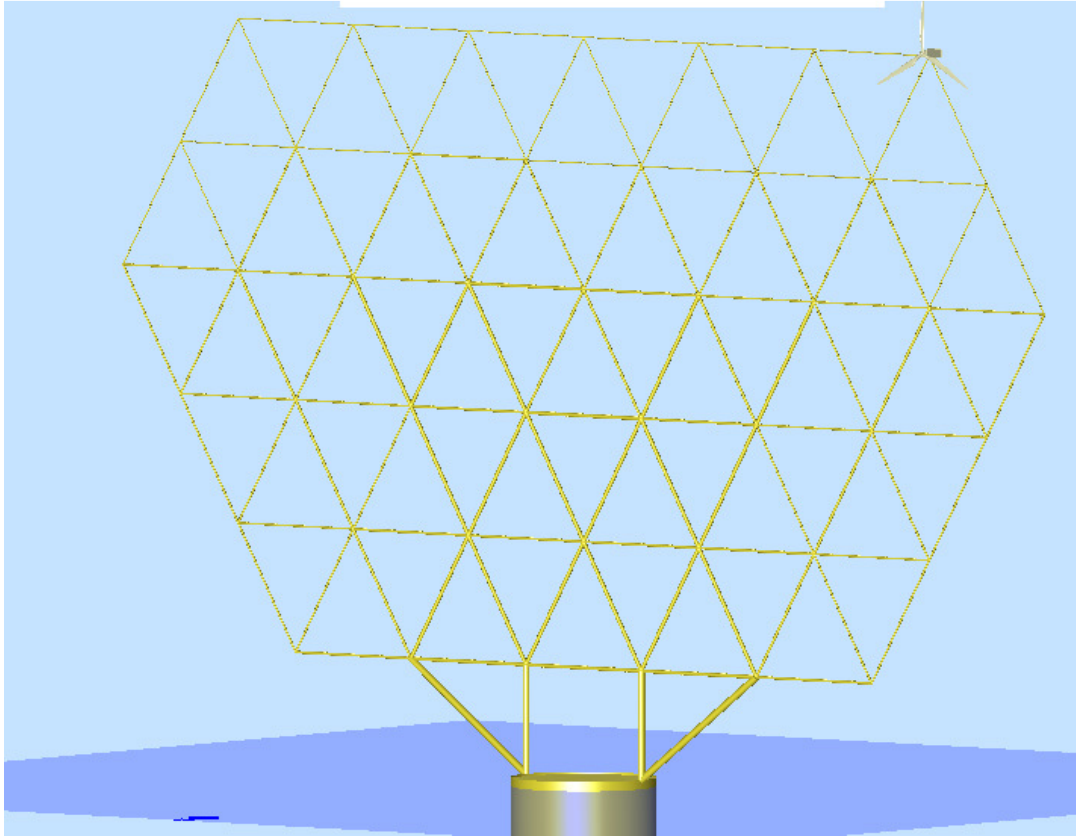


Figure 5-1 - Graphical Representation of the 45-rotor 20MW MRS Modelled in Bladed

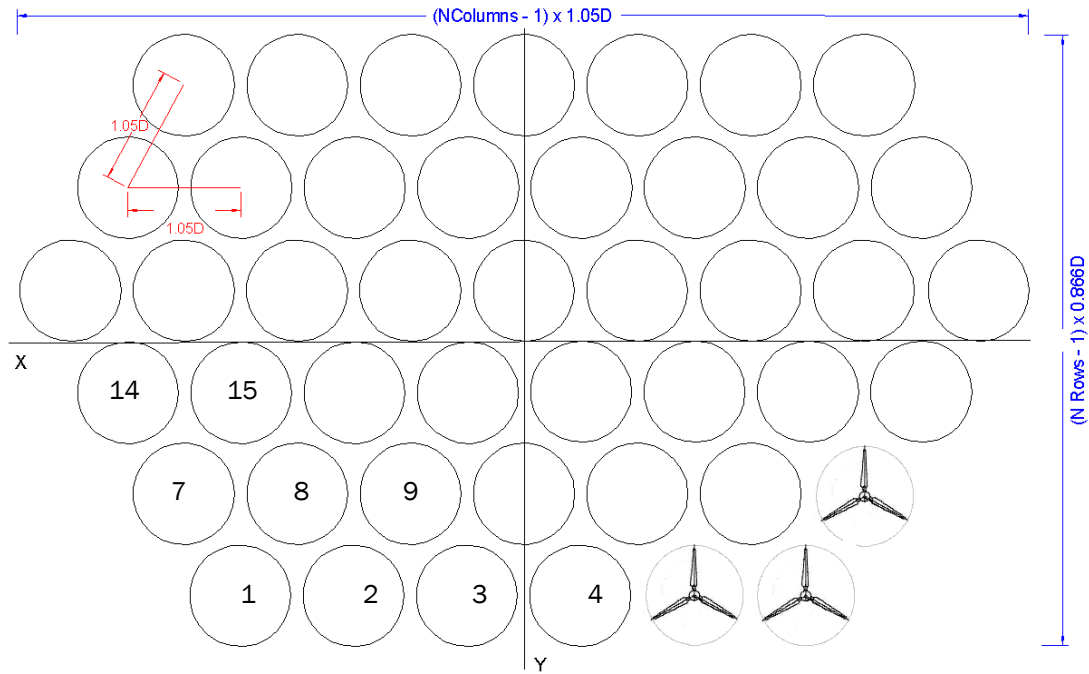


Figure 5-2 - Rotor Numbering System

5.4 Wind turbine parameters

Salient parameters are summarized in the following tables. These values are a reduced set of information from the standard Bladed project report as were used in load calculations.

Rotor diameter	40.5516	m
Number of blades	3	
Hub height	227.064	m
Tower height	226.05	m
Rotor overhang	2.32467	m
Position of rotor relative to tower	UPWIND	
Transmission	Pseudo Direct	
Aerodynamic control surfaces	Pitch	
Fixed / Variable speed	Variable	
Cut in wind speed	4	m/s
Cut out wind speed	25	m/s

The blade mass assumes that a blade design is developed using state of the art blade technology - lightweight high strength composites. The mass estimate is obtained by

descending the essentially cubic curve associated present blades for large offshore wind turbines. However the total blade weight in the MRS (unlike the single large rotor) is unimportant as a load on the structure and it may be that somewhat heavier blades are the most cost effective.

Blade Mass	550	kg
First Mass Moment	3548	kgm
Second Mass Moment	37808	kgm ²
Blade inertia about shaft	42847	kgm ²

Rotor System Mass and Inertia

Mass of hub	1500	kg
Hub inertia: about shaft	150	kgm ²
Total Rotor Mass	3285	kg
Total Rotor Inertia	128825	kgm ²

Generator

The drive train is based on a design of Magnomatics Ltd. This enables a particularly compact and high efficiency transmission system.

Pseudo Direct Drive transmission (PMG with Generator inertia)	1500	kg
	100	kgm ²

Power Production Control

Variable Speed Pitch Regulated Controller	Dynamic	
Minimum generator speed	26.42	rpm
Optimal mode quadratic speed-torque gain	4562.5	Nms ² /rad ²
Optimal mode maximum generator speed	46.63	rpm
Minimum pitch angle	0	deg
Maximum pitch angle	90	deg
Pitch direction	to Feather	
Maximum negative pitch rate	-8	deg/s
Maximum positive pitch rate	8	deg/s

PI torque control of speed

Controller values are simple placeholders defined by the auto-tune function in Bladed and therefore are in no way optimised for this particular system. Although system loads of the

MRS were generally unproblematic, there is certainly some further loading benefit to be realised in implementing a standard but appropriately designed controller.

Proportional gain	158249	Nms/rad
Integral gain	83248.5	Nm/rad
Desaturation time constant	0	s

PI pitch control of speed

Proportional gain	0.222774	s
Integral gain	0.171883	
Desaturation time constant	0	s

Gain schedule (gain divisor)

Lookup table based on	pitch
-----------------------	-------

Pitch (rad)	Gain divisor
-0.017453	1
0.087266	1
0.610847	4.99643
1.5708	4.99643

NORMAL STOP CALCULATION

Pitch rate for stopping	6	deg/s
Final pitch angle	90	deg

EMERGENCY STOP CALCULATION

Emergency pitch trip mode	Grid loss	
Emergency pitch rate	12	deg/s
Final pitch angle	90	deg
Emergency brake trip mode	Grid loss	

3 Blades	1650	kg
Hub	1500	kg
Nacelle	6500	kg

PDD Generator	1500	kg
Sundry	135	kg
Rotor System	11285	kg

5.5 LOAD CASE ANALYSIS

5.5.1 DLC-1.2 (NTM) - Fatigue loads

Fatigue loads are aggregated using Miners Rule over the design lifetime of the MRS. UoS was concerned only to provide relevant time series data to CRES for structural analysis which was conducted rigorously using local stress data rather than lifetime equivalent loads which may routinely be produced by Bladed but are only an approximate guide, useful for comparisons rather than design validation. Time-series load data for each degree of freedom derived from simulations was accumulated in wind speed bins and weighted by the annual probability distribution of 10 minute averaged mean wind speeds. Wind speed bin width used was 4m/s from cut-in wind speed to cut-out (usually bin width is 2m/s).

Weibull Calculation : DLC 1.2 / DLC 6.4					
wind speed	calc type	lower bin	upper bin	hours/year	% of total
2.5	idling	0	5	1562.8	0.18
6.5	powprod	5	8	1900.5	0.22
9.5	powprod	8	11	1913.7	0.22
13	powprod	11	15	1891.6	0.22
20	powprod	15	25	1432.7	0.16
25	idling	25	35	64.7	0.01
AMWS	10		Sum	8766.0	1.0000
shape factor	2				
α					

Due to the computing time restrictions both for UoS in generating data files and for CRES in employing the data in structural analysis, the fatigue evaluation was quite limited. A limited allocation of project resources for fatigue analysis was deliberate to the extent that early results suggested that fatigue loads were unlikely to drive structure design.

A more complete and rigorous evaluation with longer and more extensive simulations and narrower wind speed bins is best done with a fully aeroelastic model as may be developed in future work.

5.5.2 DLC-1.3 (ETM) - Ultimate Loads in Power Production

General

The extreme turbulent model (ETM) encompasses high turbulence intensity coupled with normal operating wind speeds. Ideally this would be run at wind speed intervals in the

same manner as 1.2 but peak loading generally occurs in operation between rated wind speed and cut-out. Thus simulations at both these mean speeds usually suffice.

Standard practice is followed and 6 seeds were used in generating the turbulent wind files to be associated with each mean wind speed. As the MRS has an averaging effect on loads from incoherence in individual rotor operation it is possible that this is not necessary for evaluation of structural loading. To reduce simulation time the worst minute (as subjectively judged from wind file characteristics) of each 10 minute turbulent wind file was used in the loading simulations.

Simulation Parameters;

- Simulation Time: 60s, Wind Shear Exponent: 0.14
- Wind Speed: 11 m/s (6 seeds) & 25 m/s (6 seeds)
- Kaimal Spectrum Parameters; Longitudinal: 340.2m, Lateral: 113.4m, Vertical: 27.72m, Coherency: 340.2, Decay: 12.
- Wind Parameters; Y Points: 39, Z Points: 26, Y Width: 382.5m, Z Height: 350m, Time: 600s, F: 13.65Hz

Results:

DLC1.3 was found to be the most important load case in terms of the impact of rotor induced loading on structure design and is consequently now discussed in more detail than other load cases.

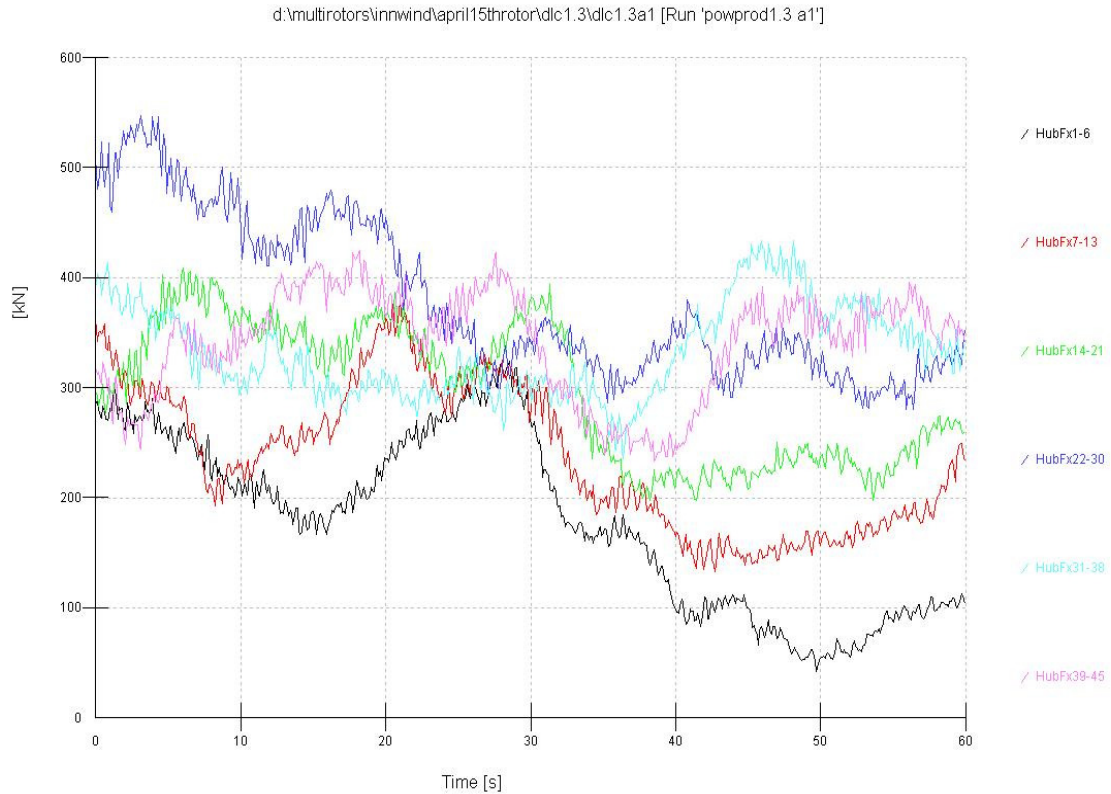


Figure 5-3 - Hub Fx by Row (DLC1.3a1)

The sum of rotor centre thrust values (hub Fx) from each row of the MRS is compared in Figure 3.

The input wind turbulence file is defined as having a mean of 11m/s at 115m height (approximately the centre of the array). Under normal wind shear conditions higher rows would on average experience higher wind speeds and this appears to be the case for a few simulation periods of 10 minutes that have been examined. As is evident in the 1 minute record of Figure 3, the pattern may vary greatly over shorter periods due to the spatial and temporal structure of turbulence.

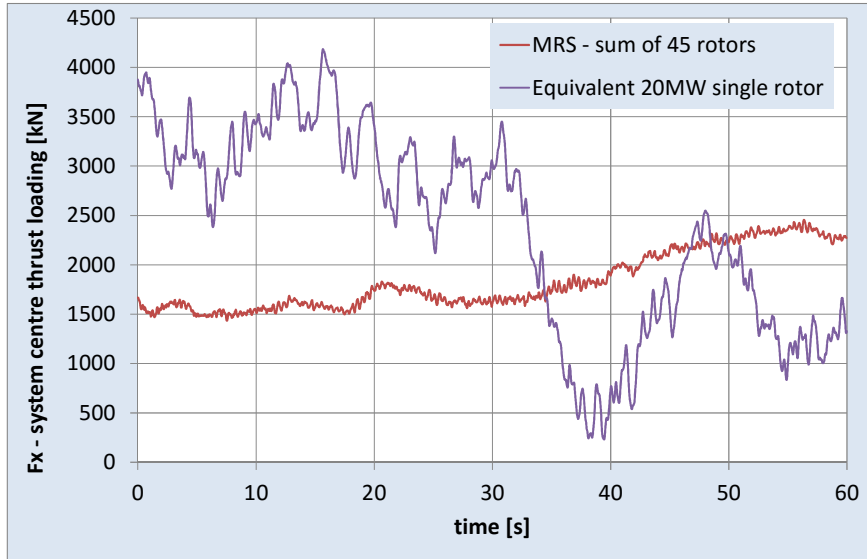


Figure 5-4: Comparison of aerodynamic thrust loading

Figure 5-4 compares the sum of rotor centre thrusts with that of a single 20 MW rotor of 275 m diameter (UPWIND upscaled) having the same total active swept area. The averaging effect of the MRS rotors operating independently in a turbulent wind field results in a huge reduction in range of load variations of the MRS as compared with the equivalent single turbine.

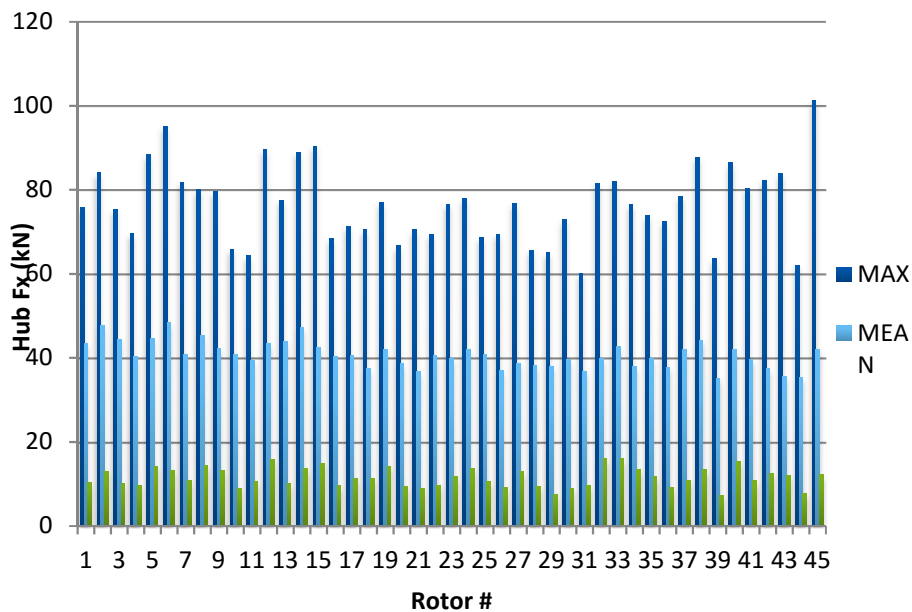


Figure 5-5 - Hub Fx by Rotor (DLC1.3a3)

Hub Fx	Aggregated Over Array sum	Average per Rotor for 45 Rotor Array	Average of Individual Maximum Time Series	Statistics of Rotor 45 (worst-case)	45 x Rotor 45 x worst-case
Mean (kN)	1830	40.67	40.72	42.05	1892.25
Maximum (kN)	2460	54.67	76.56	101.22	4554.9
Std. Deviation (kN)	297.1	6.6	11.56	12.223	550

Table 5-2 - Statistics of Hub Fx DLC1.3a3

Some statistics of the 45 rotor set from a simulation of DLC1.3a3 (run at rated wind speed) are presented in

Table 5-2 and Figure 5-6 - Hub Fx by Rotor (DLC1.3a3).

The results from this simulation are very promising from a structural standpoint. They show that while one particular turbine might experience its individual worst-case loading during a particular time period it does not contribute significantly to the overall loading on the array. As such the worst-case individual rotor loading rarely coincides with the worst case loading for the whole multi-rotor array. This bodes well for instances whereby single rotor faults lead to large localised forces which in a single rotor system would be transferred onto the tower and foundations but in the MRS will have almost negligible effect - a theory which will be tested in later sections.

The same DLC1.3 load case is run again at six seeds around cut-out speed. For the purposes of this study we are assuming that none of the rotors in the array cut-out at any point during the simulation and remain in power production. The results are presented in Figure 5-6 and

Table 5-3.

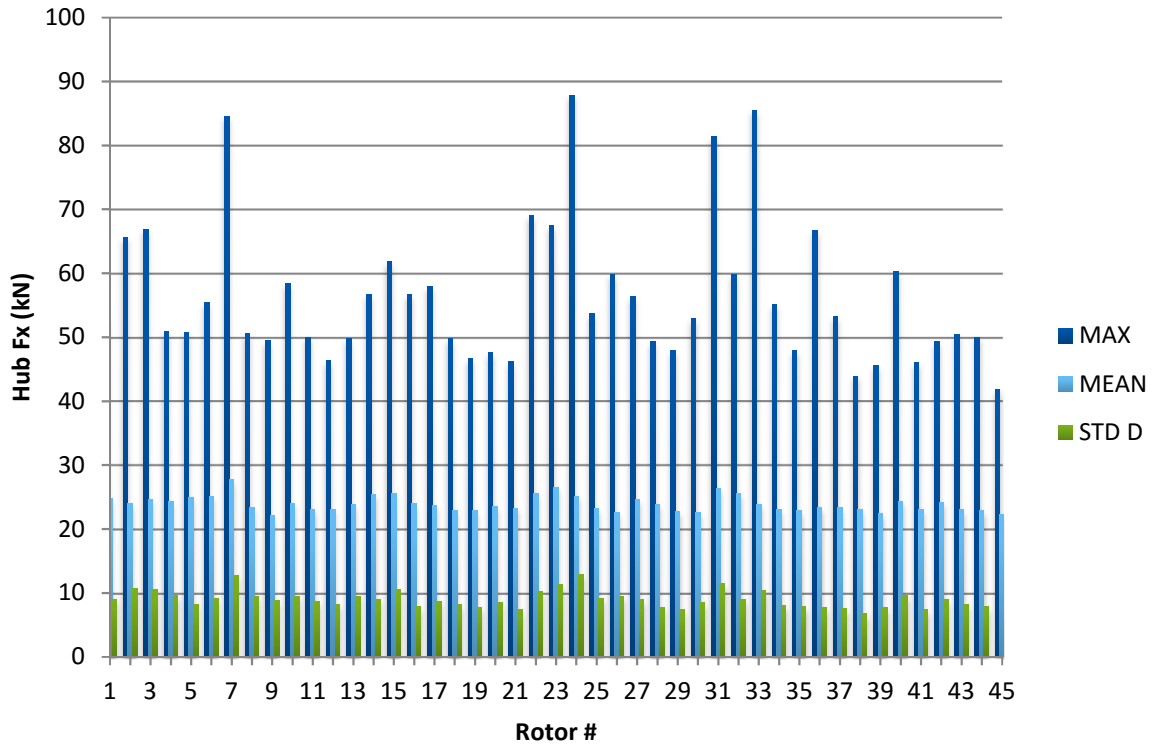


Figure 5-6 - Hub Fx by Rotor (DLC1.3a3)

Hub Fx	Aggregated Over Array	Average per Rotor for 45 Rotor Array	Average of Individual Maximum Time Series	Statistics of Rotor 24 (worst-case)	45 x Rotor 24 (coherent worst-case)
Mean (kN)	1077	23.93	23.93	25.13	1130.85
Maximum (kN)	1371	30.47	56.35	87.83	3952.35
Std. Deviation (kN)	86.05	1.91	8.96	12.89	580.05

Table 5-3 - Statistics of Hub Fx DLC1.3b4

It is clear at this stage that operation around cut-out leads to lower ultimate loading across the array irrespective of seed. We can therefore confidently state that the worst-case power production loading does occur around rated wind speed.

So far there has been some discussion about the positive effect of averaging of loads over the whole array. To better understand this we compare a typical single rotors hub Fx time plot against that of all the rotors average during the same time period.

Figure 5-7 shows a plot of a single rotor (rotor 24) from a single run (DLC1.3a1) against the rotor averages from the same period. We can see a very prominent peak in hub Fx loading for Rotor 24 around 52s into the simulation and generally a much higher average loading overall, as well as a much higher variance. This contrasts starkly with the average loading attributed to each rotor in the array which sees lower variance, a lower average and a lower peak loading. This effective averaging effect is very welcome from a structural standpoint as it undoubtedly will lead to lower fatigue loading on the structure during its lifetime and also directly result in a cheaper structure.

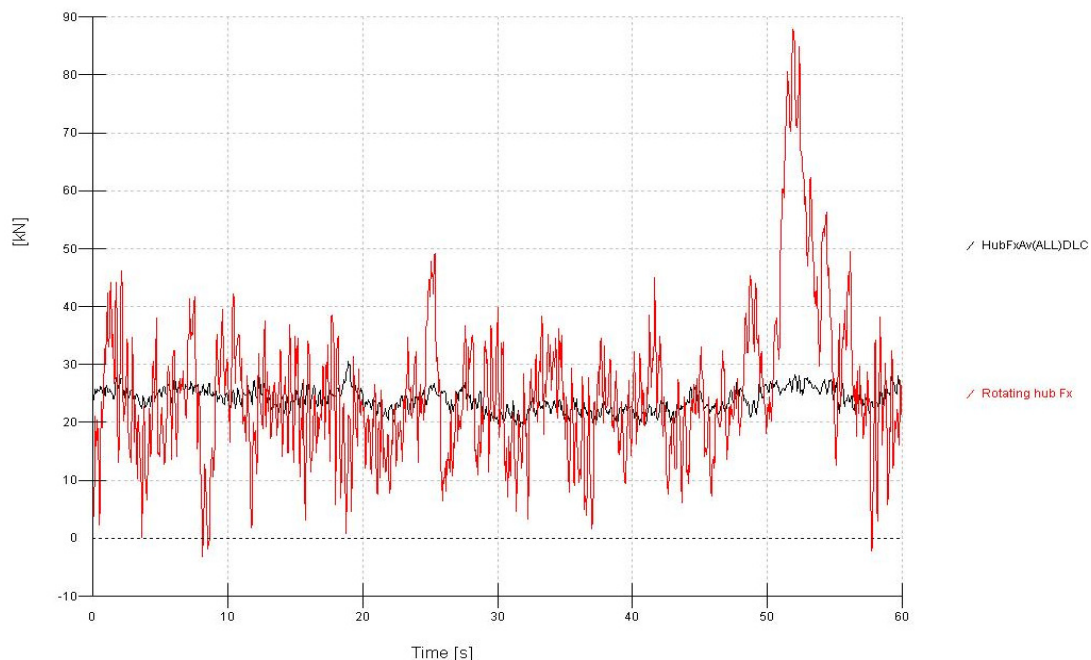


Figure 5-7 - DLC1.3a1; Comparison of MRS Average Hub Fx with Rotor 24 Hub Fx

Figure 5-8 is even more impressive, it shows the time series of hub My for the worst-case rotor (rotor 2) compared to the effective average per rotor seen over the whole array. The effective hub My averages and maximums for the array are around 1/8 of the individual worst-case rotors combined mean and maxima.

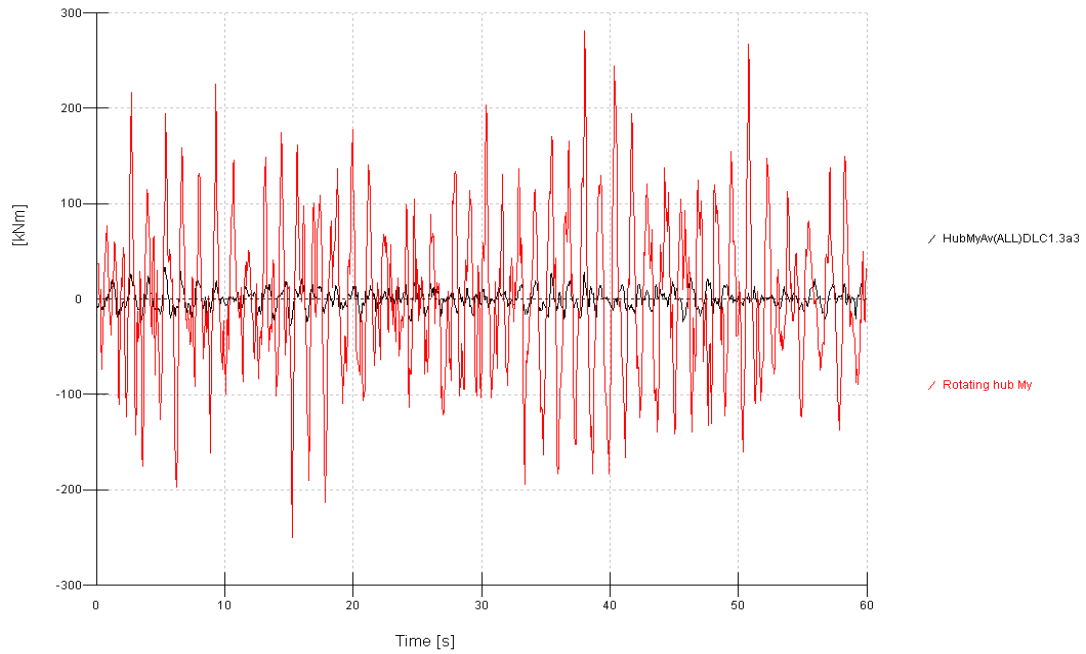


Figure 5-8 - DLC1.3a3; Comparison of MRS Average Hub My with Rotor 2 Hub My

The impressive load reduction effect is also seen in Mz (Figure 5-9) with an effective Hub Mz maximum around 1/5 of that predicted by the average maxima taken from each rotors time series.

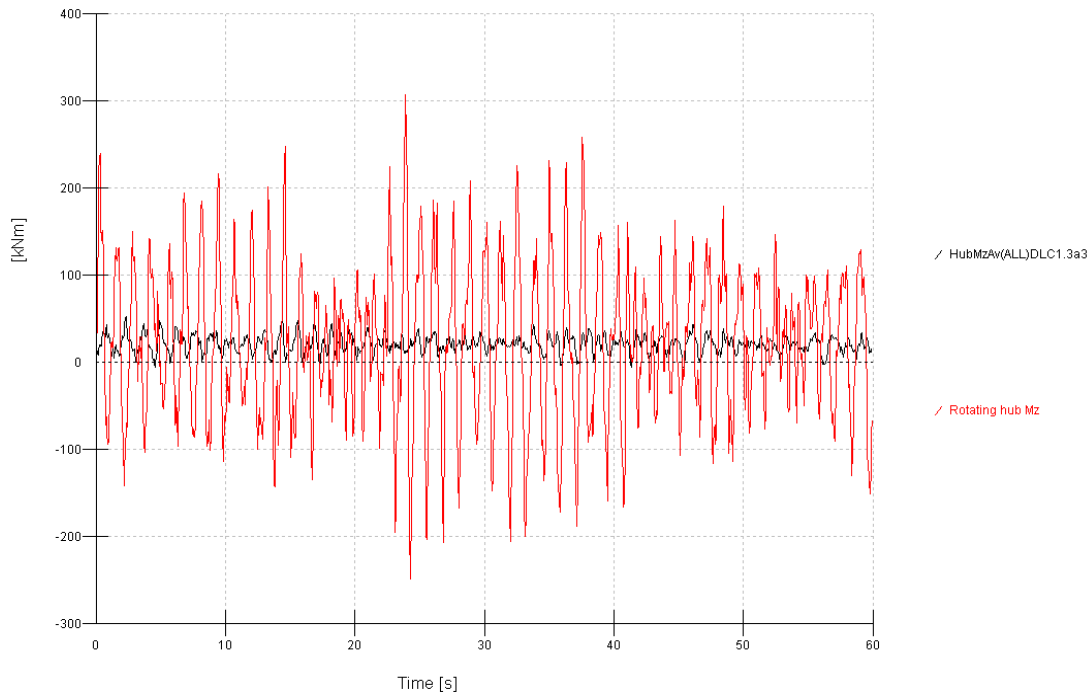


Figure 5-9 - Comparison of MRS Average Hub Mz with Rotor 30 Hub Mz (DLC 1.3a3)

Discussion

Extreme turbulence normally drives blade bending moment and is close to driving tower base bending moment in a class I storm case for large single rotors. To examine whether a similar observation can be made in the multi-rotor system, thrust loading, M_y overturning moment and M_z yawing moments are examined. For the multi-rotor system, M_y is taken to be the sum of all the individual hub M_y overturning moments plus the sum of all the individual moment arms ($F_x \cdot H$) - where H is the height of each rotor centre in metres. Similarly, M_z is taken to be the sum of all the individual hub M_z yawing moments plus the sum of all the individual moment arms ($F_x \cdot X$) - where X is the relative position of each rotor centre from the axis of rotation in metres. Figure 5-10, Figure 5-11 and Figure 5-12 present a comparison of these three loads for both the single rotor 20MW system and the 45-rotor 20MW multi-rotor system.

As predicted by the scaling-law presented in Chapter 3, the multi-rotor system as a whole exhibits reduced total hub F_x loading when compared to the 20MW single rotor system (Figure 5-10). At all points during the 5-minute simulation, the total hub F_x loading experienced by the array is 69% or less of the magnitude of that on the single 20MW rotor. This effect is found to be more pronounced in turbulent wind the reasons for which will be touched on in following sections.

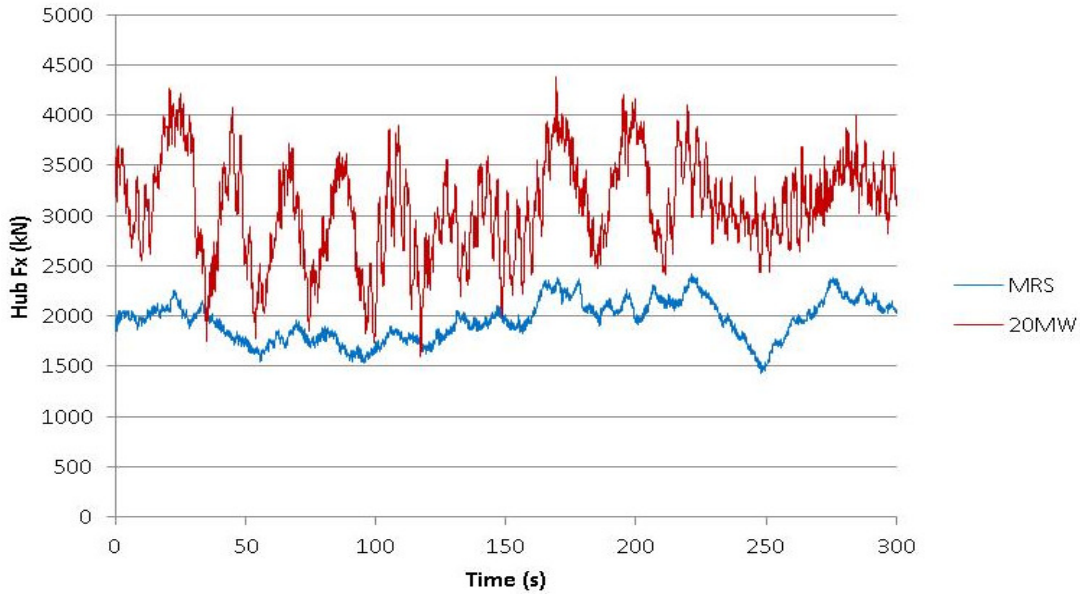


Figure 5-10 - DLC1.3a3; Hub Fx Comparison (Fx), 20MW SR + MRS

From Figure 5-11 it can be seen that the ultimate over-turning moment for the MRS is 350 MNm, when the average hub wind speed is 11 m/s at hub height. Under the same simulation parameters the single rotor 20MW system peaks at 850 MNm at a different time period. This effect was seen across all 4 other wind seeds with the ultimate loading varying only slightly for each system within each run.

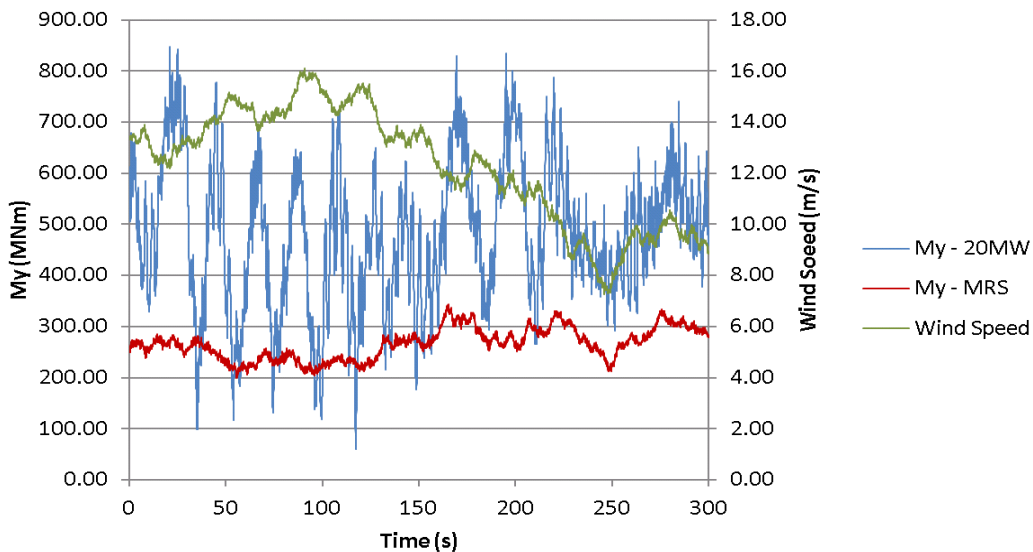


Figure 5-11 - DLC1.3a3; Overturning Moment Comparison (My), 20MW SR + MRS

These results suggest that the multi-rotor system has a lower ultimate M_y loading than the single rotor system of equivalent rating. The M_y average is also lower and has much less variance - which may be an advantage when comparing fatigue life. On average the MRS achieves a load ratio in M_y of 350:850 or 41% in comparison to the single 20MW rotor.

Figure 5-12 shows that the ultimate yawing moment for the MRS is even more significant. The M_z moment under the normal wind turbulence model is well balanced around the axis of rotation with the ultimate yawing moment not exceeding 2 MNm. Under the same wind speed conditions the single rotor 20MW system peaks at 47 MNm. This large yawing moment is unavoidable on the single 20MW rotor given the reliance of the moment on the azimuthal position of individual rotor blades (of which there is only 3) and rotor aerodynamic force imbalance under even small yaw errors. In comparison any multi-rotor system will have many more rotors and blades and therefore there will be a much greater averaging of aerodynamic yaw moments caused by blade imbalances and wind angles of attack.

On average the MRS yaw moment ratio in M_z is 2:47 or 4.25% of that of the 20MW single rotor under normal operation and without any concerted control strategy aimed at balancing yaw moments.

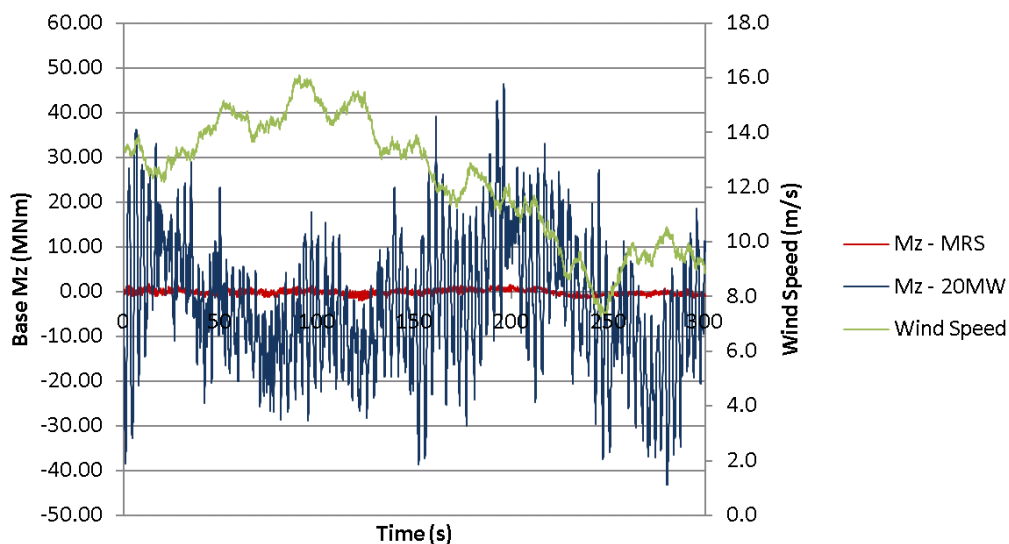


Figure 5-12 - DLC1.3a3; Yaw Moment Comparison (M_z), 20MW SR + MRS

5.5.3 DLC-1.4 (ECD) - Ultimate loads during power production

Overview;

The extreme change of direction (ECD) simulation encompasses an extreme gust coinciding with a wind direction change. These two effects occur over a short time period (10.5 seconds) to cause a sharp spike in various loads throughout the rotor and tower. The effect of azimuth and rotor direction of rotation has a larger part to play when considering the effects of both a positive and negative direction change. This effect may be less noticeable on the smaller individual multi-rotors and also due to the fact that in reality they would likely be counter rotating – offering some degree of symmetry whichever way yaw error occurs.

The whole system should perform a stop under the conditions of maximum yaw misalignment which is usually set according to individual wind speeds, with linear interpolation applied between the points. For example;

Wind Speed (m/s)	0	5	10	35
Yaw Error (deg)	60	60	45	30

Key Simulation Parameters:

- Simulation Time: 45s, Wind Shear Exponent: 0.14, Rotor Azimuths: Equal
- Wind Speed: 11 m/s, Gust speed: +6.67m/s, Start Time: 30s, Period: 10.5s
- Wind Direction: 0 deg, Direction Change: +65.45 deg, Start Time: 30s, Period: 10.5s
- Normal Stop: 6.79s seconds into event.

Results:

In this case due to the rapidly gusting wind coinciding with a direction change, the normal shutdown procedure is initiated 6.79 seconds into the event. This shutdown is initiated to avoid potential damage to the rotors and would do on an individual basis. However, in the multi-rotor array the effect is to cause a coherent shutdown of every rotor in the array which in turn leads to a large coherent loading in Fx (Figure 5-13). In reality, such increased Fx loading leads to unnecessary ultimate and fatigue loading onto the structure as a whole and should be avoided.

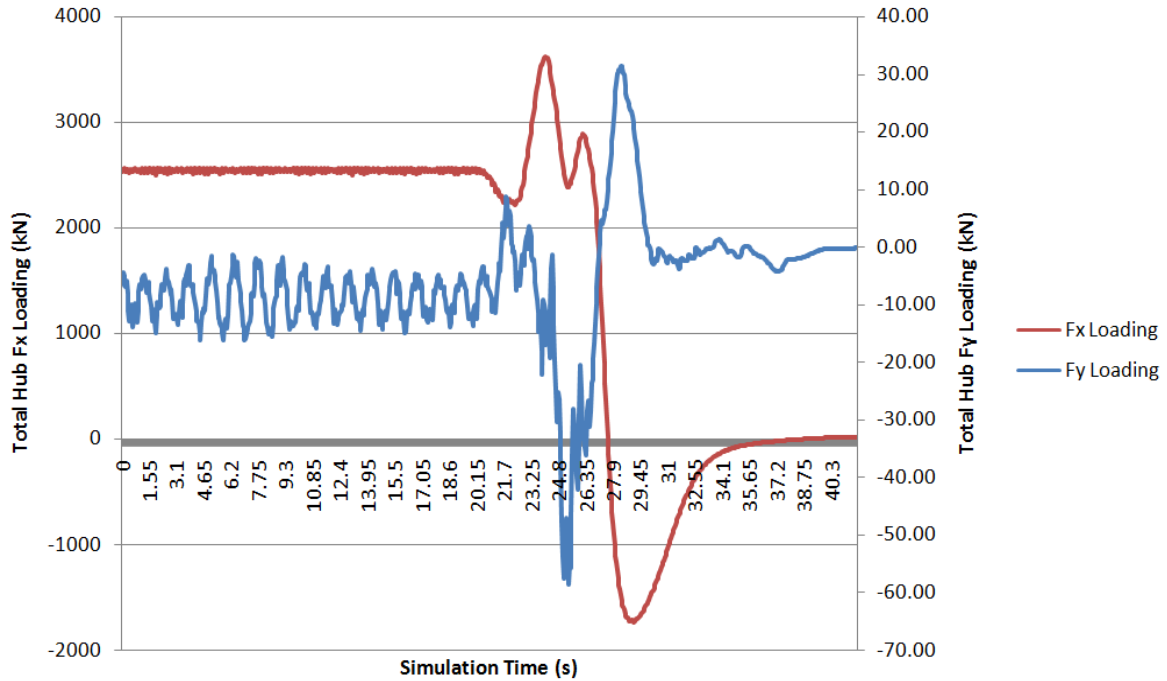


Figure 5-13 - DLC1.4: Combined Hub Fx and Fy Loading (+ve)

Hub Fx	Statistics from Total Sum of Rotors	Average per Rotor for 45 Rotor Array (sum / 45)	Averages of Individual Rotor Statistics	Statistics of Rotor 30 (worst-case)	45 x Rotor 30 (coherent worst-case)
Mean (kN)	1,534	34.1	34.1	33.1	1,490
Maximum (kN)	3,620	80.4	87.2	97.7	4,397
Std. Deviation (kN)	1,480	32.9	33.5	32.9	1,481

Table 5-4 - Statistics of Hub Fx DLC1.4a1 (+ve)

It was initially thought that due to the fact that all rotors are restrained to rotate in a uniform direction that there would be some potentially significant loading differences depending upon whether the wind was changing direction in the positive or negative direction. The same simulation was run and the results show that the loading is not significantly impacted in either hub Fx or Fy, see

Table 5-5.

Hub Fx	Statistics from Total Sum of Rotors	Average per Rotor for 45 Rotor Array	Averages of Individual Rotor	Statistics of Rotor 30 (worst-	45 x Rotor 30 (coherent
--------	-------------------------------------	--------------------------------------	------------------------------	--------------------------------	-------------------------

		(sum / 45)	Statistics	case)	worst-case)
Mean (kN)	1,535	34.11	34.12	33.12	1,490
Maximum (kN)	3,611	80.24	87.51	97.63	4,393
Std. Deviation (kN)	1,483	32.96	33.58	32.95	1,482

Table 5-5 - Statistics of Hub Fx DLC1.4b1 (-ve)

5.5.4 DLC-2.3 (EOG) - Ultimate Loads During Production with Electrical Fault

The extreme operating gust case is similar to the ECD case of DLC1.4 but without a direction change. Instead it is assumed that there is an electrical fault (causing emergency shutdown) during the transient period of the gust that combines to cause increased loading on the structure. The equation that determines the gust shape (second order Gaussian probability) causes the ‘Mexican hat’ form meaning that there is a reduction of wind speed immediately preceding and following the maximum spike. By phasing the point at which the fault occurs in relation to the gust, various potential for maximum loading can be evaluated.

Key Simulation Parameters;

- Simulation Time: 45s, Wind Shear Exponent: 0.14, Rotor Azimuths: Equal
- Wind Speed: 11 m/s, Gust speed: +6.67m/s, Start Time: 30s, Period: 10.5s
- Wind Direction: 0 deg
- Emergency Stop: 0s, 2.45s, 4s & 5.35s into gust

Results;

Simultaneous shutdown of all the rotors in the array presents one of the critical ultimate load cases to design against for the MRS system. Such a shutdown would likely be the result of a global event such as grid loss which would trip every rotors safety system and trigger emergency stop procedures. Given that a single rotor Fx is maximum at rated, it follows that the likely worst-case scenario for a emergency stop would be when the array is experiencing an average wind speed of 11m/s (at the effective hub height).

The IEC standard dictates that a check against ultimate load under DLC2.3 conditions be carried out at various gust phases.

Figure 5-14 depicts the Hub Fx loading over the event period with the emergency stop occurring at 4 different phases of the gust; 0s, 2.45s, 4s and 5.35s. The ultimate Fx loading is clearly seen to occur when the stop occurs 5.35s into the gust. This gust phasing approximately coincides with the peak of the wind gust.

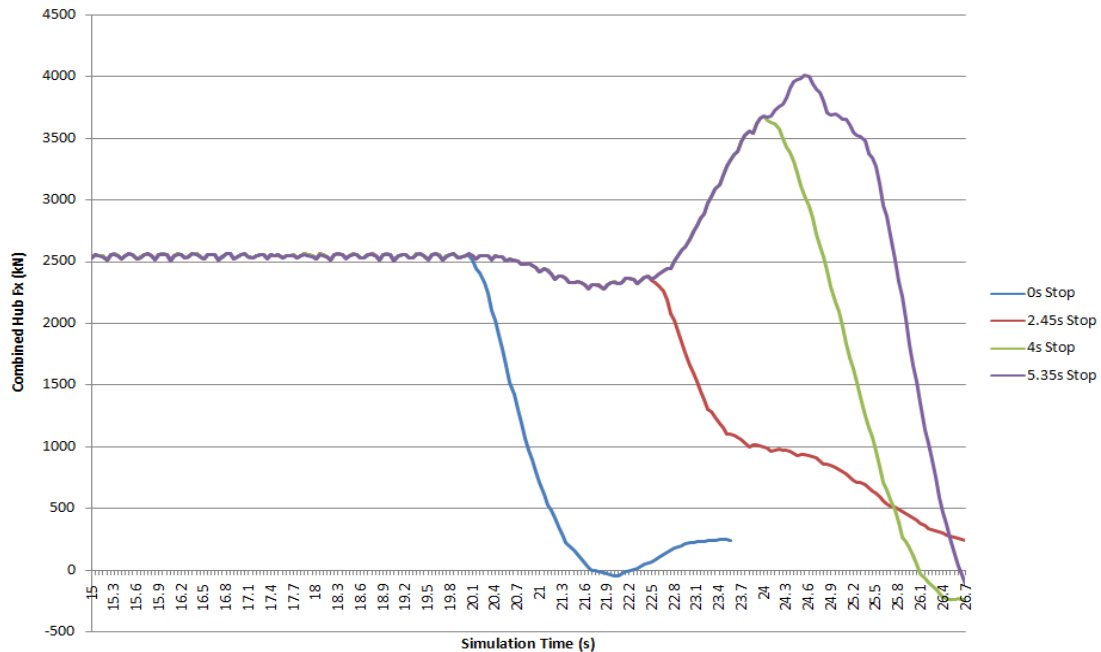


Figure 5-14 - DLC2.3: Effect of Gust Phasing on Total Hub Fx

The standard dictates that simulations be carried out at 2m/s above and below rated speed so as to check that rated speed does indeed equal the worst-case loading. It also acts as a check against the sensitivity of the rotors to small variations in wind speed.

Figure 5-15 shows the results of three different bladed simulations examining the combined hub Fx of the whole MRS array during an emergency shutdown during an extreme operating gust (DLC2.3). The shutdown is chosen to occur 4 seconds into the 10.5 period gust. The runs are labelled a3, c3 and d3 to represent the average hub wind speed of 11m/s, 13m/s and 9m/s respectively. Clearly the shutdown procedure with the average wind speed of 11m/s represents the ultimate loading on the structure.

It is worth repeating that not every rotor in the array will be experiencing a local wind speed equivalent to rated (assuming non-zero shear) and therefore its individual hub Fx may not be at a maximum even when the whole array is at its maximum. It could be suggested that an average of 11m/s over the array would see the most turbines closest to their peak hub Fx when compared to any other average and this lends credence to the practice of defining a single effective hub wind speed.

DLC2.3 - Total Hub Fx Loading (4s) at Vr, Vr+2, Vr-2

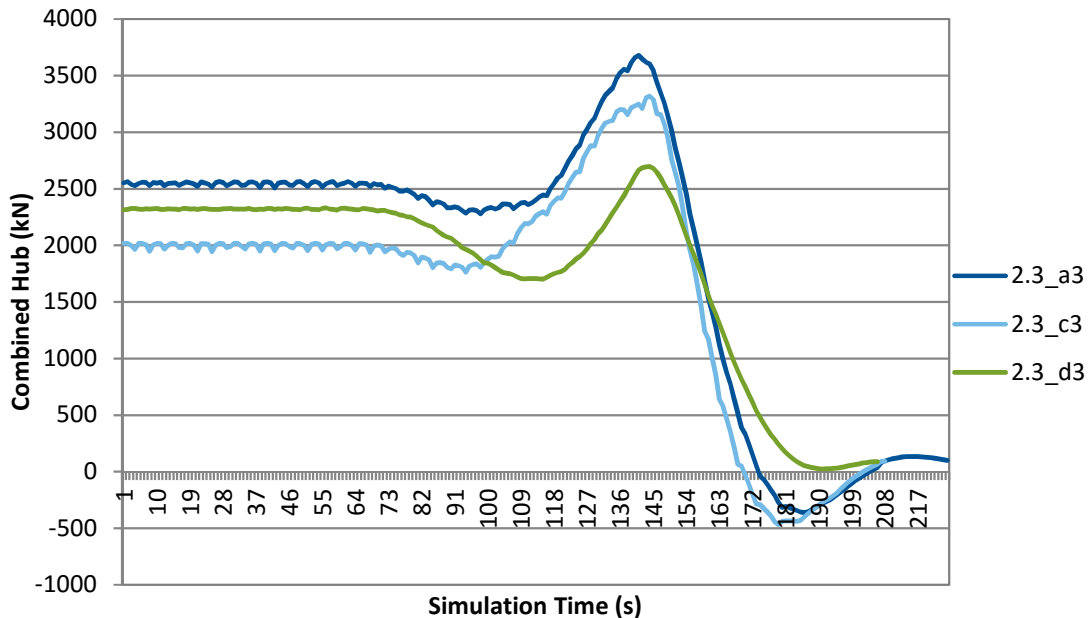


Figure 5-15 - DLC2.3; Comparison of Combined Fx during E-Stop around Rated

During the shutdown procedure the main variable controlling the rate at which the turbines shutdown before the application of any mechanical brake is the pitching of the blades. It follows that the faster the emergency pitch rate, the faster individual rotors will come to a halt. During an emergency stop procedure, the control system attempts to pitch all the rotor blades using the maximum available/defined pitch rate. This pitch rate is usually determined during the design phase and is only limited by mechanical considerations.

It was suggested that having a slow pitch rate might adversely affect the multi-rotor system – particularly if it caused multiple individual peak Fx’s to coincide. The DLC2.3 simulations were run three times at rated wind speed with the emergency stop procedure utilising pitch rates of 9, 12 and 15 deg/s.

Figure 5-16 shows the effect on the loading caused by the various pitch rates and it suggests that the problematic assumption is not the case – despite the fact that some individual rotors do experience local differences in loading of 1%.

Pitch rate therefore only determines the rate at which the rotors come to a standstill and can be set independent of overall structural considerations - though considerations of local blade forces may still be an issue.

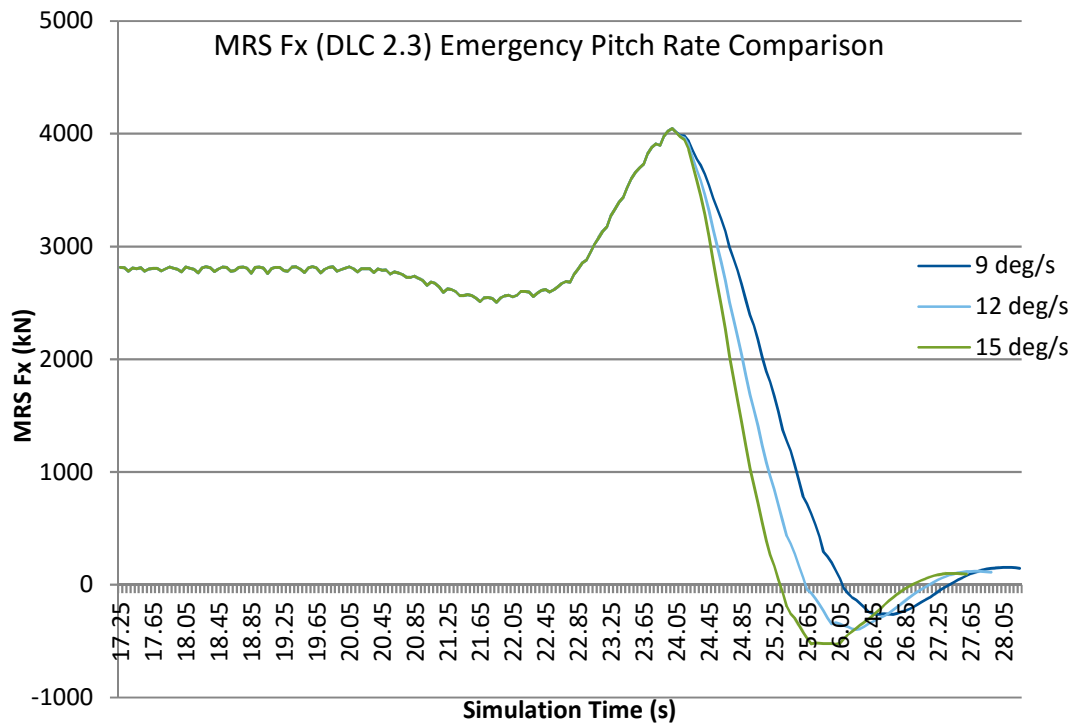


Figure 5-16 - Pitch Rate Comparison During E-stop

Due to initial software limitations in Bladed, rotor azimuths were limited to starting at zero degrees. This meant that each of the 45 rotors began at this same starting angle and as the simulation progressed would work themselves into six groups of azimuthal position due to the non turbulent nature of the wind in the transient load cases. Given that rotor thrust is dependent on azimuthal position, it was proposed that this shoe-horning of rotors into only 6 groups could potentially cause unrealistic low or high loading.

This limitation was in place during the bulk of the loading simulations due to no other alternative being in place. However, Bladed was later updated by the developers to include the option of setting rotor azimuths to random positions from the offset. This in turn would allow N amounts of rotor azimuths to be possible and potentially average out any abnormal loading previously encountered.

Figure 5-17 shows the DLC2.3 simulation run once with each rotor beginning at 0 degrees azimuthal angle and once again using random azimuthal angles for each of the rotors. While there is potentially 45 different azimuths in play whereas before there were 6, the effect of this is somewhat dampened by the fact that there is effectively only 120 degrees to play with-in a 3-rotor system before symmetry takes hold (in a coherent wind).

The only noticeable action random starting azimuths serves are to smooth out the periodic cyclic variations which are more noticeable in a system utilising only a few groups of azimuthal starting positions. One might expect this given that randomness leads to more averaging than coherence as rule.

Lastly, this final simulation confirmed that it is safe to assume that all previously run simulations remain valid despite having been subject to restrictions posed by the rotor azimuths.

DLC 2.3 - Effect of Azimuth Position on Total Hub Fx Loading

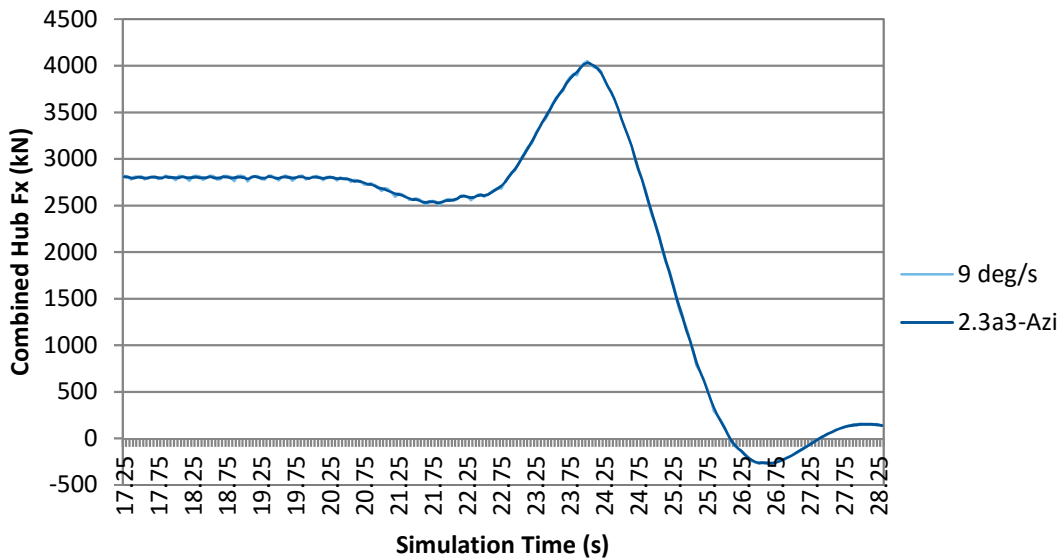


Figure 5-17 - Effect of Random Starting Azimuth Angles

For comparative purposes with the other run simulations, the statistical values for DLC2.3a3 (worst-case) are presented in

Table 5-6.

Hub Fx	Statistics from Total Sum of Rotors	Average per Rotor for 45 Rotor Array (sum / 45)	Averages of Individual Rotor Statistics	Statistics of Rotor 8 (worst-case)	45 x Rotor 16 (coherent worst-case)
Mean (kN)	2,571	57.13	51.1	60.8	2,736
Maximum (kN)	4,010	89.11	96.6	116.1	5,224

Std. Deviation (kN)	462	10.27	21.9	24.0	1,080
---------------------	-----	-------	------	------	-------

Table 5-6 - Statistics of Hub Fx DLC2.3a3

5.5.5 DLC-4.1 (NWP) - Fatigue Loads During Shutdown

Self-explanatory fatigue loads during shutdown for three different types of shutdown scenario; cut-in, cut-out and rated.

5.5.6 DLC-4.2 (EOG) - Ultimate Loads During Shutdown

Overview;

DLC4.2 refers to a normal stop under an extreme operating gust. There are two instances in which such a condition might occur; either the localised wind speed exceeds a pre-defined maximum causing the stop logic within the controller to initiate a stop or the coincidental planned or unplanned stoppage of a wind turbine during a unpredictable extreme gust. In both conditions the controller is designed to operate in such a way as to minimize loading on the rotor and thereby avoid any potential damage.

The coincidence of a normal stop with an extreme operating gust is one that can normally be avoided if the control system has measurement of the incident wind field. However, the standard dictates that the rotor and structure should still be designed to cope with such a load case.

DLC4.2 has the essentially the same simulation parameters as DLC2.3 but utilising a normal stop as opposed to emergency stop. In this load case the control requirement is less demanding and therefore designed to reduce loading.

Key Simulation Parameters;

- Simulation Time: 45s, Wind Shear Exponent: 0.14, Rotor Azimuths: Equal
- Wind Speed: 11 m/s, Gust speed: +6.67m/s, Start Time: 30s, Period: 10.5s
- Wind Direction: 0 deg
- Emergency Stop: 0s, 2.45s, 4s & 5.35s into gust

Results;

The simulations for DLC4.2 are carried out in the same way as DLC2.3 and as such 4-simulations are carried out using stops during 4 different phases of the extreme operating gust (EOG). Figure 5-18 shows that in the case of the normal stop, both the 4s and 5.35s phases can be attributed to the ultimate load scenarios within this load case. In the same way as in DLC2.3, the normal stop is modelled in bladed as a synchronous shutdown of each of the 444kW rotors and because of the synchronicity of the hub Fx loadings, the shutdown results in maximum hub Fx loading on the array.

The ultimate loading measured as the combined hub Fx is apparent with shutdown phasing 4 seconds into the EOG. The total loading of 4,195kN is marginally higher than the peak loading observed on the array during the 5.35s phased gust of DLC2.3, which was 4,000kN.

The IEC standard divides load cases into abnormal and normal load cases and attributes load modification or safety factors to each load case. In this case aerodynamic loadings taken from DLC2.3 are to be modified by a factor of 1.1 (abnormal) and loadings taken from DLC4.2 be modified by a factor of 1.35 (normal). Multiplying by these factors makes the DLC4.2 normal stop case significantly larger in comparison to the emergency stop case, see Figure 5-19.

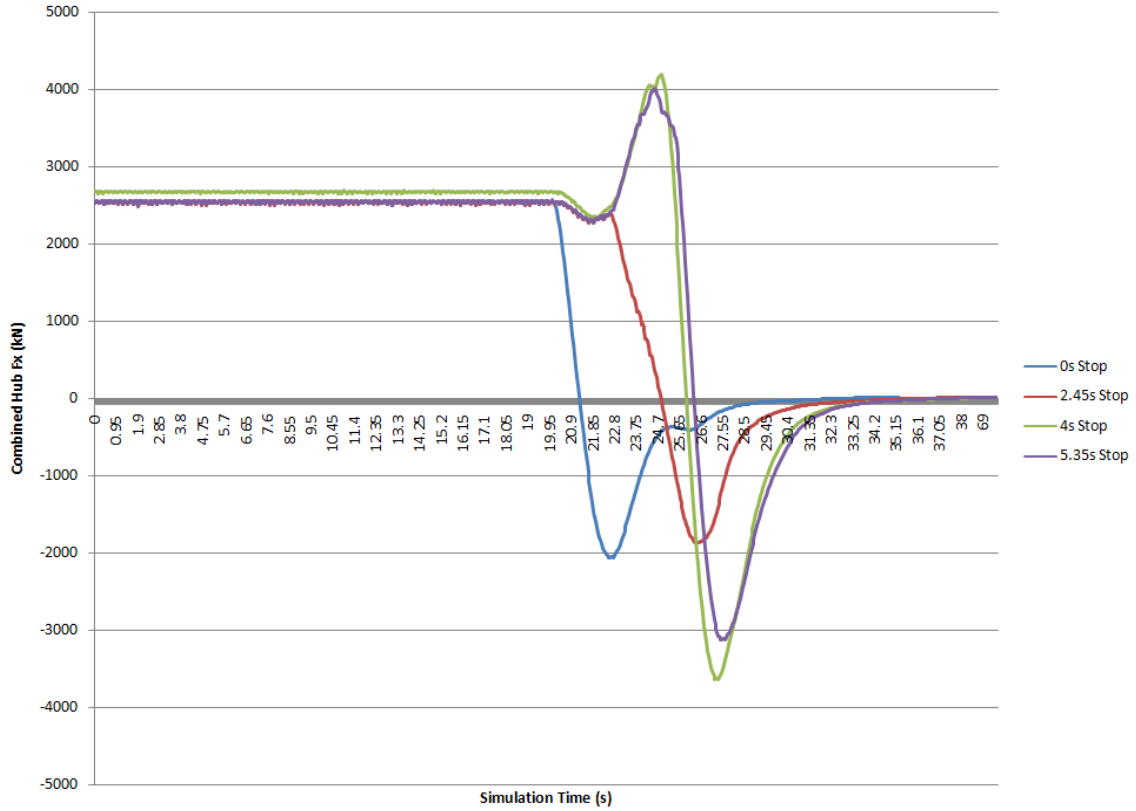


Figure 5-18 - DLC4.2: Effect of Gust Phasing on Total Hub Fx

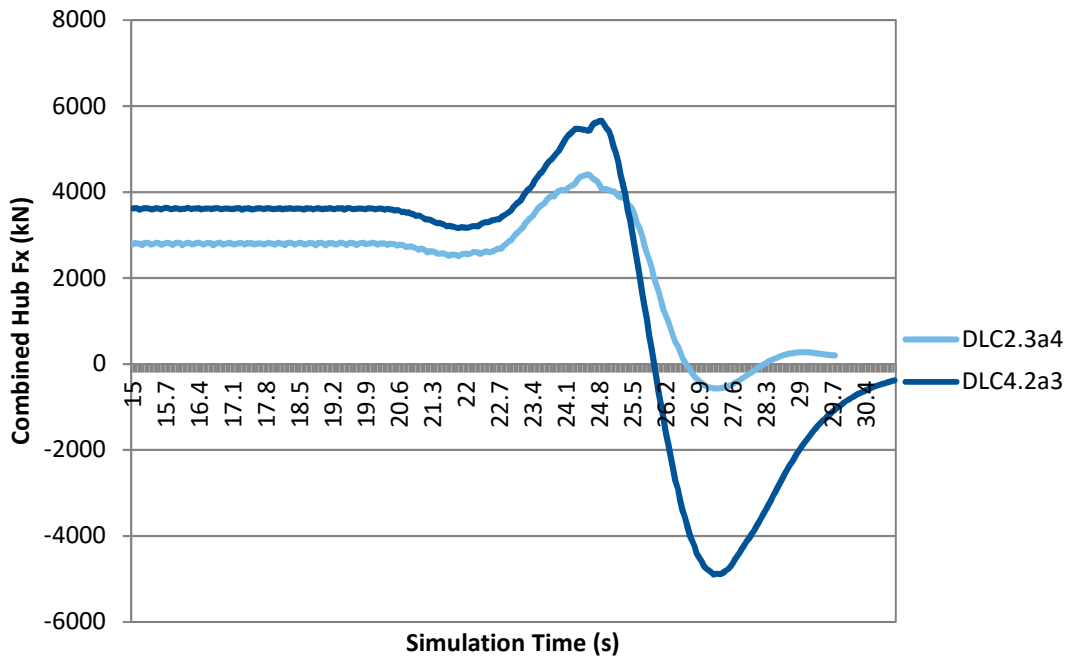


Figure 5-19 - Comparison of Shutdown Cases DLC2.3a3 and DLC4.2a3 (Safety Factors Applied)

To complete the load cases, a further set of simulations is run at cut-out wind speed using the 4 different gust phasings, Figure 5-20. It is once again assumed that single rotors do not independently trip their cut-out conditions prior to the event. Perhaps unsurprisingly, even the worst case loading at cut-out is considerably less when compared to the runs around rated for the same reasons touched in DLC2.3.

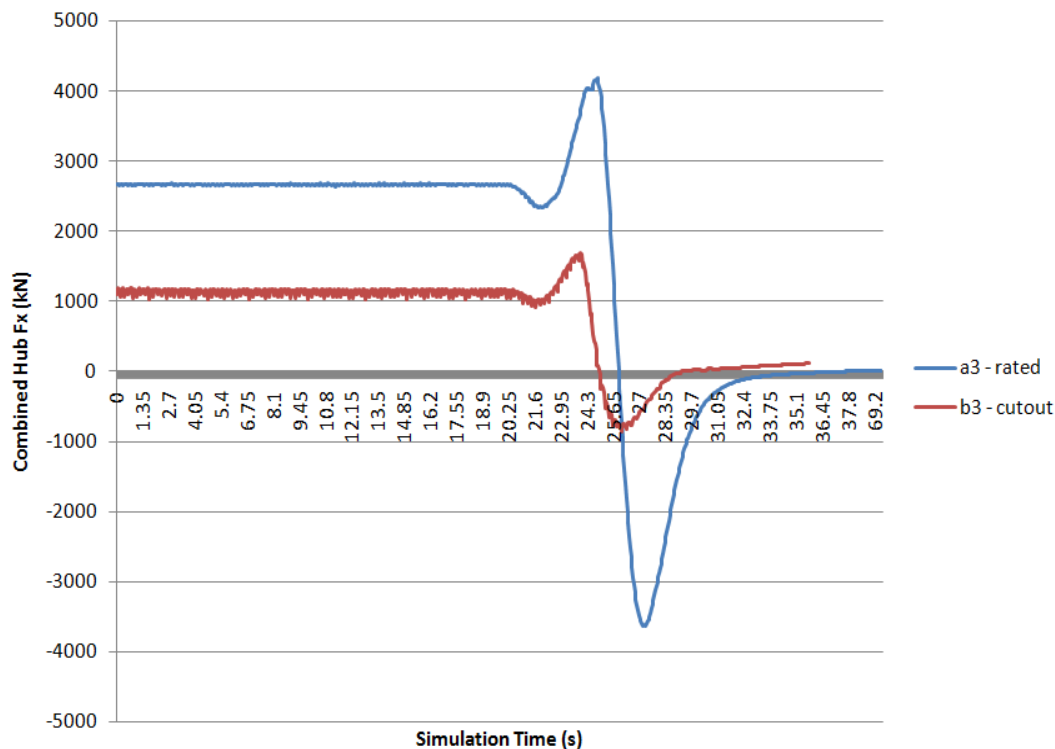


Figure 5-20 - Comparison of Hub Fx Loading at Rated and Cutout Wind Speeds

Discussion;

At this stage it is important to evaluate once again which of the load cases appear to cause the ultimate loading on the array.

Figure 5-21 shows a plot of the worst-case loading for each of the load cases already reviewed; DLC1.3/1.4/2.3 and 4.2. To make a valid comparison, safety factors have been applied in accordance with Table 5-1 - Abbreviated Load Cases taken from IEC61400-3. At this point, the normal shutdown condition of DLC4.2 appears to be the design limiting case in terms of combined hub Fx by a significant margin.

In fact, all three load cases containing normal or emergency stop procedures and coherent wind out- size the normal power production load case DLC1.3. This raises several key points that need to be addressed in the following sections;

Are the effects of coherence and turbulent wind directly opposed in loading terms on the multi-rotor array?

Can the coherent/synchronous shutdown events be phased in some way so as to destroy the peak loading present in each of the combined hub Fx time series?

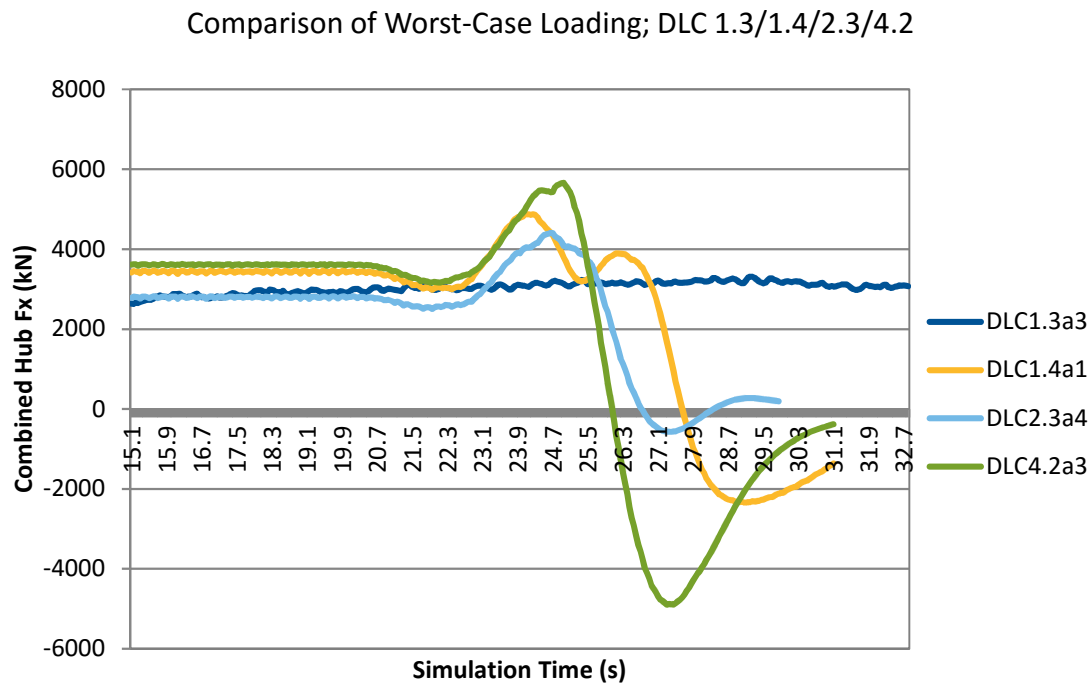


Figure 5-21 - Comparison of Total Hub Fx in all Examined Cases (Safety Factors Applied)

It is certainly the case that some of these design scenarios are so unfavourable that they should be completely avoided. With some staggering/phasing of the shutdown procedure, which may be possible under certain shutdown conditions, it is feasible to get the total Fx values much lower.

While load cases such as DLC2.3, which is an emergency stop due to a global event such as grid loss, might be limited in its ability to stagger the shutdown of the rotors. DLC4.2 on the other-hand is a normal shut-down, there is therefore some leeway with regards to the shutdown of the array in the absence of any time critical circumstances, though this is not

modelled in Figure 5-18, Figure 5-19 or Figure 5-21. It is felt therefore that normal stop conditions have a key advantage when it comes to loading on the array.

For completeness,

Table 5-7 presents the full statistics for the 4s phased shutdown for a direct comparison with the other load cases.

Hub Fx	Statistics from Total Sum of Rotors	Average per Rotor for 45 Rotor Array (sum / 45)	Averages of Individual Rotor Statistics	Statistics of Rotor 16 (worst-case)	45 x Rotor 16 (coherent worst-case)
Mean (kN)	1,536	34.13	34.15	34.35	1,545
Maximum (kN)	4,195	93.2	97.2	119.6	5,382
Std. Deviation (kN)	1,780	39.6	40.3	43.6	1,962

Table 5-7 - Statistics of Hub Fx DLC4.2

5.5.7 DLC-6.1 (EWM) - Idling Ultimate Loads due to 50 Year Gust

Overview;

The 50-year gust is an event that has a such low probability that it may occur on average once every 50 years. It is commonly assumed that over a typical turbine lifespan of 20 years the chances of the 50-year gust occurring during another major fault or extremely unfavourable event are almost negligible and for all intents and purposes the combination of the two need not be designed for. Instead, the design standard dictates that the only other condition that need be met is a yaw misalignment of plus or minus 15 degrees.

Key Simulation Parameters;

- Simulation Time: 65s, Wind Shear Exponent: 0.14, Rotor Azimuths: Equal
- Wind Speed: 70 m/s, Event Start Time: 30s, Period: 10.5s
- Starting Yaw: 0 deg, Yaw Misalignment: +-15 deg

Results;

For a Class 1A site the 50-year gust corresponds to a 70m/s local wind speed gusting for 30s with a change of direction. While the standard dictates that this gust be coherent in nature there has been recent discussion amongst academics and industry that the nature of coherent gusts may not be applicable at the scale that 20MW machines find themselves in (several hundred metres vertically and horizontally). To check against this

coherent nature and provide further validation outside the standard, an additional set of simulations were run with a turbulent wind file (of average wind speed 70m/s) as a base. The four sets of data are presented in Figure 5-22, with the turbulent and coherent cases clearly characterised by their respective plots.

The worst-case load case (DLC6.1b2) with turbulent wind represents the worst-case loading in this case and therefore it is from this run that the statistics presented in Figure 5-23,

Table 5-8 are taken from.

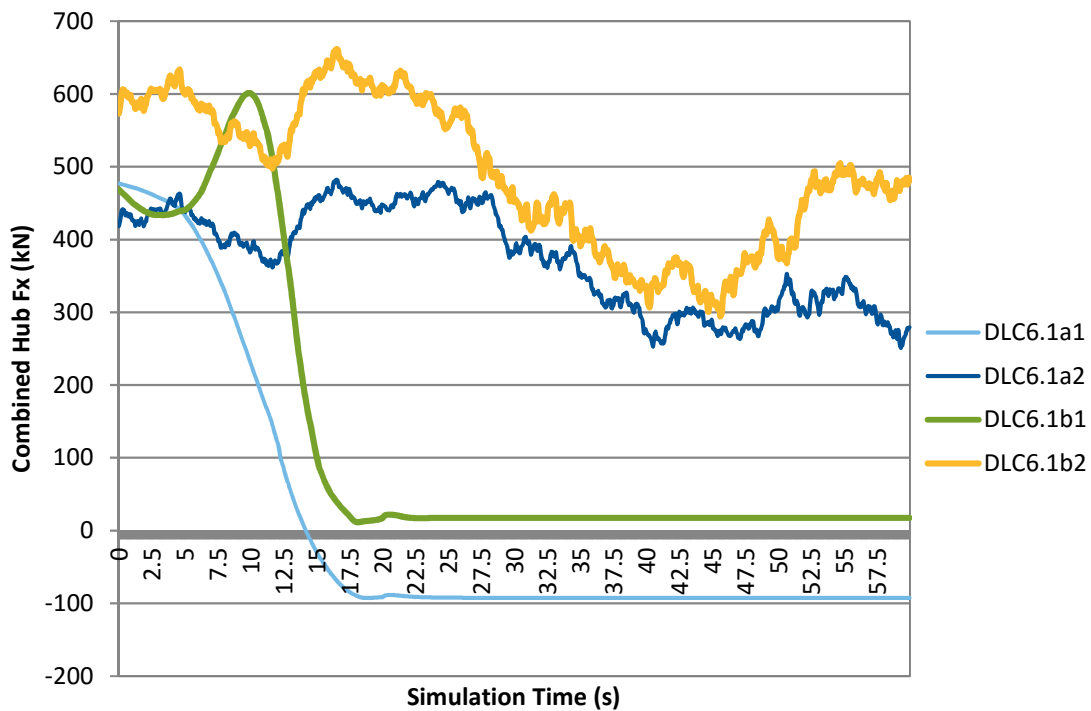


Figure 5-22 - DLC6.1a1; Comparison of Turbulent and Coherent Wind in the 50-Year Gust (Safety Factors Applied)

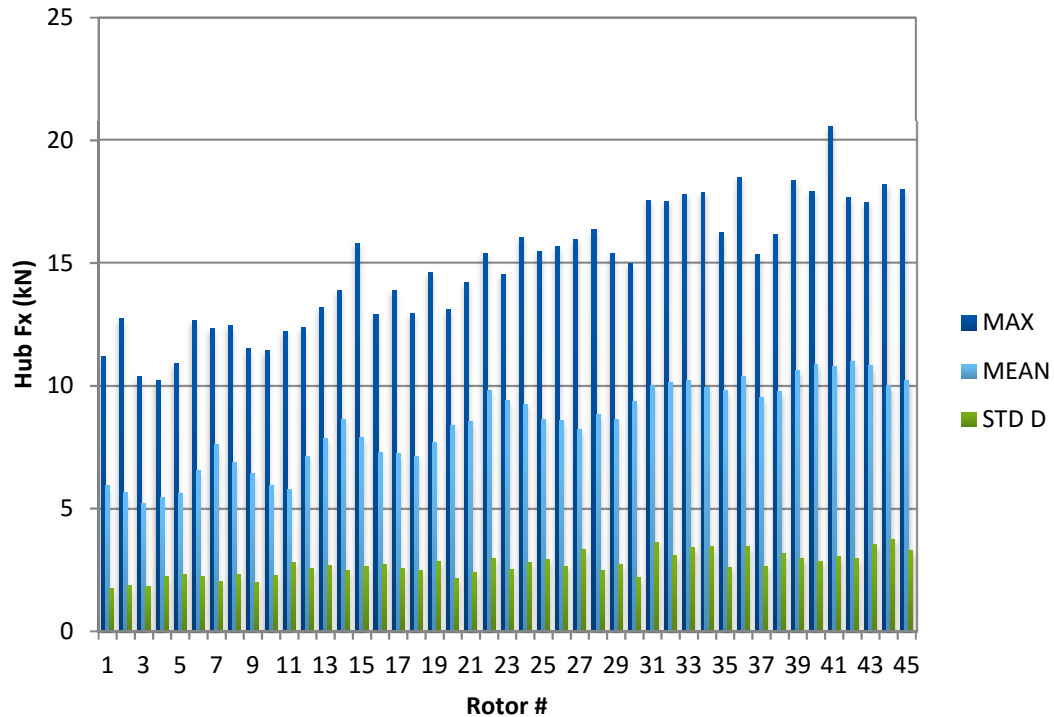


Figure 5-23 - DLC6.1b1; Individual Hub Fx Statistics

Hub Fx	Statistics from Total Sum of Rotors	Average per Rotor for 45 Rotor Array (sum / 45)	Averages of Individual Rotor Statistics	Statistics of Rotor 41 (worst-case)	45 x Rotor 41 (coherent worst-case)
Mean (kN)	374	8.31	8.44	10.8	486
Maximum (kN)	482.22	10.72	14.89	20.58	926.1
Std. Deviation (kN)	69.07	1.535	2.7	3.05	137.25

Table 5-8 - Statistics of Hub Fx DLC6.1

Discussion;

These results show that the load case DLC6.1 of a 50-year gust with a positive or negative 15 degree yaw misalignment are no-where near designing load cases in structural terms. The ultimate loading in DLC6.1b2 is only 600kN with safety factors applied whereas the likes of DLC1.3 are dealing with loads in excess of 3000kN.

Interestingly, while in DLC1.4 there was no discernible difference in a positive or negative wind direction change (in essence the same as a yaw error) in this case the wind direction

does appear to account for a small difference (around 10%) in terms of Hub Fx loading. However, we are only concerned with ultimate loadings and neither case represents that.

5.5.8 DLC-6.2 (EWM) - Idling Ultimate Loads due to 50 Year Gust and Grid Loss (Effectively Yaw System Non-Operational)

Overview;

The second case of the 50-year gust assumes that the yaw system is non operational. In the case of a single rotor this would usually be a result of grid loss – though in the multi-rotor on a water bearing the effect of such a condition is less clear. The standard dictates that the extreme wind may come from other unfavourable yaw angles and that the system may be aligned unfavourably. As such the simulation is run at various points around a full 360 degrees around the structure. In this case only the negative angles are shown as these represent higher ultimate loading than positive angles - as discussed in the previous section.

Key Simulation Parameters;

- Simulation Time: 90s, Wind Shear Exponent: 0.14, Rotor Azimuths: Equal
- Wind Speed: 70 m/s, Start Time: 20s, Period: 10s
- Wind Direction: 0 deg, Wind Change: -45, -60, -90, -120, -180 deg

Results;

Figure 5-24 presents the time series of total hub Fx for each of the 5 simulations run. In terms of hub Fx loading, the ultimate loading appears to be at both 0 degrees and 180 degrees as one would intuitively expect. While the first four runs represent a change in wind direction, the 180 degree run represent as full reversal of the wind direction, followed by a return to the original direction. In this respect it is once the wind changes direction fully that the ultimate -Fx loading is experienced and this exceeds that experienced at 0 degrees.

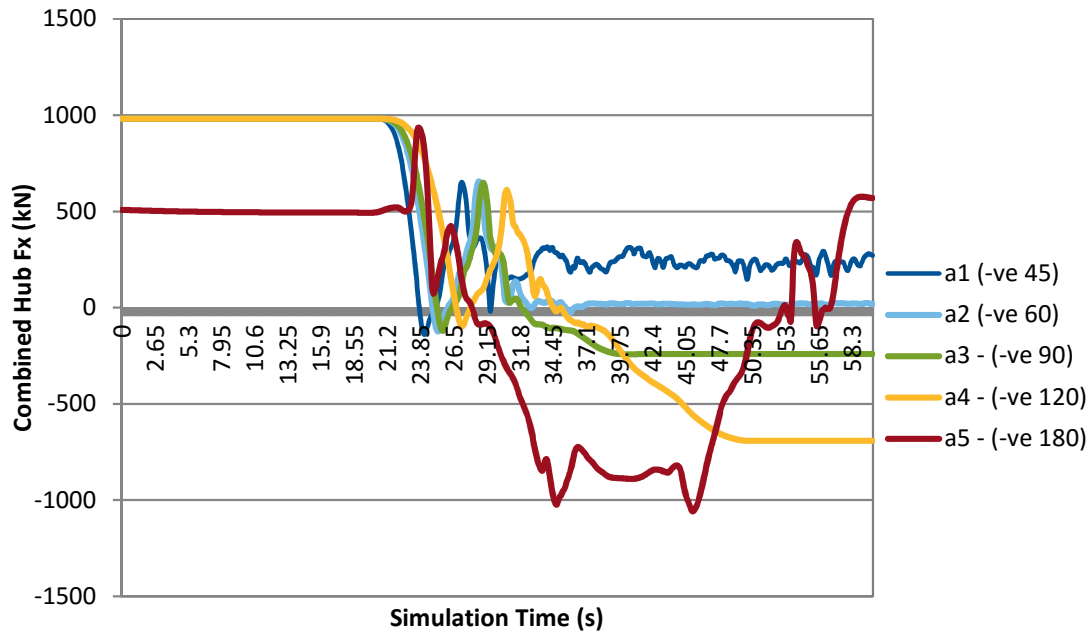


Figure 5-24 - DLC6.2; 50 Year Gust and Extreme Yaw Misalignment (Safety Factors Applied)

Again the increase in loading even at highly unfavourable yaw angles is not a driving factor in structural design for the purposes of ultimate loads – being significantly less than DLC1.3, with 1,000kN and 3,000kN respectively.

Discussion;

The only notable discussion point in DLC6.2 is as a consequence of the extreme -Fx loading when the wind has been fully reversed. This is not unexpected given that the rear of the proposed multi-rotor comprises a multitude of interconnecting members and bracing struts. It is therefore likely that the overall structural blockage is increased when the wind is blowing from the downwind direction which results in the increased loading in comparison to the normal loading from the upwind direction.

It might be proposed that aerodynamic fairings could be used to mitigate the loads on the structure in these extreme wind cases. This was a serious consideration at the start of the project when it was believed that blockage affects and structure thrust would be the overriding design case for the multi-rotor system. Both DLC6.1 and 6.2 show this to not be the case.

5.5.9 DLC-6.3 (EWM) - Idling Ultimate Loads with 1 Year Gust & Extreme Yaw Misalignment

Overview;

The final simulation of DLC6.3 is a 1 year gust of 50m/s coinciding with an extreme yaw misalignment which in this case is considered to be +/- 30 degrees. This simulation, which on its basis would appear to be less impactful than DLC6.2 is included for completeness.

Key Simulation Parameters;

- Simulation Time: 65s, Wind Shear Exponent: 0.14, Rotor Azimuths: Equal
- Wind Speed: 50 m/s, Start Time: 30s, Period: 10.5s
- Wind Direction: 0 deg, Wind Change: +/-30 deg

Results;

The total hub Fx loading in this final load case is presented in

Figure 5-25 and shows that a yaw misalignment does indeed lead to less overall hub Fx loading than any of the other considered load cases.

This lower loading is not unexpected and therefore no further discussion will be proposed at this point.

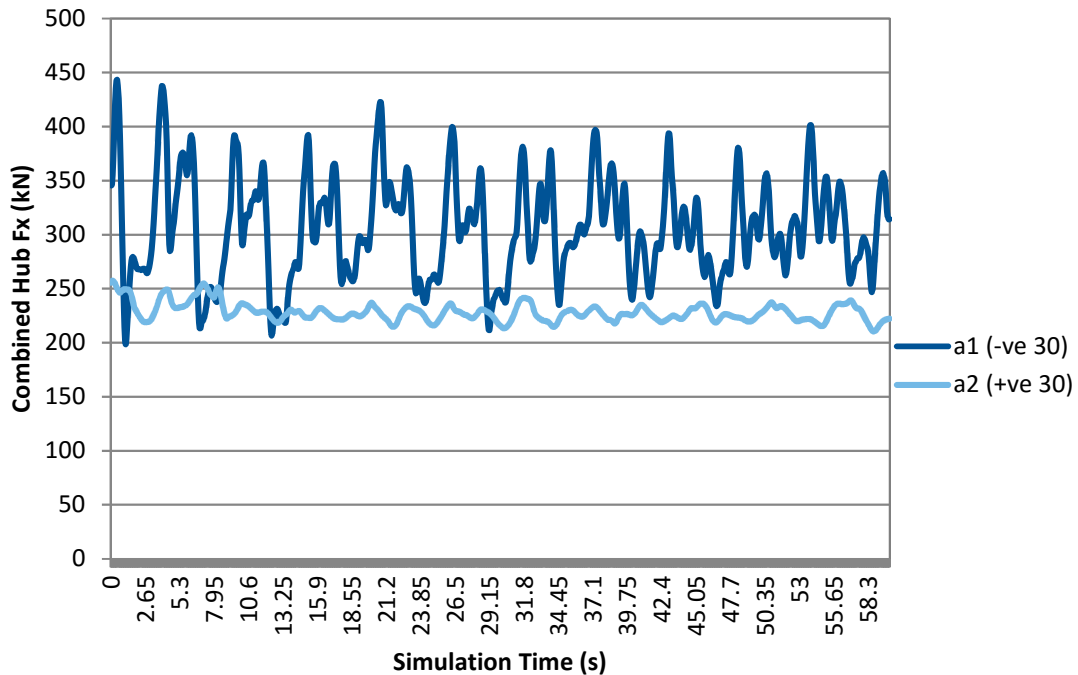


Figure 5-25 - DLC6.3; 1 Year Gust and Yaw Misalignment of +/-30 (Safety Factors Applied)

5.6 LOAD CASE OVERVIEW

In total seven load cases have been fully investigated, with a total of 37 individual simulations encompassing the full spectrum of possible environmental conditions the multi-rotor system might be subjected to. In whole these simulations provide the ultimate loads for use in later finite element modelling and structural calculations with a few caveats.

As previously stated, the primary load of interest is Fx loading and associated base moment loading which drives support structure design of both the single rotor and multi-rotor.

Table 5-9 presents a summary of the combined hub Fx loadings on the multi-rotor array for the seven examined ultimate load cases. In each case only the ultimate load and corresponding simulation run is recorded for each of the seven load cases, with the others being disregarded due to lower overall forces.

Load Case	Maximum Total Hub Fx
<i>DLC 1.3a3</i>	Constant Wind 4451kN
<i>DLC 1.4b1</i>	Fully Coherent 4875.5kN
<i>DLC 2.3a4</i>	Fully Coherent 4411.3kN
<i>DLC 4.2a3</i>	Fully Coherent 5663.7kN
<i>DLC 6.1</i>	Fully Coherent 601.2kN
<i>DLC 6.2</i>	Constant Wind 936kN
<i>DLC 6.3</i>	Constant Wind 443.4kN

Table 5-9 - DLC Comparison Summary; 1st column - load case name, 2nd column - results

The results are presented at this stage as a single column representing the maximum load for each load case in accordance with the standard and also in graphical form (Figure 5-26). They show a clear correspondence between maximum hub Fx loading and shutdown events such as DLC1.4, DLC2.3 and DLC4.2. In fact, comparing the power production case of DLC1.3 which represents maximum loading under extreme turbulence the force ratio is 4.4:5.6 when compared to the synchronous shutdown event caused by an extreme operating gust and grid loss in DLC4.2. The initial suggestion is therefore that these synchronous shutdowns represent the ultimate loading towards which the structure must be designed. However, it is very important to note that these scenarios were originally defined in the IEC 61400-1 (edition 3) standard before wind turbines designs routinely exceeded 5MW scale and therefore there is a strong case that these wind conditions may not be readily applicable at 20MW scale. These aspects of the standard are currently being debated amongst industry and academics.

To fully understand why these results may no longer be fully applicable towards the multi-rotor, or even perhaps the single 20MW rotor requires some additional investigation and inevitable re-simulation as presented in the following discussion sections.

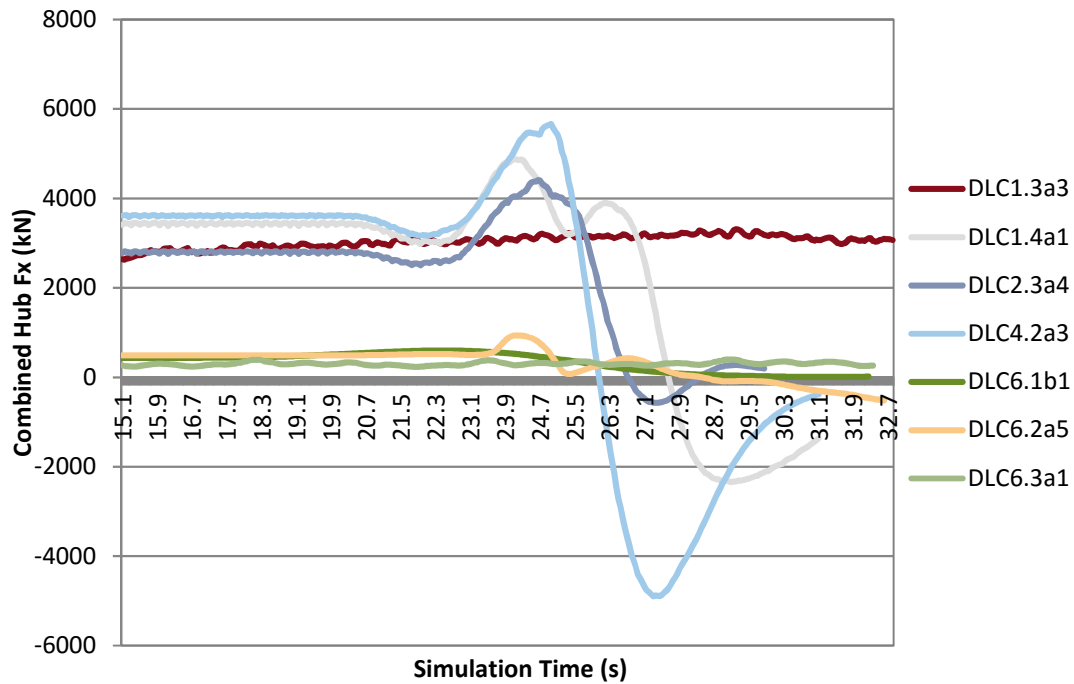


Figure 5-26 - Comparison of Total Hub Fx Loading (All Cases)

5.7 DISCUSSION

5.7.1 Load Averaging

The first and arguably the most interesting and structurally useful discussion point is that of the load averaging effect provided naturally by the multi-rotor system. This load averaging effect results in much lower ultimate loadings than would be expected from the examination of loadings on a single rotor in an array. In other words, the single worst, or even a combination of the worst individual rotor loads does not necessarily equate to the overall worst structural load. To examine this averaging aspect we must first investigate the 444kW single rotors characteristics.

Figure 5-27 shows the relationship of thrust to wind speed for the 444kW machine under power production. Configured as a pitch regulated machine, peak loading occurs at rated wind speed. The single 20MW machine by comparison retains the same relationship between thrust and wind speed – being simply an up-scaled version of the same wind turbine.

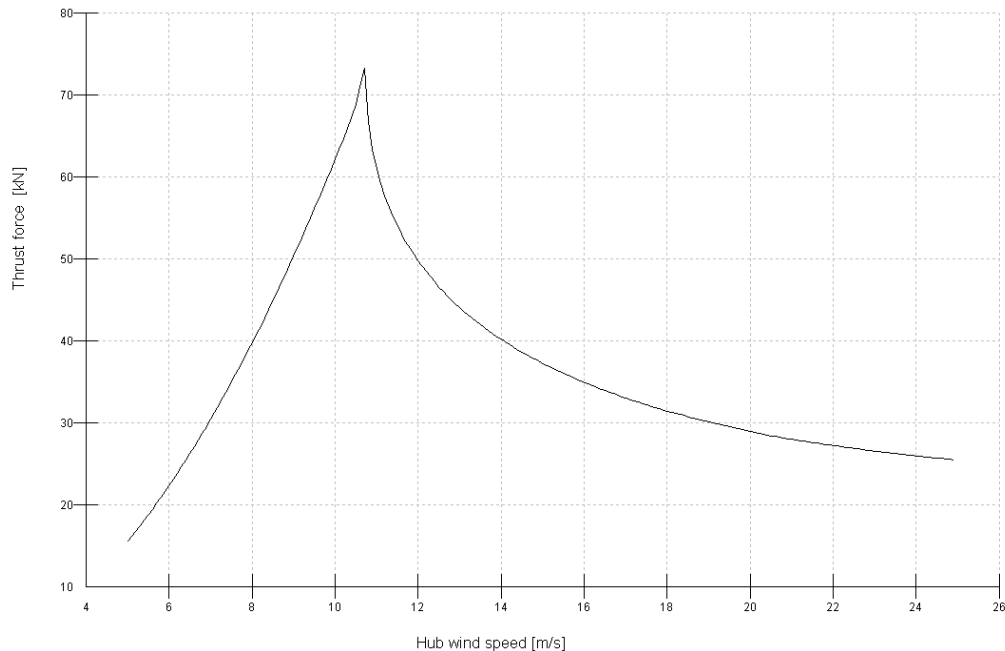


Figure 5-27 – Hub Fx Characteristic Curve

For the 444kW machine the maximum hub Fx loading 73.28kN. The theoretical maximum thrust in the multi rotor system would therefore occur if or when every turbine in the array is at rated wind speed. If these conditions were met then the thrust would be the

equivalent to a 3297.87kN (45x73.28) force at effective hub height (115m). However, this maximum is somewhat misleading given that real wind conditions should never be so coherent as to cause this maximum to occur. Any amount of spatial variation in wind strength which causes individual turbines local wind velocity to deviate away from rated wind speed will alter the total thrust and reduce it below this theoretical maximum.

For example, consider a highly coherent case of an extreme gust coupled with a normal stop, i.e. DLC4.2a3 with 0% turbulence but with a large amount of shear (0.14 exponent). The MRS system is not operating at maximum thrust due to shear across the array even when wind speed at the effective hub height is defined as being at close to rated (11m/s).

Table 5-10 presents the total hub Fx loading for each of the rows in the array, where the shear can clearly be seen in the corresponding average wind speeds.

If each of these rows is weighted according to the number of turbines present then we see that the total effective thrust (hub Fx) on the structure/tower is only 77.24% of the theoretical maximum.

To test that this is not an anomaly, a second run is carried out using a different seed and a slightly different wind speed (10.7m/s). When wind speed at hub height reaches 10.7m/s the maximum power production thrust is found to be 2,683kN or 81.38% of the theoretical maximum.

Row Number	Wind Speed (m/s)	Thrust (% of max)
1	9.59	76.59
2	10.45	92.83
3	11.02	83.29
4	11.45	74.51
5	11.80	70.06
6	12.10	66.98
Weighted		77.24

Table 5-10 - Maximum Steady-State Thrust in Coherent Load Case DLC4.2a3

These results suggest that the multi-rotor array will never actually achieve its theoretical maximum thrust under normal wind conditions. While this experiment was carried out using a value of shear more consistent with rolling hills rather than a calm sea, they were carried out with 0% turbulence. It is not considered likely that zero turbulence or shear could exist over a 350x300m² area at any average wind speed.

In normal turbulence conditions, the total thrust across the array becomes less coherent and therefore forces will drop on average. The worst-case power-production load case is considered to be DLC1.3a3, that is, power production around rated with I1, I2, and I3 turbulence intensities set at 39.9%, 24.4% and 17.47% respectively. The combined maximum thrust is determined to be 2421.59kN which represents an equivalent thrust level of 73.42% compared to that of the multi-rotor theoretical maximum. However the average thrust level is considerably lower at 1995.2kN or 60.5% of this same maximum throughout even the worst-case power production scenario. This suggests that up to 17% of maximum thrust loading can be avoided when operating under normal wind turbulence intensity.

Given that the wind speed over the whole array is not fully coherent at any point in time, the combination of rotor thrusts across the array do not necessarily follow the F_x vs. wind speed curve of a typical rotor. Taking the average thrust per rotor at each wind speed and plotting this against the average wind speed at the array centre, i.e. hub height (

Figure 5-28) shows that the MRS equivalent curve maintains the same shape as that of Figure 5-27 but with much less definition. Notice that the peak normally seen around 10.8m/s has been completely destroyed by the averaging effect of the rotors. Indeed the total thrust force has been reduced below 55kN for individual rotors and down shifted in wind speed slightly.

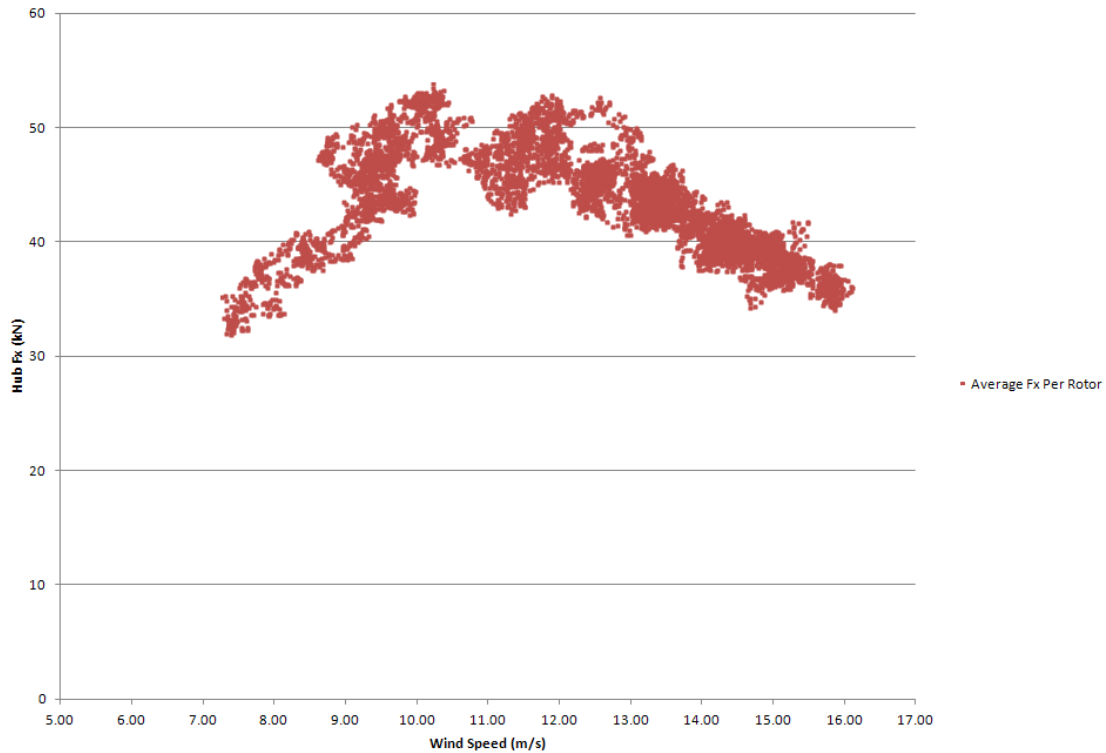


Figure 5-28 - Hub Fx vs. Wind Speed for Whole Multi-Rotor Array

These findings are partly skewed due to the fact that we can only define this curve with respect to the combined Fx's and wind speed at a single point in space but does highlight why hub Fx load reduction is possible even when the whole array is operating at rated wind speed. For convenience, the multi-rotor hub wind speed is defined as being the average wind speed seen across all the rotors in the array referred to a single point at the centre of the structure (in this example, 115m height). In contrast to the single 444kW machine example of Figure 5-27,

Figure 5-28 shows that it is not possible to identify a single equivalent or expected Fx hub loading at any particular wind speed, but rather a range of loadings in which the effective total hub Fx will fall. As a result, at normal operation at rated wind speed, the multi-rotor system will never experience a case whereby every single individual 444kW rotor is experiencing its theoretical maximum hub Fx loading at the same instant in time.

Taking this into account, the average maximum Fx per 444 kW rotor across the multi-rotor array is identified as 53.81kN – an average maximum taken from several DLC1.3 runs around rated. This calculated value is within 0.9kN of the singular worst-case hub Fx taken from the worst-case simulation (DLC1.3a3) which was found to be 52.89kN. The closeness of these two values suggests that the method of defining hub height as the

geographical centre of the array and the use of effective rotor averaging as a means of identifying likely ultimate loads is reasonable if not erring towards being conservative.

It is therefore highlighted that although it would appear that the theoretical worst-case loading for the multi-rotor array is 45×73.28 (3297.6kN), the realisable value is actually much lower (2421.6kN). This is one of the primary benefits of having many spatially distributed rotors that cannot all experience a single coherent wind speed.

5.7.2 Turbulence Loading

For a single multi-MW rotor the critical design loads nearly always arise as the result of some transient or variation in aerodynamic force across the entire length of a blade. These conditions undoubtedly occur in highly turbulent wind fields, which is why wind turbulence classification plays an important role in turbine design. One of the most unusual aspects of the multi-rotor system is that the critical design load is a result of a lack of turbulence as opposed to a high turbulence and that this contrasts sharply with a single rotor machine. This becomes more intuitive after understanding that any move towards coherent wind diminishes the desired averaging effect of loads that the multi-rotor system accomplishes.

In Figure 5-29, the total F_x is plotted for various classes of wind turbulence. The total hub F_x loading increases on average in less turbulent classes of wind (Class B and C) at rated wind speed when compared to total hub F_x under turbulence Class A. Apart from a small period where the Class 1A wind with a normal turbulence model peaked, the Class B and C normal turbulence models consistently see overall increased loading when compared to the class A wind extreme and normal turbulence models.

These results further suggest that the multi-rotor system reaches its peak load reduction capabilities in extreme wind environments. It also highlights that any form of coherent loading of individual rotors within the array will conspire to ultimately cause extreme design load cases for the whole structure. This latter point is especially critical given that the IEC-61400 standard makes use of several design load cases which base their analysis on extremely coherent wind events.

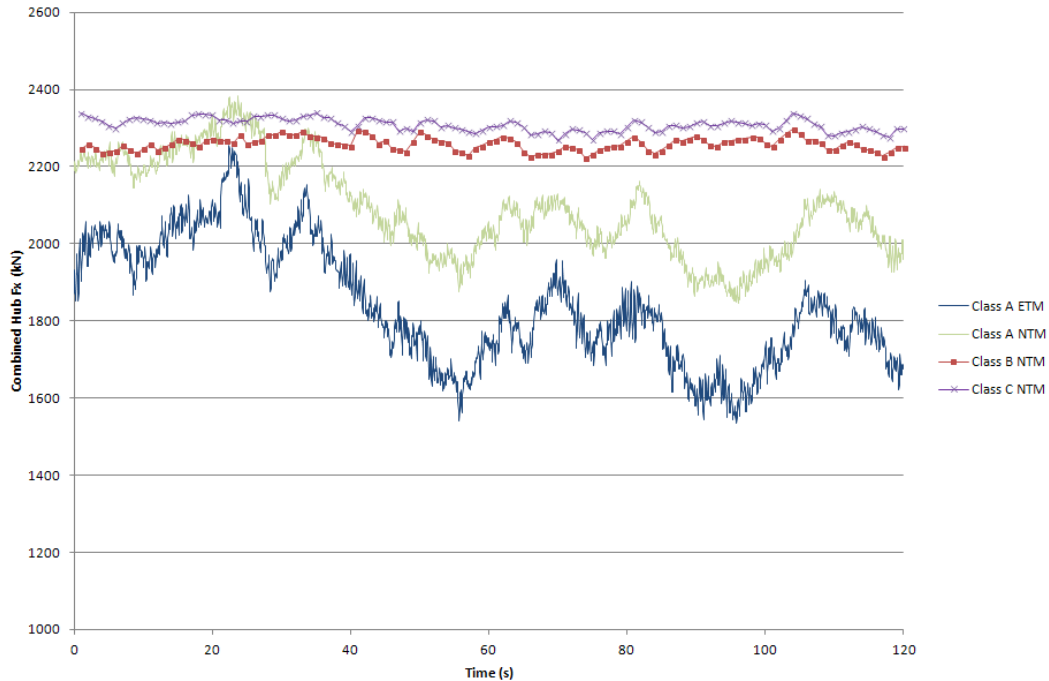


Figure 5-29 - Combined Fx Loading on MRS in Various Wind Classes

The multi-rotor system therefore finds itself in uncharted territory when considering loads from a design standpoint. Normally designers have to design against extremely turbulent events, some of which would otherwise cause the destruction of a conventional machine. For the multi-rotor the opposite effect is felt. It actually has less structural requirement the more the wind coherence is broken down by turbulence. This fact alone gives the multi-rotor some interesting advantages when considering potential turbulent sites on land where the wind speed is known to be consistently high but turbulent.

5.7.3 Phased Shutdowns

If we consider individual turbines it is likely that the general conditions that result in the shutdown of a single turbine do not apply to all 45-rotors on the array at once. Thus it may be that natural wind conditions result in a passive event caused by individual turbines tripping their shutdown conditions individually and therefore providing natural phasing of the total loading on the array. If this natural phasing does not occur, then it is not unreasonable to place limits on the controller so as to phase the shutdown of rotors, or at the very least to avoid simultaneous shutdown.

Naturally there are dozens of schemes for shutdown of the MRS array. The worst candidate is of course simultaneous shutdown of every rotor which would achieve its peak loadings as shown earlier in Figure 5-19. Regardless of gust speed, simultaneous

shutdown results in extreme loading in terms of hub Fx (as all the maximums combine in phase). The optimal choice would therefore be to shutdown the rotors one at a time.

Optimum loading is achieved by spacing the shutdown of each rotor by several seconds so as to match extreme maximum Fx with the preceding rotors minimum Fx and achieving some cancellation on the combined Fx. The phasing of shutdowns obviously depends on the gust. It is assumed that a gust period of 10.5 seconds is used as defined in the standard. The total shutdown time would therefore become $44 \times 2.35\text{s}$ (103.4s) with a phasing of 2.35s. This has the advantage of reducing the transient Fx to less than that of a single rotors maximum and brings the combined maximum in line with normal production loading as in DLC1.3.

For a relatively quick shutdown, two optional methods are 'pair phasing' and 'quad phasing'. That means shutting down the array 2 or 4 rotors at a time, utilising the symmetry of the arrangement to minimise yawing or overturning moments about the structures axis. The effect of both these methods is shown in Figure 5-30. The objective is to minimize the total maximum hub Fx while minimising the thrust reversal normally seen when shutting down, which can contribute significantly to the fatigue of a wind turbine.

Quad phasing the shutdown results in a peak Hub Fx loading of 2632kN and takes approximately 30 seconds to complete. Pair phasing shutdown yields a lower Hub Fx of 2590kN but takes twice as long. The benefits of shutting down over any longer period than the 60-seconds provided by pair phasing quickly diminishes as the theoretical minimum that could be obtained would be the steady-state average 2545.65kN plus the average standard deviation of a single rotor during shutdown (35.97kN), that is 2581.62kN.

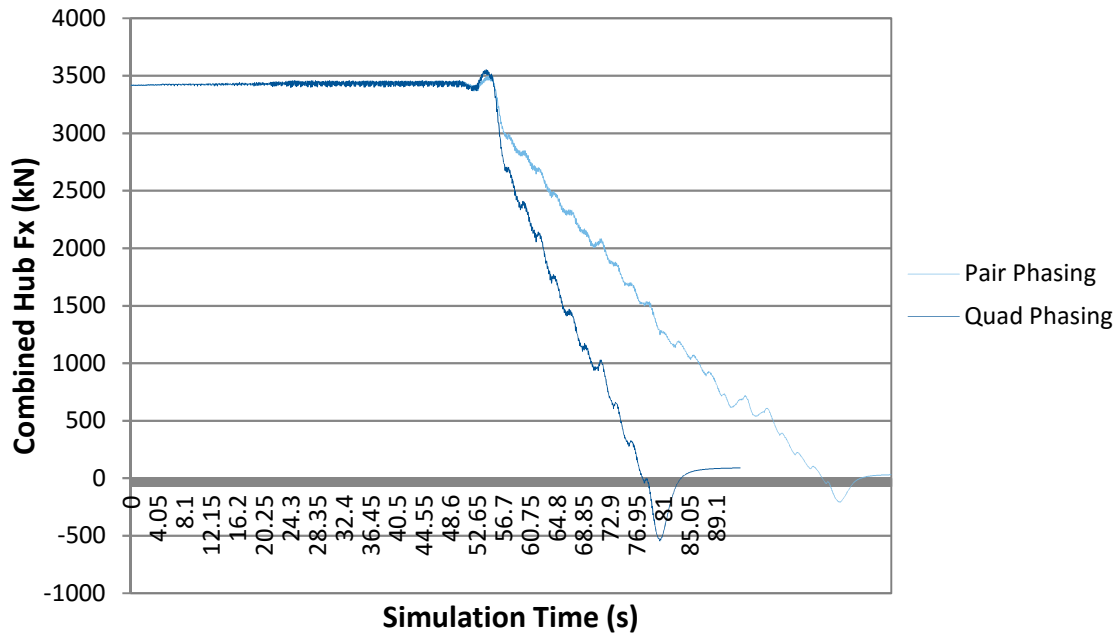


Figure 5-30 - DLC4.2; Pair and Quad Phased Normal Shutdown (Safety Factors Applied)

In quad phasing of shutdown, the thrust reversal is significantly reduced in comparison to simultaneous shutdown and even in comparison to 5MW machines. In the pair phasing, the thrust reversal is negligible.

Given that the IEC standard creates a scenario whereby the turbine happens to shutdown during the unfavourable part of an extreme gust, it can be stated with confidence that any real MRS normal shut-down procedure would never need to have more than a small number of its total rotors shutting down during an unfavourable part of a gust.

Of course emergency stop procedures are likely to require a more rapid response to avoid over speed. As a result of the reduced ability to phase shutdown through control methods, DLC2.3a3 may become the design driving load case for Hub Fx when considering ultimate loads only.

A similar method is employed in DLC2.3. For this load case given that it is caused by an emergency stop it is assumed that there is still a strong requirement to bring the rotors to a halt as quickly as possible. Two optional methods are shown in Figure 5-31; shutdown in two groups, and shutdown in four groups. In this way, the whole array can be shutdown in a matter of seconds while still destroying around 1,000kN from the peak loading.

Ultimately, the only thing determining the ultimate load cases involving shutdowns therefore becomes the rate at which total shutdown is required.

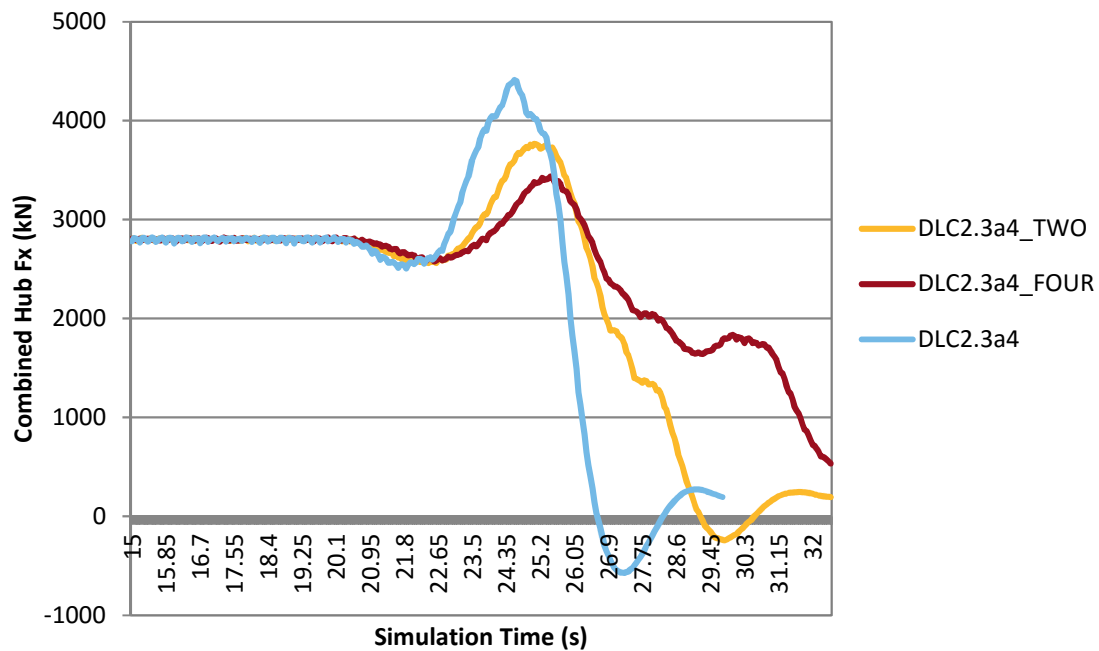


Figure 5-31 - DLC2.3; Comparison of Two Group and Four Group Shutdown (Safety Factors Applied)

The effect of phasing shutdowns is important as it allows us to bring the ultimate loads on the structure down to a level comparable with that caused by operation in extreme turbulence, see Figure 5-32. The advantages of having DLC1.3 represent the critical design loads is that it can represent design critical conditions over a period exceeding those of the shorter transients. The provision of long simulations allows for more data for the purposes of structural design and ultimately leads to higher degrees of confidence.

Of course this still does not address any perceived unfairness or unbalance in the standard that is perhaps unduly affecting the loads comparison. The final discussion will therefore be on the effect of the addition of turbulence on coherent shutdowns.

Phased Shutdown Loads Comparison; DLC 1.3/2.3/4.2

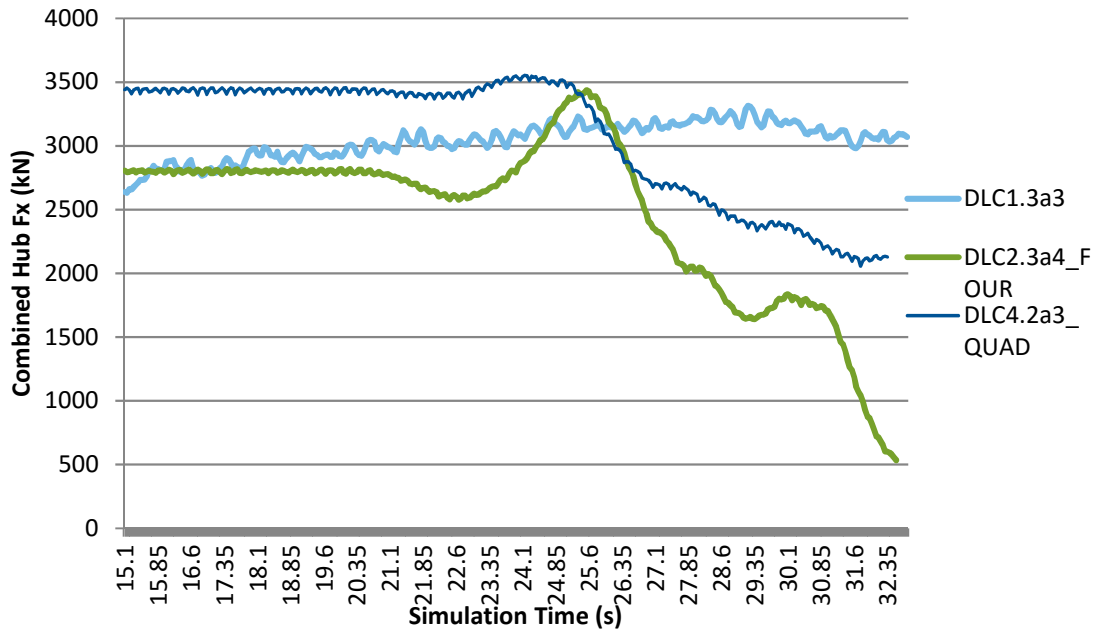


Figure 5-32 - Comparison of Shutdown Loads with Power Production Loads in Extreme Turbulence (Safety Factors Applied)

5.7.4 Addition of Turbulence to Coherent Load Cases

In its original form DLC2.3 is skewed by the assumption of extreme coherence across the whole array and simultaneous shutdown. These assumptions are reasonable at 5MW (100m scales) but over 200-300m scale the assumptions are less so. It is expected that this results in an over-estimate of average steady-state loading.

Figure 5-33 shows the effect that adding turbulence to DLC2.3 has on the combined Fx loads when the MRS enters into a shutdown scenario. As the average or steady state loading is typically lower in a turbulent wind field as opposed to a coherent one, the total additive effect of individual hub Fx's have less of an impact on the ultimate load.

This is illustrated in two ways. The first is a superimposed gust and shutdown on top of a normally turbulent wind field (during both an average and worst-case simulation period), resulting in reduction of 400kN or more on total hub Fx are observed. The second is a normal shutdown event without a gust during a normal turbulent wind field, the shutdown loading is barely noticeable above the average.

The first attempt to establish the ultimate load seems reasonable but even so still requires the following conditions to be met;

- The coincidence of an undesirable extreme operating gust with a simultaneous emergency shutdown event.
- The coherence of this gust over an area stretching 350m laterally and 250m vertically both spatially and temporally.
- Simultaneous shutdown of each individual rotor during the worst phase of the gust.

If any of these conditions are not met then the ultimate loading should by nature or design become less than that of the ultimate loading present under normal power production operation at rated wind speeds (Figure 5-33). It is therefore expected that the multi-rotor system need only be designed on the basis of the worst-case power production loading design case DCL1.3.

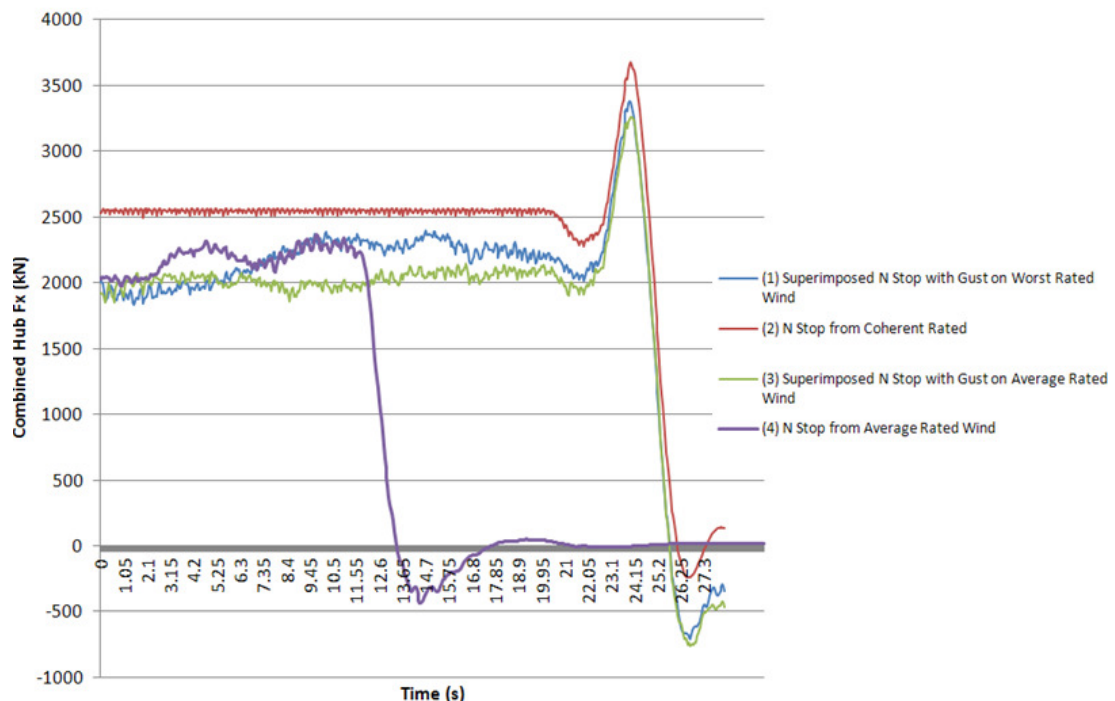


Figure 5-33 - Normal Stop Loading Comparisons (No Safety Factors)

5.8 LOAD CASE COMPARISON

The final aspect of this chapter calls for the complete load case overview and comparison.

Table 5-11 presents the abbreviated results, showing only the maximum total hub Fx for each of the seven load cases investigated.

Scenario	Maximum Total Hub Fx			
<i>DLC 1.3a3</i>	Constant Wind	Turb. Worst-case		
	4451kN	3314.3kN		
<i>DLC 1.4b1</i>	Fully Coherent	Turb. Worst-Case	Turb. Average	
	4875.5kN	3309kN	3200kN	
<i>DLC 2.3a4</i>	Fully Coherent	Turb. Worst-Case	Turb. Average	
	4411.3kN	3362.4kN	3216kN	
<i>DLC 4.2a3</i>	Fully Coherent	Turb. Worst-Case	Coh. Phased Shut	Turb. Phased Shut
	5663.7kN	3500kN	3553.6kN	2468kN
<i>DLC 6.1</i>	Fully Coherent	Turb. Worst-Case		
	601.2kN	661.8kN		
<i>DLC 6.2</i>	Constant Wind			
	936kN			
<i>DLC 6.3</i>	Constant Wind			
	443.4kN			

Table 5-11 - Full Load Case Comparison

The third and fourth columns represent adjustments (made outside the scope of the standard) to each of the coherent load cases as discussed in the previous section. To adjust for the coherent nature of the wind defined in these three transient cases, the transient event is summed with total hub fx under normal operation (both in average operation and in operational worst-case). This adjustment better reflects the actual realisable loading across the multi-rotor array and ultimately lowers the coherent steady-state loading. These adjustments are also shown under the Turbulent Worst-Case and Turbulent Average headings in Table 5.6-1

Table 5-9 also presents the reduced total hub Fx caused by staging rotor shutdowns both under coherent and turbulent wind conditions. The results suggest that it is possible to reduce the peak magnitude of the total hub Fx loading during shutdown in both DLC2.3 and DLC4.2 (normal and emergency stop) to a magnitude similar to that experienced during normal power production.

The case is therefore made that the load production case around rated wind speed (DLC1.3) is likely to be the ultimate load case. This load case is examined in more detail in the following chapter for both the 20MW single rotor and 20MW multi-rotor for comparative purposes.

5.9 DISCUSSION

The total hub Fx loads combined with a fault are reduced in DLC2.3 and 4.2 compared to DLC1.3 in the multi-rotor system due to reduced probability of simultaneous independent faults across the array. Extreme loading due to loss of grid, which would result in worst-case loading, can be designed against using resistor banks which allow for phasing of the rotor shutdown - a method for which will be discussed in Chapter 6. Lateral coherence of gusts are such that individual blade bending moments are not design drivers in the MRS and that overall tower loading is more distributed comparing favourably with single rotor machines of equivalent power rating. A multi-rotor system consisting of 45x41m diameter rotors can almost ignore extreme negative wind shear (IEC DLC1.5): normally driving (or close to driving) tip-to-tower closest approach in larger single rotor machines. Extreme coherent gust with direction change (IEC DLC1.4): normally driving bending moments at hub and yaw bearing overturning moment and which is very sensitive to tuning of the supervisory control for a single large rotor is lowered in the MRS with more degrees of freedom and the ability to yaw.

Comparing the loads from each design driving case shows that the MRS benefits from decreased loads overall compared to other equivalently rated single rotor systems in all examined IEC 61400-1 design load cases. Significant load reductions of 50% or more have been seen in total hub Fx, total hub My and total hub Mz on the multi-rotor system when compared to a single 20MW rotor.

Reduced loading leads to reduced structural mass and cost, competitive with or less than single rotor systems at large scale. The MRS also benefits from many more degrees of freedom, inherent redundancy, and increased part commonality compared to single or several single rotors of equivalent rating.

CHAPTER 6 MULTI ROTOR SYSTEM SUPPORT STRUCTURE DESIGN

6.1 Brief description of the structural analysis tool

For the structural analysis of the MRS support structure the in-house structural tool CRES-Frame is used. CRES-Frame is capable of doing the static and dynamic analysis of 3-D structures. Its main capabilities involve determining the member displacements and loads, and structural reactions for:

- Static loading
- Applied transient load history
- Modal analysis

The support structure of the Multi-Rotor system is modelled as a space frame of Euler beams, each of them having 12 degrees of freedom (2 nodes X 3 rotations and 3 translations each). The details of the formulation are presented in ref [19].

The structural damping is introduced as proportional mass and stiffness damping using the assembled matrices. The detailed formula for the structural damping is the following

$$C_S = aM + bK \quad (1)$$

where M and K are the global mass and stiffness matrices and the a and b coefficients are computed using two characteristic system eigen-frequencies ω_1 , ω_2 and their desired damping ratios ξ_1 , ξ_2 . The formulas used in that are the following

$$a = 2\omega_1\omega_2(\omega_1\xi_2 - \omega_2\xi_1) / (\omega_1\omega_1 - \omega_2\omega_2) \quad , \quad b = 2(\omega_1\xi_1 - \omega_2\xi_2) / (\omega_1\omega_1 - \omega_2\omega_2) \quad (2)$$

In transient load calculations, the numerical integration of the linear(ized) dynamic system is performed using Newmark's method (see ref. [20], [21] for details). To achieve an unconditionally stable scheme with zero numerical damping the Newmark scheme is to be applied with characteristic coefficient values $\beta=0.25$ and $\gamma=0.5$.

Two alternative formulations are available for modal analysis, either a) the vector iteration method for finding the lowest eigenvalues, and by use of shifting the other eigenvalues or

b) the generalized Jacobi method for getting all the eigenvalues (but not the mode shapes in the present implementation) simultaneously.

Using the static or dynamic loads and the sectional properties of the members CRES-Frame calculates the equivalent stress σ_v for the failure criterion (748) of ref [22] and also two Buckling Indices, one for the lateral buckling (section 3.5 of ref [23]) and one for the local buckling (section 4.2 of [24]). In our convention a member fails in buckling when one of its two buckling indices (Bl_1 and Bl_2) gets lower than -1 (minus denotes compression). The equivalent stress is to be compared against the limit stress $\sigma_{R,d} = f_{y,k}/\gamma_M$ where $f_{y,k}$ is the characteristic value of the material's yield stress and γ_M is a partial safety factor.

CRES-Frame can cope with the following external forces:

- The weight of concentrated masses applied on the nodes of the structure
- The self-weight of the structure members, applied at the centre of the elements
- The aerodynamic drag of the members subjected to a uniform wind speed coming from a given wind direction (applied at the centre of the elements). For cylindrical sections, as those assumed here, the drag coefficient is set at 0.6.
- Any other external forces corresponding to a static or dynamic load case (applied on the nodes)

6.2 Initial shape

The proposed design assumes a 20MW multi-rotor system comprising 45 horizontal axis rotors of rating 444kW in a planar arrangement supported by interlocking frame. The initial shape of the support structure (Figure 6-1) was provided by UoS [25] along with a library of possible cross-section characteristics. The members will be assumed to be hollow cylinders fabricated by construction steel. The geometry of the cross section is defined from its outer and inner diameters (or outer diameter and thickness, as normally described in the manufacturers' product lists).

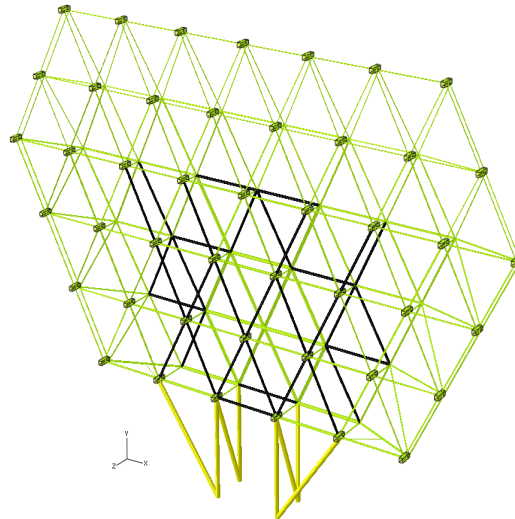


Figure 6-1: Layout (left) of the multi-rotor system and first design of its support structure (right)

6.3 Selection of candidate cross sections

To select a proper family of cross sections we set up the following numerical optimization problem in Mathematica [26], where a similar implementation of the CRES-Frame structural tests has been programmed:

Given a cylindrical tube of length $L = 40\text{m}$, optimize the design variables (outer and inner diameters D_o and D_i), with the object of minimizing the linear mass of the cylindrical cross section. The structural members are clamped at both sides and subjected to a variable axial compression load F_{ax} and a bending moment which is proportional to the outer diameter (corresponding to the drag force of the cylinder subjected to an extreme wind speed equal to $V_{e50} = 50\text{m/s}$). The optimization is constrained by the structural failure criteria ($\sigma_v \leq \sigma_{R,d}$, $-1 \leq BI1$ and $BI2$).

The L value is selected as a characteristic length for the present application corresponding to the distances between the front (and the back) nodes of the support structure. The result of this exercise is presented Figure 6-2 as a function of F_{ax} .

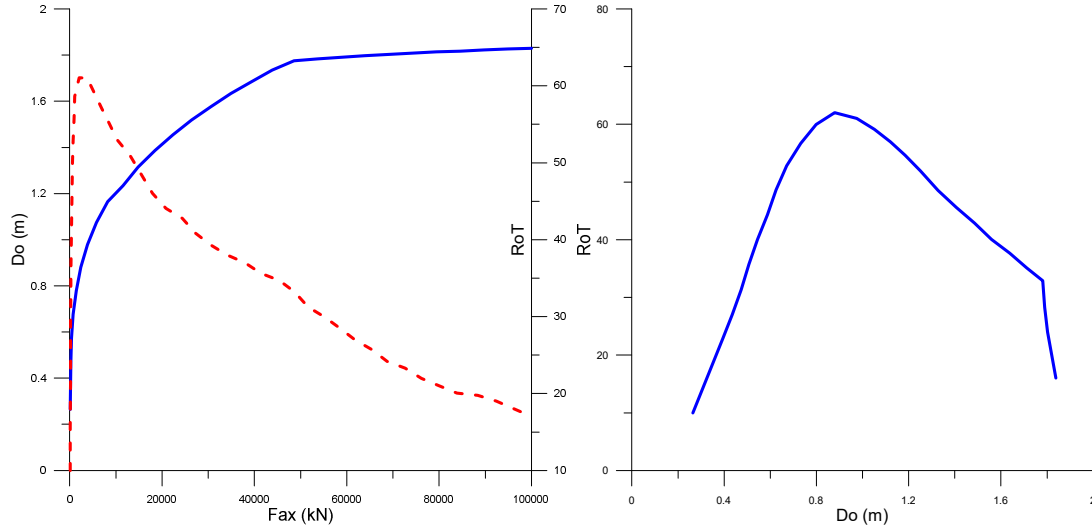


Figure 6-2: Left: Optimal sectional properties as a function of the axial compression load (F_{ax}). The y-axes present the outer diameter of the cylinder D_o and the mean radius over thickness RoT . Right: RoT vs D_o .

The inclusion of the drag-driven bending moment term into the cross section optimization problem has two interesting effects:

- The optimization does not allow solutions of very big diameters at high axial loads because of the drag effect. It can be seen that after 1.8 m the diameter plot flattens out
- At low axial forces the optimal solution does not allow for cross-sections of large ToR (this would be the case if the bending moment was zero). There is a point (for D_o around 0.8 m in this case) where ToR gets its maximum value, around 60 in this example. The actual D_o value where ToR gets its maximum as well as the maximum value itself depend on the level of the applied bending moment.

Nominal Yield Stress of 355 MPA / 52 KSI	PIPE LENGTH 12.500 mm / 13.200 mm																PIPE LENGTH 4.200 mm / 4.800 mm																							
	4,8 mm		5,2 mm		5,6 mm		6,4 mm		7,1 mm		7,9 mm		8,7 mm		9,5 mm		10,3 mm		11,1 mm		11,9 mm		12,7 mm		19,1 mm		25,4 mm		31,8 mm		38,1 mm		44,5 mm		50,8 mm		54 mm			
406,4	4,8				6,4	7,1	7,9	8,7	9,5	10,3	11,1	11,9	12,7	19,1	25,4	31,8	38,1																							
508,0		5,2		5,6	6,4	7,1	7,9	8,7	9,5	10,3	11,1	11,9	12,7	19,1	25,4	31,8	38,1	44,5																						
609,6			5,6	6,4	7,1	7,9	8,7	9,5	10,3	11,1	11,9	12,7	19,1	25,4	31,8	38,1	44,5	50,8																						
711,2				6,4	7,1	7,9	8,7	9,5	10,3	11,1	11,9	12,7	19,1	25,4	31,8	38,1	44,5	50,8																						
812,8				6,4	7,1	7,9	8,7	9,5	10,3	11,1	11,9	12,7	19,1	25,4	31,8	38,1	44,5	50,8																						
914,4				6,4	7,1	7,9	8,7	9,5	10,3	11,1	11,9	12,7	19,1	25,4	31,8	38,1	44,5	50,8																						
1016,0					7,9	8,7	9,5	10,3	11,1	11,9	12,7	19,1	25,4	31,8	38,1	44,5	50,8																							
1117,6						8,7	9,5	10,3	11,1	11,9	12,7	19,1	25,4	31,8	38,1	44,5	50,8																							
1219,2							8,7	9,5	10,3	11,1	11,9	12,7	19,1	25,4	31,8	38,1	44,5	50,8																						
1320,8							7,9	8,7	9,5	10,3	11,1	11,9	12,7	19,1	25,4	31,8	38,1	44,5	50,8																					
1422,4							7,9	8,7	9,5	10,3	11,1	11,9	12,7	19,1	25,4	31,8	38,1	44,5	50,8																					
1524,0							7,9	8,7	9,5	10,3	11,1	11,9	12,7	19,1	25,4	31,8	38,1	44,5	50,8																					
1625,6								8,7	9,5	10,3	11,1	11,9	12,7	19,1	25,4	31,8	38,1	44,5	50,8	54,0																				
1727,2								8,7	9,5	10,3	11,1	11,9	12,7	19,1	25,4	31,8	38,1	44,5	50,8	54,0																				
1828,8									9,5	10,3	11,1	11,9	12,7	19,1	25,4	31,8	38,1	44,5	50,8	54,0																				

Table 6-1: The selected family of welded pipes cross-sections

Figure 6-2 is further used for selecting a family of cross sections for the present designs. The dimensions of steel pipes (seamless or welded) are standardized following the ANSI B

36.10 or the ASTM norms. There is a given, relatively small, number of possible outer diameters which are combined with a number of possible thicknesses (look in [27] for instance). Individual pipe manufacturers build a smaller or larger part of these combinations (see [28] as an example of a pipe manufacturer who is involved in wind energy applications). Table 6-1 presents outer diameter and thickness combinations as offered by a welded pipes manufacturer. Using Figure 6-2 we are able to select a family of 15 cross-sections by selecting for each available outer diameter the single thickness that comes closer to the RoT-D_o curve of the figure. These 15 combinations are highlighted in yellow. Note that neither the outer diameter nor the thickness values (in mm) are round, since the standardisation was historically based in inches rather than millimetres.

6.4 Load cases

Following [29] we have selected the loads of DLC 1.3a1 (at rated wind speed) for designing the support structure. The wind turbulence file is defined as having a mean of 11m/s at 115m height (approximately the centre of the array). Two variants have been considered:

1. A Static variant applying point loads at the turbine nodes equal to the maximum value of each row for those loads having a non-zero expected value and zero for the rest. The resulting values are shown in Table 6-2
2. A Dynamic variant where the actual load time series are applied as point loads

The above rotor/nacelle loads apply on the 45 turbine nodes. Parasitic drag forces acting on the members of the support structure are also considered. Being in the operational range of wind speeds, parasitic drag is calculated conservatively for the cut-out wind speed (25 m/s).

Row number	F _x (kN)	F _y (kN)	F _z (kN)	M _x (kNm)	M _y (kNm)	M _z (kNm)
1	104,173	0	-36,458	94,113	0	0
2	100,807	0	-38,334	94,102	0	0
3	99,583	0	-37,411	94,112	0	0
4	101,471	0	-37,843	94,113	0	0
5	94,493	0	-38,419	94,101	0	0
6	101,162	0	-39,329	94,113	0	0

Table 6-2: Static variant of DLC 1.3a1. CRES' coordinate system is now used. Row numbering: bottom to top

In addition, the multi-rotor support structure should be able to sustain its ultimate loading due to a 50 year gust. If no other provision is taken (active or passive yawing during the incidence), this extreme gust can come from any wind direction. This all-directional

extreme gust, assumed equal to the 10 min averaged V_{e50} for Class I (50 m/s), will form an additional load case for assessing our support structure designs. In our implementation we scan the 0-360° flow direction range with 1° step.

6.5 Preliminary Designs

The common assumptions for the designs presented in this section are the following:

- The space-frame topology (the way the members are connected to each other) of Figure 6-1 is maintained.
- The cross-section of any member should coincide with one of the 15 outer-diameter/thickness combinations of Figure 6-2.
- The depth of the structure is changing proportionally to its bottom (base) value which is a free parameter of the design.

The design is performed in the following simple, still very efficient way:

- STEP 1:** Select the bottom depth value of the structure
- STEP 2:** Initiate the design assuming that all members are built with the lighter material ($IMAT = 1$)
- STEP 3:** “Iterate” applying loads on the structure. When designing with the dynamic load case the iterations are the actual time steps. For the extreme all-directional gust the iterations correspond to the different wind directions. Calculate the loads and stresses of the entire structure at each iteration.
- STEP 4:** When one of the three structural failure criteria (equivalent stress, two buckling tests) is violated for a specific member, increase its material class by one ($IMAT = IMAT + 1$)
- STEP 5:** Continue until no failure criteria is violated for any member
- Interestingly this loop works well. This is because the non-linearity of the design problem, associated to the own-weight and the drag-external diameter connection of the changing members, is rather weak.

Bottom Depth (m)	MASS OF THE SUPPORT STRUCTURE (t)				
	DLC 1.3 DYNAMIC			GUST ALL DIRECTIONS	
	SF = 1,00	SF = 1,35	Overhead	SF = 1,00	Overhead
20	1472				
30	1371	1564	14%	2857	108%
40	1377			3053	122%
50	1370				

Table 6-3: Mass of the support structure as a function of the bottom depth and the safety factor applied on the transient loads

Table 6-3 presents the mass of alternative designs performed for the DLC 1.3 Dynamic load case and the all-directions 50-year gust for different bottom depth (BD) values of the structure. The following remarks are made:

- Designing for the DLC 1.3 Dynamic with safety factor (SF) 1.00 results in light-weight constructions which have their minimum mass at BDs larger than 30m. The designs after BD=30m look mass-insensitive.
- Designing for the all-directional extreme gust the mass of the support structure is more than doubled. Also, larger BDs increase the mass due to larger side-wind resistances.
- Combining the above two remarks we only consider solutions with fixed BD =30 m in the following.
- The DLC 1.3 Dynamic design with safety factor 1.35 increases the mass by 14% compared to the no-safety factor design. None of the two designs can withstand the extreme gust of 50 years at any wind direction. The 1564 t design can also withstand the DLC 3.1 Static with no safety factor but not the DLC 3.1 Static with SF 1.35.
- The all-directional extreme gust increases the total mass of the DLC 1.3 Dynamic, no-safety factor design by 108%. Still, this 2857 t design is able to undertake the DLC 1.3 Dynamic and Static loads with (and obviously without) safety factor 1.35.

6.6 Final Design

Using the experience of the earlier designs we proceeded in what we shall call ‘Final Design’ fixing the BD at 30 m and applying properly the IEC-61400-3 load and material safety factors of Table 6-4 for the two load cases considered, the DLC 1.3 (extreme turbulence model) and the DLC 6.2 (all directional 50 year gust, assuming that no active or passive yaw mechanism is in place when during the extreme incidence). The load safety factors apply i) on the external loads (turbine loads), ii) on the aerodynamic loads of the

structure itself (parasitic drag) and iii) the weight loads which we handle with safety factor 1. The material safety factors are the γ_M of the limit stress of the introductory section and γ_{BLat} used in the lateral buckling analysis. The local buckling analysis uses already its own safety factor (see ref [24]) and, thus, no extra safety factor is needed.

The 'Final Design' derives after designing for both load cases and symmetrizing the resulting space-frame around the x-z plane. Its total mass is 2,938.5 tonnes and the way this mass is split to the members of the cross-sections family (IMAT: 1 to 15) is shown in Table 6-5. Other gross-properties of the structure are presented in Table 6-6.

Load Case	Load Safety Factors			Material Safety Factors		
	Turbine Loads	Parasitic Drag	Weight Loads	γ_M	γ_{BLat}	γ_{BLoc}
<i>DLC 1.3 DYNAMIC</i>	1.35	1.35	1.00	1.10	1.20	-
<i>DLC 6.2 GUST All DIRECTIONS</i>	1.35	1.10	1.00	1.10	1.10	-

Table 6-4: Load cases and load and material safety factors for the 'Final Design'

IMAT	MASS (kg)	IMAT	MASS (kg)	IMAT	MASS (kg)
1	25,256	6	297,212	11	300,860
2	75,303	7	150,655	12	187,409
3	66,837	8	64,850	13	707,235
4	148,183	9	286,532	14	215,116
5	187,797	10	225,258	15	0

Table 6-5: 'Final Design', mass per cross-sections family member

Table 6-6: Gross properties of the 'Final Design'

GROSS PROPERTIES	
Center of Gravity - X (m)	7.40
Center of Gravity - Y (m)	0.00
Center of Gravity - Z (m)	97.38
Moment of Inertia - X (kg*m2)	60,461,070,877
Moment of Inertia - Y (kg*m2)	45,269,607,881
Moment of Inertia - Z (kg*m2)	16,248,817,194
Total MASS (kg)	2,938,500

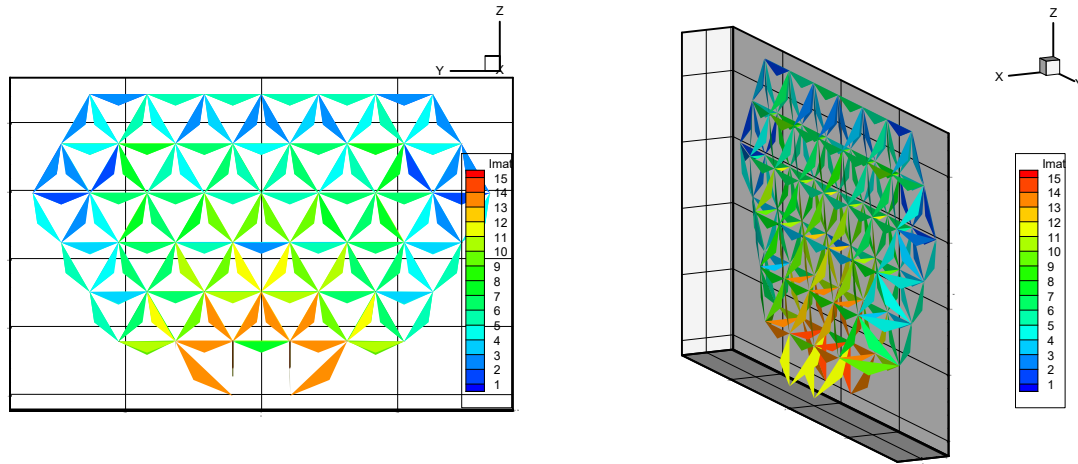
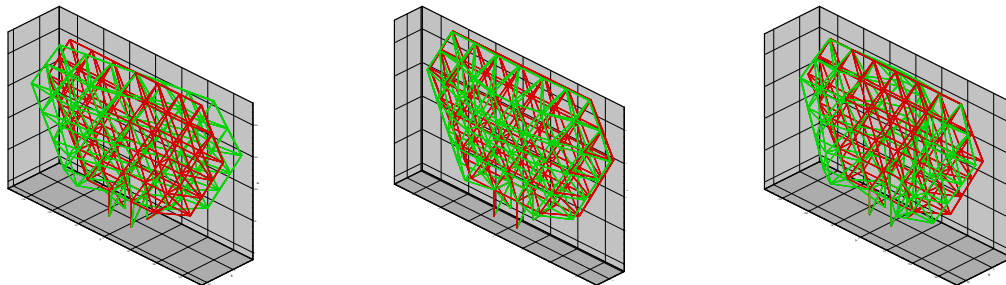


Figure 6-3: Front and side view of the 'Final Design' members following for cross-sections identification (*Imat* increases from smaller to larger diameters)

Figure 6-3 presents a front and a side view of the IMAT members of the 'Final Design'.

6.7 Structural Analysis - Eigenvalue analysis

Table 6-7 present the first 200 natural frequencies of the 'Final Design'. Following [25] the P1 operating range of the rotors is within the range of 0.44 Hz to 0.78 Hz. One can notice that the design does have a large number of natural frequencies within the range of rotors excitation 1P-3P. The corresponding mode shapes are shown in Figure 6-4. In general, such a multi-member support structure is expected to have a large number of closely placed natural frequencies, some of them lying within with the excitation frequency range of the operating rotors. The unavoidable resonance is expected to penalize to some extent the fatigue loading of the support structure.



MODE 1

MODE 2

MODE 3

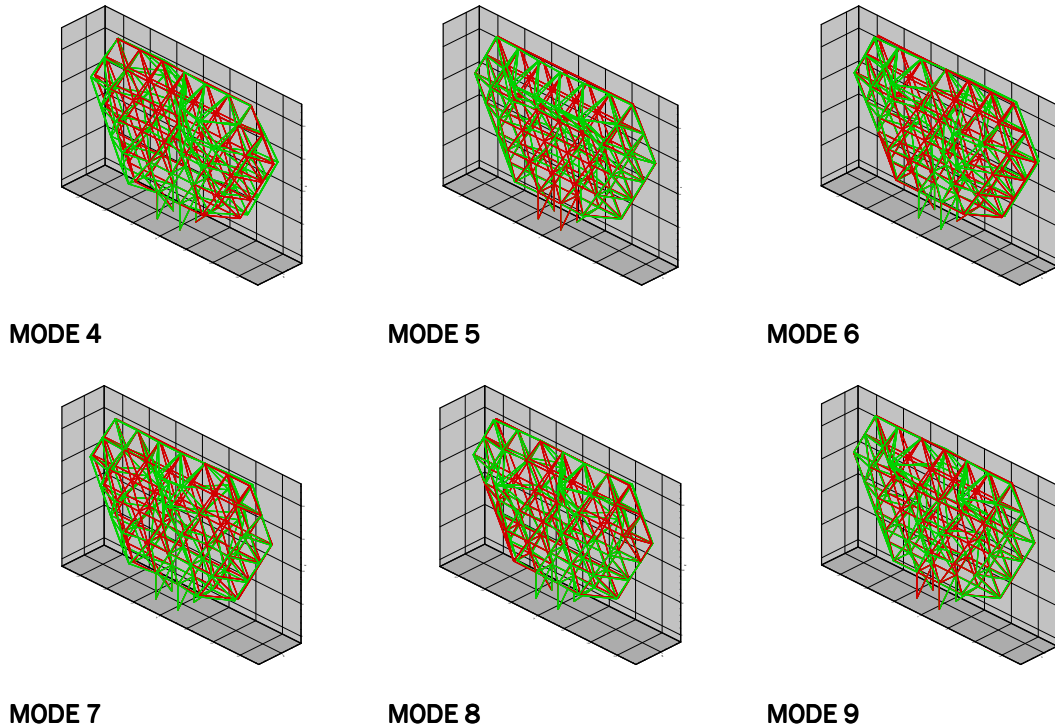


Figure 6-4: First nine eigenmodes of the “Final Design”

N/N	Hz																		
1	0.36	21	1.35	41	2.12	61	3.10	81	3.63	101	4.27	121	5.03	141	6.10	161	7.03	181	8.21
2	0.40	22	1.37	42	2.17	62	3.10	82	3.65	102	4.33	122	5.07	142	6.15	162	7.12	182	8.46
3	0.50	23	1.49	43	2.27	63	3.12	83	3.66	103	4.37	123	5.07	143	6.16	163	7.23	183	8.50
4	0.58	24	1.53	44	2.31	64	3.13	84	3.78	104	4.39	124	5.09	144	6.28	164	7.26	184	8.56
5	0.62	25	1.57	45	2.34	65	3.18	85	3.79	105	4.44	125	5.15	145	6.30	165	7.37	185	8.64
6	0.67	26	1.57	46	2.39	66	3.23	86	3.83	106	4.45	126	5.17	146	6.34	166	7.39	186	8.74
7	0.69	27	1.71	47	2.49	67	3.23	87	3.91	107	4.57	127	5.24	147	6.35	167	7.48	187	8.82
8	0.77	28	1.73	48	2.51	68	3.28	88	3.94	108	4.58	128	5.27	148	6.47	168	7.53	188	8.85
9	0.81	29	1.73	49	2.57	69	3.29	89	3.97	109	4.64	129	5.35	149	6.49	169	7.59	189	8.90
10	0.82	30	1.75	50	2.59	70	3.32	90	4.00	110	4.65	130	5.47	150	6.54	170	7.63	190	8.92
11	0.84	31	1.80	51	2.65	71	3.33	91	4.03	111	4.68	131	5.55	151	6.60	171	7.67	191	8.98
12	0.86	32	1.86	52	2.69	72	3.34	92	4.05	112	4.73	132	5.59	152	6.65	172	7.67	192	9.01
13	0.91	33	1.86	53	2.72	73	3.35	93	4.07	113	4.76	133	5.66	153	6.68	173	7.70	193	9.09
14	0.92	34	1.90	54	2.75	74	3.37	94	4.16	114	4.83	134	5.67	154	6.77	174	7.72	194	9.13
15	0.98	35	1.99	55	2.77	75	3.37	95	4.18	115	4.84	135	5.71	155	6.77	175	7.75	195	9.15
16	1.03	36	2.02	56	2.80	76	3.44	96	4.18	116	4.85	136	5.78	156	6.81	176	7.82	196	9.20
17	1.04	37	2.02	57	2.82	77	3.46	97	4.21	117	4.86	137	5.81	157	6.84	177	7.94	197	9.21
18	1.15	38	2.09	58	2.88	78	3.53	98	4.23	118	4.88	138	5.93	158	6.91	178	8.05	198	9.32
19	1.17	39	2.09	59	2.91	79	3.57	99	4.25	119	4.93	139	5.96	159	7.01	179	8.14	199	9.36
20	1.32	40	2.10	60	3.01	80	3.58	100	4.26	120	4.99	140	6.01	160	7.02	180	8.18	200	9.40

Table 6-7: Eigenvalues of ‘Final Design’

6.8 Structural Analysis - Ultimate Loading

Figure 6-5 and Figure 6-6 present the equivalent stress and the two Buckling Indices resulting from the two load cases (DLC 6.2 and DLC 1.3) of 'Final Design'. For each member we plot the "worst" value encountered during the design process.

We remind from an earlier section that, in our convention, a member fails in buckling when one of its two buckling indices (BI_1 and BI_2) gets lower than -1 (minus denotes compression). The equivalent stress is to be compared against the limit stress $\sigma_{R,d} = f_{y,k}/\gamma_M$ where $f_{y,k}$ is the characteristic value of the material's yield stress and γ_M is a partial safety factor.

It is seen from the figures that there is no failing member in ultimate loading as the later was introduced through the load cases and safety factors of Table 6-4.

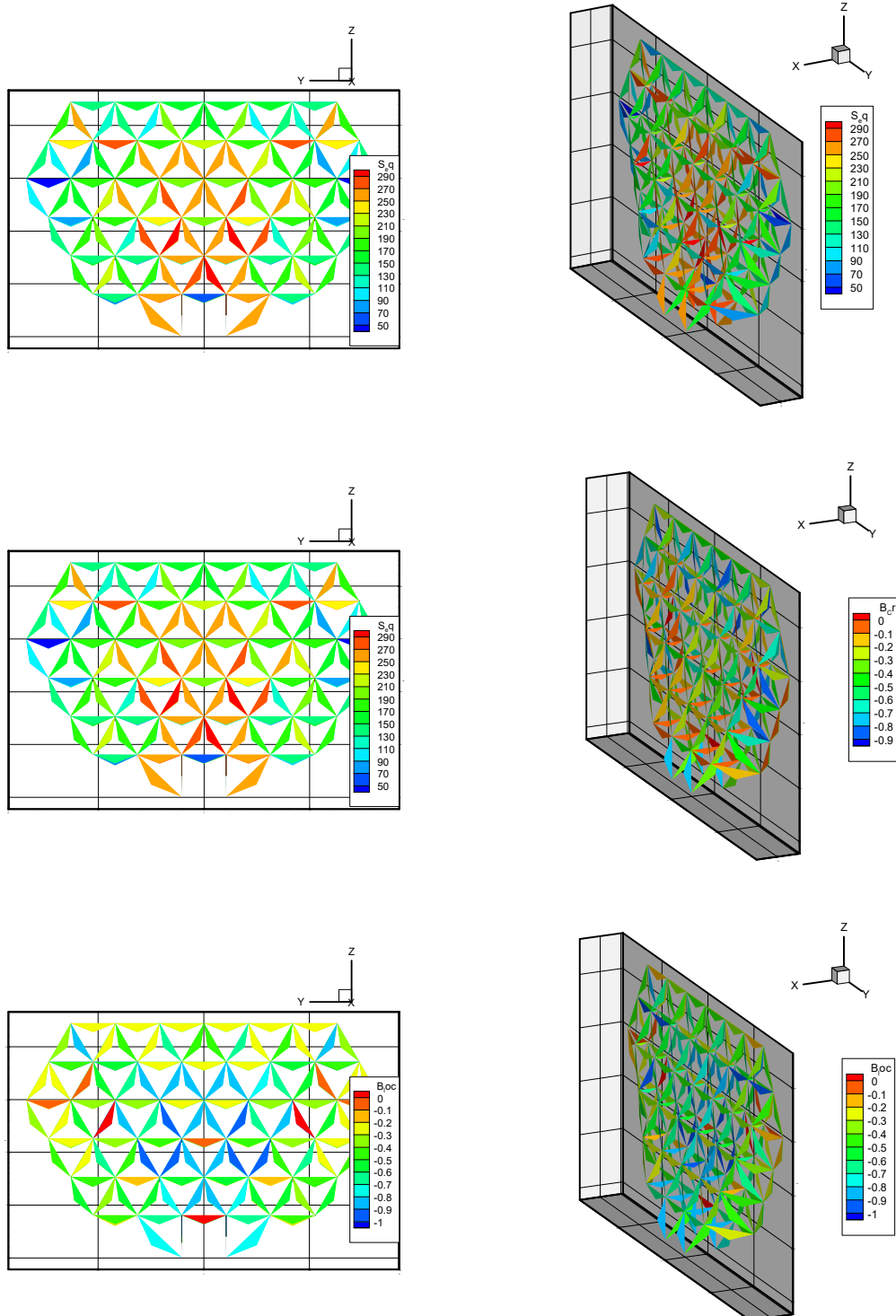


Figure 6-5: Maximum loading under DLC 6.2. From top to bottom, front and side views of: equivalent stress (in MPa), lateral buckling (BI1) and local buckling (BI2).

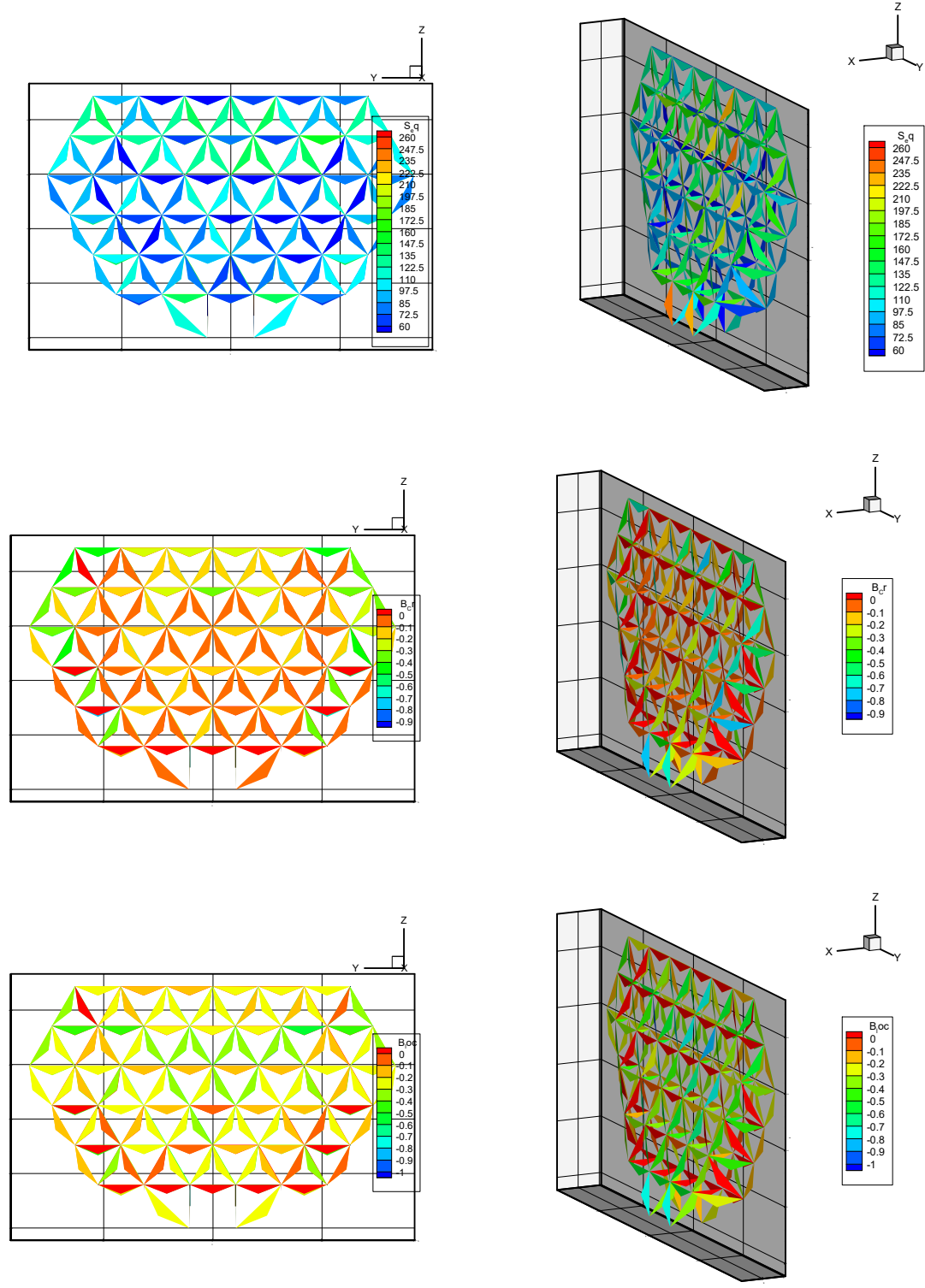


Figure 6-6: Maximum loading under DLC 3.1 Dynamic". From top to bottom, front and side views of: equivalent stress (in MPa), lateral buckling (B1) and local buckling (B12).

6.9 Structural Analysis - Fatigue Loading

A full fatigue analysis for the resulting structure is quite complicated and would require:

- A series of operation states that describes the loads on the turbine during normal operation. In a typical formulation, these states are taken to be a function of the inflow velocity, where the range of the inflow velocity is from the cut-in velocity $V_{\text{cut-in}}$ of the turbine to its cut-out velocity $V_{\text{cut-off}}$.
- A series of “start/stop” operation states that describes the loads on the turbine during normal stops, emergency stops, etc.
- A series of “buffeting” operational states that describes the loads on the turbine while it is stopped, but its blades and other structural components are being buffeted by the inflow.
- Any additional operational states that impose significant fatigue loads on the structure that are not covered by the other three operational states.

This division of load cases falls within the standard set of load cases that has been established by the International Electrotechnical Commission, IEC, for the design of wind turbines [17].

Due to the preliminary nature of the analysis and the difficulties in obtaining the required data, a simplified analysis is performed to get an initial picture of the structure behaviour under fatigue loads. For this analysis, a number of simplifying assumptions are made, for the MRS structure described in the previous sections. The analysis is based on the load calculation for two DLC 1.2 design cases, one with an incoming velocity of 11m/s (rated speed) and one with a wind speed of 20m/s (near-shut-down). Spatially coherent time series for the resulting forces and moments on the wind turbines were produced by UoS for these cases and the response of the supporting structure was calculated, in terms of resulting stresses and displacements. The length of the produced time series was 300sec. Data for different wind speeds was extrapolated based on the available data at the two speeds for which calculations were available. A single seed has been used for each wind speed, increasing the uncertainty of the derived results.

An initial check of the resulting displacements was performed using an FFT transformation of the displacements in order to check the resulting spectrum. Indicative results for some of the nodes are shown in Figure 6-7. It can be seen that the expected increase near the 1P and 3P frequencies of the wind turbines is indeed there.

Using a typical rain flow counting method, the occurrence of different equivalent stress values was calculated. The results are only indicative, as there are calculations for two wind speeds only, that were used for the entire wind speed regime. In addition to that

there is no information concerning the low cycle fatigue, as the lowest number of cycles that can be discretised with a 300sec simulation is of the order of 1.e6.

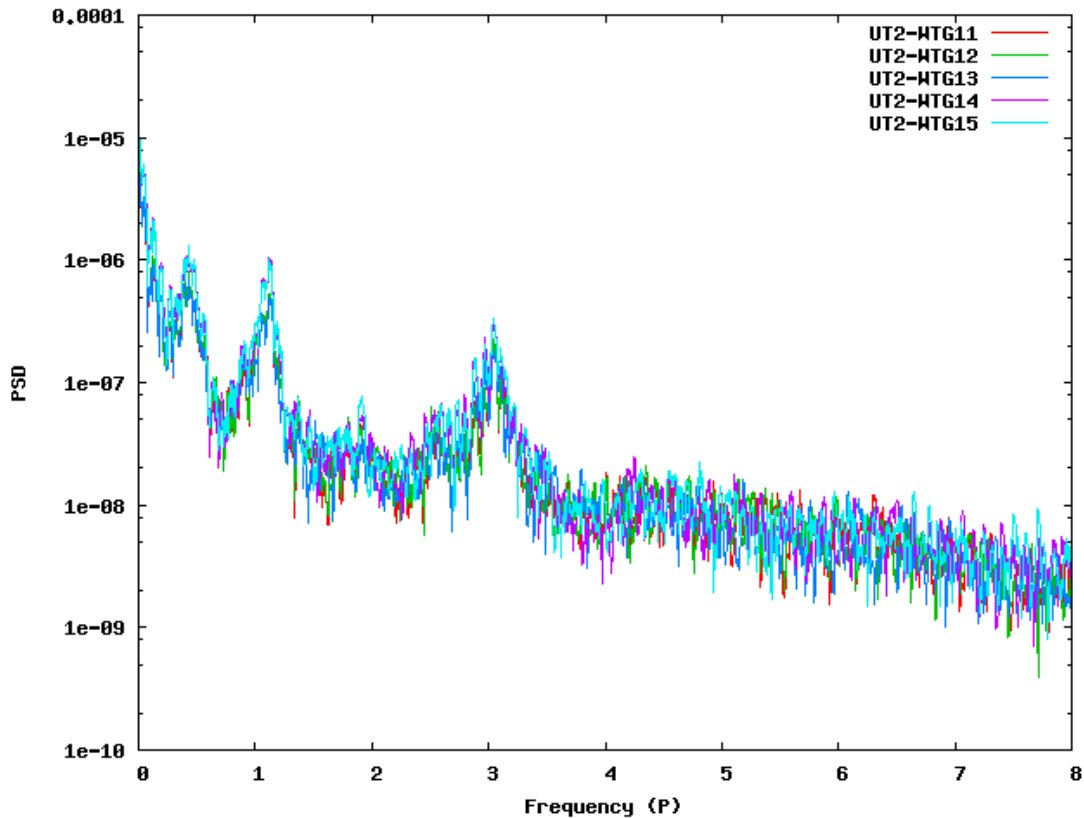


Figure 6-7: Spectral analysis of the displacements for nodes 11-15

The initial fatigue analysis showed that there exist a number of members suffering from high fatigue loads.

To remedy that, in the present revised form of the deliverable we conducted a more detailed fatigue analysis following the S-N curves of the Recommended Practice of DNV-GL [30] for offshore steel structures. To reduce fatigue loads we reapplied the design procedure of sections 6.5 and 6.6 lowering the allowable maximum (instantaneous) stress for normal operation at wind speed 20m/s to 150 MPa. This resulted to a reselection of the cross-sectional properties for the critical members (always from Table 6-1), reducing the maximum but also the mean and standard deviation of the equivalent stresses, increasing the robustness but also the weight of the structure. The gross properties of this “fatigue driven” design are presented in Table 6-8.

GROSS PROPERTIES	Table 6-6	Present
Center of Gravity - X (m)	7.40	7.87
Center of Gravity - Y (m)	0.00	0.00
Center of Gravity - Z (m)	97.38	104.74
Moment of Inertia - X (kg*m2)	60,461,070,877	83,723,434,308
Moment of Inertia - Y (kg*m2)	45,269,607,881	63,081,955,007
Moment of Inertia - Z (kg*m2)	16,248,817,194	22,000,885,361
Total MASS (kg)	2,938,500	3,759,275

Table 6-8: Gross properties of the 'Fatigue-driven Design'

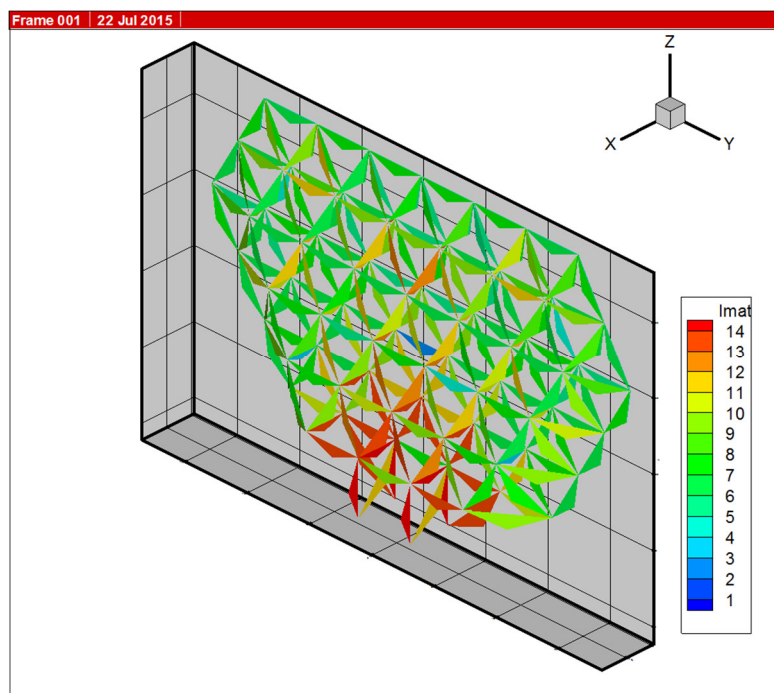


Figure 6-8: Cross sections properties of the 'Fatigue-driven Design'

It is seen that the mass increase of this last design is about 820tn, (corresponding to 28% surcharge to the total mass). The new design has passed successfully, as expected, the ultimate loading analysis of section 6.8. Its cross section properties (to be compared against Figure 6-3 is shown below. The comparison shows that IMAT = 1 members (the most light weight of the material family) are no more present while IMAT = 2 are also drastically reduced.

For the lifetime analysis, the equivalent damage for a 20-year life cycle is calculated using the standard Miner rule. The reference S-N curve used is the bilinear one for tubular structures described in [30], characterised by parameters of $(m = 3.0, \log \bar{a} = 12.164)$ and $(m = 5.0, \log \bar{a} 15.606)$ for the two parts. The equivalent stress at 10^7 cycles is 52.36MPa, meaning that for the members where the maximum variation is below this threshold no further fatigue investigation is necessary.

The resulting equivalent stress for all members is shown in Figure 6-9, where it is seen that ~50% of the elements have an equivalent stress that is below the fatigue limit at 10^7 cycles. For the remaining members a full analysis based on the number of cycles at each stress level is performed and the results are summarised in Figure 6-10. Based on the analysis 76% of the members have a life consumption parameter $D < 1$, while there is small number of elements (8-10) where this is significantly exceeded, indicating that a redesign of these would be necessary for the final design, based on more accurate simulations.

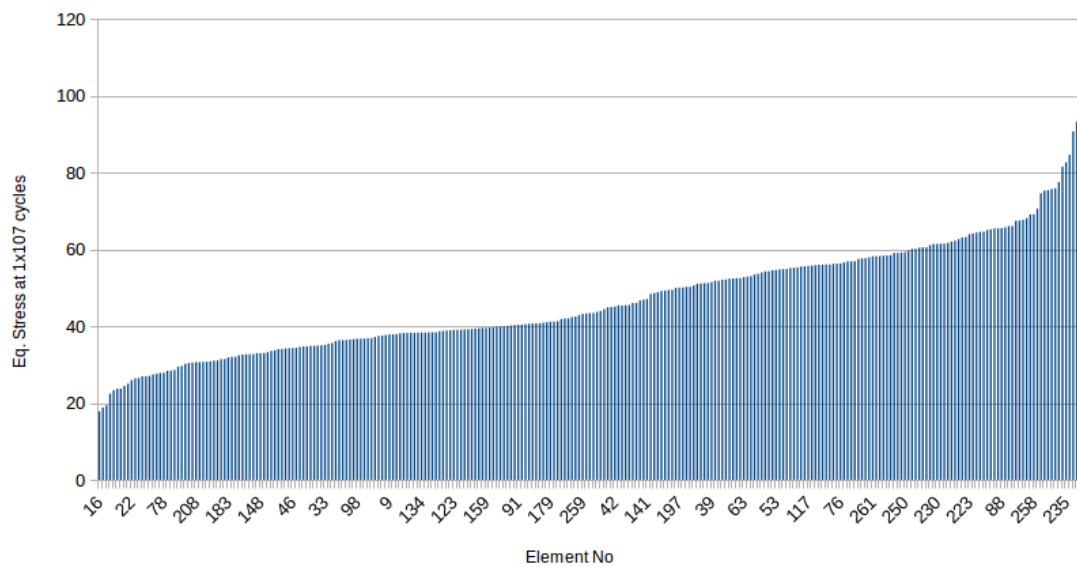


Figure 6-9: Equivalent load at 10^7 cycles for all members of the support structure.

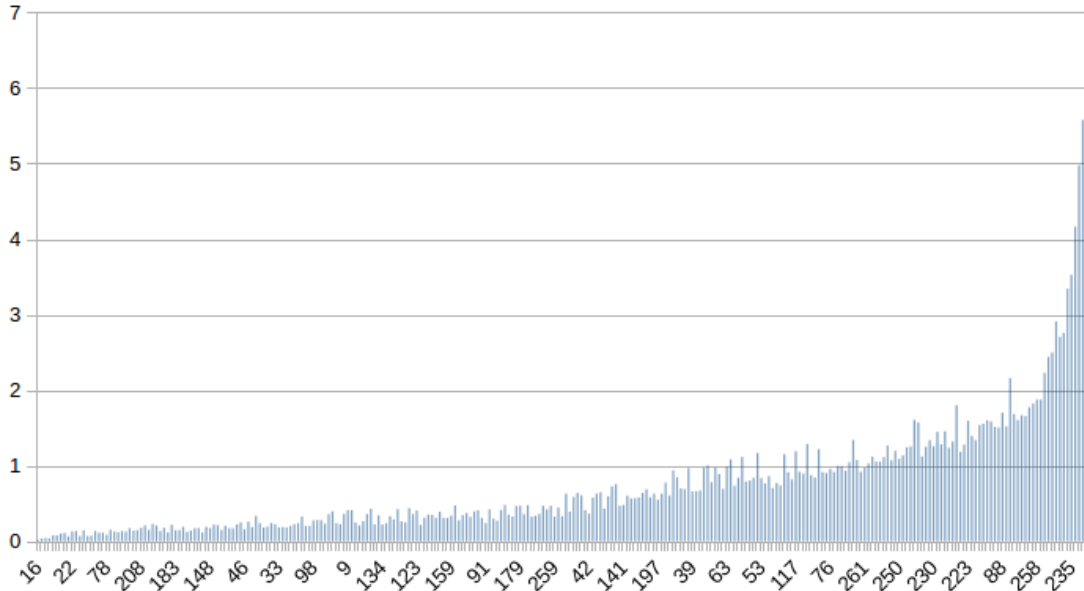


Figure 6-10: Life “consumption” for all members of the support structure.

Based on the analysis that was performed, and keeping in mind the substantial simplifying assumptions that have been made it seems that the support structure *is* driven by fatigue concerns. A full analysis would be required to determine the exact loads and engineering solutions required. Indicative results, for selected member, are presented in Appendix A.

6.10 Structural Analysis – Robustness

The robustness of the MRS support structure is evaluated in this section. This is done by assuming that one of the critical members of the structure has failed and the question to be answered is whether the structure can still withstand its normal operation loads in the absence of these members.

The check is performed for normal operation at 20 m/s using the load time-series that are available for this speed. These are the same stochastic loads applied for the “fatigue driven design” of the MRS support structure presented in the previous section.

Four critical members are selected for the analysis. They are those bearing the maximum equivalent stress in the 11 m/s stochastic run. These four members are listed in Table 6-9 where N is the member’s number, X,Y,X its mid-node coordinates, L its length, S_min S_max S_mean and S_sdv are the minimum, maximum, mean value and standard deviation of the member’s equivalent stress during the turbulent run.

N	X (m)	Y (m)	Z (m)	L (m)	S_min (MPa)	S_max (MPa)	S_mean (MPa)	S_sdv (MPa)
207	0.000	-94.500	203.679	42.000	2	150	33	38
242	0.000	115.500	203.679	42.000	5	143	32	36
244	3.659	94.500	203.679	42.406	4	139	35	40
84	0.000	115.500	94.560	42.000	4	137	29	32

Table 6-9: Critical members for robustness check

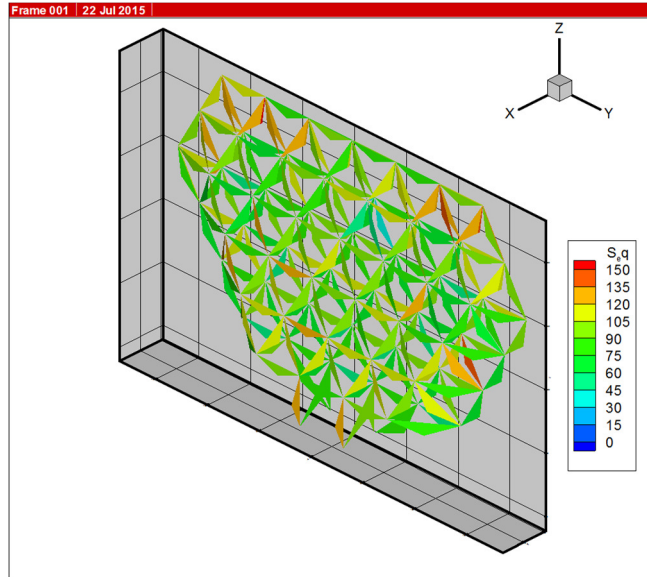
In the following Table 6-10 we present equivalent stress statistics when one of the above members is missing from the structure. The stress values given are those corresponding to the remaining member having the highest S_{max}.

Missing N	S_min (MPa)	S_max (MPa)	S_mean (MPa)	S_sdv (MPa)
207	4	189	49	57
242	4	154	44	49
244	6	167	36	42
84	5	145	43	48

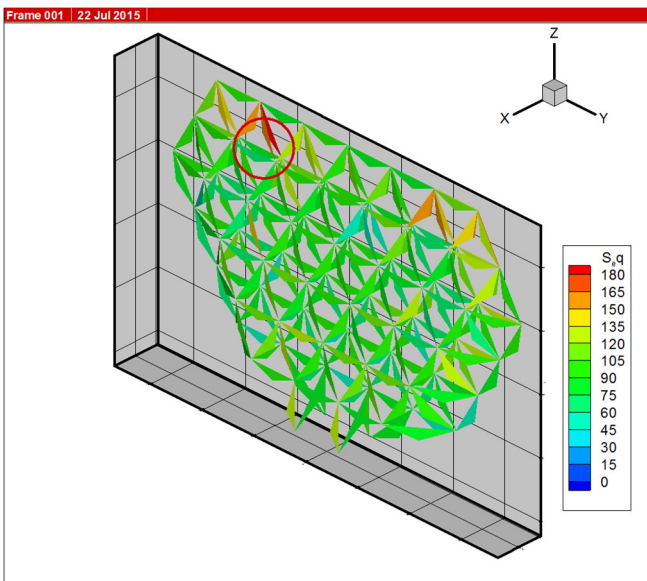
Table 6-10: Consequences of missing members on S-max of the remaining ones

Equivalent S_{max} plots for all MRS support structure members, when one of them is missing, are shown in Figure 6-11. A red circle on the plots indicates the position of the missing member. Clearly, when one of the members is missing stress concentration is taking place at its neighbourhood which, in the cases of N=244 and N=84 is not restricted there.

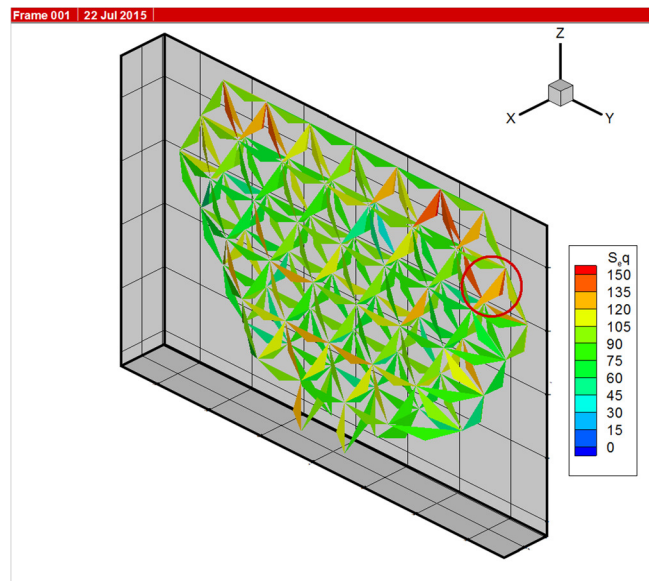
From Table 6-10 it is seen that the failure of any of the four members examined is not creating catastrophic stresses in its neighbourhood or other parts of the structure. The maximum stress attained by the remaining elements is well below the design stress. We can therefore conclude that the presented MRS support structure design is adequately robust.



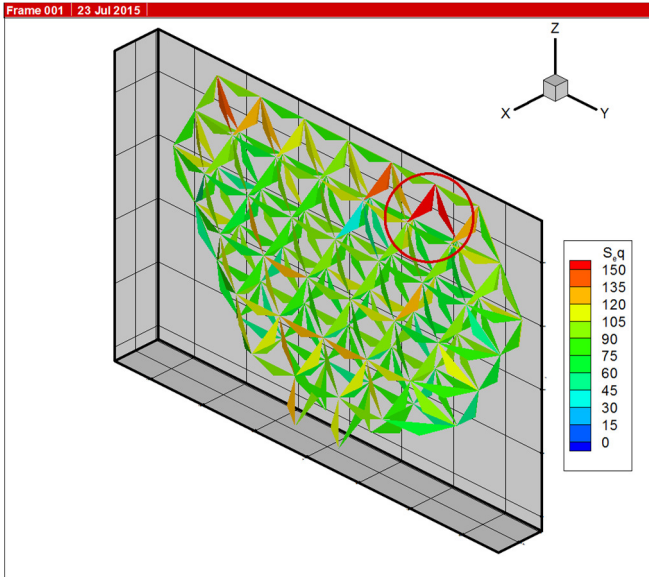
No missing member



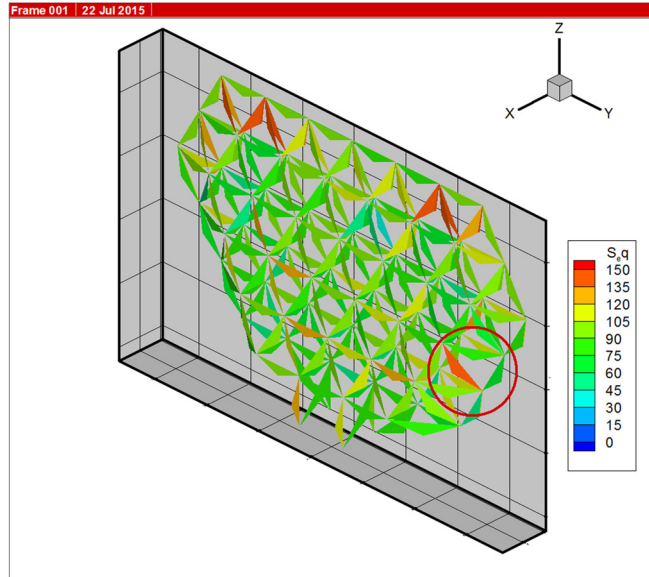
Missing N=207



Missing N=242



Missing N=244



Missing N=84

Figure 6-11: S_{max} of the remaining members when one is missing

CHAPTER 7 FLOATING PLATFORM – PRELIMINARY DESIGN

7.1 Scope

In the initial work plan CRES was assigned the task of designing and evaluating a yawing mechanism for MRS. It is indeed a challenge to yaw a 3000+ tonnes structure having a footprint of 40X30 m. A previous study [8] of a much smaller 5 MW, 36-rotor, MRS adopted a different design solution. The rotors were supported on a frame which yawed using twin bearings located at top and near mid-level on a conventional tubular tower. Such a solution could be also followed here combined with a jacket structure. However, since the initial decision was to go for a full- truss design instead of a hybrid truss-tubular (which is less efficient material wise) it was not possible any more to combine the MRS with the specific yaw mechanism. The possibility of employing a non-conventional hydrostatic yaw bearing placed at the MRS base is discussed in another section of this report.

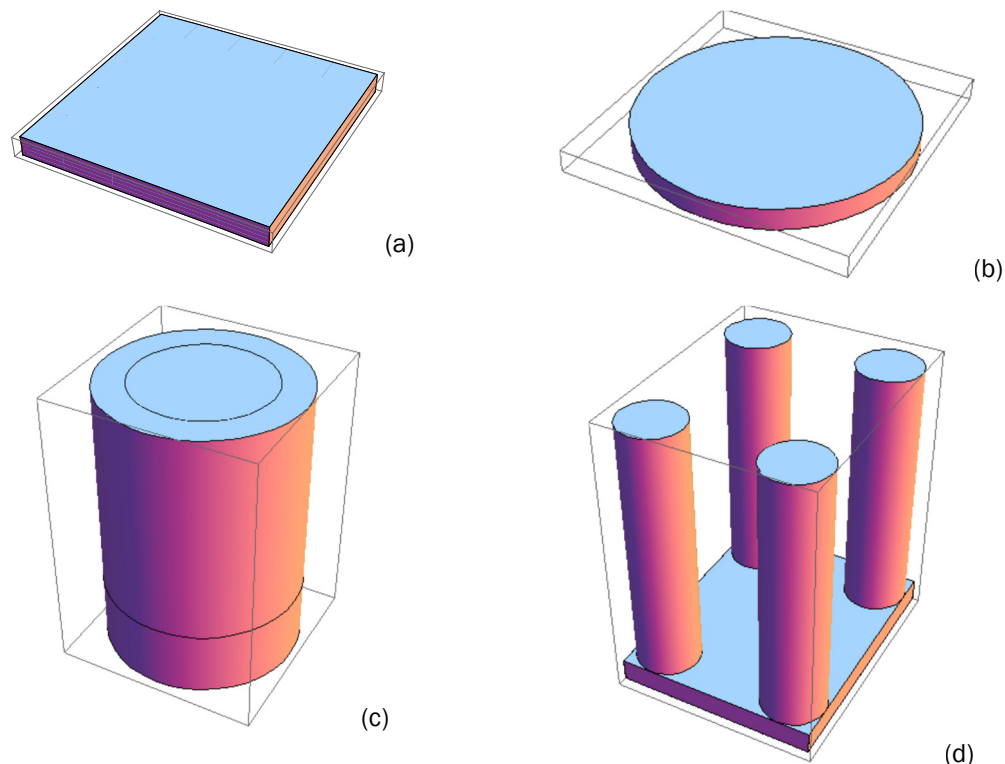


Figure 7-1: Floater configurations considered: a) rectangular barge, b) cylindrical barge, c) annular floater with a solid bottom ring and d) four cylindrical floaters on a solid plate

Given that such a huge structure is rather intended for deep offshore operation we investigate the alternative of mounting the system on a floating platform yawing in the sea.

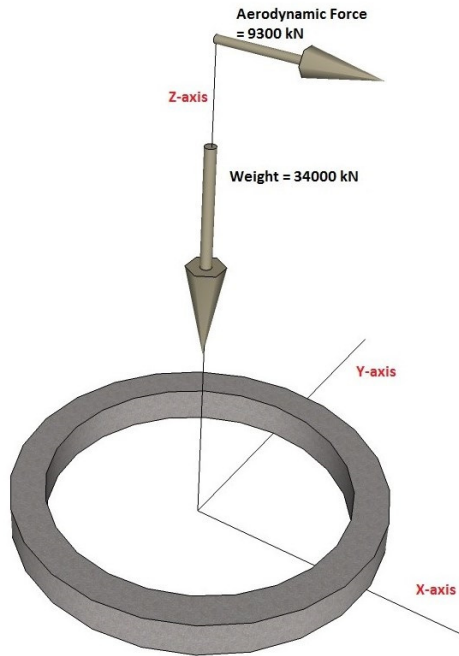
A barge-type floater seems then to be ideal for undertaking the large weight and footprint of the structure, making at the same time yawing easier. The main advantages of floating concrete structures lie in the economy of the materials used (concrete is very well suited to a marine environment) and in the fact that it is easy to make concrete structures buoyant in the construction stage. Four different floater configurations have been investigated in the present context, as presented in Figure 7-1, a rectangular and a cylindrical barge, an annular floater with a solid concrete bottom ring and a combination of four cylindrical floaters sitting on a solid concrete plate.

The scope of the present investigation is the dimensioning of the floaters (lengths, inner and outer diameters, submerged and above mean-sea-level heights) and, from that, the estimation of their construction cost, needed for the LCoE analysis of the multi-rotor system.

The initial analysis of D1.33 did not include any constraints on the natural frequencies of the floaters. During the course of the project WP4 came along with D4.33 which includes specifications for the designs of the INNWIND.EU floaters. Non-surprisingly important restrictions are suggested for the system frequencies in connection to the wave energy spectrum. Under these conditions the D1.33 floater section had to be revised accordingly. New parametric designs were performed attempting to lower the heaving and pitching frequencies below 1/20 and 1/25 Hz respectively.

7.2 Design method and assumptions made

The dimensioning of the concrete floater is done for hydrostatic stability. Using the extreme MRS thrust (deriving from DLC 6.2 and DLC 1.3) we are looking for the size of the floater that can withstand their overturning moments and providing the buoyancy needed. The coordinate system used, the magnitude of the applied forces and the coordinates of the aerodynamic and gravity centres of the MRS are given in Figure 7-2.



Coordinate System and MRS Forces		
Coord System:	{0,0,0}	at sea level, along Z-symmetry axis
Aerodynamic Force :	(kN)	{-9310, 0, 0}
Weight :	(kN)	{0,0,-34000}
Aeodynamic Center :	(m)	{0.9,0,122}
Center of MRS Gravity :	(m)	{0,0,98}

Figure 7-2: MRS forces for floater design

The calculations for hydrostatic stability are done with relevant scripts that have been programmed in Mathematica [26]. When the floater dimensions are calculated, it's mass and cost is estimated using data from Table 7-1.

Concrete density	(kg/m ³)	2500, Ref [31]
Sea water density	(kg/m ³)	1030
Mean Floater density (<i>hollow</i>)	(kg/m ³)	500, Ref [32]
Structural Concrete Price	(US\$/m ³)	800, Ref [33]
Structural Steel for Concrete Reinforcement	(kg/m ³)	400, Ref [31], [32]
Structural Steel price	(US\$/kg)	2.1, Ref [33]

Table 7-1: Assumptions made for concrete floaters

7.3 Results

Table 7-2 and Table 7-3 present a summary of the results obtained for the rectangular and cylindrical barge configurations of Figure 7-1. The columns of the tables represent alternative designs having the same topology. The first rows are listing the basic floater dimensions, the last one being the total height. Then, the height is split in its over-water (h-above MSL) and under-water (draft) parts. Finally, the floater buoyancy is presented along with cost estimation (concrete, steel and total cost). We end-up with the heaving and pitching natural frequencies.

Mean Floater Density	(kg/m ³)	500	500	500	500	500	500	600	700
Diameter	(m)	100	90	80	70	60	55	55	55
Height	(m)	3.219	4.432	6.510	10.745	23.869	44.001	51.917	65.525
h - above MSL	(m)	1.228	1.752	2.680	4.654	11.092	21.225	20.258	19.960
h-submerged	(m)	1.991	2.680	3.830	6.091	12.777	22.776	31.659	45.565
Floater Mass	(tn)	12643	14098	16363	20677	33743	52270	74007	108973
Boyancy	(kN)	158027	172303	194518	236838	365024	546764	760013	1093850
Structural concrete volume	(m ³)	5057	5639	6545	8270	13497	20908	29603	43589
Structural steel mass	(tn)	2023	2256	2618	3308	5399	8363	11841	17436
Concrete cost	(Mil US\$)	4.046	4.511	5.236	6.616	10.798	16.726	23.682	34.871
Steel cost	(Mil US\$)	4.248	4.737	5.498	6.947	11.337	17.563	24.867	36.615
Total Cost	(Mil US\$)	8.293	9.248	10.734	13.563	22.135	34.289	48.549	71.486
Natural freq heaving	(Hz)	0.353	0.304	0.255	0.202	0.139	0.104	0.088	0.073
Natural freq pitching	(Hz)	0.187	0.148	0.113	0.080	0.046	0.022	0.018	0.013

Table 7-3

Mean Floater Density	(kg/m ³)	500	500	500	500	500	500	600	700
X-Size	(m)	100	90	80	70	60	50	50	50
Y-Size	(m)	100	90	80	70	60	50	50	50
Height	(m)	2.019	2.722	3.858	5.918	10.582	31.462	42.071	62.517
h - above MSL	(m)	0.702	0.985	1.460	2.358	4.510	14.844	16.218	18.683
h-submerged	(m)	1.317	1.737	2.398	3.560	6.072	16.618	25.853	43.834

Floater Mass	(tn)	10095	11023	12346	14500	19048	39327	63106	109406
Boyancy	(kN)	133035	142133	155116	176245	220866	419800	653069	1107270
Structural concrete volume	(m3)	4038	4409	4938	5800	7619	15731	25242	43762
Structural steel mass	(tn)	1615	1764	1975	2320	3048	6292	10097	17505
Concrete cost	(Mil US\$)	3.230	3.527	3.950	4.640	6.095	12.585	20.194	35.010
Steel cost	(Mil US\$)	3.392	3.704	4.148	4.872	6.400	13.214	21.203	36.760
Total Cost	(Mil US\$)	6.622	7.231	8.098	9.512	12.495	25.799	41.397	71.770
Natural freq heaving	(Hz)	0.434	0.378	0.322	0.264	0.202	0.122	0.098	0.075
Natural freq pitching	(Hz)	0.248	0.199	0.154	0.113	0.075	0.033	0.029	0.018

Table 7-2: Alternative designs for the rectangular barge (a)

Mean Floater Density	(kg/m3)	500	500	500	500	500	500	600	700
Diameter	(m)	100	90	80	70	60	55	55	55
Height	(m)	3.219	4.432	6.510	10.745	23.869	44.001	51.917	65.525
h - above MSL	(m)	1.228	1.752	2.680	4.654	11.092	21.225	20.258	19.960
h-submerged	(m)	1.991	2.680	3.830	6.091	12.777	22.776	31.659	45.565
Floater Mass	(tn)	12643	14098	16363	20677	33743	52270	74007	108973
Boyancy	(kN)	158027	172303	194518	236838	365024	546764	760013	1093850
Structural concrete volume	(m3)	5057	5639	6545	8270	13497	20908	29603	43589
Structural steel mass	(tn)	2023	2256	2618	3308	5399	8363	11841	17436
Concrete cost	(Mil US\$)	4.046	4.511	5.236	6.616	10.798	16.726	23.682	34.871
Steel cost	(Mil US\$)	4.248	4.737	5.498	6.947	11.337	17.563	24.867	36.615
Total Cost	(Mil US\$)	8.293	9.248	10.734	13.563	22.135	34.289	48.549	71.486
Natural freq heaving	(Hz)	0.353	0.304	0.255	0.202	0.139	0.104	0.088	0.073
Natural freq pitching	(Hz)	0.187	0.148	0.113	0.080	0.046	0.022	0.018	0.013

Table 7-3: Alternative designs for the cylindrical barge (b)

It can be seen in Figure 7-3 for the cylindrical barge case that low frequency floater designs are characterized by a significant increase of mass and cost. Lowering the heaving frequency below 1/20 Hz would require an extremely heavy and expensive floater. Similar conclusions can be drawn for the rectangular barge. Although the simple barge designs look cost efficient when natural frequencies are not constrained they lose this advantage when low frequency designs are sought. On the other hand stiff designs, that over-exceed the critical wave frequency range, are unrealistic because of their extremely high width to height ratio. Given their high cost these simple designs are not considered suitable for the present application.

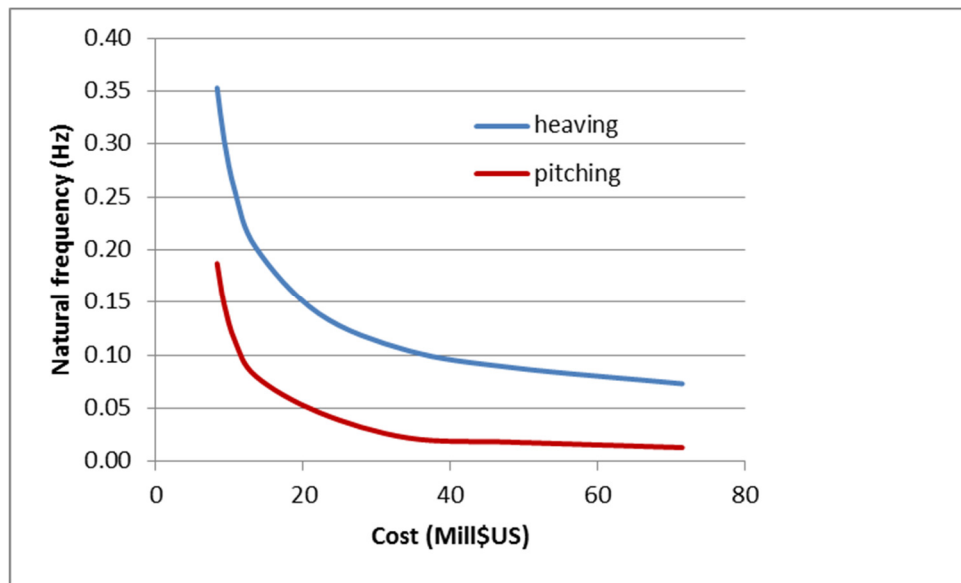


Figure 7-3: Cost-frequency dependence of a cylindrical barge for the 20MW MRS

Mean Floater Density	(kg/m ³)	500	500	500	500	500	500	500
Dmin	(m)	29.500	34.200	37.000	41.800	45.000	46.800	45.550
Dmax	(m)	70.500	65.800	63.000	58.200	55.000	53.300	54.450
Concrete bottom height	(m)	0.000	0.000	5.000	10.000	15.000	20.000	20.000
Height	(m)	11.750	20.120	39.550	60.280	82.360	105.800	94.550
h - above MSL	(m)	5.000	9.000	9.000	9.000	9.000	9.000	5.000
h-submerged	(m)	6.750	11.120	30.550	51.280	73.360	96.800	89.550
Floater Mass	(tn)	18876	25008	60924	64853	56266	47634	60945
Boyancy	(kN)	219175	279326	631667	670210	585975	501295	631870

Structural concrete volume	(m3)	7550	10003	24369	25941	22507	19054	24378
Structural steel mass	(tn)	3020	4001	9748	10376	9003	7622	9751
Concrete cost	(Mil US\$)	6.040	8.002	19.495	20.753	18.006	15.243	19.502
Steel cost	(Mil US\$)	6.342	8.403	20.470	21.790	18.906	16.005	20.478
Total Cost	(Mil US\$)	12.382	16.405	39.965	42.543	36.911	31.249	39.980
Natural freq heaving	(Hz)	0.192	0.149	0.109	0.088	0.075	0.065	0.070
Natural freq pitching	(Hz)	0.077	0.054	0.047	0.039	0.033	0.028	0.039

Table 7-4: Alternative designs for the annular barge with a solid concrete bottom ring (c)

Table 7-5 presents different designs for concept (c), the annular barge with a solid concrete bottom ring of given height (from 0 to 20m). Compared to earlier designs it is now possible to reach heaving and pitching frequencies as low as 0.065 and 0,028 Hz with floater cost of 31.2 Mil US\$ (see the yellow highlighted column). Nevertheless, this particular design is characterized by a very long draft of 97m resulting to an uncomfortably large aspect ratio $2H/(D_{max}-D_{min})$ which might be difficult to construct.

Table 7-5 presents five alternative designs of concept (d). In this case we have restricted the design window to configurations with low natural frequencies. The highlighted design is our preferred option combining relative low frequencies 0.056 and 0.026 Hz along with a relative low cost *31.1 Mil US\$) and draft (41.5m).

Mean Floater Density	(kg/m3)	500	500	500	500	500
Cylinder Diameter	(m)	27.700	25.630	10.038	11.320	14.020
Cylinder Height (CH)	(m)	40.730	47.140	131.750	118.430	57.450
CH - above MSL	(m)	8.000	10.000	12.000	15.000	16.000
CH-submerged	(m)	32.730	37.140	119.750	103.430	41.450
Plate thickness	(m)	5.000	5.000	5.000	5.000	5.000
X-distance bet cylinders	(m)	30.000	30.000	30.000	30.000	30.000
Y-distance bet cylinders	(m)	40.000	40.000	40.000	40.000	40.000
Floater Mass	(tn)	97933	94272	45895	50350	47467

Boyancy	(kN)	994728	958812	484233	527941	378828
Structural concrete volume	(m3)	39173	37709	18358	20140	18987
Structural steel mass	(tn)	15669	15084	7343	8056	7595
Concrete cost	(Mil US\$)	31.338	30.167	14.686	16.112	15.190
Steel cost	(Mil US\$)	32.905	31.676	15.421	16.918	15.949
Total Cost	(Mil US\$)	64.244	61.843	30.107	33.030	31.139
Natural freq heaving	(Hz)	0.073	0.073	0.041	0.044	0.056
Natural freq pitching	(Hz)	0.030	0.030	0.013	0.013	0.026

Table 7-5: Alternative designs for the four cylindrical floaters on a solid plate (d)

7.4 Discussion on the results

We are reporting the following conclusions from the concrete floater designs exercise:

1. The simpler concepts (a) and (b) are becoming extremely expensive when low frequency solutions are sought. Because of that they are not further considered.
2. The floater mass and cost sensitivity to system natural frequencies appeared in all cases examined to be extremely high, especially at the low frequency part of our concern. This might be explain why earlier alternative floater designs in INN WIND.EU presented an unusually large mass and cost scatter.
3. Concept (c) and especially (d) provide better possibilities for low frequency designs at reasonable cost. Indicative mass and cost figures for the highlighted solutions for the 20MW MRS are: Mass ~48 ktn, Cost ~32 Million US\$.

CHAPTER 8 ELECTRICAL SYSTEMS DESIGN

8.1 General

The main aims of the MRS electrical design were to:

- a) Investigate in a preliminary way the impact of clustering the turbines electrically in groups
- b) Develop wiring arrangements among the turbines that were not unduly expensive whilst ensuring that any single fault did not compromise a large amount of output power.
- c) Ensure that fault conditions e.g. grid loss did not result in design driving loads

8.2 Electrical Infrastructure

The choice of having many small turbines in the MRS implies more electrical interconnections. However with the MRS aggregating greater output capacity on a single structure than would be possible with the single turbine concept the requirement for expensive intra-turbine cable laying on the seabed is reduced and overall any cable maintenance/replacement required is significantly easier.

It is possible and perhaps desirable to aggregate expensive power electronics into small clusters of multi-rotors. In this way, several wind turbines could share key costly components (such as transformers) while retaining essential components such as a generator and back-to-back converter. Cost and complexity could be reduced at the expense of some operational adaptability. There may also be the potential to improve overall reliability through the use of an entire redundant link for several individual turbines located in a cluster.

8.2.1 Inverters

Self-commutated inverters are capable of providing power conversion capabilities in the range of 200kW to 1MW, which should be suitable for most conceivable multi-rotor systems.

8.2.2 Electrical Clusters

An indication of the power performance implications of clustering is now presented. It is not yet feasible to determine if there is a LCOE benefit in any trade off involving

performance loss in clustering, with electrical component cost reduction. Local electrical clusters are a trade-off between controllability and maximum energy capture versus cost. The theory is to aggregate many parts of the electrical network into a single network of equivalent capacity.

In Figure 1, the rotors are presented as circles with the dark lines indicating which turbines are linked together. Thus there are 15 clusters of between 2 and 4 machines. In this configuration there is the possibility to reduce the number of DC-links, transformers, circuit-breakers and protection equipment by 1/3.

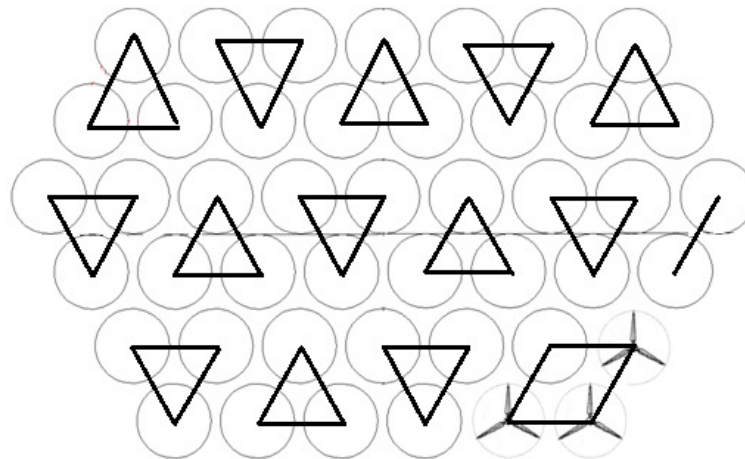


Figure 8-1 - Small Clusters of 2, 3, or 4 Machines.

Consider the cluster at the top left of the array. This constitutes turbines 31, 32 and 39 according to a bottom to top, left to right numbering system. Investigating the longitudinal components of the point history wind speed of wind field passing through this cluster at the three hub points leads to the plot of Figure 8-2. Each of the three turbines experience a very similar overall change in longitudinal wind speed but over the course of several cycles (<5s scale) there can be significant difference. In effect, clustering will act to remove any local variations in power production and average out the effective wind (essentially reducing the turbulence).

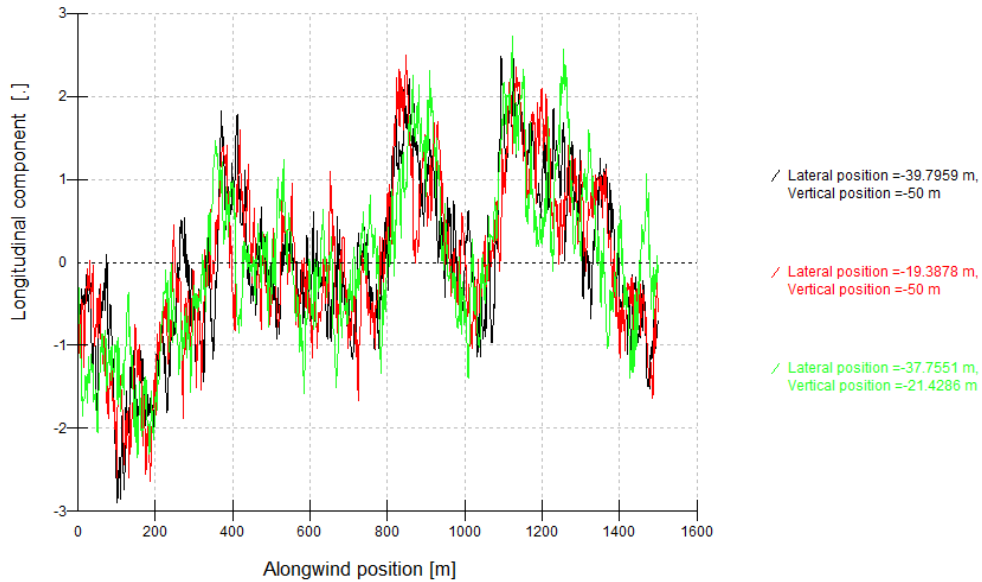
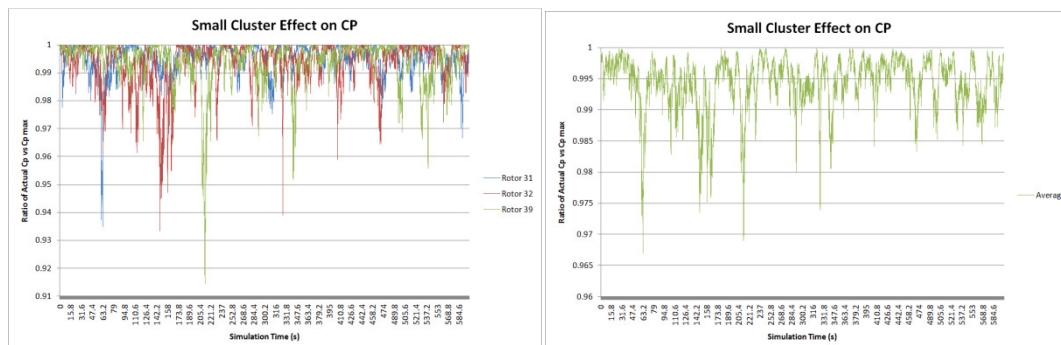


Figure 8-2 - Wind Longitudinal Component Point History of Turbines 31, 32 and 39

To examine the potential trade-off in terms of power loss for simplicity in the electrical configuration we examine the wind speed across the cluster at a single time point. At this point we will assume that the rotor speed is configured to obtain maximum power coefficient for an average wind speed of 11m/s. This corresponds to a tip speed ratio of 8.5 and therefore a rotor speed for a 40.55 m diameter rotor of 2.3 rad/s. Assuming that the electrical frequency of the three systems is to remain in phase these three rotors will rotate at the same speed of 2.3 rad/s.

In this particular wind field, an average wind speed of 11.04 m/s is measured across this cluster at 92.4 seconds. This corresponds to a longitudinal wind speed of 10.94 m/s at turbine 31, 10.59 m/s at turbine 32 and 11.63 m/s at turbine 39. Assuming a constant rotor speed, the tip speed ratios of turbines 31, 32 & 39 are calculated as 8.52, 8.80 and 8.02 respectively.



Relating these values with the C_p - λ characteristic on an MRS turbine, clearly the 3 rotors cannot all operate at maximum power coefficient. Rotor 31 remains at $C_{p_{max}}$ while rotor 32 experiences a 1.659% decrease in C_p and rotor 39 experiences a 0.945% decrease in C_p . Total C_p loss for the cluster is therefore averaged at 0.238% for the time point 92.4 seconds

The same analysis is conducted on a slightly larger cluster using the same wind field and the same time frame. The top left cluster now contains 5 turbines in this instance with the addition of turbines 40 and 33 (see Figure 8-3).

Although only two turbines were added to the cluster the total C_p loss for the cluster in this case is 0.712%, which is nearly three times the loss in the previous example. This confirms the hypothesis that by increasing the cluster size the spatial coherence of the wind begins to take its toll on each turbine's ability to respond optimally to average control inputs.

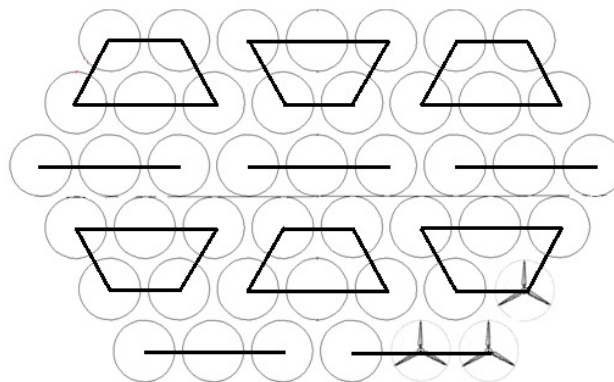


Figure 8-3 - Medium Clusters

The same procedure is carried out on an even larger cluster set. In this case Figure 8-4 presents a cluster containing 8 turbines. Using the same averaging control strategy a total C_p loss of 2% is expected over the cluster, again nearly a three-fold increase in the loss.

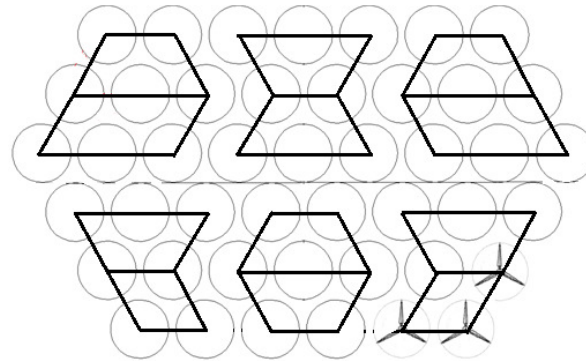


Figure 8-4 - Large Clusters

At present the impact of clustering has not been investigated further. The MRS CAPEX without clustering is affordable and the benefit of independent, asynchronous operation of rotors on loads is clear. This still leaves open the possibility of some further LCOE benefit through an appropriate extent of clustering when a sufficiently refined LCOE model is available to assess this.

8.2.3 Provisional wiring arrangement for MRS

An optimisation of the interconnections between turbines was conducted having regard to redundancy to limit loss of capacity from a single fault. The chosen arrangement is illustrated in Figure 5 where any single wiring fault will at most cause a loss of 9% of output

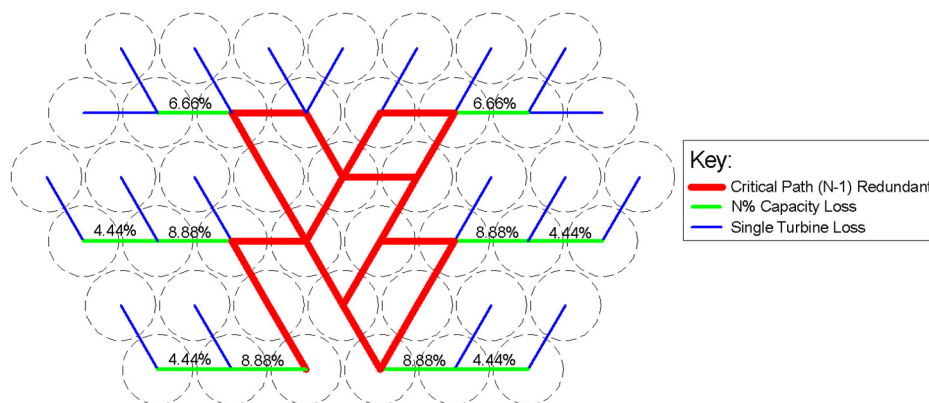


Figure 8-5: Optimised Electrical Interconnections with Redundancy

8.2.4 Control strategy

One proposed strategy is to control generator torque through a Field Orientated Control (FOC) which controls the converter side. The turbine, despite being decoupled from the grid will experience a small increase in speed in the presence of a grid fault.

To provide fault-ride through capability, the inverter is controlled so as to provide minimum active power and maximum injection of reactive power so as to compensate for a low grid side voltage and maintain maximum current until clearance of the voltage fault.

8.2.5 Resistors for load dump

The extreme designing load case for the multi-rotor system would occur if all the rotors in the array were simultaneously shutdown - for example, in an attempt to avoid over-speed after a system wide fault. This corresponds to the IEC design cases DLC2.3 and DLC4.2.

The ability to stagger the shutdown of rotors in the array - by only a few seconds - is enough to prevent loads arising that may be design driving for the space frame structure and otherwise add mass and cost to the structure.

One method of enabling a staged shutdown is to provide dump load resistors for each rotor or for groups of rotors. In this way loss of the grid does not immediately result in a loss of load and dangerous over speed of any rotor is avoided. The requirements for such a load dump would be that it would draw power for a set period of time while enabling a staged shutdown of all the rotors in the array. The load itself would need to be capable of drawing the full rated power from the array, though the total power through the load would reduce gradually over this period.

There are two types of load dump that might be contemplated either in isolation or partnership. The first would be an auxiliary battery bank which would be charged - but limited by current input and therefore of limited capability. The second is a set of simple load dump resistors whose only job is to absorb the power and convert it to heat safely, for dissipation into the surrounding environment. The latter would be limited only by size and weight considerations.

For a 45 rotor array rated at 20MW a potential load dump system has been investigated. This would comprise of 900 individual resistors in the form of 45 parallel paths of 20 resistors formed from a mixture of iron and copper, each with an individual resistance of 21.5Ω , a specific heat capacity, C , of 20 J/kg.K and mass of 5kg. The resistors have been

sized according to a requirement of dual-staged (pairs of rotors) shutdown with stages offset by 2.35s each.

Initial ohmic heating could raise resistor temperatures at a rate of $222\text{ C}^\circ/\text{s}$ (assuming no loss). However the system load will be successively reduced such that no individual load resistor will exceed a safe percentage of melting point. With the addition of a fin heat-sink array and potentially (offshore) the use of water cooling will help ensure that the load dump system can safely dissipate the MRS load for the duration of the shutdown.

All this could be achieved using individual resistors with sizes in the region of: $0.1 \times 0.075 \times 0.075\text{m}$ resistors weighing in at 5kg for a total system weight of only 4.5t. Both in absolute terms and in comparison to the additional structural requirements to fully design for DLC2.3 and DLC4.2 without the proposed measures which may add 200-300t, this added weight cost is inconsequential.

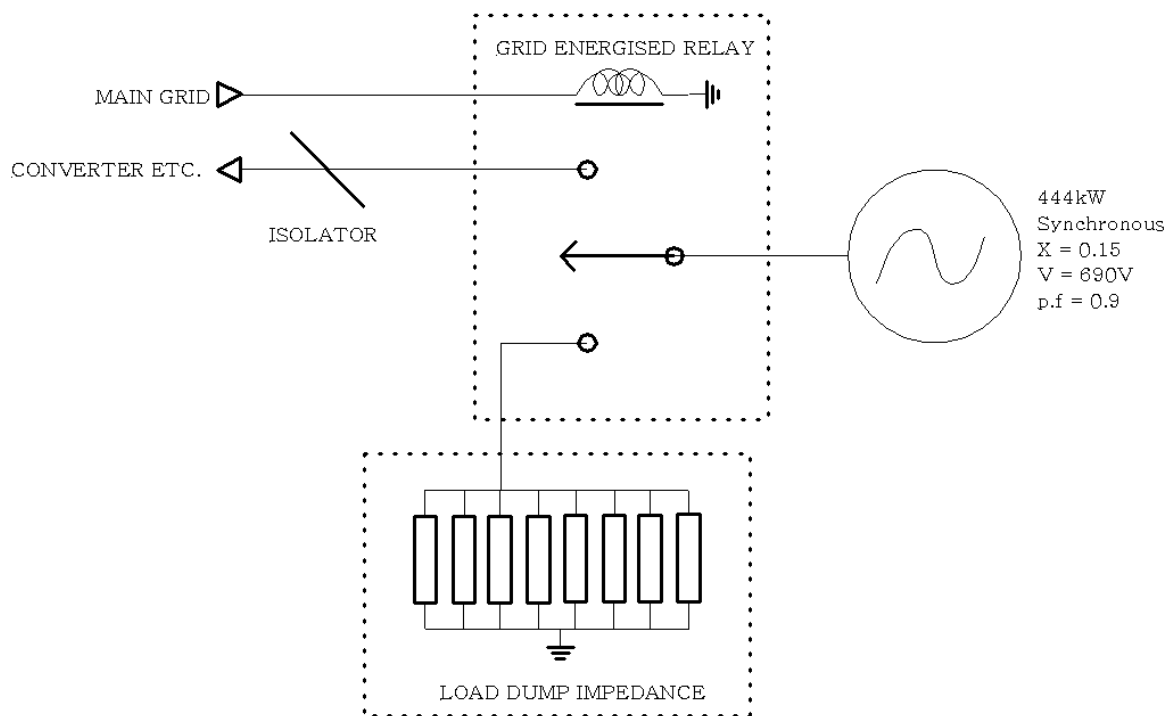


Figure 8-6 - Turbine Side Load Dump Resistor

The load dump consists of coils of wire, and so is inductive as-well as resistive. It may also be placed on the collector side. Ideally it should be placed as close to generator as possible so as to provide fail-safe protection in event of a local fault and the potential for

fault-ride through. It may also be located on the DC-link where the inductance will become zero after the initial relay switch.

CHAPTER 9 YAWING OF THE MRS

9.1 Yaw system design

Although many options are available for active and passive control of yawing in normal operation, a system which will neither depend on active pitch control nor on auxiliary power systems to maintain a safe yaw alignment in fault cases is preferred. A load specification is obviously one key requirement for design of a yaw system. Existing load calculations (Chapter 5) give a very good indication of dynamic load variations in the yaw moments and overturning moments and these are substantially averaged out by turbulence when the rotors are operational. In order to evaluate requirements for yaw actuation and regulation, and to see if yaw motor and brakes (excluding a parking or locking mechanism) are required, two sources of steady yaw moments are evaluated.

- Yawing moments arising from aerodynamic drag on the space frame structure members
- Yawing moments that could be created by active control of rotor thrusts via blade pitch control

9.1.1 Yaw moments due to structure drag

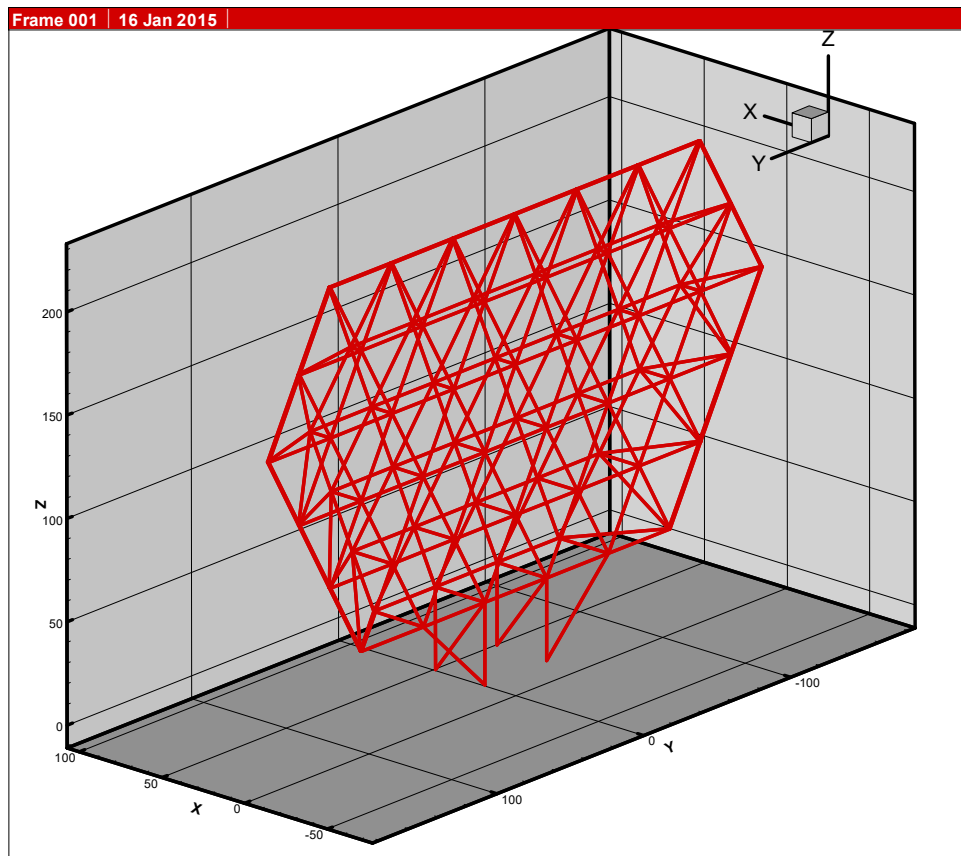


Figure 9-1 Axes definition in relation to structure

NOTES

The force and moment components are given in the X,Y,Z system which is fixed to the support structure (Figure 9-1).

The origin of the X,Y,Z system (0,0,0) is at the ground level (z=0) at the front face of the structure (x=0) where the turbines are mounted and at (y=0) the symmetry level of the structure

The yaw angle is the angle of the wind speed with the x-axis

Fz is the total weight of the structure

MASS (kg) = 3446325

Center of Gravity -x (m) = 7.399

Center of Gravity -y (m) = 0

Center of Gravity -z (m) = 97.379

Moment of Inertia -x axis (kg*m²) = 60461070877

Moment of Inertia -y axis (kg*m²) = 45269607881

Moment of Inertia -z axis (kg*m²) = 16248817194

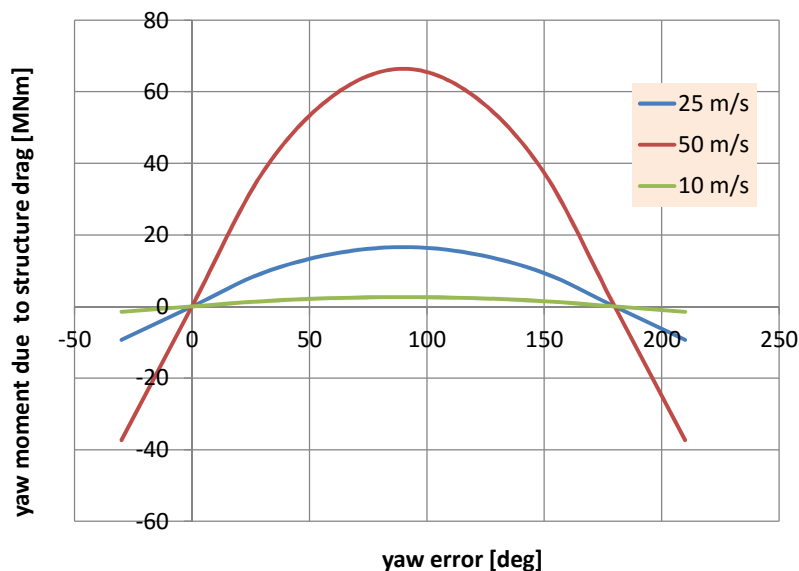


Figure 9-2 Yaw moments due to drag on the structure

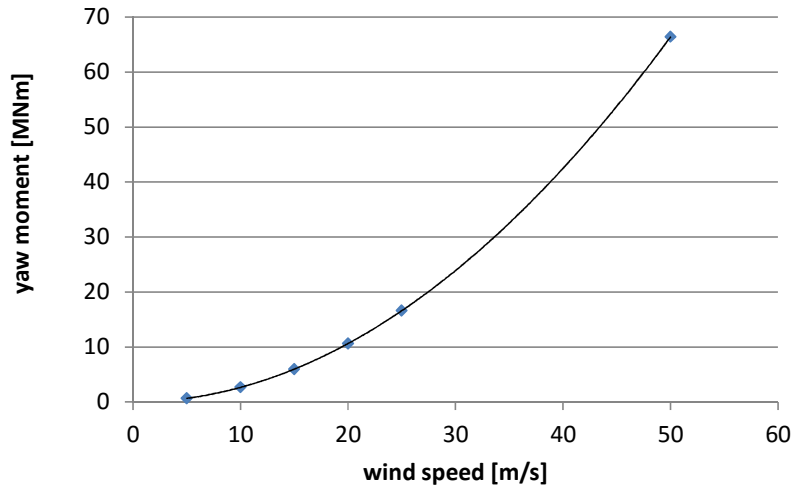


Figure 9-3 Yaw moment from drag on the structure in 90° yaw error

9.1.2 Effect of yaw system centre location on yaw stability

Dx	h	4	m			
wind speed	U	50	m/s			
	unit Mz	unit Fy	unit Mz(h)	Mz	Fy	Mz(h)
0	0.000	0.0000	0.0000	0.00	0.00	0.00
30	14.937	2.5351	4.7961	37.34	6.34	11.99
60	23.534	3.9243	7.8364	58.83	9.81	19.59
90	26.568	3.2086	13.7331	66.42	8.02	34.33
120	23.534	3.9243	7.8364	58.83	9.81	19.59
150	14.937	2.5351	4.7961	37.34	6.34	11.99
180	0.000	0.0000	0.0000	0.00	0.00	0.00
210	-14.937	-2.5351	-4.7961	37.34	-6.34	-11.99
240	-23.534	-3.9243	-7.8364	58.83	-9.81	-19.59
270	-26.568	-3.2086	-13.7331	66.42	-8.02	-34.33
300	-23.534	-3.9243	-7.8364	58.83	-9.81	-19.59
330	-14.937	-2.5351	-4.7961	37.34	-6.34	-11.99
360	0.000	0.0000	0.0000	0.00	0.00	0.00

Table 9-1 Yaw moment components

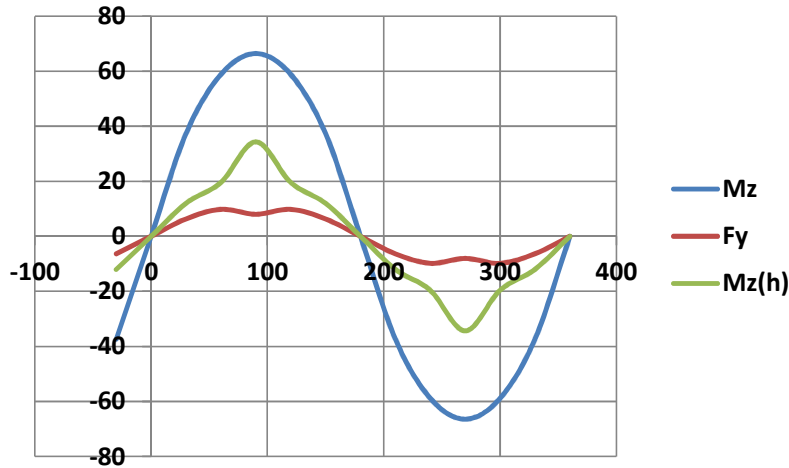


Figure 9-4 Yaw moment from drag on the structure with $h=4m$

From Figure 9-1 it is evident that yawing moments on the structure associated with drag on the structural members will depend primarily on the moment $M_z(h)$, about a vertical axis and the moment due to a lateral force F_y acting at the aerodynamic centre of the array at a distance h from the centre of rotation. Drag forces and moments will be simply proportional to the dynamic pressure of the wind and thus will vary as square of wind speed (Figure 9-2). Table 9-1 shows values for unit wind speed and for 50 m/s wind speed in the case where the centre of rotation is 4m upwind of the aero centre. In the structural analysis (Chapter 6) a convention was adopted in which the positive yaw moment and positive yaw error angle are in opposite senses. Figure 9-3 shows the magnitude of yaw moments at 90 yaw error and reinforces the desirability of such moments being stabilizing, this tending to reduce yaw error. It is clearly important that yawing activity does not require to oppose structure drag moments in any major way.

In Figure 9-4, a positive slope of $M_z(h)$ represents a stable condition with the moment acting to reduce yaw error. The choice of design centre of yaw rotation is clearly critical. The further upwind, i.e. the more negative h is, the greater are the restoring moments with a possible result that the system may self-yaw based on structure drag forces possibly without assistance from control of rotor thrust. Very large self-yawing moments can be generated by having the centre of rotation sufficiently far upwind. However the choice of centre of rotation will affect design and cost of the support structure and also the distribution of loading over the yaw ring.

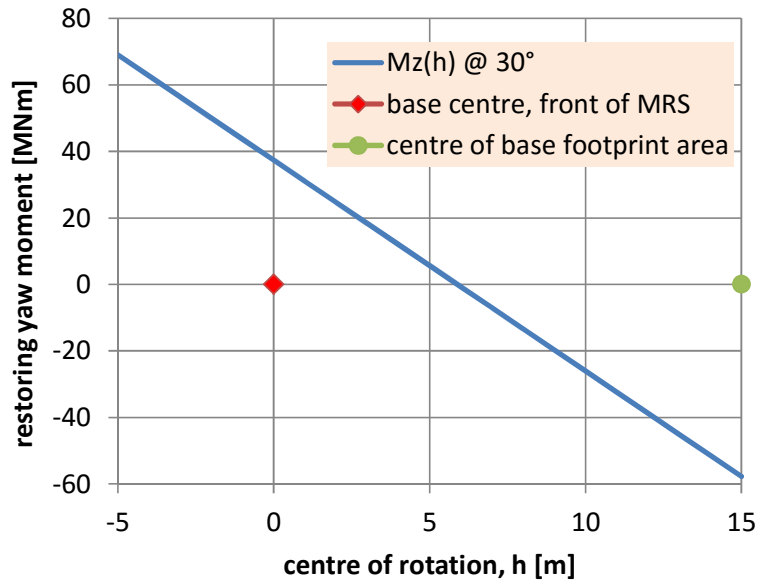


Figure 9-5 Yaw moment from drag on the structure with $h=4\text{m}$

From Figure 9-5, it is evident that the centre of rotation must be at position $h < 6$ m for structure drag moments to be stabilising. This is equivalent to the centre of rotation being more than 9 m upwind of the centre of the 40 x 30 m base footprint. It seems desirable to have such a position as the system will then be stable in yaw in the event of a loss of grid connection to the MRS.

9.1.3 Active control of yaw using rotor thrust

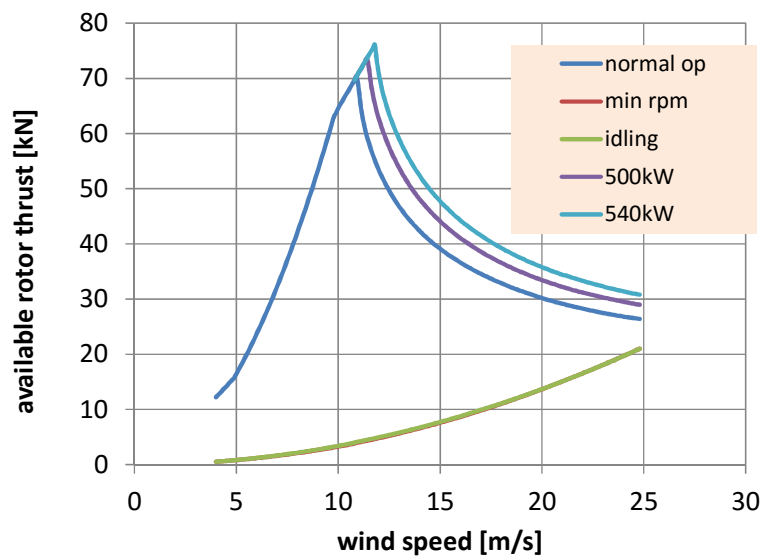


Figure 9-6 Available thrust per rotor depending on operational state

The rotors of the MRS are nominally rated at 444 kW so that all 45 provide the design system output rating of 20 MW. However the individual turbines may be up-rated with various benefits;

- Greater safety margins on generator temperature and improved reliability,
- Capability of individual rotors to operate above 444 kW gaining extra energy in turbulent conditions where some rotors operate above rated wind speed and some below,
- Extra margins on thrust range which may assist control functions

Of course there will be added cost in proportion to generator up-rating but there need not be much further added cost in major downstream electrical systems providing the array output is always limited to 20 MW. At this stage there is no conclusive analysis but the uprating option may show cost benefit. Steady state thrust characteristics are illustrated in Figure 9-6. From the steady state thrust characteristics with or without over-rating on generator output capacity, moments that can be generated by differential control of rotor thrust over the array (including having some rotors idling but generally preferably not) can be evaluated.

This is studied in detail in Innwind Task 1.42 and only a summary of salient findings is presented here. The scope of MRS work for deliverable 1.42 was to examine methods to maximally exploit the additional capability of distributed control to improve the performance relative to current control systems; specifically multi-rotor wind turbine control as a distributed control scheme was to be examined, involving:

- a) Management of power and distributed thrust loadings over the array of a multi rotor
- b) Stabilization of floating structure via low frequency pitch activity and torque reaction

The work on yaw control and fore-aft concerns the management of distributed thrust loadings over the array of a multi-rotor, as well as stabilization of the MRS on a floating structure via low frequency pitch activity and torque reaction.

Management of power over the array of a multi-rotor is explored in the work on droop control and synthetic inertia.

It was found that it is feasible to control the yaw of a multi-rotor system using distributed control via the incorporation of power adjusting controllers on each RPC system on the multi-rotor. The yaw of the multi-rotor is stabilised through control of the thrust on the rotors.

A suitable spar floater was designed for the multi-rotor, taking into account both the aerodynamic and hydrodynamic loads. This model was used to demonstrate the feasibility of damping the fore-aft pitching of the multi-rotor through distributed control. It was demonstrated that without remedial action the fore aft motion of the multi-rotor could cause instability of the RPC system controllers. Distributed control reduces the fore-aft

pitching motion, maintaining stability of the RPC system controllers and improving power quality.

The capability of the multi-rotor to provide synthetic inertia was examined. The multi-rotor does not have the capability to provide synthetic inertia at the same levels as a conventional wind turbine largely because of the much reduced overall mass and rotational inertia of the sum of MRS rotors compared to a single equivalent rotor. However it is possible to provide synthetic inertia equivalent to the inertia of synchronous machines at most wind speeds.

9.2 Engineering of yaw systems

9.2.1 Concepts for yawing

Yawing in the sea may ultimately be the optimum solution especially for deployment at water depths where jackets are impractical. However, within the resources of the present project, there is no possibility to undertake the design of a moored yawing turret, mooring connections to floater and, as would be necessary for a quantitative analysis, including the important dynamics of wave and wind interacting with the degrees of freedom of the floater as affecting yawing behaviour.

Therefore in order to bound the problem of estimating yaw system feasibility and cost and achieve more direct comparability with the RWT as a 10 MW turbine mounted on a jacket, it is proposed to consider options for yawing the system using bearing arrangements that would suit an MRS mounted on a jacket (or for that matter land based).

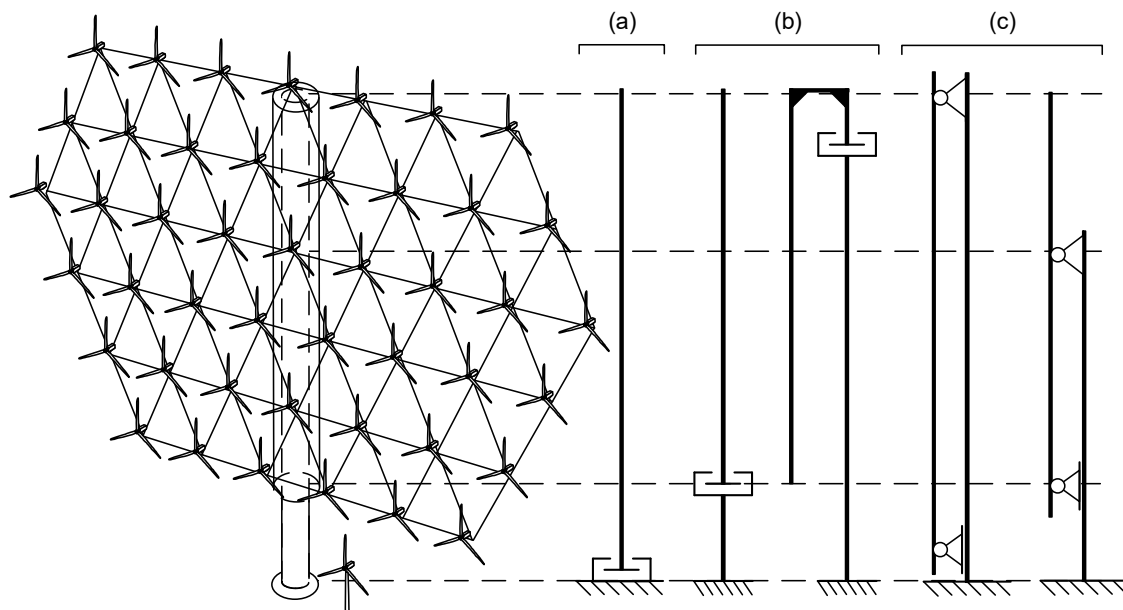


Figure 9-7 Yawing bearing arrangements for a 20 MW MRS

The Hamburg University of Applied Sciences (HAW Hamburg) is conducting research on multi rotor systems and has contributed a study on Yaw Bearing Concepts for Multi Rotor Systems. Much of the work presented in this section is based on that study.

Concept arrangements for yawing of the system are presented in Figure 9-7. Figure 9-7 (a) shows a base bearing which may either be mechanical or may correspond to rotation of an MRS system rigidly attached to a floater turning in the sea about a mooring turret.

Yawing with a single bearing, the norm for large single rotor turbines, is shown in Figure 9-7 (b). The bearing supports radial- and axial forces as well as bending moments. Bending moments from the rotor support structure are carried through the single bearing so that bearing and support structure are highly loaded.

Figure 9-7 (c) shows a bearing concept with locating and non locating bearings. The locating bearing supports radial and axial loads while the non locating bearing supports mainly radial loads. The bending moment support is controlled by the distance between the bearings. The concept of utilizing two bearings arranged in the upper tower section with a locating and a non-locating bearing has been considered (see patent documents, US20120134841A1, EP2402599A2). It has been implemented in an early Enercon wind turbine design and currently by Mervento.

This concept was adopted in previous work on an MRS system [4] at 5MW scale. The frame supporting the rotor nacelle systems is then considerably lighter than the structure such as in Chapter 6 that is designed to accept base levels overturning moments. In the specific design developed in the previous project, the mass of frame, rotors and nacelles was less than for the rotor blades and hub of an equivalent single turbine. The tower is an added cost and weight but the yaw rings themselves have reduced loading compared to a loads on the yaw ring of an equivalent single rotor turbine. The reduction in dynamic loading of an MRS compared to an equivalent single rotor is very substantial as may be obvious considering the difference between yawing and overturning moments of the MRS array compared with a 20 MW single rotor (Figure 5-11 and Figure 5-12).

Whether a solution such as in Figure 9-7 (c) is optimum it enables the use of bearings in a size range presently used in wind turbines and large cranes. Also the argument presented in the previous paragraph indicates that, if yaw bearing arrangements are feasible for a single 20 MW turbine as has been considered in the UPWIND project [6], they should also be feasible for the 20 MW MRS. Thus while optimisation of design, cost and weight will remain unclear until much more extensive work has been undertaken, there is little doubt regarding the fundamental feasibility of yawing a 20 MW MRS.

9.2.2 Development of tower-frame concepts

Based on the CRES design (Chapter 6), Dalhoff and Kim (HAW Hamburg) set up the design of Figure 9-8 as a reference. This design is then compared with solutions (Figure 9-9) based on a central tower column. The space frame is connected to the tower via two

bearings, a fixed bearing at tower top position (transmitting axial and radial forces) and a loose bearing at tower bottom position transmitting only radial forces. This approach may seem odd at first sight as all the vertical loads have to flow up to the top bearing and then down the tower. However when the space frame hangs on the top bearing, many space frame members are under tension reducing buckling concerns whereas they would experience compression under self-weight loading in an arrangement with a base level slew ring.

The designs of Figure 9-9 employ diagonal stiffeners across structure nodes in various planes in the fore-aft directions and these are considered helpful in reducing bending loads in the main beams and hence may benefit overall structure mass. Bearings in these initial designs of Figure 9-9 are at top and bottom of the tower sections.

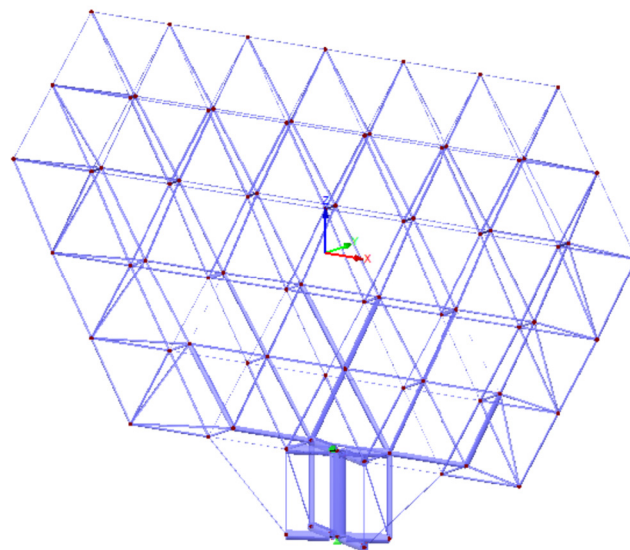


Figure 9-8 Reference design for development of yaw bearing solutions

Structural analysis was performed at HAW Hamburg using RSTAB, a commercial analysis program for 3D beam structures. As in the analyses of CRES, a set of standard tubular beam sections (11 in this case, see Table 9-2) were selected and optimisations run to meet loads with minimum system mass.

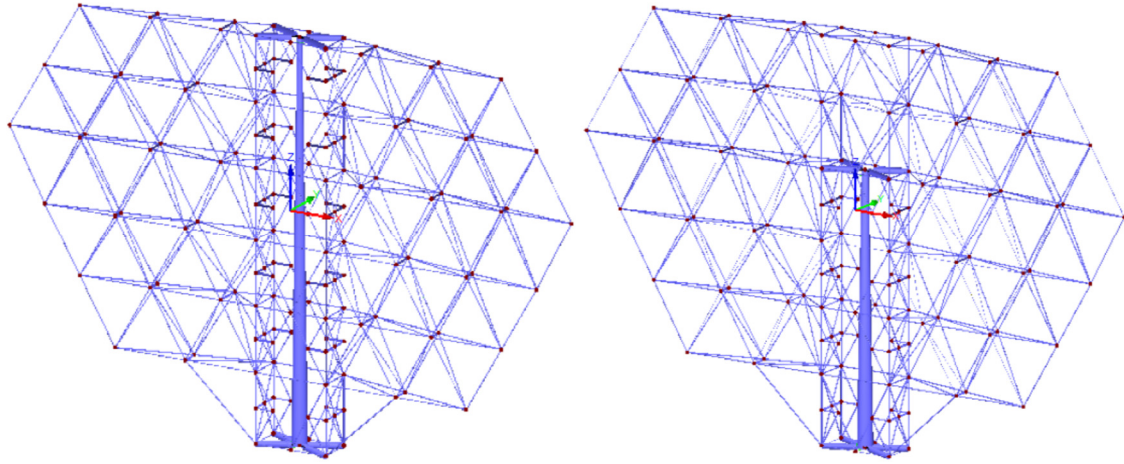


Figure 9-9 Full tower (left) and semi-tower solutions

Component	OD [mm]	thickness [mm]
space frame	114	2.5
space frame	219	4.0
space frame	273	5.0
space frame	300	10.0
space frame	356	6.0
space frame	711	4.0
yaw bearing	500	15.0
yaw bearing	2800	50.0
tower	3800	30.0
tower	6100	50.0
tower	7100	50.0

Table 9-2 Tubular cross sections

The much more comprehensive work of CRES is naturally the benchmark for structural design of MRS in the Innwind project, but the work of HAW Hamburg is very useful in making preliminary comparisons between design options for yawing.

In order to relate their work to the design of CRES, Dalhoff and Kim of HAW Hamburg developed design comparisons based on the DLC 1.3 loads as provided by UoS both to CRES and HAW Hamburg. To manage resources in studying a number of alternative solutions, the loads were then simplified in a way that allows very reasonable comparison of concepts but loses much of the advantage of the MRS averaging effects discussed in Section 5.7.1. Thus their design can be considered to be conservative in that respect.

	Semi-tower design	Reference MRS design
	Mass [t]	Mass [t]
Yaw Bearing connection top	389.75	-
Yaw Bearing connection bottom	17.03	-
Tower	834.51	-
Space Frame	1015.76	1371.00
Overall support structure	2257.05	1371.00

Table 9-3 Design Comparisons based on DLC1.3a1 excluding load safety factors.

A yield strength check based on such a conservative envelope of load case DLC1.3a1, but without load safety factors was performed. The total weight of the semi tower MRS support structure is 2,257 tons, of which 1,016 tons are space frame weight, 835 tons tower weight and 407 tons for the yaw connection between space frame and tower (Table 9-3).

Weight of the yaw bearings has not been considered, but the weight of the connecting members between space frame and tower with 407 tons is considered over conservative by Dalhoff and will cover some weight reserve for a yaw bearing arrangement.

The tower weight comes close to that of the space frame and could be reduced substantially by using a lattice tower. Lattice towers are stiff in bending and weak in torsion compared to tubular steel towers and can run into resonance problems for fixed yaw system turbines where yaw moments are transferred from rotor to tower. Since the MRS yaw system is designed as a free yaw system, the tower is free of torque. Thus the best solution may involve continuing the jacket above water as a lattice tower for attachment of MRS yaw bearings

Although the system weight for the semi-tower solution is higher than the MRS reference design weight calculated by CRES, the space frame itself is naturally lighter for the semi-tower solution and provides a solution for yawing. Dalhoff considers that tower and yaw bearing supports have substantial potential for further weight reduction.

The design in a previous project [4] of MRS at 5 MW scale produced the same result that tubular tower and space frame were of similar mass. .

The mass estimates of Table 9-3 relate to DLC 1.3 and, after fatigue calculations were performed as is noted in Section 6.6, a considerable increase in structure mass was required. This led to a final mass MRS system mass estimate of CRES at 3760 t. The space frame and tower masses in Table 9-3 relating to DLC 1.3 without safety factor were factored up in the ratio of $(3760/1371) \times 0.85$ as being the ratio determined by CRES of final mass to DLC 1.3 based value reduced by the factor 0.85 on account of HAW-Hamburg using conservative estimates of the DLC 1.3 loads. The yaw attachment structures were not further factored being considered to be quite conservative estimates

in the first place. This gives rise to rough estimates for a finished design based on space frame tower concept, now with yawing capability as in

Table 9-4.

	Semi-tower design	Reference design
	Mass [t]	Mass [t]
Yaw Bearing connection top	390	-
Yaw Bearing connection bottom	17	-
Yaw bearings	78	
Tower	1520	-
Space Frame with rotor nacelle assemblies	1850	3760
Overall support structure	3855	3760

Table 9-4 Final Design Comparisons of System Mass.

These estimates are of course rather crude and would need to be verified with more detailed design effort. However it does suggest that the tower-frame concept may have merit in providing a yaw solution avoiding a very large diameter single bearing and possibly without much added mass (especially as the reference design will inevitably incur extra mass for the yawing solution).

9.2.3 Yaw bearing solutions

Yawing the whole structure on a single base bearing (considering the scale of the MRS system) may be optimally achieved with innovative solutions possibly along the lines of bogies on tracks as in railway engineering but in arrangements that can contain uplifting loads. There is not resource to explore such possibilities in sufficient detail to arrive at mass and cost estimates.

However one solution established in industry for rotation of very heavy machinery including large telescopes is the hydrostatic bearing. A design from UoS for turbines ~ 500 kW rating, originally developed in collaboration with Rolls Royce, Allen Gears, has been up-scaled by CRES to suit the 20 MW MRS. The bearing can be designed in a modular fashion and assembled in sectors. It does not require the level of precision engineering demanded in rolling element bearings nor has it the sensitivity to failure associated with various types of fatigue and wear in such bearings. This type of bearing is consequently

much simpler than the sophisticated rolling element bearings that dominate the market for slewing of cranes and in wind turbine pitch and yaw systems. The hydrostatic bearing would probably be very effective and less expensive for such applications if ever established in volume production and certainly comes into its own in applications for large systems where very high loads are involved.

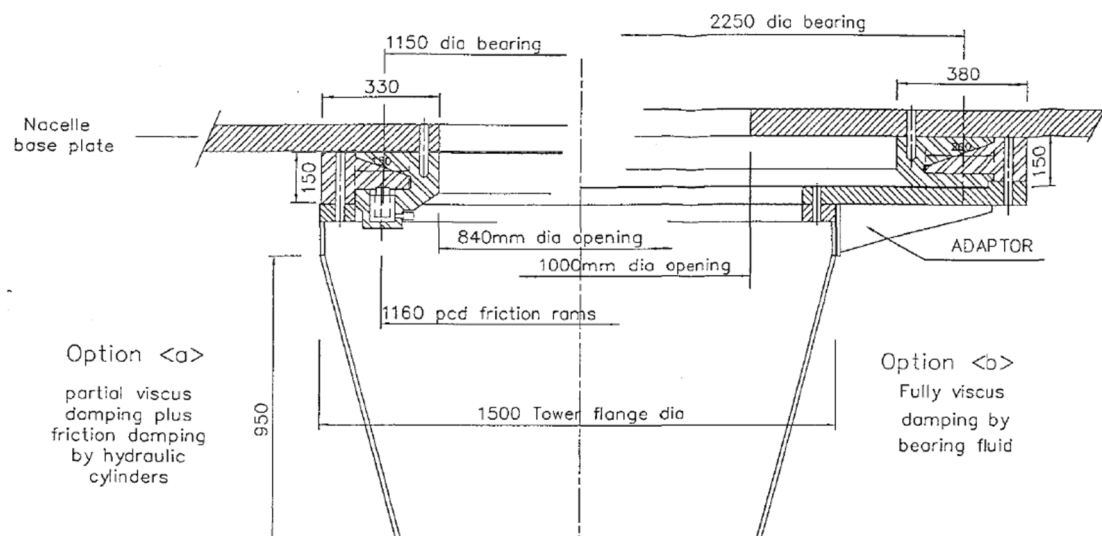


Figure 9-10 Hydrostatic bearing designs for a yaw system of 500 kW wind turbine

Two alternative bearing designs (at 500 kW scale) are illustrated in Figure 9-10. The operational principle is to pressurise the bearing when yaw movement is required. This releases the mating surfaces which are normally effectively clamped by friction related to structure weight. The working medium rather than the usual low viscosity hydraulic oil is a viscous grease with viscosity typically $\sim 10 \text{ Ns/m}^2$.

Among a number of advantages of this design concept are;

- the surface loading is not in a range where surface fatigue is an issue
- the stiffness and damping of the bearing can be controlled by its construction and choice of lubricant
- braking, damping of the yawing motion can be controlled by active control of lubricant pressure
- the low surface stresses permit the use of unhardened components which simplifies manufacture

A hydrostatic bearing design of the types illustrated in Figure 9-10 is up-scaled to 20 MW in Table 9-5. The working pressure 3.5 MPa ($\sim 500 \text{ psi}$) is quite low and the fluid viscosity is high helping to avoid longer term sealing problems.

DESIGN CHARACTERISTICS	MRS 20MW
Mean bearing diameter (m)	32
Outside bearing diameter (m)	37
Contact length (m)	0.526
Outer-inner diameter (m)	0.994
Height	0.499
Supply pressure (N/m ²)	3500000
Axial capacity of bearing (N)	175750650
Radial capacity of bearing (N)	33932283
Moment capacity of bearing (kN)	1622198000
Moment capacity force at radius (kN)	101387375
Radial to Axial Force Ratio	0.19
Moment eq. Force to Axial Force Ratio	0.58
Approx Volume (m ³)	47.52
Approx Weight (kg)	416278
Cost per unit (€/kg)	10.94
Cost (€)	4555177

Table 9-5 Design characteristics of a hydrostatic bearing for the 20 MW MRS

The main alternatives to a base yawing solution are the tower-frame systems discussed in Section 9.2.2. As has been mentioned this enables the use of more conventional bearing solutions. Some bearing concepts are illustrated in Figure 9-11.

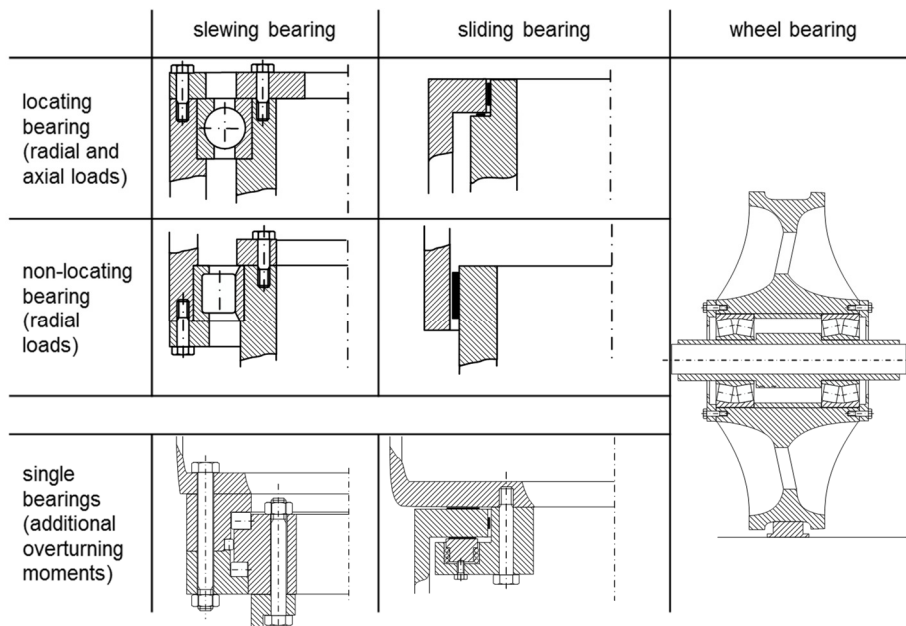


Figure 9-11 Bearing concepts for MRS

Figure 9-11 illustrates bearing concepts that would suit the arrangements of Figure 9-7. The locating bearing is at the top of the fixed support structure providing axial and radial support.

Usually four-point contact bearing types are used for slewing rings. Double-row bearing types are also utilized as they have an increased fatigue life due to reduced Hertzian stress. However the manufacturing costs are higher compared to their single row equivalent. For bearing arrangements in the tower bottom, three-row roller bearings are able to support the high axial loads but the overturning moments are still a challenge.

Sliding bearings usually consist of friction plates made from a lubricated polymer. With suitably designed actuators and integrated brake motors, these bearings may avoid any need for additional yaw brakes. Friction plate bearings however are dependent on wear and temperature. The starting friction coefficient is often designed with a tolerance of $\pm 20\%$ leading to high uncertainties during the design stage. An advantage however is that they can be separated thus enabling maintenance and replacement without removing the bearing itself [34]. In addition the separated bearing systems are not limited in diameter in the way that present roller bearings are limited due to supply chain constraints [35]. The friction torque can be adjusted by the normal force of the plates as shown in the single sliding bearing (Figure 9-11).

Wheel bearings as shown in Figure 9-11 (right) are utilized in offshore crane applications. As with the friction plates this bearing concept is not constrained by the diameter of the support structure.

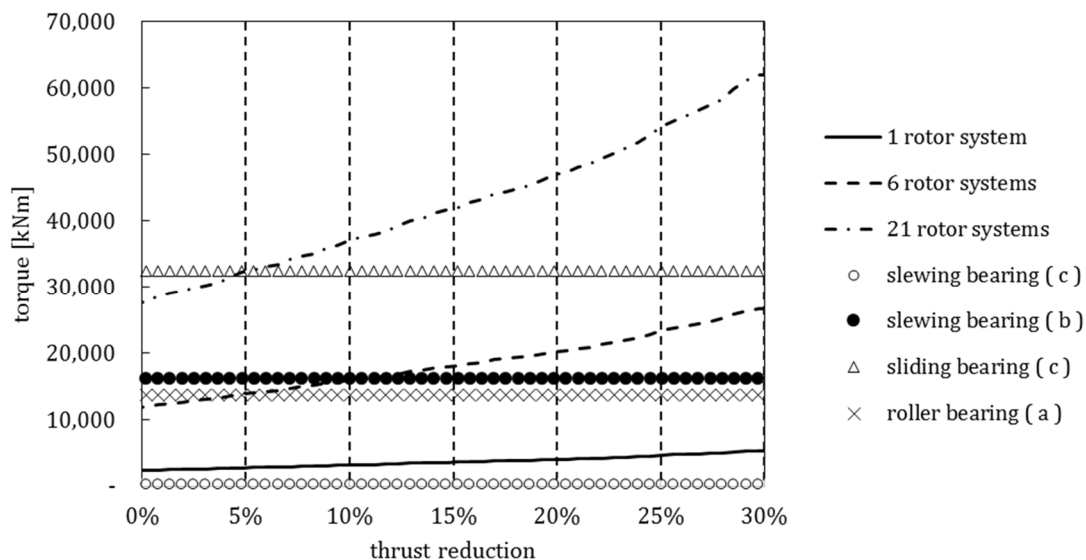


Figure 9-12 Friction torque related to bearing concepts

By differential control of rotor thrust on a set of MRS rotors, a yaw torque can be created. When this aerodynamic yaw torque exceeds the yaw bearing friction torque, the MRS will start yawing. Depending on the yaw system geometry, principally the yaw axis centerline in

relation to the system aerodynamic center, structure drag may generate high restoring yaw moments. To investigate the implications of bearing friction for yawing operation, the friction torque associated with the various yaw bearing concepts of Figure 9-11 was estimated. Figure 9-12 shows the different friction torques for the presented bearing concepts. The letters (a), (b) and (c) in the legend of this figure relate to the concepts of Figure 9-7. The friction torque is related to the aerodynamic yawing torque that can be created by various numbers of wind turbines of the MRS system based on the thrust at rated wind speed.

Twin bearing concepts have in general a lower overall friction torque than single bearing options. This is due to the lower overturning moment resulting from the reduced distance of the bearing placement to the point of attack of the aerodynamic thrust. It is also due to the reduced diameter of bearings when a pair are compared to a single bearing. The friction of the sliding bearing concept is presently calculated from the applied loads (weight and aerodynamic thrust) without considering any additional friction torque from pre-load. With most of the bearing concepts, the thrust of a single rotor is not enough to overcome bearing friction. At least 6 or 21 rotors have to be utilized to overcome the friction alone. Because of the heavy weight of the MRS structure, the sliding bearing concepts generate a high friction torque making the free yaw concept difficult to implement for below rated wind conditions. These considerations make it all the more likely that an arrangement where structure drag generates comparatively large stabilizing yaw moments will be preferred.

A distributed control scheme to provide droop control was implemented and demonstrated. The control scheme includes a priority system to ensure that the RPC systems least useful for yaw and fore aft pitch control are used first. The control scheme is shown to be able to provide accurate droop control with a droop capability of 4%, similar to conventional synchronous machines.

9.3 Overview of yaw system issues

9.3.1 Yaw torques and operational aspects

It would appear that with appropriate engineering design, a solution can be developed that is inherently yaw stable due to structure drag forces. Yaw control of an MRS using rotor thrusts was investigated in Task 4 on the basis of no-benefit (or hindrance) to yawing from structure drag. This was found to be feasible in general but most demanding around rated wind speed. Thus a system where yaw stability is primarily achieved through structure drag with fine tuning and control of dynamic response (especially in the case of a floating system) may be optimum. Not unexpectedly, it is clearly important to develop integrated designs of structure including yawing capability considering all aspects of loads and control function from the outset. The work of HAW Hamburg also highlights that bearing friction must be accounted in the evaluation of yaw torques and yaw system operation.

9.3.2 Bearing design and interaction with structural solutions

With almost all of the major costs of development and testing of main components of giant single turbines avoided in the use of proven turbine technology and proven structural frame solutions, the major fresh engineering challenge for an MRS is in the means of yawing. At present it is only feasible to attempt to bound this problem with rough mass and cost estimates. The solution with a space frame carrying the rotors yawing about a tower on twin bearings should be feasible since the yaw system loads are generally less (dynamic loads very much less) than for an equivalent single turbine and the twin bearings are of smaller diameter than an equivalent bearing for a single large turbine. It looks like this can be engineered at acceptable cost in relation of overall LCOE. Whether a single base bearing system may be more economic is less clear. Again such a system should be feasible but, at the scale required for the MRS, may require an innovative approach and special solutions such as wheels on tracks etc. rather than effort in the direction of up-scaling standard bearing technology.

CHAPTER 10 OPERATION AND MAINTENANCE

10.1 O&M Modelling of the MRS

There are many challenges in developing appropriate O&M modelling of the MRS. The approach adopted is to employ a detailed O&M modelling tool previously developed by UoS to predict O&M costs and optimise O&M planning of conventional wind farms [36]. Adaptations are then introduced which aim to capture the most significant differences in O&M that are specific to the MRS concept, specifically:

- a) With MRS there is no offshore installation of turbine units and no use of large floating cranes or jack up vessels for rotor maintenance. The offshore activity comprises towing a complete assembly to site with connection to an established jacket or if floating system to mooring lines. In the case of deployment on a jacket a jack up vessel would be used for installation but never for maintenance.
- b) There is little unscheduled maintenance directly associated with MRS because the system is engineered to have considerable independence between the turbine units. Thus a single turbine fault will compromise only a few percent of capacity and there is no urgency to remedy. Consequently most maintenance requirements can be accumulated and can wait for favourable weather windows. Obviously, as with a conventional wind farm, any fault that compromises total power output of an MRS unit or any fault with turbine interconnection and wind farm substation etc. may need more urgent attention.

The model [36] is a very detailed one with ~ 75 inputs reflecting climatic conditions, weather constraints, transportation options, maintenance equipment options, wind turbine characteristics, wind farm characteristics and cost factors.

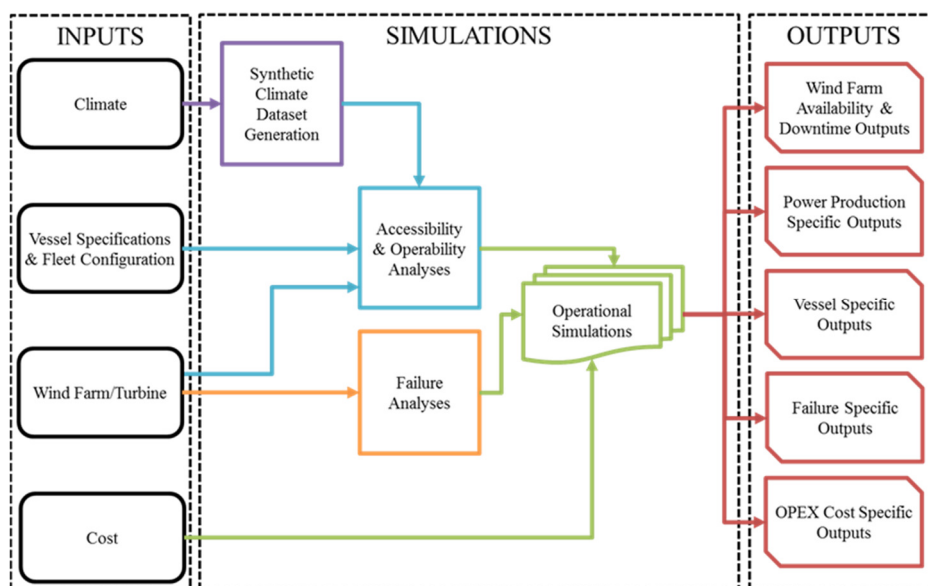


Figure 10-1 O&M Methodology

An illustration of its general structure is presented in Figure 10-1. The model has previously been used to determine the most cost-effective approach to allocate O&M resources which may include helicopter, crew transfer vessels, offshore access vessels, and jack-up vessels. It employs a time domain Monte-Carlo simulation approach which includes analysis of environmental conditions (wind speed, wave height, and wave period), operational analysis of transportation systems, investigation of failures (type and frequency), and simulation of repairs. An illustration of some of many available outputs is provided in Figure 10-2

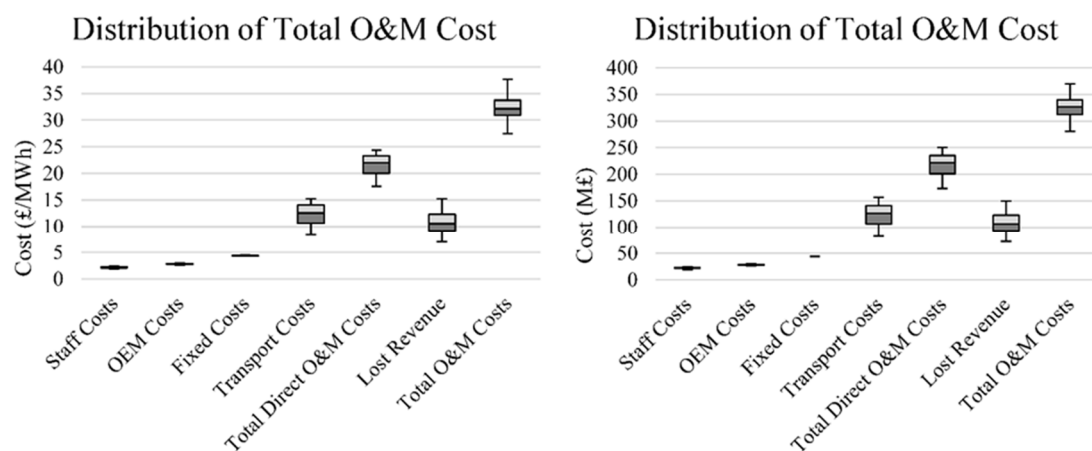


Figure 10-2 Distribution of O&M Cost

10.2 Validation of baseline O&M impact of LCOE

A preliminary task was to use this O&M model to verify the baseline O&M as employed in the evaluation of the RWT. This has been set in the cost model of Task 1.2 at 28.12 €/MWh. The UoS O&M model, as applied to a wind farm comprising 50 of the 10 MW RWTs, predicted a value of 24.94 €/MWh. Without detailed knowledge of the background assumptions on which the reference value is based, this can be considered fair agreement. In all analyses of LCOE within this project, O&M cost results of the UoS model are factored by $(28.12/24.94) = 1.13$, i.e. increased by 13 % as a calibration to provide consistent comparisons with the RWT.

10.3 Results for the MRS

The UoS O&M model adapted for the MRS and calibrated to the reference O&M value of 28.12 €/MWh produced a value of 24.37 €/MWh representing a 13% reduction in O&M cost (note that this value being equal to the 13% increase required for calibration is entirely co-incidental and the factors have no fundamental relationship whatever).

The reduction in direct transport cost (~€10 million/yr) from the removal of utilising jack-up vessels is very significant in reducing O&M costs. This is consistent with the analysis in Chapter 11 of Task 1.34 deliverable [37] which acknowledges a likely significant cost

reduction in avoiding the use of jack-up vessels for all categories of MRS faults. The estimates for MRS availability in the analysis of this chapter and in Task 1.34 are in general agreement. It would appear that there is a significant penalty to availability of the MRS (already included and accepted in the present evaluation) associated with stopping the whole array for the duration of Class 1 repairs (manual re-start after inspection). This is unnecessary although turbines around the one being serviced may be stopped. Also if a number of MRS turbines require manual re-start it may be best to have more technicians and work in parallel rather than accumulate repair time in series operation. Gintautas [37] acknowledges this. Understandably there has not been resource to model such details nor have the maintenance system and procedures yet been designed and specified in sufficient detail.

The UoS analysis determines a lower availability for the RWT and hence the difference in lost revenue indicated in Figure 10-3 favouring the MRS. However as far as establishing O&M costs and LCOE, there is no conflict in evaluation of the MRS arising from availability estimates and the availability for the RWT as estimated in Innwind.EU Task 1.2 is used in comparisons.

There is a penalty in increased repair costs (it was assumed that cost of a single multi rotor component is ~ 2/5 of the cost of a single large rotor blade/drive train component repair. Considering only component cost, this is excessively pessimistic as the direct cost (=spare part cost) and weight of major MRS components (blades, drive train etc.) are generally less than the corresponding reference turbine components by factors over 100. However the overall repair cost per failure cannot be modelled realistically without further detailing of procedures for maintenance and for that reason a very conservative factor has been employed. The distribution of major O&M cost elements (units of M€) of the reference wind turbine (REF) and MRS is presented in Figure 10-3

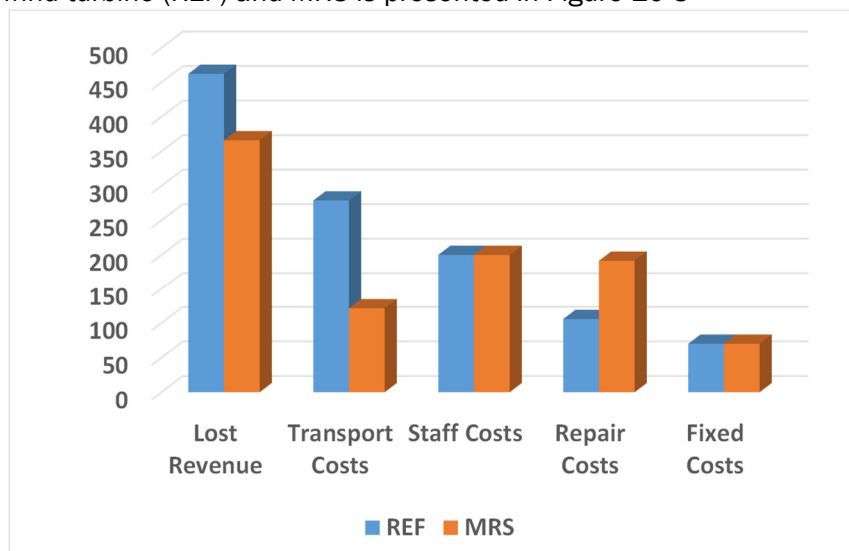


Figure 10-3 Distribution of O&M costs

There are elements in the necessarily simplified modelling of the new features specific to the MRS that are not conservative. The MRS case is slightly optimistic due to the way the model is coded. When a partial failure occurs, the system can only transition to a

completely failed state, i.e. the transition to 3 or 4 of the multi rotors failed in a single structure is not captured correctly. This can be fixed but not in available project timescales.

However the 13% reduction in MRS O&M cost predicted is also particularly conservative in that it does not account for any improvement in unit reliability whereas reliability improvements of MRS turbines relative to the RWT can readily result due to the MRS having;

- 1) Simpler rotor nacelle systems without local yawing
- 2) Greater production quantities per installed MW of wind farm capacity
- 3) Production of units at a scale where the technology is already well proven
- 4) Opportunity to increase design margins on key components (at added cost). The rotor and nacelle CAPEX of the MRS is relatively such a low proportion of lifetime cost that it almost certainly will improve LCOE to pay for reliability enhancement.

A greater reliability of MRS turbines relative to RWT is not quantified but is logically definite for the reasons in 1) to 4) preceding. This will reduce required no of site visits, improve availability and reduce O&M costs. There has not been resource in Tasks 1.33 or 1.34 to further model impacts of enhanced reliability except in a few specific aspects, For that reason there is no credit from enhanced reliability of RNA systems in the present O&M and LCOE estimates.

Figure 10-4 and Figure 10-5 provide a comparison of monthly costs for 500 MW wind farms based on RWTs and MRSs.

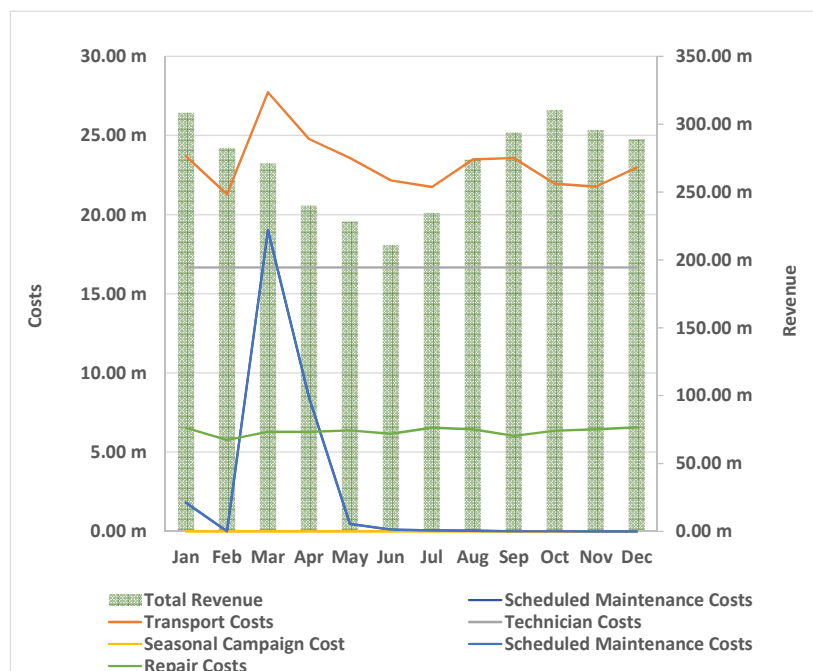


Figure 10-4 Average Monthly Wind Farm Costs (RWT)

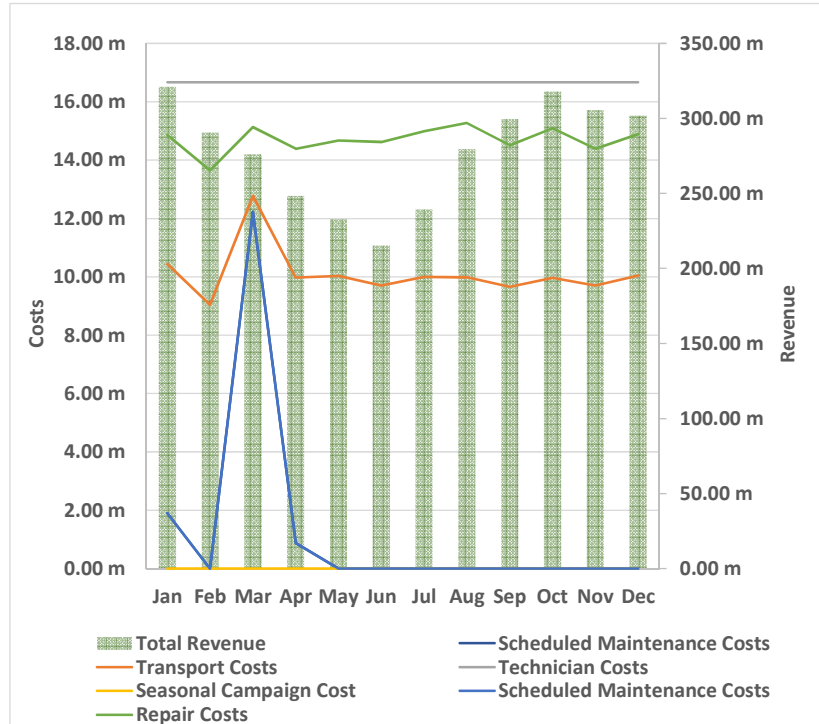


Figure 10-5 Average Monthly Wind Farm Costs (MRS)

CHAPTER 11 COST OF ENERGY EVALUATION

11.1 General

Levelised Cost of Energy (LCOE) modelling was developed within Innwind.EU in Task 1.2 [1]. The model and assumptions and adjustments relating to its use in MRS comparisons will be discussed in Section 11.4. Turbine CAPEX and energy capture can be reasonably well estimated for the MRS. O&M costs have been estimated as discussed in Chapter 6 but with much greater uncertainty because it was beyond the resources of this project to develop detailed O&M procedures and match the sophistication in O&M modelling that presently exists for conventional wind farms. Moreover the present project was suggested to have a primary focus on CAPEX. Well differentiated BoP and O&M impacts may be less consequential in evaluating innovations related to the single rotor concepts. O&M especially is however significantly different for the MRS. Important differences are avoidance of use of jack-ups as would be needed for the RWT if a major component such as a blade failed, much reduced impact of single turbine faults and consequently less urgency for repair but on the other hand the need for effective automated handling of MRS rotors using the in-built travelling crane so that the impact of having more components and more frequent faults is well managed.

For any renewable technology, energy is “the bottom line” as far as LCOE is concerned and some distinctive impacts on energy capture of the MRS are now discussed.

11.2 Energy Capture – Impact of Wind Turbulence

The MRS with many smaller rotors than the equivalent large single rotor provides a more complete spatial coverage of the input turbulent wind field. Moreover, each MRS rotor as a smaller entity is capable of faster response and therefore in principle capable of extracting higher frequency turbulent energy than a larger rotor. An attempt to quantify this effect is now described.

Using the Garrad Hassan (now DNV GL Energy) design tool, Bladed, simulations of dynamic operation of the MRS array and the UPWIND 20 MW wind turbine were compared. At each mean wind speed, turbulent wind files were generated using 3 different turbulence seeds and dynamic operation both of MRS and the UPWIND turbine were simulated. Energy production is determined by integrating the power over the time interval simulated (600 s).

As key parameters of each system (swept area especially and power performance characteristics etc.) differ, the basis of this comparison was to compare the gains as the ratio of energy captured in dynamic operation to that corresponding to steady state operation at the mean longitudinal wind speed of the turbulent wind file.

Energy capture in turbulent wind operation was determined by integrating the power time series. Figure 11-1 shows the ratio of gains of MRS to single rotor. In general the MRS extracted some very small additional energy from turbulence (gain~1.01) while the single rotor with its much higher inertia could not respond as effectively and lost energy (gains in

a range 0.93 to 0.98). This comparison was based on wind records with turbulence intensity (TI) of 8%.

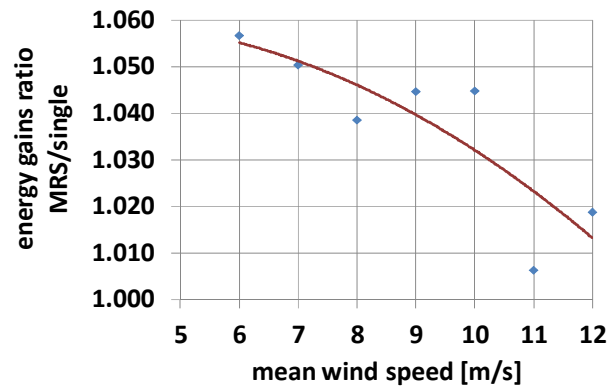


Figure 11-1: Energy gain comparison

The benefit to the MRS system would increase markedly with increase in TI. It is not appropriate to use the 90 percentile values of TI as commonly specified for load calculations. These are extreme values chosen to ensure that safe loading estimates are made and do not reflect the turbulence levels that may be typical over a period of a year at the design site location and therefore representative for energy capture evaluation.

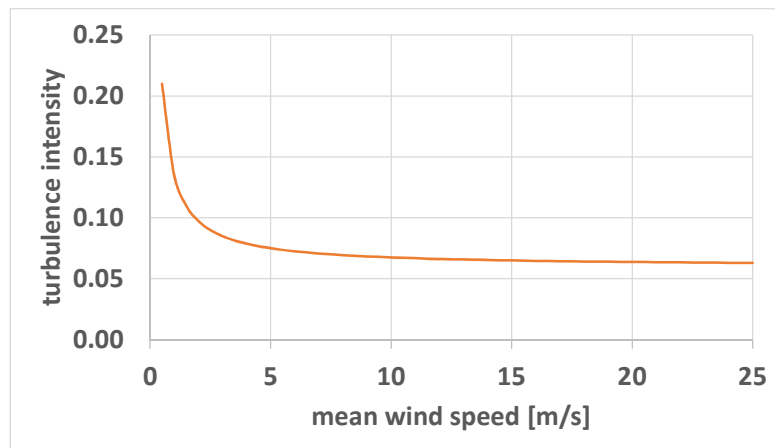


Figure 11-2: Turbulence intensity

The impact of turbulence on annual energy production was also considered using a simplified theoretical model. As in the IEC wind turbine loads standard, the form of the variation of turbulence intensity with mean wind speed was determined by estimating the standard deviation of wind speed as the product of a reference TI values and a linear function of mean wind speed. The coefficients in that linear function were determined and related to site data (low turbulence land based site provided by DNV GL Energy). The

assumed turbulence distribution is shown in Figure 11-2. This expresses the variation of TI with 10 minute mean wind speed for a reference TI of 0.065 at 15 m/s.

A power curve in turbulent wind corresponding to 10 minute averaged data may be estimated with the assumption that the turbulence has a Gaussian distribution about the mean values. For a mean wind speed of 9 m/s using the turbulence data of Figure 11-2 a power curve is derived as in Figure 11-3. The ideal 0% TI power curve (solid line) is compared with the effective power curve in turbulent wind (dotted line) with 6.5% TI at 15 m/s mean wind speed. The 3 MW rating applied here is arbitrary as the final output is a factor of energy gain in turbulence which is considered to be turbine and control system independent. In reality it cannot be, but some validation of this approach with dynamic simulations [8] of specific turbines gave reasonable agreement suggesting a convergence in behaviour of well-designed wind turbines with effective control systems.

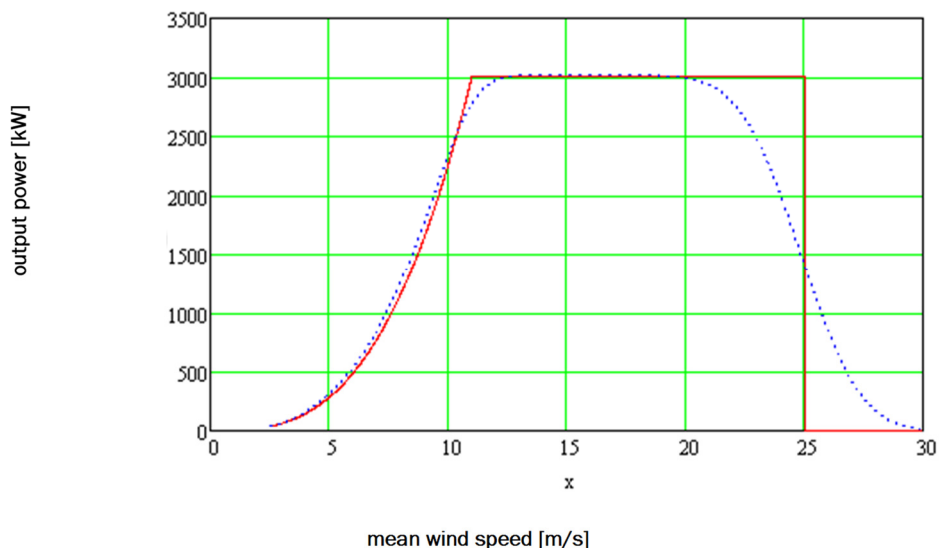


Figure 11-3: Power curve.

Using this model the gain in annual energy production (AEP) was estimated by combining the TI data of Figure 11-2 with the turbulent power curve of Figure 11-3 and assuming a Rayleigh distribution of mean wind speeds. Figure 11-4 suggests that for a reference TI around 5 to 6% at good offshore sites with mean wind speed of ~ 9 m/s ~ 2% gain in energy may be obtained from operation in turbulent wind. This approach reveals trends and may or may not be a reasonable quantitative estimate. In order to produce a more secure estimate of the effect of turbulence on annual energy production, a joint annual distribution of TI and mean wind speed based on 10 minute averaged data is required for relevant offshore conditions.

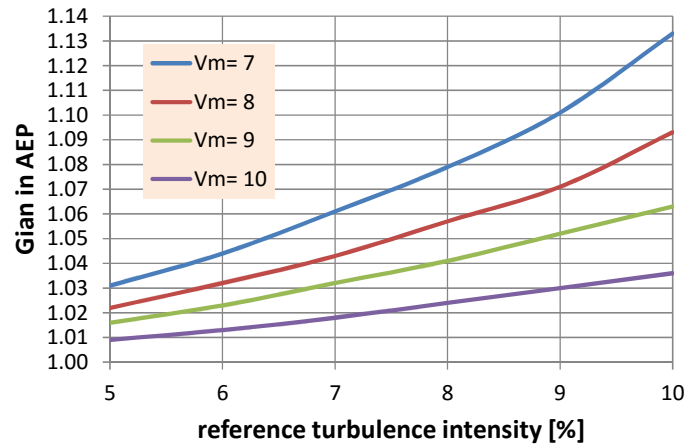


Figure 11-4: Gain in AEP.

At present no credit for turbulent energy gain of the MRS is applied to base case LCOE estimates (discussed later). The possibility of overall annual energy increase from this effect of 1% on MRS production and also some annual energy capture penalty of a few percent to the RWT, as justified by the dynamic simulation studies of Figure 11-1, is considered in sensitivity studies.

11.3 Energy Capture – Effect of Rotor Interaction

The effect of aerodynamic interaction of rotors in the MRS was discussed in Section 4.4. An 8% power gain is projected, associated perhaps with flow acceleration through the spaces between the rotors increasing mass flow through the most outboard parts of blade span.

The aerodynamic studies of NTUA did not include the effect of support structure blockage. However in the load calculations of UoS, the structure members were included and modelled as individual “tower shadows” and there was no significant effect on power production associated with this. This result was essentially for a rotor in isolation as the software, Bladed, could not account for aerodynamic interactions between rotors. This is line with experience of single rotors where the tower shadow can introduce some additional fatigue loading but has negligible impact on energy capture.

No structural elements lie directly downwind of the free spaces between the rotors that may impede the flow acceleration through the spaces. It is therefore quite likely that energy gains will be realised from the MRS rotor interactions although further aerodynamic investigation will be needed to have high confidence in this. In the LCOE modelling, no benefit is assumed in the base case but energy gain scenarios are explored in sensitivity studies.

11.4 LCOE Cost Model

The following equations show the cost calculations for the multi-rotor wind turbine sub-components. All the resulting costs are presented in 2012 Euros. The equations represent an original model based on 2002 US dollars updated to 2012 costs and converted to Euros. In the equations, the factor of 1.32 represents the conversion of dollars to euro based on 2002 conversion rates. The PPI(x%) represents the percentage change in material cost from 2002 to 2012.

Following outline design and costing of yaw system solutions in Chapter 6, the LCOE evaluation is principally based on the concept of mounting the MRS on a jacket as thus will give a more direct comparison with the RWT.

The system of cost equations embodied in the MRS version of the cost model of Task 1.2 is as follow.

Cost equations – (2012) €

Components of the rotor cost:

$$\text{Blade} = 13 \times \text{Blade Mass(kg)} \times (1 + \text{PPI}(9\%))/1.32$$

$$\text{Hub} = 4.25 \times \text{Hub Mass(kg)} \times (1 + \text{PPI}(55\%))/1.32$$

$$\text{Pitch Mechanism} = 9 \times \text{Pitch Mechanism Mass(kg)} \times (1 + \text{PPI}(48\%))/1.32$$

$$\text{Nose Cone} = 5.57 \times \text{Nose Cone Mass(kg)} \times (1 + \text{PPI}(55\%))/1.32$$

Components of the drivetrain cost :

$$\text{Low Speed Shaft} = 3 \times \text{Low Speed Shaft Mass(kg)} \times (1 + \text{PPI}(67\%))/1.32$$

$$\text{Main Bearing} = 17.6 \times \text{Main Bearing Mass(kg)} \times (1 + \text{PPI}(44\%))/1.32$$

$$\text{Brake \% Couplings} = 1.9894 \times \text{Rating(kW)} - 0.1141 \times (1 + \text{PPI}(6\%))/1.32$$

$$\text{Generator} = \left(\frac{\text{Turbine rating(kW)}}{\text{Total MRS rating(kW)}} \right)^{3.15/2} \times 1160000$$

$$\text{Power Electronics} = 79 \times \text{Turbine rating(kW)} \times \frac{1 + \text{PPI}(37\%)}{1.32}$$

$$\text{Bed Plate} = (\text{Turbine rating(kW)})^{0.85} \times 627.28$$

$$\text{Hydraulic \& Cooling System} = 12 \times \text{Turbine rating(kW)} \times (1 + \text{PPI}(30\%))/1.32$$

$$\text{Nacelle Cover Cost} = 4 \times \text{Nacelle Cover Mass(kg)} \times (1 + \text{PPI}(13\%))/1.32$$

$$\text{Electrical Connections Cost} = 40 \times \text{Turbine rating(kW)} \times (1 + \text{PPI}(13\%))/1.32$$

Space Frame Structures (for various design solutions):

$$\text{Spaceframe cost} = 4.8 \times \text{Mass}$$

$$\text{Mass per joint for spaceframe} = 2,500\text{kg}$$

$$\text{Spaceframe joints cost} = 15 \times \text{Mass}$$

Conventional Bearing Cost

$$\text{Yaw bearing cost} = 7.7 \times \text{Mass}$$

This is based on the RWT relation between yaw bearing cost and mass

Floating Structure:

$$\text{Cost estimate for 20MW MRS (2012€)} = 32,000,000/1.32$$

Modelling of the 10MW RWT is taken from the cost model provided as Deliverable D1.23 (April 2014). The foregoing cost equations are from a subsequent version developed by CRES adapted by CRES and UoS to suit the MRS. The I/O areas of the two models (RWT and MRS) are nearly identical with the following few exceptions:

In the MRS Turbine Input Parameters panel

- The number of rotors has been added.
- Dedicated MRS blade and floater models have been developed, the latter following the findings of the previous section.

In the MRS Wind Farm Data panel

- A provision for MRS-specific aerodynamic losses (or gains) due to the interaction of the rotors has been put in place. The actual value is set to zero at this moment.
- For the MRS wake losses of 7% compared to the 9% losses of the RWT are assumed. This is due to the larger capacity of MRS (20 MW instead of 10MW). Although it is highly speculative at this stage, it is possible that an MRS in wake immersion can extract relatively more of the turbulent energy and also that in overall wind farm control wakes in an MRS wind farm could be managed more sensitively than for single rotors.
- A slight improvement of the availability (from 95% RWT to 96% MRS is credited to the MRS. The large number of rotors reduce the need for unscheduled maintenance)

In the MRS Intermediate Turbine Results panel

- The MRS rotor is modelled with the same C_p -max as the RWT blade (0.48). The single large rotor at very high Reynolds number could in principle have superior aerodynamic performance but in reality the small one is much less constrained by performance compromises for structural comfort of to facilitate load relief through aeroelastic characteristics.
- Drive train efficiencies appropriate to the Magnomatics PDD are used.
- The capacity factor of each single MRS turbine is evidently higher than the RWT. This is due to a choice of a lower power density (336 W/m^2) in the design. Power density is here defined as the ratio of rated electrical output per turbine to rotor swept area. Industry average onshore and for early offshore is $\sim 400 \text{ W/m}^2$ whereas latest largest turbines of Siemens, Vestas, Samsung and others have power densities nearer 300 W/m^2 .

In the MRS Site Conditions panel, no change

In the MRS Other Data panel

- Nacelle and rotors in the MRS system would be simpler and manufactured in volume production rates ~ 20 times that of 10 MW turbines. On the basis of economies of scale and faster learning curves the turbine cost multiplier (including assembling costs and manufacturers overheads and costs) is reduced from 1.4 (RWT value) to 1.2 (MRS).

The cost model as delivered in 1.32 and subsequently modified by CRES has been further developed by UoS prior to use in LCOE estimation and these further changes are now discussed:

Structure cost – Joints in the structure add weight and cost and were not included. In order to have some account of this, joints were estimated on average to be of 2500 kg mass and at a premium cost for a complex casting of $12\text{€}/\text{kg}$. There may be some double accounting here in this sense that the structure is already costed as a jacket allowing for fully welded joints. However there will definitely be some significant extra cost in the MRS joints which also provide for connection of rotor-nacelle assemblies.

Control System and Pitch System Costs - In some internal review of these costs by UoS it is considered that the MRS pitch system costs are too low (possibly due to inadequacy of the NREL based cost model to scale down well) and the MRS control system costs too high. In

reviewing the RWT design, the control system costs seem too low as being similar to known costs for 5 MW technology. Although control system costs are to some extent scale independent, there are elements of hardware that do scale. With very large turbines it may be considered advantageous to have more sensors and additional condition monitoring equipment all of which is assumed to be embraced in the cost model definition of “control system”.

No changes were made. There was not sufficient information to sensibly alter the costs and also the effects are to some extent cancelling at least for the comparison of MRS LCOE with RWT.

11.5 CAPEX Comparisons

The base cases are those which directly follow the best estimates used in the cost model. Some additional cases are subsequently investigated as sensitivity studies where the impact of varying selected critical parameters are considered.

Following the design work in Chapter 9 considering means of yawing the MRS, three base case options for the MRS are evaluated. These comprise;

- A. The MRS rotor nacelle systems are located on a lattice frame which can yaw on twin bearings about a tubular tower sited on a jacket foundation
- B. The MRS rotor nacelle systems are located on a lattice frame that yaws from a base level hydrostatic bearing also sited on a jacket foundation
- C. The MRS rotor nacelle systems are located on a lattice frame rigidly attached to a floating platform capable of yawing in the sea about a central mooring turret.

Case C is presented for indicative purposes only. The floater, as is evident from the work in Chapter 7, is designed with acceptable frequencies but according to experience of the naval architecture department at UoS, who designed (for a wind turbine at 5 MW scale) a simple barge type floater (among other solutions) in a previous project, there is a strong likelihood of over large angular displacements occurring in extreme weather and the semi-submersible, tri-floater concept such as employed in the designs of Principle Power may be the most appropriate for the MRS. Moreover systems mounted on jackets will afford a more direct comparison with the RWT.

Mass and cost results for CAPEX associated with these three options are compared in Table 11-1.

Option A appears as the most economic solution. A comparison of CAPEX is significant in terms of LCOE as there are no major differences foreseen in other LCOE impacts, certainly between options A and B. The total cost of option C appears similar to option B but the cost of option C may increase when a more detailed design is developed and costed. This is in line with current experience of floating technology being somewhat more expensive than jackets but depending strongly on water depth.

Table 11-1 Mass and CAPEX of MRS Options

Option A - space frame yawing on tower	mass tonne	cost M€
Space frame with bearing attachment structures	1904	9.1392
Space frame joints	113	1.688
Bearings (tower top and lower ring bearing)	78	0.601
Tubular tower	1520	3.800
Rotors	170	1.887
Nacelles	183	5.971
Sub-total for above water assembly	3968	23.086
Jacket	3459	17.351
Total MRS CAPEX	7427	40.437
Option B - space frame yawing from base level	mass tonne	cost M€
Space frame	3407	16.3536
Space frame joints	113	1.688
Base bearing (hydrostatic)	416	4.555
Rotors	169.965	1.887
Nacelles	183	5.971
Sub-total for above water assembly	4289	30.455
Jacket	3459	17.351
Total MRS CAPEX	7748	47.806
Option C - space frame attached to floater	mass tonne	cost M€
Space frame	3407	16.3536
Space frame joints	113	1.688
Rotors	169.965	1.887
Nacelles	183.42	5.971
Sub-total for above water assembly	3873	25.900
Floating platform	47634	24.242
Total MRS CAPEX	51507	50.142

In addition to the recent work on yaw system solutions in Section 9.2, a previous project considered the solution of yawing on a tower with twin bearings for a system at 5MW scale. Lacking the capability to model turbulent wind loading spanning a large set of rotors as has now been done in this project, very conservative (ultimate) loads were used but detailed structure designs were done as in this project using finite element type analyses accounting for extreme loading and buckling. It was also found in that previous

project [4] that the space frame yawing on tower seemed the most economic solution. This, Option A will be used as the base design of MRS for comparison purposes although the other concepts are included in sensitivity studies.

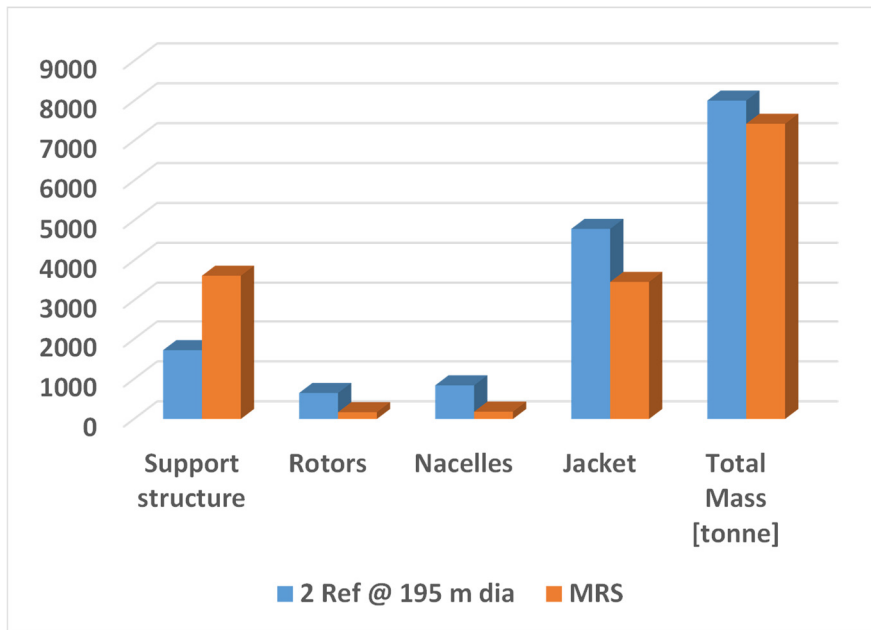


Figure 11-5 Comparison of mass – MRS v 2 x RWT

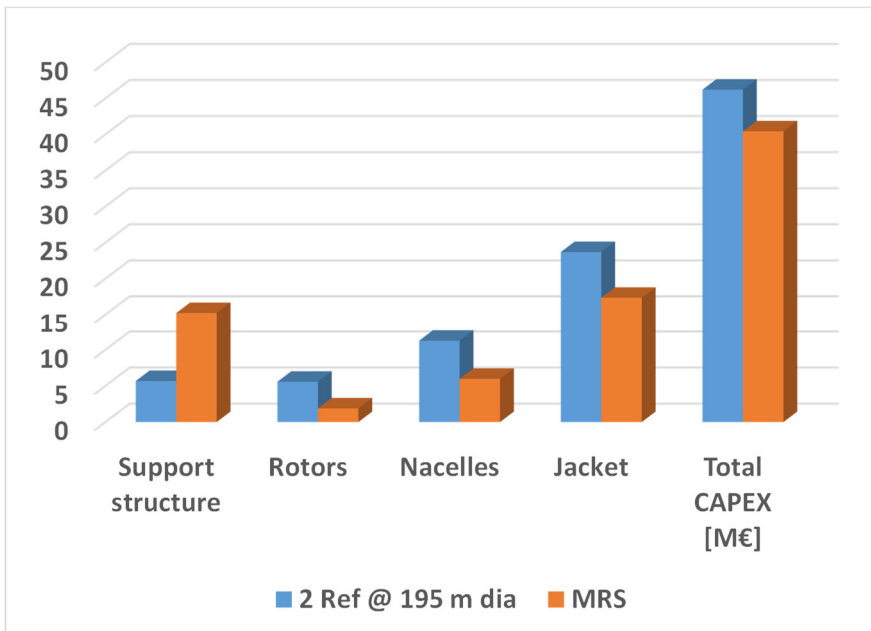


Figure 11-6 Comparisons of cost – MRS v 2 x RWT

Continuing initially with a CAPEX comparison, comparisons of MRS Option A are now made with the 10 MW RWT. In order to make a valid comparison of CAPEX in isolation, the comparisons is made of Option A with two reference turbines equalizing

- a) Total rated capacity at 20 MW
- b) Estimated annual energy production.

Achieving a) is an automatic result of having 2 turbines rated at 10 MW. Achieving b) requires a diameter increase of the RWT from 178 m to 194.5 m and power density consequently reduced to 337 W/m² approximately matching energy production of the MRS, more in line with commercial practice of the largest turbines being designed for offshore. Results of the CAPEX comparisons of mass and cost are presented in Figure 11-5 and Figure 11-6.

11.6 Baseline LCOE Comparison

Option A is taken as the baseline for the MRS concept. The LCOE for a wind farm of 500 MW rating is evaluated using the cost models of Task1.2 in a comparison of 25 x 20 MW MRS with 50 x 10 MW RWTs. In the evaluation of the MRS, structure costs are based on the results presented in Chapter 6 and Chapter 9 of this report. O&M estimates are based on the modelling discussed in Chapter 10. The baseline comparison is summarized in Table 11-2 which shows a 16% reduction in LCOE of the MRS wind farm (80.2 €/MWh) as compared to one based on RWT technology (95.6 €/MWh).

Table 11-2: Cost comparison between MRS and RWT.

Parameter (All include marinization and cost scaling factor where appropriate)	Wind Turbine System				Ratio (MRS/2x10MW turbines)
	Multi-rotor system wind turbines 20MW (45x44kW)		Single Turbines 2x10MW (20MW)		
	Single MRS rotor	All MRS rotors	Single 10MW	2x10MW	
Rotor System(s) cost (€)	41,943	1,887,431	3,415,042	6,830,084	0.276
Blades (€)	24,615	1,107,668	2,174,323	4,348,646	0.255
Hub (€)	9,969	448,594	688,242	1,376,484	0.326
Pitch mechanism (€)	5,359	241,148	524,303	1,048,606	0.230
Nose cone (€)	2,000	90,021	28,173	56,346	1.598
Drivetrain and Nacelle cost (€)	132,693	5,971,175	7,041,092	14,082,184	0.424
Low speed shaft (€)	3,613	162,604	450,599	901,198	0.180
Main bearing (€)	2,520	113,386	547,098	1,094,196	0.104
Gearbox (€)	0	0	1,694,765	3,389,530	-
Mechanical brake and couplings (€)	988	44,444	25,955	51,910	0.856
Generator (€)	11,545	519,536	1,109,011	2,218,022	0.234
Power electronics (€)	49,110	2,209,931	1,290,417	2,580,834	0.856
Bed plate (€)	22,825	1,027,134	139,676	279,352	3.677
Hydraulic and cooling system (€)	7,121	320,428	187,104	374,208	0.856
Nacelle Cover (€)	1,621	72,959	142,964	285,928	0.255
Electrical connections (€)	33,350	1,500,752	876,315	1,752,630	0.856
Yaw system (€)	0	0	577,189	1,154,378	-
Control/Condition Monitoring system (€)	35,455	1,595,455	75,833	151,666	10.520
Turbine Cost (excluding tower/support structure) (€)	210,090	9,454,061	10,531,967	21,063,934	0.449
Support Structure/Tower (€)		22,377,633	3,519,533	7,039,066	3.179
Complete Turbine Cost including tower/spaceframe (€)		31,831,694	14,051,500	28,103,000	1.133
Balance of Plant (€)		28,146,552	16,949,603	33,899,206	0.830
Underwater Foundation system (€)		14,446,327	9,496,800	18,993,600	0.761
Offshore transportation (€)		3,224,045	1,613,636	3,227,273	0.999
Port and staging equipment (€)		432,900	216,667	433,333	0.999
Offshore turbine installation (€)		3,246,750	1,625,000	3,250,000	0.999
Offshore electrical I&C (€)		6,796,530	3,401,667	6,803,333	0.999
Scour Protection (€)		0	595,833	1,191,667	-
Total CAPEX (€)		59,978,246	31,001,103	62,002,206	0.967
500 MW Windfarm LCOE Comparison between MRS and 10 MW single wind turbines					
Power per wind turbine (MW)		20	10		2.000
Number of rotors per wind turbine unit		45	1		45.000
Number of wind turbine units		25	50		0.500
Availability (%)		96	95		1.011
Wake losses (%)		7	9		0.778
Wind farm capacity factor		0.495	0.43		1.151
Balance of Plant (Million€/MW)		1.506	1.695		0.888
Operation and Maintenance cost (€/MWh)		24.45	28.12		0.869
Annual Energy Production of wind farm (GWh/y)		2169	1,886		1.150
Windfarm (500 MW capacity) LCOE (€/MWh)		80.17	95.58		0.839

The BoP CAPEX regarding offshore transportation, port and staging, offshore installation, and electrical installation and commissioning are not differentiated in Table 11-2 for want of detailed modelling of this in the cost model. The impact of having half as many maintenance sites with 20 MW MRS technology versus 10 MW RWT and other impacts on cost of equipment are however implicit in the O&M modelling of Chapter 10.

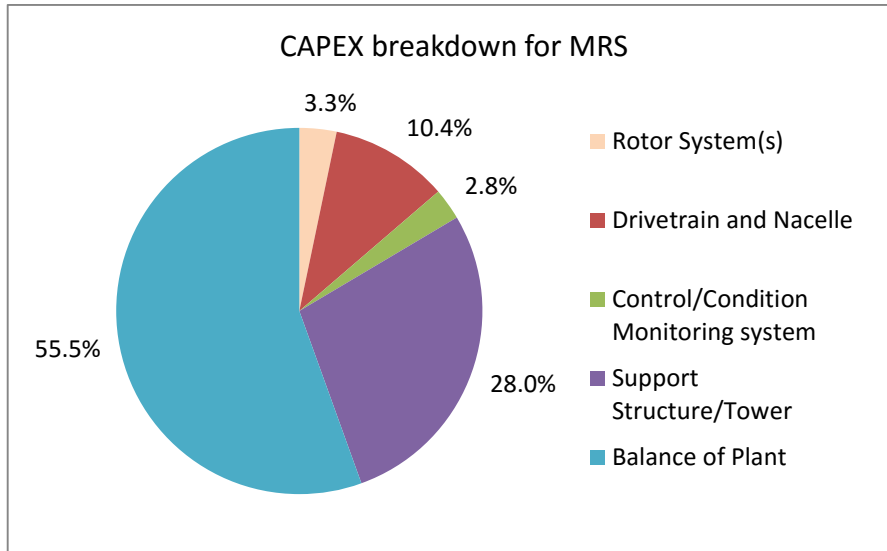


Figure 11-7: CAPEX breakdown of the MRS

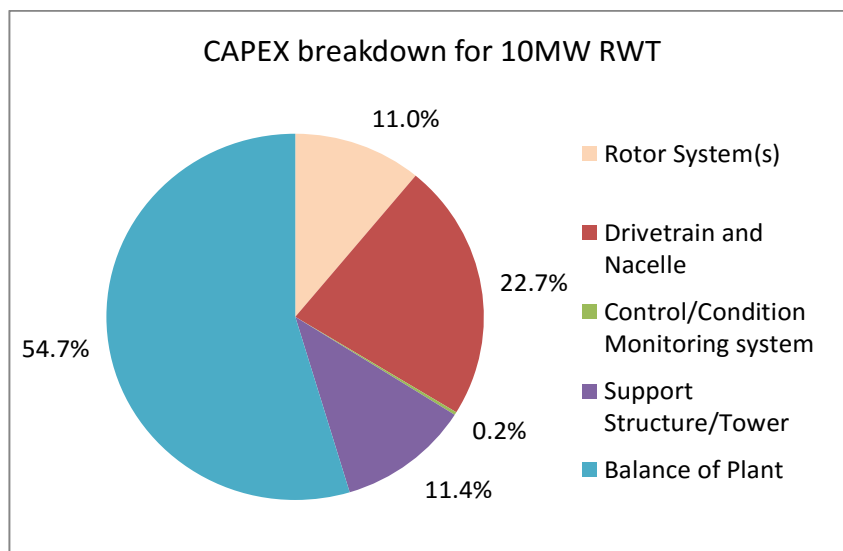


Figure 11-8: CAPEX breakdown of 10MW RWT

The overall CAPEX reduction of MRS compared to RWT is rather small (~3 %) but within this, there are very large savings specifically in the rotor-nacelle systems (>60%). These for the single turbine concept are the high risk components that are particularly

demanding to develop at ever larger scale. Moreover the CAPEX comparison here is not very relevant as the MRS has greater active swept area than two RWT turbines with consequently relatively higher CAPEX, higher capacity factor and greater energy production (from increased swept area without accounting for possible further energy gains due to specific features of the MRS, better response to turbulence and enhanced flow between the rotors). The more relevant CAPEX comparison was made in Figure 11-6 where the diameter (and CAPEX) of the RWT is increased to equalise energy output.

Sensitivities to a number of input parameters and design variables of the MRS and RWT are now considered.

11.7 LCOE Sensitivity Study

A sensitivity study was conducted to assess the impact of key parameters within the LCOE model.

In this study a 500 MW MRS wind farm is evaluated in comparison to a conventional wind farm of 10 MW RWTs. The most critical LCOE sensitivities for the MRS reflect areas where significant new design is required compared to established wind technology or where new system characteristics exist. They comprise:

- a) MRS structure cost – (the structure like a jacket is conventional but mass and cost need to be contained acceptably)
- b) Yaw system cost – (new solutions are required to yaw the complete assembly)
- c) AEP – (performance of a planar array of closely spaced turbines is a new issue)
- d) O&M – (quite different strategies apply to the MRS)
- e) Rotor-nacelle assembly (RNA) cost (scaling advantages are key to MRS concept)
- f) Turbine availability – (essentially part of AEP but specifically related to reliability)

Figure 11-11 compares MRS (Design A) with the RWT. The magnitude of each sensitivity relates to magnitude of the slope of the line relative to horizontal (zero sensitivity). As expected both systems are most sensitive to firstly energy capture including availability loss and secondly O&M. The MRS differs from the conventional RWT principally in a way that will already be obvious. The RNA cost shows a reduced sensitivity of the MRS compared to the RWT () with two implications;

- In an MRS wind farm there is much less project cost associated with relatively high complexity, high risk turbine systems compared to RWT
- It is thus more affordable to increase MRS turbine CAPEX if it enhances reliability

For MRS design A (Figure 11-9) it requires around a 100% increase in structure cost to lose all LCOE benefit relative to the RWT. MRS design B (Figure 11-10) is less competitive and would lose relative benefit with a 50 % increase in structure cost or a 10% deficit in energy production. Although the present state of MRS design is preliminary and lacks great detail, the structure cost will almost certainly not increase by 50% and all aspects of

power performance as yet investigated suggest gains rather than losses in production for the MRS as compared with RWT.

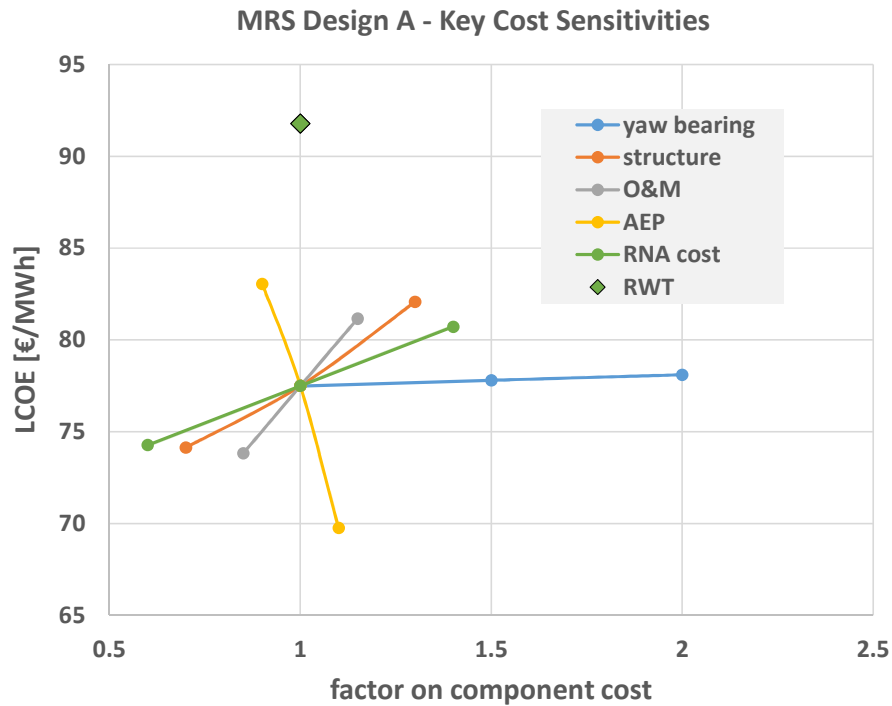


Figure 11-9 Sensitivity to cost factors of MRS Design A (tower-frame concept)

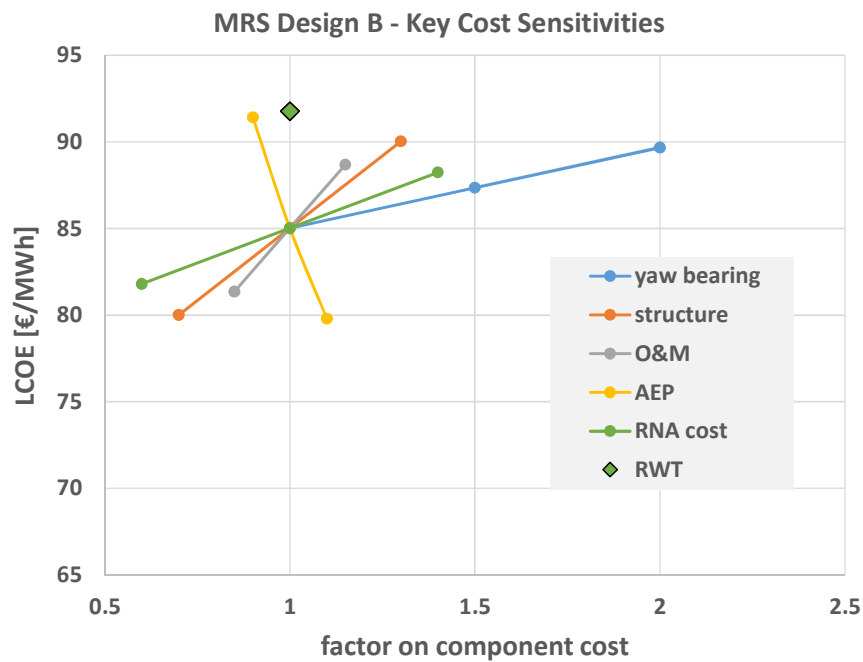


Figure 11-10 Sensitivity to cost factors of MRS Design B (base yaw bearing)

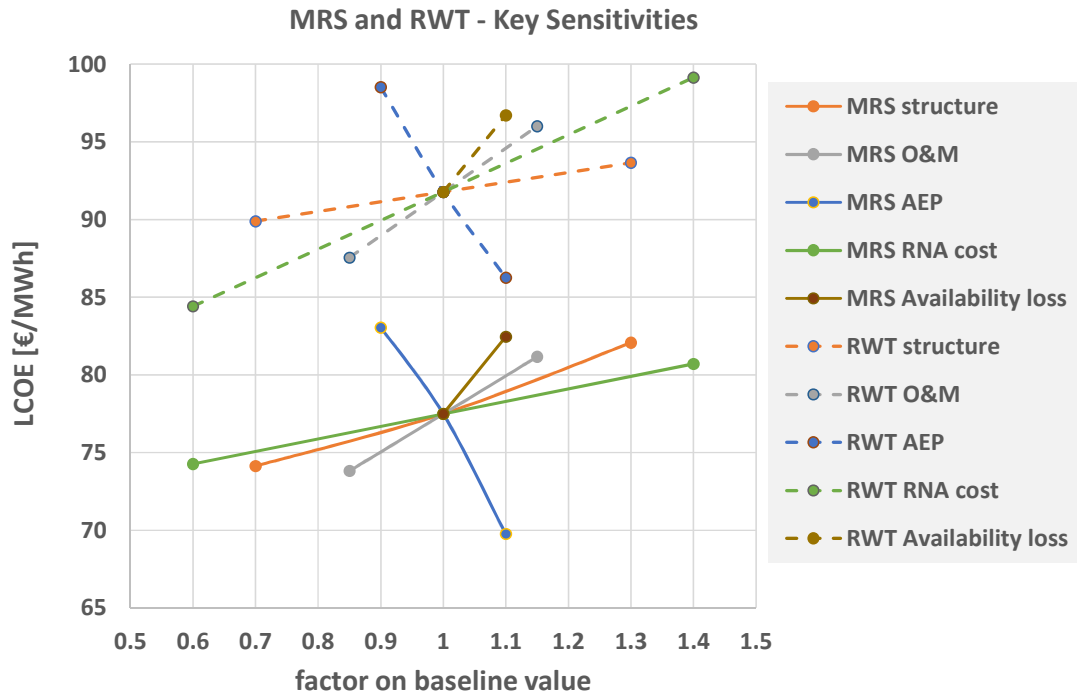


Figure 11-11 Comparison of cost sensitivities of MRS and RWT

In addition to the sensitivities discussed, some other factors are investigated

Wake losses (Figure 11-12) affect the wind farm capacity factor and so influence the LCOE of the project. Differential control of the turbines of the MRS could in principle more sensitively alter the overall wake and the state of immersion or partial immersion of downstream turbines than in wind farms of single turbines.

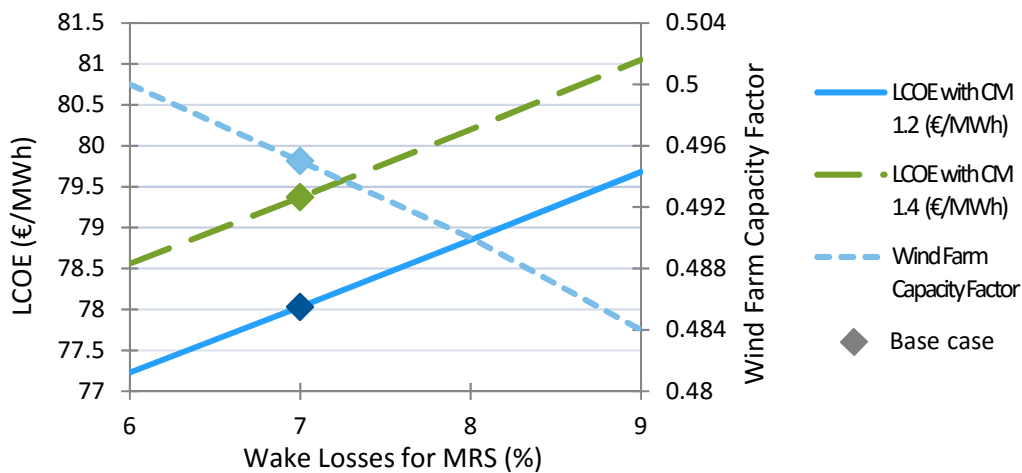


Figure 11-12: MRS LCOE sensitivity to Wake losses.

The MRS aerodynamic losses (Figure 11-13) represent the effect of the support structure and turbine arrangement on aerodynamic performance. The studies of NTUA (Chapter 4) indicate that accelerated air flow in the spaces between rotors may increase the turbine power and wind farm capacity factor. At present there is a likely performance gain and no sign of any penalty in aerodynamic performance of an MRS with very closely spaced turbines. Moreover the analyses of NTUA suggested that an 8% power gain is maintained with the rotor spacing reduced from 5% of diameter to 2.5%. However a secure position on aerodynamic performance estimates will not be achieved until the aerodynamic performance of complete structure and rotors has been simulated in a turbulent wind field over a range of the range of yaw angles associated with normal power production. It is almost certain that the MRS will have superior power performance to single large turbines in turbulent wind conditions and modelling/simulation (Section 11.2) predicts significant energy gains increasing markedly with increasing TI. However it will require further work to quantify this as a gain on annual energy production.

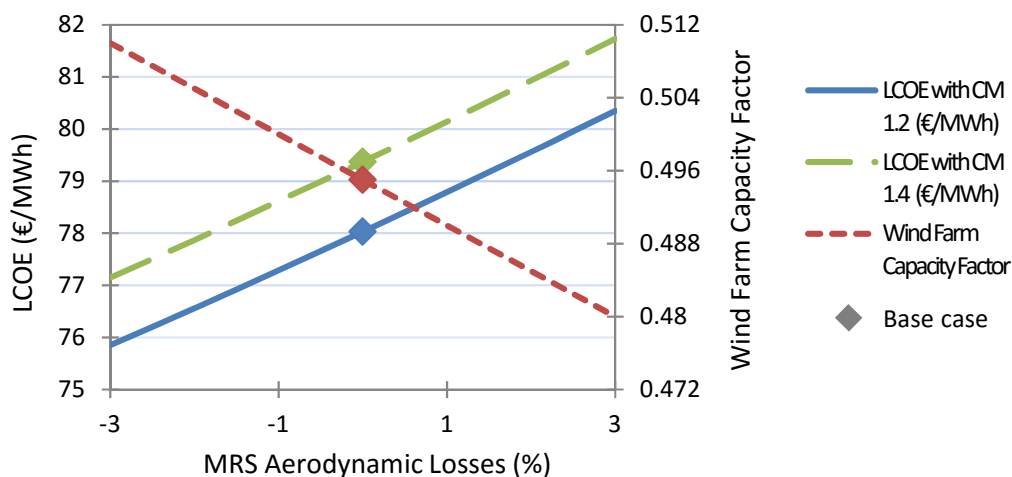


Figure 11-13: MRS LCOE sensitivity to MRS aerodynamic losses.

The turbine costs are partly based on scaling rules and partly on historic models as used in Deliverable 2.3. Costs based on scaling have regard to the fact that rotor and nacelle costs are mostly fundamentally cubic with rotor diameter [8]. Commercial data often seems to violate this scaling but largely because components are compared at different stages of technology development. A key argument for the MRS is that most of the projected advantages from cubic downscaling of say rotor blade cost requires no further advance in technology, merely a rigorous application of best current materials and methods to component manufacture of turbines in the hundreds of kW range.

The MRS structure cost is based on general similarity to a jacket as a large welded space frame with a cost for structure joints included as discussed in Section 11.4. The cost value is derived considering the ratio of cost of steel tubes per kg to cost in an all welded jacket

structure. The cost per kg of jackets could decrease but this would require a demand driven development of automated processes for large welded joints.

Power rating the MRS (Figure 11-14 and Figure 11-15) in relation to diameter may not be optimized. This is the issue discussed of power density which is generally optimum at a lower value offshore than on land because total costs related to electrical output form a much larger proportion of CAPEX and of lifetime cost in the offshore situation. The MRS cost model would not readily adapt to a change of rotor diameter. However, as structure costs primarily relate to storm loading on the structure itself, the rated output of MRS may be reduced from the nominal 20 MW and, assuming no impact on structure cost, the cost impacts on electrical components and systems can be accounted.

Obviously as the MRS is de-rated, more systems are required to make up the total wind farm capacity (500 MW). An assumption was made that O&M costs rise in proportional to the number of systems making up wind farm capacity or equivalently that O&M costs were factored as $(444 / P)$ where P is the unit turbine rating chosen. Figure 11-14 suggests that a unit de-rating to about 15 MW (power density 265 W/m²) could further reduce LCOE. However the LCOE modelling is too crude to have confidence in the precision of this assessment. There is however general confirmation that the lower power densities now favoured by the industry for very large offshore turbines are appropriate.

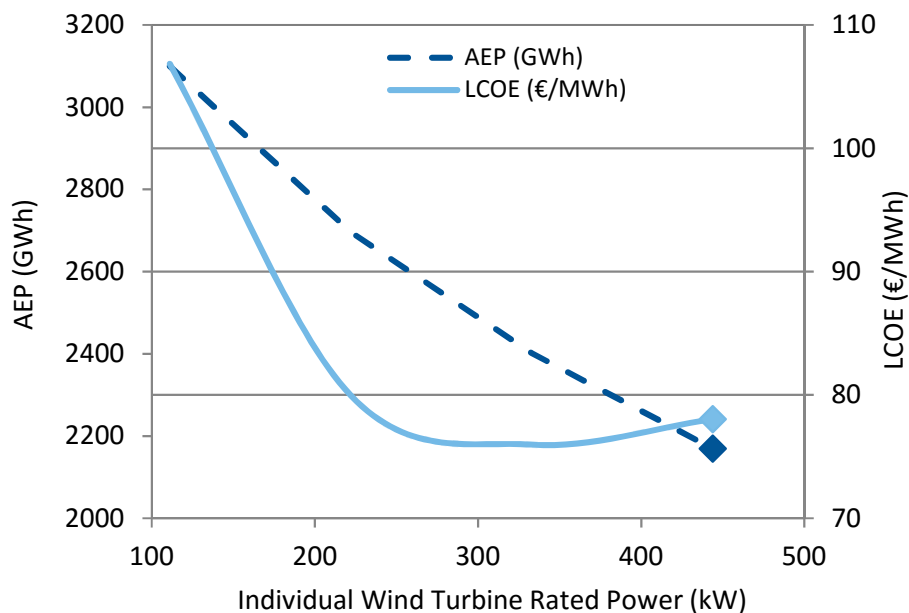


Figure 11-14 Individual Wind Turbine Rated Power (kW)

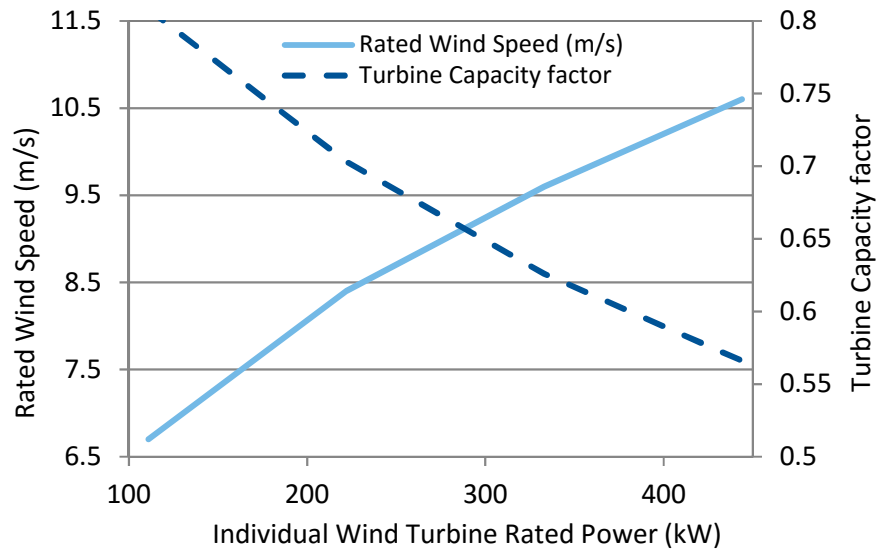


Figure 11-15 Individual Wind Turbine Rated Power (kW)

11.8 40 MW MRS

A claim for the MRS concept is that it may upscale well beyond levels that are economic or generally feasible for the single rotor concept. To test this, a 40 MW MRS is evaluated. The general principle in upscaling the MRS design is that there are more turbines and not larger ones so that turbine cost of a 40 MW MRS is effectively twice that of a 20 MW unit. It is then assumed that the space frame structure cost will scale cubically with any characteristic linear dimension of the structure. This is modelled by scaling structure cost as $2^{(3/2)}$. The power is doubled (from 20 MW) and is assumed to follow a square law as related to linear dimensions. The results are then compared with 4 x RWT (10 MW DTU wind turbine). O&M costs are as given in the LCOE model. In going from 20 to 40 MW unit rating the number of offshore sites per installed MW is halved and maintenance cost should reduce. Projected O&M reduction is after all a main part of the motivation in upscaling size of the single rotor turbine.

Table 11-3 offers CAPEX comparisons between the 20 and 40 MW MRS designs. The Jacket mass and cost is based on the LCOE modelling established in Innwind.EU, Task 1.2. Rotor and nacelle costs are simply doubled as is the number of MRS turbines from 45 to 90. This is the essence of the scaling of the MRS concept completely avoiding the impact of the square-cube law on these components that are much more expensive per kg than structure. All other mass values relating to structure and yaw bearings are scaled as $(40/20)^{(3/2)} = 2^{(3/2)}$ with consequent effect on costs.

	MRS 20 MW		MRS 40 MW	
	kg	M€	kg	M€
Bearings	78	0.601	221	1.699
Tower	1520	3.800	4299	10.748
Rotors	170	1.887	340	3.775
Nacelles	183	5.971	367	11.942
Space frame	1904	9.139	5385	25.850
Joints	113	1.688	318	4.773
Jacket	3459	17.351	9783	27.026
Totals	7427	40.437	20713	85.813

Table 11-3 CAPEX Comparison of 20 and 40 MW MRS

	LCOE	Reduction	
	€/MWh	% relative to RWT	
RWT	91.77	0	RWT baseline value
20 MW MRS	77.49	15.6	Baseline value for MRS Design A
40 MW MRS	86.33	5.9	No credit for O&M benefit
40 MW MRS	79.31	13.6	With 15% reduction in O&M

Table 11-4 LCOE Comparisons

The effect of upscaling the MRs from 20 MW to 40 MW is significantly adverse on LCOE if no credit is given for reduction in O&M costs which is unreasonable. LCOE will reduce unacceptably at some scale above 20 MW basically because in scaling structure costs it is hard to avoid the square cube law although the jacket can apparently do this mainly because the variable design water depth may not be scaled.

It will be obvious that the LCOE model and the level of design engineering that has been possible to date are too crude to regard this result at all definitive but it does not contradict the idea that the MRS concept may upscale far beyond single rotor concepts.

CHAPTER 12 CONCLUSIONS AND OVERALL EVALUATION

The conclusions and overall evaluation of the MRS concept covers the following areas:

- Key results from the detailed analyses, of aerodynamics, loads and structures
- Results of the LCOE evaluations
- Limitations of modelling and scope of investigation

Loads

As compared with large single rotors, many large reductions in structure loads were noted for the MRS arising from averaging effects associated with the independent operation of the small rotors all running at slightly different speeds in turbulent wind. After refinement of operational aspects, storm wind loading on the structure itself with rotors idling rather than rotor induced loading was the most significant source of extreme loading for the structure. Fault cases of a single rotor (blade stuck in pitch for example) are not significant for structure design. The most recent analyses indicate that fatigue loading is designing for the structure although the possibility to mitigate this by control action – possibly something as simple as having slight variations in the rated rotor speed – has not been explored.

Space Frame Structure

A preliminary design by CRES of a 20MW MRS structure has been presented. This design uses 45 horizontal axis rotors each rated at 444kW in a planar arrangement supported by an interlocking space frame. An optimisation of the supporting structure for minimum weight was performed, leading to a solution using standardised tubular steel sections with an overall weight of ~3750 t. A single 20 MW turbine with the same total swept area would be of larger diameter than the UPWIND 20 MW design and expected to have a tower weight ~ 3500 t. The present MRS design solution was checked for ultimate loading and fatigue in selected representative cases. It has been validated as robust in the event of failure of the most highly stressed member.

Floating Support Structure

Different configurations for the floating support structure were examined for the proposed Multi-Rotor system. A concrete floater design was chosen with an estimated mass of 48,000 t. The project was initiated with focus on the floater solution as also providing a means of yawing in the sea. Latterly it has seemed much preferable to have a clear comparison with the RWT with both designs using jacket foundations.

Aerodynamic Evaluation

Aerodynamic modelling of NTUA showed no adverse interaction in a large array of closely spaced rotors and revealed a likely mechanism of increased power performance associated with augmented flow through spaces between the rotors. An 8% power gain, comparing the total power of a 45 rotor MRS with 45 x power of a rotor operating in

isolation, resulted both from analyses using (viscous) CFD modelling and (inviscid) vortex based models.

Simulation and modelling of UoS indicated an additional mechanism of energy gain for the MRS in having superior performance extracting energy in turbulent wind conditions. The gain may be small $\sim 1\%$ depending very much on site turbulence levels but increasing strongly with increasing turbulence. However this must be seen in the context where large single turbines regardless of sophistication of control cannot extract turbulent wind energy as effectively. The high rotor inertia filters higher frequencies in the wind and may in similar turbulence levels lose 2% or 3% energy compared to operation in steady wind conditions.

Thus comparing MRS and single rotor systems at equal swept area, an overall an energy gain $\sim 10\%$ is predicted. No credit for this is assumed in the baseline estimate for LCOE of the MRS.

Wind Farm Wakes

The aerodynamic modelling of NTUA was restricted (not in principle but by project resource) to an examination of the 45 rotors of the MRS operating in synchronism in steady wind (with a vertical shear). In reality the wind flow will be turbulent and the rotors will not operate precisely at the same speeds. As was demonstrated in Section 5.7.1, especially near rated wind speed, the averaging effects of wind turbulence will reduce the aggregate total thrust on the MRS compared to an equivalent large wind turbine and thrust is the primary determinant of wake deficit. Moreover partial wake immersion, which is considered the most damaging situation for added rotor fatigue, will be mitigated on the MRS where, if the system as a whole is operating partially in the wake of another upstream MRS, individual rotors will mostly be totally immersed or not immersed.

LCOE Evaluation

In the base case scenarios for the MRS and RWT, the LCOE of the MRS is estimated to be reduced by 15%. This is a huge benefit. To put it in perspective, if the giant blades of the 10 MW RWT were provided at no cost, the reduction in LCOE of the RWT would be only 4%. Also the RWT is in itself a low mass advanced design aiming to capture what may be achieved in technology development of the conventional solution over the timeframe in which competing innovative technologies may appear. In the Innwind project, the reference value for present offshore LCOE is 107 €/MWh. In relation to that value the MRS technology promises $\sim 30\%$ LCOE reduction.

In addition to the base case analysis a wide range of sensitivities were explored.

Using a very detailed model for offshore O&M costs but with limited adaptations to address the MRS, a reduction in O&M costs of 13 % was predicted for the MRS. This is sensitive to details of design for O&M and to O&M procedures which have not been fully developed. No credit is taken for this in the baseline LCOE for the MRS of 77 €/MWh.

Considering CAPEX, the net saving in the base case comparing MRS and RWT is apparently only 3%. However and it is misleading to draw as a general conclusion that the penalty in MRS structure cost will nearly cancel the benefit of an MRS in very low turbine CAPEX. The MRS, in line with present offshore practice for very large turbines, has a lower power density (337 W/m^2) than the RWT (402 W/m^2). Increasing the diameter of the RWT to match power densities and hence equalise swept areas increases blade, pitch system and tower costs of RWT in a range 20% -30%. Comparing at equal energy output, the MRS has overall CAPEX savings ~13%.

Limitation in modelling and scope of study

Areas not yet addressed or studied in sufficient detail are:

1. Rotor (size) optimisation and structure shape optimisation
2. O&M (especially)
3. Aerodynamic performance in yawed flow
4. Integrated structure design with yaw bearing(s) to suit jacket foundations
5. Complete system engineering including design for maintenance, assembly and installation with the more extensive loads analysis and general modelling that will be associated with this.

The optimum size of rotor for an MRS may be determined by consideration of handling and maintenance logistics more than by the economics of scale which certainly demand a large number of rotors but in isolation do not determine an optimum size. Performance in yawed flow was assessed outside of Innwind.EU in a previous project [4]. Whilst no sign of any serious performance penalty beyond the expected reduction in power with yaw angle was detected, the tests were rather limited and inconclusive. Structures have been analysed with some rigour but not optimised in relation to yaw system solutions nevertheless allowing credible estimates of mass and cost. However there is a need for a more complete integrated design to be developed addressing all necessary aspects,

CHAPTER 13 MRS CONCEPT OVERVIEW

13.1 Evaluation of MRS as an innovation

In the evaluation of an innovation there are three main aspects;

- 1) What are the benefits if successful?
- 2) Is it thoroughly feasible?
- 3) If technically feasible will it be economic?

The level of benefit is the starting point. Clearly an innovation is pointless if there is not a significant level of benefit should it be successfully engineered.

13.2 The level of benefit

The MRS as a complete system solution can potentially have greater impact on LCOE than any innovation that addresses components only such as blade or generator for example. Some key areas of potential benefit are listed here with some explanations following.

- a) Technical LCOE reduction addressed in the present project
- b) Commercial LCOE reduction from de-risking turbine technology
- c) Shortening of production and development cycles accelerating turbine cost reduction and reliability improvement
- d) Potentially much larger unit capacities than conventional technology reducing the number of offshore sites per installed MW
- e) Savings, perhaps ~ 80% reduction, in the use of non-recyclable glass-resin products per installed MW
- f) Faster market implementation

LCOE can loosely be regarded as having two separate main components, one technology related and the other commercial relating to market circumstances, perceived investment risk etc. From a purely technology related stance as is the main interest in the present project, the MRS aims to achieve reduction in LCOE from a fundamental scaling advantage which leads to large savings in mass and cost of rotor-nacelle systems when the same total swept area is spanned by a multiplicity of small rotors rather than one large one.

Employing a fixed size of a technology that is already proven should reduce the commercial risk to turbine manufacturers, developers and investors with further benefit to LCOE. This could be the most major factor of all and more significant the technology related cost reduction potential.

The potential benefits of offshore wind turbines being manufactured in greater quantity at a standard size, where the technology is well proven, are huge. Compared to the single equivalent turbine, the units are less complex without individual yaw systems and are being made in quantities over 20 times greater per installed MW (as compared with 10 MW single rotors) yet using ~ 80% less raw materials per installed MW. Unit reliability can increase and unit cost decrease (experience curves for a wide range of industries show 10 -25% cost reduction with each doubling of output). However the focus will be on improving

reliability and hence availability which have prime impact on LCOE. The turbine CAPEX is inherently reduced by the MRS concept to a level where it is not a dominant influence on LCOE.

Another benefit is the shortening of production and development cycles accelerating turbine cost reduction and reliability improvement.

Suppose in the context of a blade of the 10 MW RWT, a new development in blade design offers useful LCOE reduction but requires a new blade design. Consider then the timescale and R&D costs in implementation through design of blade and tooling, manufacturing trial, component and full scale testing plus prototype experience. Compare this to the situation of an MRS where a new set of blades at several orders of magnitude of less cost and materials volume and much faster development cycle time may be tested on one or two turbines of a pre-existing MRS with little disruption to availability. Thus the whole process of technology development, product enhancement, reliability improvement and cost reduction can be much faster and cheaper with MRS technology.

The present drive towards up-scaling wind turbines is about cost reduction through reducing number of offshore sites per installed MW with benefit to BoP and O&M cost per MW. The MRS achieves this without the huge costs and risks of developing new super-scale single turbine technology and also may be feasible at unit capacities above 20 MW and thus beyond what is likely ever to be economic for single turbine technology.

The mass of blades and other composite components per installed MW is greatly reduced to a level $\sim 20\%$ of the mass of material required for 10 MW single turbines. As the composites used in the wind industry are generally very difficult to recycle, this is also a major advantage from an EU perspective.

Finally, regarding potential benefit of the MRS, while there is clearly an initial time lag for adequate design development, once past the MRS technology can be implemented much faster in the market than large scale single turbine systems.

13.3 Feasibility, economics and possible show stoppers

At the deepest level there is no question that the MRS is feasible. In the array of turbines and structures, there is no inherently new technology in the whole system. However if any of the technical challenges led to excessive cost, it could in effect render the system unfeasible. So items 2) and 3) of Section 13.1 are bound together and now discussed in that light.

Possible show stoppers

The development of the MRS design, the approach taken in this project has been to systematically address what may appear to be showstoppers:

- a) **Energy Capture** – is there an adverse aerodynamic interaction in having closely spaced rotors that would compromise energy output in relation to installed swept area?

- b) **Structure** – although the lattice frame structure is well proven in general engineering being essentially a jacket above water, are there unusual loads or problems in carrying the rotor nacelle systems that would add prohibitively to capital cost?
- c) **O&M** – the MRS has superior fault tolerance in terms of implications of a turbine fault for total system output. It also has less urgency for maintenance especially in challenging weather periods. However, there will be more faults per system per annum on turbines that may be located at any position in the array. Although no major cranes will be required for individual turbine maintenance (as would be needed to replace a blade on a 10 MW turbine), can the maintenance operations be sufficiently automated using the intended built-in travelling crane to keep maintenance time and cost to acceptable levels?
- d) **Yawing** – are the demands in yawing a complete assembly of support structure and rotor nacelle systems so severe as to render it unfeasible or uneconomic?

The present outcome in relation to these possible showstoppers is;

- a) **Energy Capture** – following extensive aerodynamic modelling exploiting very powerful computing resource, there appear to be energy gains from the closely spaced array of rotors to the extent that minimal spacing is optimum. It remains important to confirm that aerodynamics in yawed flow are not especially problematic.
- b) **Support structure for rotor-nacelle systems**– tubular lattice structures are long established and there is clearly no fundamental problem. Many loads of the MRS system are reduced compared to the single equivalent turbine. However fatigue evaluation needs to be more extensive. Although many detailed analyses have been conducted, there has not been resource to re-optimize design in any major ways in relation to findings of the analyses. Thus there are factors that may be adverse or beneficial still to be accounted. However the structure has been quite rigorously and robustly designed to present load specifications and very large cost increases are affordable before LCOE benefit would be badly compromised.
- c) **O&M** – the relatively automated maintenance proposed with an overhead crane allowing rotor nacelle systems to be removed automatically has been discussed with various experienced engineers who consider it quite feasible. However there has not been resource to address detailed design of assembly and maintenance and this remains a key area for further work. Studies of O&M within this task 1..33 and the reliability work of Task 1.34 lead to consistent preliminary views of O&M impacts in a range that will not compromise the LCOE benefit of the MRS
- d) **Yawing** – yawing concepts have been explored and a first level of analysis applied to systems based on yawing on bearing(s). Basic feasibility seems assured and mass and cost implications of engineering yawing do not seem especially problematic.

13.4 Perception of the MRS concept

Basic Concept

In the context of familiarity with trends in many recent years of wind turbine development, the MRS may seem to be a strange exotic system. However, it should be noted that in many engineering situations (e.g. lighting a very large building), whether optimum or not, the first thought is to seek a solution using standard proven components rather than develop new ones. In the earliest periods dating from 1930's, multi rotors were only considered because of the difficulties of up-scaling wind turbines based on steel material systems. Other major merits of MRS technology, especially in relation to scaling implications, were overlooked. In consequence there has been a curious reversal of approach to the extent that the common sense first approach of looking at up-scaling with a multiplicity of established turbine systems rather developing massive scale new turbines has been neglected.

Visual Impact

The MRS has a complex appearance at close range which may be off-putting even if visual impact in relatively deep water offshore sites may not be of great importance. The crude line drawings of Figure 3-1 or Figure 3-4 give rather a false impression of the scale and visibility of most of the tubular members. The view in Figure 3-5 is realistic. It is not an arbitrary visual representation but is based on a structure designed with very conservative loads and showing the rotors and structure members in accurate proportions. With no very large parts in the MRS system and reduced height compared to the tip height of an equivalent single rotor, the MRS will most probably have reduced visual impact at distance compared to the equivalent single turbine.

Technical Perception

The natural reaction to an MRS is that the system has a large number of parts which looks to be problematic for assembly and maintenance and the requirement to yaw the turbines collectively seems to be a very demanding in engineering terms. All of this is true.

However the central advantages of the concept are less visible but very substantial, at the core being a huge reduction in mass and cost of rotor and nacelle systems and, possibly above all, the standardisation of turbine technology at a very manageable scale leading to large cost and reliability benefits. The engineering of collective yawing is demanding and expensive but appears to be affordable while there are useful benefits as well as disadvantage in O&M aspects.

Disruption of Innovation

If MRS technology were adopted in a significant way it would admittedly disrupt present R&D directions. However to established manufacturers of the horizontal axis wind turbines which dominate the market place, it would be far less disruptive than say a vertical axis concept which would render years of developments experience in horizontal axis systems less relevant. In fact it would offer manufacturers a route to stable

production with much reduced development overheads and potentially much better profit margins.

13.5 Status of MRS at conclusion of Task 1.33

Unquestionably more detailed work is required in a number of areas to confirm the MRS as a convincing solution to up-scaling. This has been inevitable. Problems of rotor/nacelle design are bypassed with such technology being taken for granted at 444 kW scale, but beyond that in the MRS a new system concept is involved requiring major adaptations of tools for load prediction and aerodynamic evaluation, involving new concepts for support structure and yaw systems, requiring new models for O&M prediction etc. By comparison, other types of innovation (say a new generator) can effectively “bolt on” to the RWT and use most of the established design (tower, jacket etc.) and modelling with little change required. In addition the tools and design methods for the standard 3 bladed turbine are now long established. Thus it is not possible immediately to bring the new MRS design to comparable levels of detail and refinement. The present MRS design is not mature in the least leaving many uncertainties but also the capability for much more optimisation and refinement.

While the uncertainties in design evaluation at the present preliminary stage are highlighted, the MRS looks to have potential for substantial LCOE reduction from purely technical aspects as are addressed in the present Innwind.EU project. However considering LCOE in the wider commercial context, the de-risking of turbine technology and the reduced probability and impact of any serial fault in design or productions will greatly facilitate investment and may be more important in reducing overall LCOE than any of the technology factors evaluated within this project.

Based on scaling laws validated by existing commercial data, the MRS concept will typically enable a reduction ~ 80% per installed MW in the quantity of rather non-recyclable glass epoxy material systems used in large wind turbine blades.

The predicted LCOE reduction of the MRS ~ 15% relative to the RWT is attended by many uncertainties. However it is largely deriving from the fundamental scaling advantage which is confirmed by commercial data and current cost models.

The work done suggests that the MRS may be inherently more productive with about 10% power gain in below rated operation. Considering production volumes, unit scale and affordability of paying for increased design margins, it seems irrefutable that the MRS rotors can in time develop appreciably more unit reliability than giant single turbines. It also seems likely that overall O&M costs can be less. While all these possible benefits are modelled and approximately quantified, in the baseline MRS case, no credit is taken for these probable benefits. Moreover in examining sensitivities to variation in major costs such as the structure and yawing system, the MRS can tolerate very substantial cost increases and still remain usefully advantageous in LCOE.

REFERENCES

- [1] P. Chaviaropoulos et al., "PI-based assessment of innovative concepts (methodology)", *Innwind.EU Deliverable 1.23*, April 2014.
- [2] Jamieson P, *The Prospects and Cost Benefits of Advanced Horizontal Axis Wind Turbine Design*. Garrad Hassan Report, No 317/GR/02, February 1995.
- [3] Smulders PT, Orbons S, Moes C. *Aerodynamic Interaction between Two Wind Rotors set next to each other in One Plane*. EWEC, October 1984 Hamburg..
- [4] Ransom D, Moore JJ, Heronemus-Pate M. *Performance of Wind Turbines in a Closely Spaced Array*. *Renewable Energy World*. May/June 2010, Volume 2:3, pp 32-36..
- [5] Jamieson P, *Future Vision of the Technology*. Presentation to US, DOE Deepwater Wind Energy Workshop. Washington DC, October 2004..
- [6] UPWIND 2011, "Design Limits and Solutions for Very Large Wind Turbines", EWEA.
- [7] Branney, M. *PhD Thesis in preparation as at August 2014*.
- [8] Jamieson,P, "*Innovation in Wind Turbine Design*", Wiley and Sons Ltd., August 2011.
- [9] Chaviaropoulos, P. K. and Douvikas, D. I., 1998, "Mean-flow-field Simulations over Complex Terrain Using a 3D Reynolds Averaged Navier–Stokes Solver," *Proceedings of ECCOMAS '98*, Vol. I, Part II, pp. 842-848.
- [10] Wilcox, D.C., 1993, "Turbulence Modelling for CFD", DCW Industries Inc., La Canada, California, ISBN 0-9636051-0-0..
- [11] Stull, R.B., 1988. "An Introduction to Boundary Layer Meteorology". Kluwer Academic Publishers, Dordrecht..
- [12] Prospathopoulos, J.M., Politis, E.S., Chaviaropoulos, P.K., 2008. "Modelling wind turbines in complex terrain". *Proceedings of the 2008 EWEC & Exhibition*, Brussels. EWEA 42–46..
- [13] Monin A.S., Obukhov A.M., 1954, "Basic Laws of Turbulent Mixing in the Atmospheric Surface Layer", *Trudy Geofiz. Inst. Acad. Sci. U.S.S.R.*, 24(151), pp.163-187.
- [14] Voutsinas, S.G., 2006 "Vortex Methods in Aeronautics: How to make things work", *Int. Journal of Computational Fluid Dynamics*, Vol 20, No 1.
- [15] Petot, D.,1989."Differential Equation Modelling of Dynamic Stall," *Recherché Aerosp.* 5,59–72.
- [16] Riziotis, V.A., Voutsinas, S.,G., "Dynamic stall modeling on airfoils based on strong viscous-inviscid interaction coupling," *Int. J. Numer. Meth. Fluids*, 56, 185-208, 2008.
- [17] IEC, "International Standard:IEC61400-1", 3rd Edition 2005-08.

- [18] Germanischer Lloyd, "Guideline for the Certification of Wind Turbines", Edition 2003 (Hamburg).
- [19] P. Chaviaropoulos, "Development of a State-of-the-art Aeroelastic Simulator for Horizontal Axis Wind Turbines. Part 1: Structural Aspects", *Journal Wind Engineering*, Vol 20, No. 6, pp. 405-421, (1996)..
- [20] Doyle, J.F., "Static and Dynamic Analysis of Structures with An Emphasis on Mechanics and Computer Matrix Methods", Kluwer Academic Publishers, 1991..
- [21] Bathe, K.J., "Finite Element Procedures in Engineering Analysis", Prentice-Hall, ISBN 0-13-317305-4, 1982..
- [22] DIN 18800 Part 1, "Structural steelwork, Design and construction", Nov. 1990.
- [23] DIN 18800 Part 2, "Structural steelwork, Analysis of safety against buckling of linear members and frames", Nov. 1990.
- [24] DNVGL-RP-0005:2014-06, "Recommended Practice, RP-C203: Fatigue Design of Offshore Steel Structures, 2014.
- [25] Jamieson, P, et al., "Initial geometry and Concept Specification", Innwind Internal Communication from UoS.
- [26] "Mathematica: a system for doing mathematics by computer", computer program by Wolfram Research Inc..
- [27] Tube & Pipe Sizes, 5th Edition, TPS Technitube, Röhrenwerke GMBH, www.tpsd.de.
- [28] www.eew-group.com/downloads/?eID=dam_frontend_push...2299, 10. eew global pipe company - EEW Group in:.
- [29] Jamieson P, et al., "Design Loads for a 20 MW Multi Rotor System", Innwind Internal Communication from UoS.
- [30] DNVGL-RP-0005:2014-06, RP-C203: Fatigue design of offshore steel structures, 2014.
- [31] K. Sandvik at al., "Offshore Structures – A new challenge. How can experience from the marine concrete industry be utilized", *Proc. XIV National Conference on Structural Engineering, Acapulco, 2004.*
- [32] E.G. Nawy. *Concrete Construction Engineering Handbook. 2nd Edition*, CRC Press, 2008, ISBN-13:978-0-8493-7492.
- [33] <http://www.wsdot.wa.gov/nr/rdonlyres/f764fc61-e749-4f5d-b5ee-ed6da0c71f89/0/ci.pdf>.
- [34] Wagner, "Wagner J, Horn M & Manz J. Die neue P3000 - ein Entwicklungsbericht von TEMBRA. *Wind-Kraft Journal*, (2), 2–4, 2013."
- [35] Liew, "Liew K W. On the Yaw Dynamics of Floating Wind Turbines. (2013).".
- [36] Dalgic, "Dalgic Y, Lazakis I, Dinwoodie I, McMillan D, Revie M. Advanced Logistics Planning for Offshore Wind Farm Operation, *Ocean Engineering*, Volume 101, 1 June 2015, Pages 211–

226”.

[37] Gin, “Gintautas T, Sørensen J D. Integrated system reliability analysis. Task 1.34 Report for Innwind.EU, September 2015”.

APPENDIX A FATIGUE ANALYSIS OF THE SUPPORT STRUCTURE MEMBERS, S-N CURVES

Indicative results from rainflow counting for individual members are presented below. The reference S-N curve depicted is the one corresponding to tubular structures, according to [24], characterised by parameters a, m (3.0, 12.164) and (5.0, 15.606) for the two linear parts. Low cycle fatigue is not shown, as it has not been calculated.

